Author:
Deakin, William J

Title:
The Role of Mechanical Function in the Evolution of Skeletal Morphology

THE ROLE OF MECHANICAL FUNCTION IN THE EVOLUTION OF SKELETAL MORPHOLOGY

By
William J. Deakin

Bristol Palaeobiology Group
School of Earth Sciences
University of Bristol

A dissertation submitted to the University of Bristol in accordance with the requirements of the degree of Doctor of Philosophy in the Faculty of Science.

April 2023

Word count: 34,724

Abstract

The role of mechanical function in the evolution of morphology is important to our understanding of the dynamics of morphological macroevolution. Our understanding of the fossil record and therefore Earth's natural history is largely based on morphological evidence. Many epistemological arguments have been discussed regarding what should be assumed about morphological adaptation to function, ranging from an assumption that all structures are optimised, to an assumption that no structure is. In this thesis, I develop upon previous methodologies such as theoretical morphology, Pareto optimality and biomechanics, to test whether morphological structures are optimised or not, and to measure the relative strength of functional bias on form. I apply this to a wide range of 2D vertebrate jaw morphologies throughout their fossil record, and find that many of these jaws are optimised within the trade-off for rotational efficiency and stress dissipation in response to biting. Furthermore, I find a negative correlation between optimality and complexity in the theoretical morphospace of mammal jaws, which provides a mechanism through which natural selection can actively reduce complexity over time. Finally, I develop more models for the theoretical morphology of 3D biological 'tubes', such as the shaft of the humerus in birds. These algorithms are intended to be broadly applicable to a wide range of biological structures. The morphology of the limb shaft is constrained in aquatic and aerial birds compared to terrestrial and insessorial birds. I conclude in this thesis that theoretical morphology is an extremely powerful tool in modern evolutionary biology, and more work is needed to develop new morphological models and apply their concepts to a wide range of biological structures. The role of mechanical function in skeletal morphology is testable in certain structures like the jaw, and with more development, we can ask similar questions of many biological forms.

Acknowledgements

This work was not possible without my supervisors, Emily Rayfield and Phil Donoghue. I understand that the same could be said of any supervisor of any PhD thesis. That being said, I find it hard to believe I could have received their tireless support, their extensive knowledge and their unconditional care anywhere else.

The Bristol Palaeobiology Group has been a welcoming atmosphere since my very first introduction, and everyone within has always had something interesting to show, something helpful to share, or just something funny to bring to a conversation to take the mind off of work. Collaborators have provided resources and feedback during my PhD projects, and were very helpful during my first interaction with the scientific publishing process.

My friends and family have been a solid foundation from which this thesis was built. You know who you are and, hopefully, you know how grateful I am.

I am immeasurably grateful to you all.

Author's declaration

I declare that the work in this dissertation was carried out in accordance with the requirements of the University's Regulations and Code of Practice for Research Degree Programmes and that it has not been submitted for any other academic award. Except where indicated by specific reference in the text, the work is the candidate's own work. Work done in collaboration with, or with the assistance of, others, is indicated as such. Any views expressed in the dissertation are those of the author.

William J. Deakin
13/04/2023

Contents

List of Figures

List of Tables

Chapter 1

Introduction

Author's contribution This chapter was written by William J. Deakin.

1.1 The importance of shape in evolutionary biology

It is generally accepted that biological shape has evolved [1–4]. The wide variety of phenotypes we observe today in nature are but a slice of a billions-year long landscape of weird and wonderful biological structures, shifting and warping as new taxa speciate and old ones die out. The phenotype, as it is quoted in biological literature, refers to the overall structure of an organism – of which morphology (shape) is an integral part. Indeed, it was largely through careful observation of shape that Darwin first formulated his theories of evolution and selection. Similarly, before the onset of molecular biology and phylogenetics, shape was the comparative anatomist's primary tool in organising the hierarchy of life.

Considering shape alone was not perfect, however. Many taxa were historically placed within the wrong clades due to evolutionary convergence. Despite this, many higher taxonomic groups created at the time remain monophyletic branches of our most up to date evolutionary trees, including mammals and birds. Therefore, it is uncontroversial to say that shape has evolved not only via selection, but also via genetic drift and passive evolutionary processes [5–8]. With this, one fundamental question of biology remains: how much of shape over large evolutionary timescales is controlled by selection, and how much is contingent on an organism's phylogenetic and ontogenetic history?

Understanding these processes controlling evolutionary morphology is critical to macroevolutionary science. An overwhelming proportion of palaeontological data is considered through shape, as the primary data source from fossils. Further, fossils are now understood to be imperative data sources in any macroevolutionary analysis, as they provide thresholds in time to which we can calibrate models of molecular and morphological evolution [9–11]. This was not always the case. In the mid-20th century, palaeontology was often viewed by biologists as a lesser science. George Gaylord Simpson wrote: "The palaeontologist, [the biologists] believed, is like a person who undertakes to study the principles of the internal combustion engine by standing on a street corner and watching the motor cars whiz by." [12] During the latter half of the 1900s, the palaeobiological revolution - in which long term trends in evolution were measured, mass extinctions were discovered in the fossil record and laws of macroevolution were formulated – convinced wider biological science of its merit as both a nomothetic and idiographic field of study [13]. All of this information had, at its core, a basis in morphological analysis.

Contemporary palaeobiology is a multidisciplinary science, with fossil data providing much more information than just shape. CT scanning, biomechanics, geochemistry and taphonomical analyses provide a myriad of anatomical, behavioural and molecular data that has only been feasible with modern techniques [14–20]. But still, shape remains the primary source of data through which we observe macroevolution. Anatomy is largely characterised by difference and similarity in shape, the physical principles of biomechanics act on shape, and a large goal of taphonomical analysis is to unpick the deformation and loss of shape.

Therefore, morphology is perhaps the palaeobiologist's most ubiquitous and versatile tool, which can present some issues. If morphology is a Swiss army knife, then it is the palaeobiologist's job to pull from it the specific tool for the specific job the organism wishes to perform. If I want to reconstruct the diet of an extinct pelycosaur, which shapes should I look at? Its skull? Its teeth? Its legs? If I want to resolve the phylogenetic positions of ancient turtles, which shapes should I look at? The neck? The shell? The beak? Which parts of which organisms are controlled by their environment, and which are contingent on their biological history?

These questions are important to palaeobiology, and I argue they are also important to the rest of biological sciences. As evolutionary morphology is a critical component of modern biological science, understanding the controls of its construction can provide key insights to future biological research. These are not new questions, however. The integration of natural selection and evolution into biology carried with it old ideas of perfect natural systems, optimised and balanced in a neat natural order. The difference was that the role of an intelligent designer had been passed on to the 'neutral' evolutionary process. This assumption, that the natural process of evolution optimises all aspects of organismal biology, was termed adaptationism, and critiqued by Gould and Lewontin in 1979 in the famous 'spandrels' paper [21]. They noted that biologists – in particular, palaeontologists – tended to assign function to all modules even when there may not be one. The solution, they claimed, came with adopting the new framework of morphodynamics.

1.2 Morphodynamics

In 1970, Dolf Seilacher published the 'Konstruktions-Morphologie', in which he argued for the interpretation of three critical factors in the evolution of form: function and selection; phylogenetic history and evolutionary contingency; and morphogenesis, the physical processes that build an organism from conception (figure 1.1) [22]. Later he would add a fourth point, environment, to his triangle, developing the 'constructional morphology' tetrahedron [23, 24]. Any evolving module of a biological system can be considered as lying at some point within the bounds of this tetrahedron, with its distance to each point conveying the relative importance of function, phylogeny, environment, and development in the construction of its shape. This framework has since adopted the name morphodynamics [23, 24].

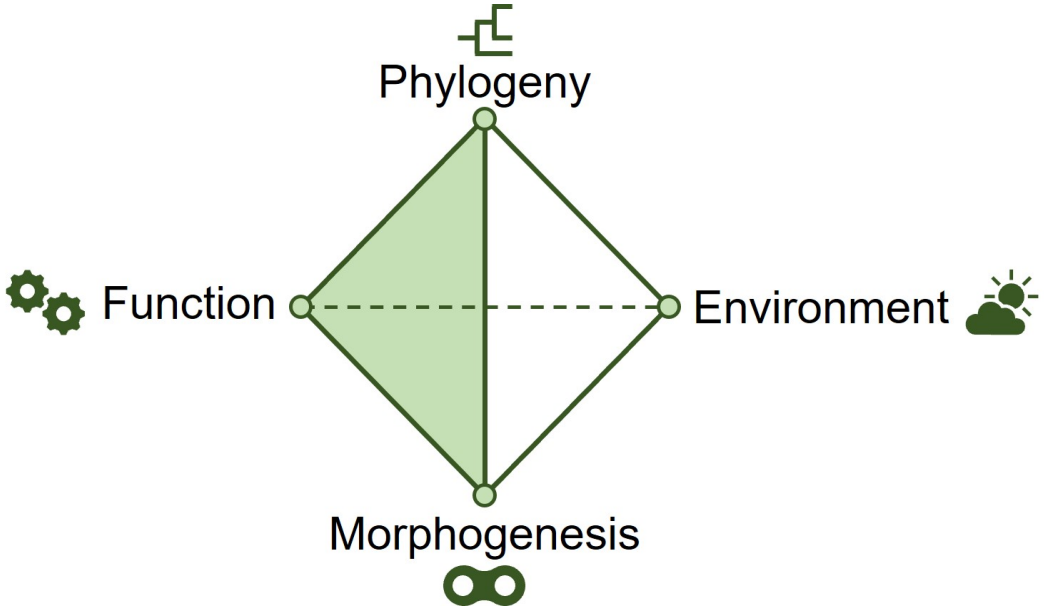

Figure 1.1: Morphodynamic tetrahedron. Points represent four individual biases on the evolution of morphology. Seilacher's original morphodynamic triangle, represented by the biases of phylogeny, function and morphogenesis, is highlighted in light green.

1.2.1 Functional bias

The functional component of morphodynamics has been central to the study of evolutionary biology since the publication of *On the Origin of Species* [1]. Generally, it refers to the aspects of shape that are controlled by selection, both natural and sexual. As an example, a finch's beak must perform the role of collecting and processing its specific diet. Short, thick beaks can distribute stress efficiently, while generating large bite forces due to their high mechanical advantage. This allows them to crush seeds and nuts and other hard foods more efficiently, so finches that prefer those hard foods are biased towards shorter and deeper beak shapes [25–29]. Thus, the shape of a finch's beak is controlled by its function.

Selection is one of the primary lenses through which many naturalists understand shape, and not without good reason – there is a large amount of evidence to support the idea that function has a strong evolutionary bias on shape [30–37]. The most convincing examples are those that point to cases of convergent evolution, the phenomenon where different organisms form different branches of the tree of life develop similar shapes for performing similar functions. Consider the body shapes of aquatic vertebrates throughout their evolutionary history. Sharks, dolphins, whales, and ichthyosaurs have all solved the problem of hydrodynamic drag in the same way; by generating a hydrodynamically efficient body plan, often referred to as streamlined, 'teardrop' or 'cigar shaped' [35, 38–40]. Many thousands of fish species also exhibit this shape [41–43]. This shape has since been adopted by engineers designing submarines to optimise efficiency [44].

Indeed, engineering has often used biological systems as inspiration for solving technical issues. When the Shinkansen bullet train entered a tunnel, the increase in air pressure was equivalent to a change in fluid medium – like a kingfisher diving from air to water. The engineers turned to nature for inspiration, and designed the nose cone to resemble the

kingfisher's beak, assuming that selection had solved this problem for them. Not only did it solve their problem, but it increased the train's efficiency overall [45]. Many engineers are now adopting biomimetic practices where they use biology to inspire design [46], and some are looking further to the evolution of form for design guidance [47].

Together, this evidence may convince you that function plays a strong role in the evolution of shape. However, these examples are cherry-picked. There are many cases of biological systems that are surprisingly inefficient [48]. While many will criticise Gould and Lewontin for patronising (to say the least) and oversimplifying the logic of their contemporary evolutionary biologists, the adaptationist bias still has influence within and without biology. This view of evolution almost on par with an intelligent designer has not only constricted the science, but has spawned outright dangerous pseudoscience and political theories, including race 'science' and social Darwinism [49]. A 'post-spandrels' critique of adaptationism, which provides analytical methodology for assessing the strength of function in controlling form, is therefore necessary.

1.2.2 Phylogenetic bias

Adaptationism was not ubiquitous within evolutionary science. While some were ascribing form to function alone, others were continuing the Linnaean tradition of classifying organisms within hierarchical groups based on their morphology [50]. Within the new context of evolution in the 19th and 20th century, this meant defining the evolutionary tree of life. The implicit assumption was that organisms that share similar morphological features share earlier common ancestors (note that this contradicts all examples of convergent evolution). This is apparent in Linnaeus' original taxonomy, where paraphyletic groups of plants were classified by their number of stamens, and invertebrate animals were sorted into insects and worms [51]. Phylogeneticists and cladisticians now incorporate convergence into their definition of homology, which can be split into primary homology (structures that share morphological features) and secondary homology (structures that share morphological features that are directly ascribable to their common ancestry) [52]. These components of homology are important when considering morphometric methodology, as I will discuss in part 3 of this introduction.

With the advent of molecular biology and genetics, the field of phylogenetics relied less and less on morphology except in the case of long extinct organisms. Still, the control of phylogeny on form was apparent, and consistent with evolutionary theory – evolution can only work with what it has been given. We can expect that the change in shape between an ancestor and its descendent is some function of the evolutionary time between them. The dynamics of this shift are currently debated, between two models of macroevolution: phyletic gradualism and punctuated equilibrium [53, 54]. The former states that morphological change through time is always gradual and varies consistently at any point along the branches of the evolutionary tree. The latter states that much of the genetic and morphological change that has accumulated in the tree of life happened within short bursts of evolution at each node (speciation) within the tree, which is then followed by long periods of evolutionary stasis within each branch. Macroevolutionary studies have found evidence supporting both these hypotheses in the fossil record [55, 56].

How can shape be controlled by function, while it is also biased by ancestral states? Within the morphodynamic framework, the answer is simple – shape is contingent on both phenomena, and neither has complete control of shape. Understanding how strong the phylogenetic bias is compared to function and morphogenesis may provide insight into these phylogenetic problems. If a system is heavily functionally controlled, for example, it may make sense to omit it from morphological phylogenetic analyses. Similarly, the punctuated equilibrium versus phyletic gradualism debate may be understood through the controls on morphospace exploration, which I will discuss in part four of this introduction. Understanding the tempo and mode of morphological evolution is heavily intertwined with our understanding of the morphodynamic process.

1.2.3 Morphogenetic bias

The final vertex of the morphodynamic triangle represents the morphogenetic bias on form. Morphogenesis is the process through which organismal form is created through growth, whether from seed to sapling to tree or embryo to juvenile to adult. It encapsulates the molecular processes that build cells and tissues, and the physical forces that guide this. While a large proportion of phenotypic data is stored in an organism's DNA or RNA, the life history of an organism has the final say on how shape is made. For example, scars and pathologies that an organism receives during its lifetime can have major effects on morphology. These can even be noted in fossils [57, 58]. Identical twins may seem very similar, but they have enough differences caused by morphogenesis to be distinguished from one another. Morphogenetic processes do not always manifest between individuals, however – they can have significant effects on body shape within individuals. Many dolphins and whales have medio-laterally asymmetrical crania, which develop from more symmetrical shapes during ontogeny [59–61].

The most significant kinds of morphogenetic bias are those generated by the growth process. Many shapes in nature are generated through strict methods, like biological algorithms, where varying input parameters can vary shape slightly while remaining constrained to the algorithm's process. As an example, the logarithmic spiral has been identified in many natural systems, including plant seed patterns, shells, teeth, claws, and horns [62–64]. This may promote some idea of evolutionary convergence; perhaps there is a functional optimality to the logarithmic spiral (and in the case of plant seeds, this may be the case [63]). However, one can also find logarithmic spirals in the structure of clouds and hurricanes, and in the shape of spiral galaxies (figure 1.2). This geometric pattern just arises from the natural forces associated with self-similar growth [65]. In the case of shells, teeth, claws and horns, the logarithmic spiral arises from linear changes in growth rate at different points in development. Specifically, by changing the growth rate over time and varying the growth rate either side of the developing tip, the structure naturally curves in a logarithmic fashion (figure 1.2) [64].

There are many such biases that limit the variety of organismal form. In the case of bones, they must perform functions not as individuals but together as a skeleton. The humerus must articulate with the radius and ulna, while the pelvis must make a smooth joint with the femora. Furthermore, the bones are not all individually created at conception

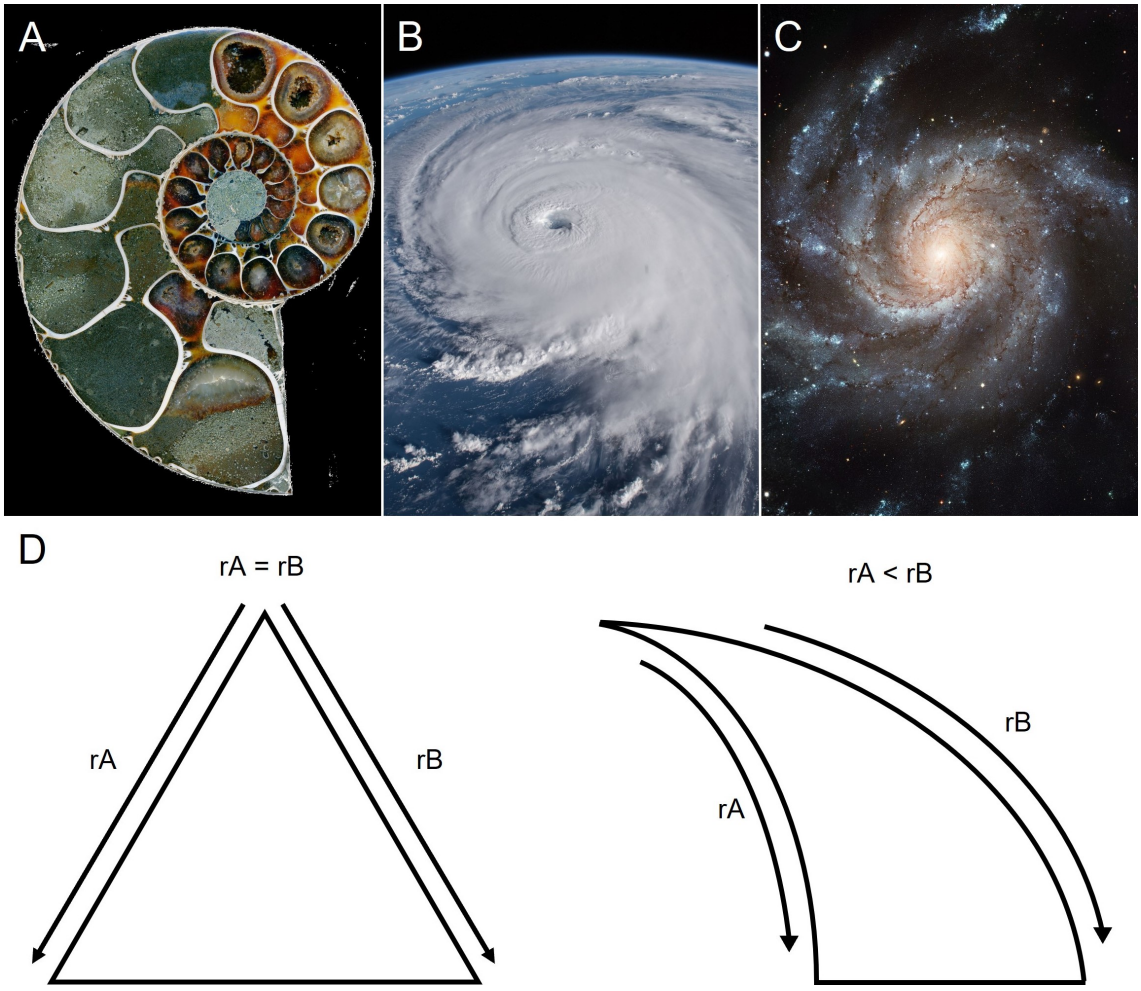

Figure 1.2: Logarithmic spirals in nature. (A) Fossilised shell of the ammonite *Argonauticeras*. Adapted from Dr. René Hoffmann (https://creativecommons.org/licenses/by-sa/3.0/deed.en). **(B)** Hurricane Florence, image courtesy NASA. **(C)** The Pinwheel Galaxy (Messier 101), from ESA/Hubble (https://esahubble.org/copyright/). **(D)** Logarithmic spirals arise naturally via spatially heterogeneous growth patterns, where the outer surface has a greater rate of growth than the inner surface. Adapted from [64].

– they form from the same mass of unspecialized cells during gastrulation, as with any other part of the body. During the skeleton's developmental process, those bones that are connected (or even just located close to one another) have distinct biases on one another's morphology. This phenomenon of biological structures developing connected 'modules' has been named modularity. Modularity is key aspect of morphological bias within bones. While modularity refers to the individual evolving parts of a system, the term 'integration' refers to the specific ways they bias one another's shape [66–68].

1.2.4 Environmental bias

The morphodynamic tetrahedron includes one more vertex – environmental bias. There are many examples in nature of the environment controlling phenotype. Think of the colour and shape change of a tree through the four seasons of the year. A famous example of extreme morphological change brought about by environment is the egg incubation of the American alligator (*Alligator mississipiensis*). Alligator eggs incubated at $< 30°C$ are all

born female, whereas eggs incubated $> 34°C$ are all male [69]. The morphological change associated with sexual dimorphism can therefore be attributed to environmental change during incubation. This is perhaps an overstatement – there are a myriad of developmental, functional, and genetic factors that determine the sex of an alligator. In my opinion, while environmental bias is important, the bias only acts through the other biases in the morphodynamic triangle (mainly morphogenesis and function). For this reason and for the sake of simplicity, I will not consider it heavily during this thesis. I will note, however, that the methods developed here to understand the controls on form may be used to explore this bias more in the future. The effects of climate change on organismal morphology have been documented in many different taxa [70–73]. This is currently an extremely important field of research in understanding the effects of anthropogenic climate change and will only become more important in the years to come.

Is there a way we can assess the relative importance of these biases on form? Great work has been done in each field of functional morphology, phylogenetics and developmental biology. In my opinion, after reading the literature of methodology, we can statistically test phylogenetic bias and some aspects of morphogenetic bias (which I will discuss in part 4 of this introduction), but understanding functional bias is still not totally possible. There are some convincing answers about the nature of these biases – for example, the evidence suggests that the biases have different strengths between different clades, and even within species between different modules [74–77]. In this thesis, I will attempt to further develop the current analytical methods, with a focus on creating informed models for assessing the role of mechanical function in defining the form of modules within the vertebrate skeleton.

1.3 Testing functional limits in morphospace

The constraints on morphology can be interpreted through the limits of morphospace (figure 1.3). A morphospace is an N-Dimensional (ND) set of axes that together represent major variation in morphology within a dataset [78]. Each point in morphospace represents a particular form, and the space close by to this point represents similar shapes. Translation along a particular vector represents a particular change in morphology. This is a useful framework because it pairs well with morphometric methods and is visually intuitive – like a map of shapes, it is immediately apparent which taxa within a dataset are more similar to one another. Following the construction of morphospace, the properties of the shapes within each region can be investigated and compared with the actual pathways that evolution has traversed through morphospace. In the case of functional optimality, this process will be used to build adaptive landscapes.

The metaphor of the adaptive (or fitness) landscape was first introduced by Sewall Wright in 1932 (figure 1.4) [79, 80]. Wright used it purely in a descriptive sense, as a thought experiment about how evolution might move populations to phenotypes with higher fitness, while also constraining some populations away from the most optimal phenotype. Firstly, a genotype space is constructed. For the sake of simplicity, we can imagine a Two-Dimensional (2D) set of axes, where each point in space represents a unique genotype. From here, it is theoretically possible to extrapolate a phenotype space – where each unique genotype maps to a singular phenotype. This may not be a unique mapping,

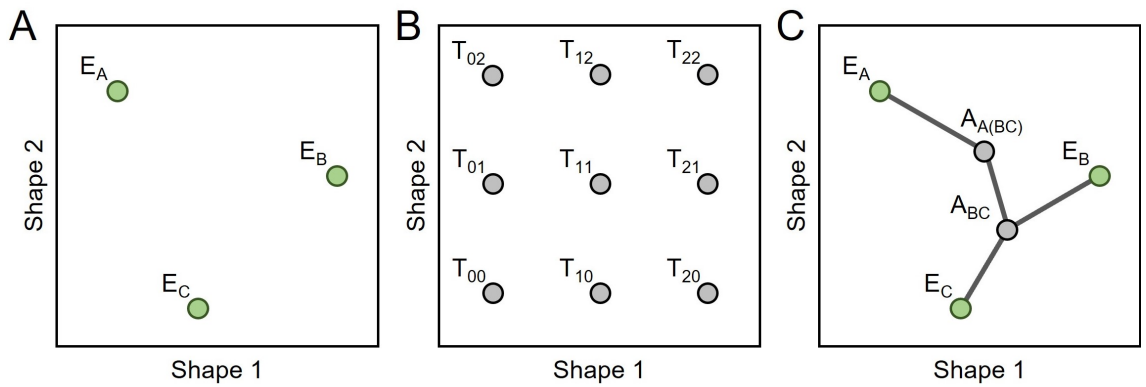

Figure 1.3: Types of morphospace. (A) Empirical morphospace is a visualisation of the proportional similarity between a set of empirical morphologies (E_i). The axes represent the different metrics defining shape, or the component scores of a PCA of the shape data. Empirical data is then plotted within these axes. **(B)** Theoretical morphospace is a set of generated theoretical morphologies (T_{ij}) and the area of morphospace that they cover. These represent the shape at an arbitrary position in morphospace, defined in this example as an evenly spaced 3-by-3 grid that covers the entire empirical morphospace. **(C)** A phylomorphospace is a visualisation of the morphological evolution of empirical morphospace. ASR is used to generate the ancestral state morphologies (A_i), which are plotted within empirical morphospace, and connected via their ancestry with lines. Empirical morphologies are represented by green circles and theoretical morphologies are represented by grey circles. Note that ancestral states can be considered theoretical morphologies.

as many genotypes may map to the same phenotype. Note also that this introduction has so far shown that a singular genotype may not map to a singular phenotype. Each point in phenotype space has particular properties that denote its fitness within that population at one moment in time. Some phenotypes will be more likely to successfully produce offspring than others, and these relative differences in success can be visualized as a surface- or landscape – in the z axis above the original genotype landscape. Wright noted that populations would move at measurable rates through this landscape towards the peaks of the landscape [79, 80].

While it was originally only intended as a metaphor, the concepts have since been employed within an analytical framework to further understand the macroevolutionary dynamics of a group of taxa within morphospace. In some cases, the genotype space has been mapped to the phenotype space to produce a true fitness landscape [81–84]. In the case of macroevolutionary morphology, this genotype-phenotype mapping is not currently possible and thus the phenotype space is directly constructed through morphometrics [85]. It is still useful to many questions of disparity to understand which areas of morphospace are functionally explorable. For example, disparity within a system may not accumulate any more if it has already explored all different functionally optimal morphologies. Most importantly to this thesis, the adaptive landscape is a powerful tool in measuring the strength of the functional bias on form. If a phenotype-function mapping is possible, then we can observe where biological structures lie on the adaptive landscape. If they

are constrained to optimal peaks, we can conclude that these morphologies are heavily controlled by function. If not, then there are other factors biasing form.

Note that the adaptive landscape requires functional analysis of both explored and unexplored regions of morphospace. In order to investigate whether evolution has generated the most optimal morphologies, it is necessary to test the morphologies that evolution has not generated for comparison. But how can we test a shape that, by definition, does not exist in nature? We can extrapolate the range of natural shapes mathematically, a concept known as theoretical morphology [86, 87]. Here, I will use four terms that I will define clearly to avoid the confusion with different definitions in the literature [88]: **1) Theoretical morphology:** the shape of a non-existent structure, generated mathematically, and the mathematical process through which it is generated. **2) Theoretical morphospace:** a set of distinct theoretical morphologies, and the area within morphospace that they span. **3) Empirical morphology:** the shape of an existent biological structure, measured directly via morphometric methods. **4) Empirical morphospace:** a set of distinct empirical morphologies, and the area within morphospace that they span (figure 1.3).

While the empirical morphospace has proven a useful tool by itself in many studies [89–95], here it will largely be used in combination with theoretical morphospace to generate adaptive landscapes. Adaptive landscapes can be generated without the use of theoretical morphology, by interpolating functional or survivorship data from empirical taxa [96, 97]. However, this approach misses morphological variation in unoccupied morphospace, which limits its potential to interrogate the constraints on the evolution of morphology. To investigate the optimality of evolved shapes, one must have a sample of unevolved shapes for comparison [98]. Therefore, theoretical morphology is critical to investigating functional optimality.

The analytical pipeline of generating the adaptive landscape from a theoretical morphospace is as follows: 1) An empirical morphological dataset is collected of a particular study sample of interest; 2) A theoretical morphospace is generated through some mathematical shape generation algorithm (often informed, but not defined by empirical morphospace); 3) the functional performance of each theoretical morphology within theoretical morphospace is measured through biomechanical analysis; 4) multiple functional performance landscapes are combined into one single adaptive landscape; 5) the positions of empirical morphologies and empirical morphospace within theoretical morphospace and the adaptive landscape are observed. The following subsections will discuss the variety of available methodology for completing each stage in this process.

1.3.1 Empirical morphology

In order to investigate the controls of shape, one must first assess shape itself. Morphometrics, or the process of mathematically defining shape such that differences between shapes can be measured, is an old and mature aspect of biology. Morphometric methods can be as simple as the length of a limb shaft, or as complex as assigning a high dimensional matrix to capture the all the bumps and crevices of a Three-Dimensional (3D) skull shape [99]. The most common form of morphological measurement is the landmark [99]. In fact, all morphometric analysis relies on some form of landmarking at some point in its

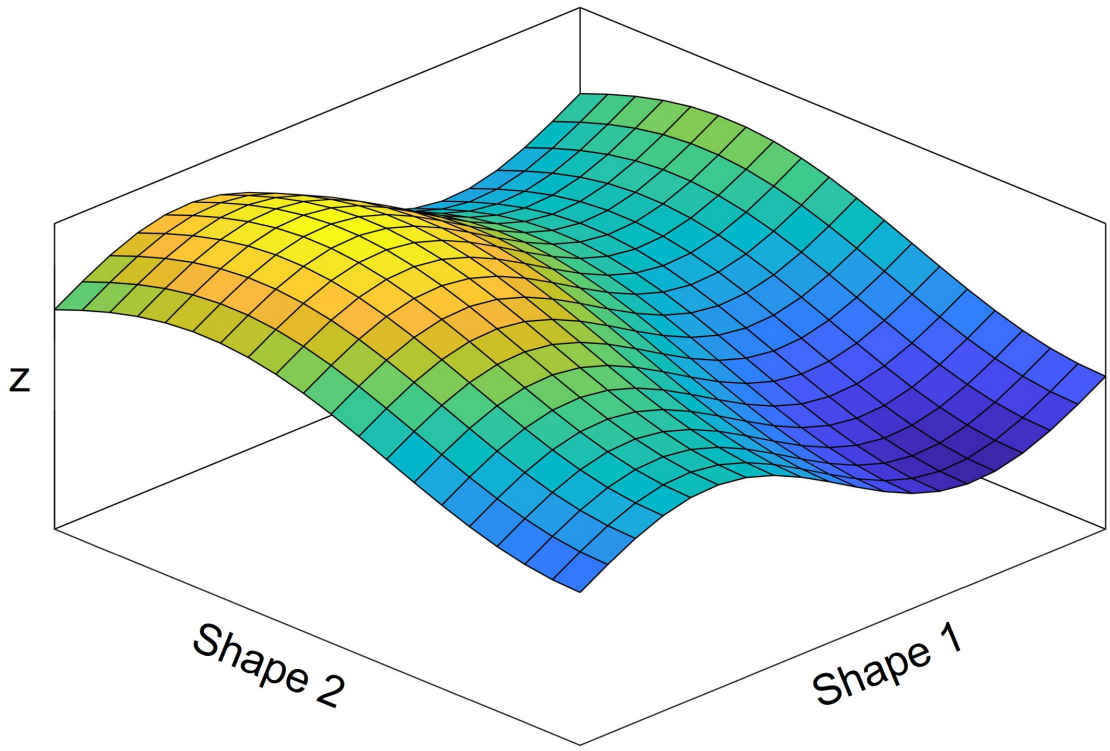

Figure 1.4: The adaptive landscape. The adaptive landscape of a 2D morphospace can be visualised as a surface above morphospace, where the z axis represents a measure of how fitness varies across morphospace. As a clade evolves, it will move in morphospace towards the peaks of the adaptive landscape. However, biases on shape will limit the regions of accessible morphospace, which may prevent taxa from reaching the peak of the landscape.

methodology. Landmarking is the process of identifying points in a space (usually 2 or 3 dimensional), where each point represents some aspect of morphology you wish to capture. For example, when measuring the length of a femur, a researcher must first 'place' two landmarks: the first being where they put the zero mark of their ruler, and the second being where they read the length measurement. Alternatively, when characterizing the 3D shape of each bone in a skull, a researcher must place many landmarks on the surface of bone (usually done in 3D computer software) to capture as much of the intricacies of shape as possible. The output data will be a list of 3D coordinates.

The number and positions of the landmarks is a decision made by the researcher. There are three flavours of landmarks, referred to as Type I, Type II and Type III [100, 101]. Type I landmarks represent points that are directly corresponding between different individuals, and that correspondence can be attributed to phylogenetic ancestry (secondarily homologous). Type I landmarks can also be placed with arbitrary accuracy. These are landmarks that, if you described their position to 100 different researchers and asked them to place it, they should produce almost identical results. For example, the point where multiple bone sutures cross, or a particular narrow foramen in a bone. Type II landmarks are similar but have a subtle difference. These still represent secondary homologies, but they do not represent precisely identifiable points and so may incur some human error.

Examples are the tips of specific processes, that are identifiable and homologous, but the exact position of a tip may not be certain. The tip may also not represent developmentally identical points between taxa anyway. Finally, Type III landmarks represent those that are not secondarily homologous, but are instead defined geometrically. For example, if our researcher defined the length of the humerus as 'the longest distance between two points on the bone's surface', then the landmarks that they 'placed' during measurement would be Type III. Other popular examples include the narrowest point of a bone, or the midpoint of the orbit. These still convey important shape data but are strictly non-homologous. There are also semi-landmarks, which are usually mathematically spaced along an outline between two landmarks. These are not necessarily considered Type III landmarks, despite them fitting most definitions of the terms [100]. Semi-landmarks can be considered separately from placed landmarks because they are partly self-correlated.

These three types of landmarks can be lumped into a higher organization between two groups of landmarks – those that are secondarily homologous, and those that are not. Generally, Type I and Type II landmarks belong to the former and Type III landmarks belong to the latter. Homologous landmarks may be powerful in identifying the phylogenetic aspects of shape and allow a more reliable comparison of shape difference between different organisms [102, 103]. Non homologous landmarks are more susceptible to error and may not represent true evolutionary shape difference. However, they are very powerful when trying to capture the morphological intricacies of more complex structures and can be used to reconstruct shapes more accurately. This reconstructive capability will be critical to many of the analyses I perform in this thesis, particularly when constructing theoretical morphology, which I will discuss in the next subsection.

Raw landmark positions do not suffice on their own when characterizing and comparing shapes. In their purest form, landmarks contain a mathematical mixture of shape, size, and rotation data. This is where different morphological analyses differ, in their transformation of landmark data to disentangle these aspects of raw landmark data. The most successful of these methods in contemporary literature is the generalised Procrustes analysis, or partial Procrustes superimposition, which utilises properties of a triangulation of the sets of landmark points within a dataset. Each triangle is located within Kendall's triangular shape space, where each unique triangle is represented by a point on the sphere, then all the triangles can be projected into a plane tangent to the mean of the sample to be plotted in a 2D space, generating a set of coordinates for each form [78, 99, 100, 104–106]. Shapes can then be scaled to a centroid size, to remove or separate size from shape depending on the particular analysis. Generally, these pipelines of shape characterization have been termed Geometric Morphometrics (GM) and have been widely utilized in many morphological studies [107]. Following this transformation, one can compare distances between organisms through the differences in their transformed landmark positions, or by assigning a thin plate spline to the data, which shows how the points are deformed by assigning a continuous deformation grid to each set of landmarks [102, 108, 109].

Alternatively, raw landmark data can be used to characterize shape through Fourier deconstruction. In the case of the 2D example, imagine an outline as a particularly stiff

string. By tying its ends together, we can create a loop, and we can push and pull points along the edge to create any 2D continuous shape. We can then untie the string, being careful not to lose the peaks and troughs along its edge, and unwrap it so that it varies along a single axis. We have created a continuous, periodic signal that can be deconstructed into its infinite component sine and cosine waves via a Fourier transform. Every shape will do so uniquely, and the factors defining each of its major wave components can be used to interpret unique shapes. This results in a very dimensionally efficient characterization of shape. Not only this, but these shapes can be reconstructed mathematically with variable resolution [110, 111].

One such algorithm is Elliptical Fourier Analysis (EFA) [112–114]. EFA splits a 2D closed loop into its component elliptical harmonics (figure 1.5). There are an infinite number of such ellipses comprising each shape, however the amount of shape data they contribute to the final shape (harmonic power) diminishes exponentially with increasing harmonic number. This diminishing return can be visualised by the size of each ellipse decreasing with harmonic number (figure 1.5) Therefore, 99.9% of each shape can be characterized with a finite number of harmonics. Each harmonic is characterized by four numbers, A, B, C and D. These describe the major and minor axis of each ellipse as a vector in 2D space, as well as the phase shift the ellipse at $t = 0$. So, a set of N elliptical harmonics can be characterized by $4N$ parameters, generating a $4N$ dimensional morphospace. We can go a step further, however, because this deconstruction contains size and rotation data. We can remove these aspects of form, to isolate shape, by taking the first elliptical harmonic (which generally contains the major information of size and rotation) and transforming it such that its major axis has a magnitude of 1 and is aligned with the x axis $(A, C) = (1, 0)$. Note that when we do this, we also ensure that $B = 0$, as the minor axis must now align with the y axis. Thus, a set of N size and rotation corrected elliptical harmonics can be represented by $4N$–3 parameters.

Morphology is an intrinsically high dimensional structure to measure. High dimensional data can capture a large proportion of organismal shape and is often paired with a Principal Component Analysis (PCA) to find the components of shape that capture the greatest variation within a dataset. The major axes of variation are then often plotted against one another, creating a morphospace. In this thesis, I will utilize this concept of morphospace heavily. The mathematical structure of morphospace can sometimes be misleading [78]. Many morphospaces built in literature represent non-Euclidean spaces, where distances are not consistent at every point in space. Think of the Mercator projection of the Earth. Although it provides some information about locality, countries close to the equator are relatively smaller compared to those closer to the poles. This concept will be important in discussion of the fifth chapter of this thesis. The other three research chapters will deal strictly with Euclidean data. It is also worth noting that some morphospaces in literature are not even affine spaces – that is they may not represent any aspect of locality [78]. These will be avoided entirely within this thesis.

These morphometric measures can be paired with other statistical analyses to answer questions about the nature of morphological evolution. The most common is an analysis of

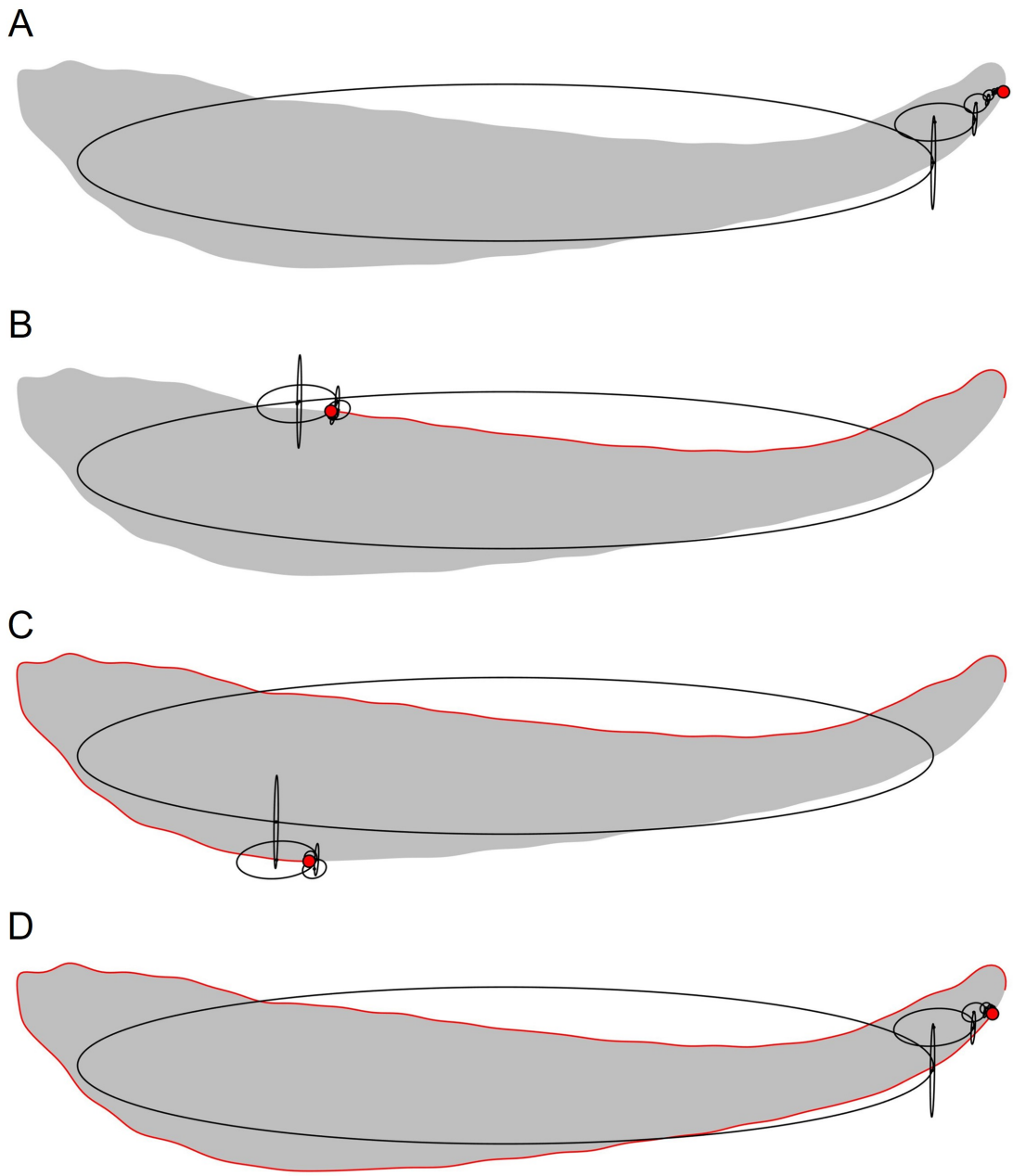

Figure 1.5: Elliptical Fourier Analysis (EFA). EFA splits a 2D closed loop into a set of ordered component ellipses, called harmonics. Any arbitrary co-ordinate along the outline is a function of the set of elliptical harmonics and its distance along the outline, t, where $0 \leq t < 2\pi$. The co-ordinates on each ellipse at nt, where n is the harmonic number of the ellipse, are summed together to produce the outline. Grey shapes represent the total lateral view jaw outline of *Acanthostega*, black ellipses represent each harmonic. The red circle represents the outline co-ordinate at t, and the red line represents the total outline generated from 0 to t, where: **(A)** $t = 0$, **(B)** $t = \frac{2\pi}{3}$, **(C)** $t = \frac{4\pi}{3}$, and **(D)** $t = 0.99 \times 2\pi$.

disparity, or the variety of morphology within a clade or geological time period [3, 115, 116]. Morphological disparity has been a staple metric in the palaeobiologist's toolkit since at least the 1990s. Systematic biology aims to understand how organismal variety came to be; in order to answer that question the variety of organisms must first be measured. In short, diversity is the number of individuals within a sample, whereas disparity is the scale of the differences between individuals within a sample. Within this thesis, I will link the morphological controls of the morphodynamic framework with disparity accumulation. Considering the punctuated equilibria versus phyletic gradualism debate, does disparity accumulate at different rates depending on the nature of morphological controls? We might expect so. To achieve this, the individual links between morphology and phylogeny, morphogenesis or function must be measured.

1.3.2 Theoretical morphology

Theoretical morphology is a difficult subject to define, due to subtle difference in definition within the literature [88]. For the purposes of this thesis, I will refer to the more general definition of theoretical morphology, as noted by McGhee: "Two quite different conceptual areas are understood today under the umbrella term of theoretical morphology: (1) the mathematical simulation of form, and (2) the analysis of the possible spectra of form via hypothetical morphospace construction" [86]. Classic examples include Raup's shell coiling morphospace, in which the shape of many mollusc shells can be constructed with a three parameter formula [62, 117, 118]. Empirical shell morphologies can then be plotted within these axes, and theoretical morphologies can be constructed at any point in the morphospace. There is one issue with this morphospace, however – as each axis represents a parameter measured in different units (angles and lengths), it can be described as a non-Euclidean affine space. This means that, while locality is preserved, distances in this morphospace will change depending on direction [78].

Some Euclidean methods for the construction of theoretical morphology exist. They can also be more general, allowing consistent application to a wide variety of structures instead of being limited to just shells, for example. Some methodology has utilized a mean shape to generate theoretical morphologies. The mean shape can be warped and shifted to fit the dimensions of any particular point in theoretical morphospace to generate a theoretical morphospace [119]. The mean shape is usually taken as the closest empirical shape to the mean of a morphometric dataset. Thus, this shape generation is not entirely free of bias from empirical shape. In the previous subsection I discussed EFA as a shape measuring and reconstruction tool. EFA allows for the construction of theoretical morphologies at all points in morphospace, with the limitation that it is constrained to 2D shape. It is also unique, in the sense that all points in morphospace represent unique shapes. This, combined with its reliance on non-homologous landmarks and its reconstructive ability at arbitrary resolutions, makes EFA a powerful tool in the construction of theoretical morphology.

The next step is to generate a theoretical morphospace, by generating a set of theoretical morphologies. Generally, this requires the researcher to make two decisions: how many theoretical shapes should be generated, and how should the position of each theoretical

morphology be decided? The common solution in the literature is to generate a uniform grid of theoretical morphologies spanning a finite region of interest in morphospace [48, 85, 120–123]. This has the benefit of allowing precise definition of the size and shape of theoretical morphospace, as well as facilitating interpolation of the functional/adaptive landscapes in morphospace between theoretical morphologies. This grid is usually generated in such a way that it is centred on the mean of empirical morphospace and covers an area greater than the area of empirical morphospace. Note that this means that the theoretical morphologies generated are biased by the empirical morphological variety.

The density of this grid remains an arbitrary decision, however. Recent studies have shown that very low-density sampling of morphospace can perform adequately in reconstructing performance landscapes, but whether this phenomenon is ubiquitous amongst different morphometric and functional analyses remains to be tested [97]. As there is no drawback to extreme sampling density other than computational time, usually as many theoretical morphologies as feasible are generated, with no strict rules about how many is enough. This highlights a central issue with the grid theoretical morphospace. The number of theoretical morphologies in a grid of consistent density increases exponentially as more dimensions of morphospace are sampled. Combined with the lack of standardised sampling rules, this makes including higher dimensions of shape variation in a grid very difficult. Thus, grid theoretical morphospaces are usually limited to two or three morphological dimensions. Combined with PCA, this can capture a measurable percentage of morphological variation within an empirical dataset. Depending on empirical sample size and morphometric methodology, this percentage of variation on two PC axes can vary substantially. For example, in this thesis, the percentage of morphological variation captured on the first two axes varies from $\sim 71\%$ of the dataset in chapter 2 to $\sim 59\%$ of the dataset in chapter 4.

Alternatively, theoretical morphospaces can be built from random point clouds in empirical morphospace [124]. These can be built to vary in any arbitrary number of axes, eliminating the bias in morphological variation from limited axis number. However, due to their random generation, uniform sampling through morphospace is not guaranteed, and the area of morphospace covered cannot be specified precisely. Also, the sampling density of the dataset still suffers the same issues as the theoretical grid when incorporating higher dimensional axes of morphospace. In cases where a large majority of shape variation is captured by the first two Principal Component (PC) axes of morphospace, such as chapter 2 of this thesis, I will prefer the theoretical grid. However, it is not clear which approach is more beneficial in cases where morphological variation is spread over more axes, like in chapter 4 of this thesis. Thus, in that chapter, I will attempt to compare the results from both a 2D grid theoretical morphospace and a ND random point cloud theoretical morphospace.

Theoretical morphospace is not the final stage when assessing the limits of morphospace evolution, but it does provide some hard limits before any functional analysis of theoretical morphologies has been performed. Due to the nature of characterising the physical phenomenon of biological form (which must abide by the universal physical laws) using mathematical form (which is abstract and does not necessarily abide by these laws) there are

sometimes regions of theoretical morphospace in which those laws are broken. Impossible morphologies (a sub-set of theoretical morphologies which cannot physically exist) have been reconstructed in many theoretical morphospaces, and usually together form strict sub-regions of theoretical morphospace known as impossible morphospace [87, 98, 125]. As an example, such structures exist in an EFA theoretical morphospace. EFA can reconstruct self-intersecting loops – which are not a physically possible property of the outline of a 2D projection of a 3D object. These represent hard boundaries in morphospace, in which there must be no empirical morphologies. Due to the dimensionality reduction and rotation of PCA, some high dimensional empirical data points can be 'squashed' down into the impossible regions of a 2D theoretical morphospace. This is an artefact of the morphological data lost when reducing the number of axes in a morphological dataset. Like a photo of a tourist at the Leaning Tower of Pisa, the reduction of a 3D environment to a 2D photo 'squashes' the space such that things are not what they seem.

1.3.3 Functional performance

The function of a structure represents each component of its active role in an organism's life and the functional performance of that structure is a measure of its ability in each of those individual functional components. For example, a primary function of many display structures is to attract a mate. In the case where a larger display structure is more likely to attract a mate, the functional performance of a particular structure in attracting a mate may be measured by its size [126]. There are, of course, many other attributes of a display structure that may make an organism more attractive, like colour and shape, which would each have their own individual functional performance metrics. Additionally, the attractiveness of a display structure is not its only functional role – in some cases it may need to be strong to resist the forces of a battle for a mate, and in general a more conservative structure can have high functional performance with regard to its low energy requirement to grow and maintain in an organism's life [126, 127]. Thus, functional performance represents a single component of a structure's ability to perform its role. I chose to include the example of the performance of a sexually selected structure as it shows that functional performance can be a difficult attribute to measure. 'Attractiveness' is an inherently arbitrary metric, the value of which may vary between different observers. Therefore, when attempting to build adaptive landscapes to assess the functional bias on form, it is important to choose structures that perform roles which have a large proportion of measurable functional performances.

For this reason, I will limit the assessment of functional performance to mechanical performance. While mechanical function is only one part of the function of a structure, in some structures it makes up the majority of its utility. An example I will investigate in chapters 2, 3 and 4 of this thesis is the vertebrate lower jaw. In almost all cases in nature, it performs a highly conserved function – to capture and process food. The performance of this is measurable, as it must be rotationally efficient in order to open and close during feeding, and it must be structurally strong to withstand the bite stresses involved in feeding. Many studies have shown a tight link between form and mechanical function in jaws. A wide variety of formulae and methodology from engineering and classical physics

has been utilised in the biological literature to measure such performances in the field of biomechanics [128–148].

In this thesis, I will utilise shape dependent biomechanical metrics to assess functional performance. Computationally assessing the physical properties of complex shapes is not feasible, so they are often broken into a finite set of mathematically simpler elements which can be assessed in parallel to approximate the overall physical properties of a system. The accuracy of this analysis increases with increasing number of elements, at the cost of higher computational power requirement. This is known as Finite Element Analysis (FEA), and has had decades of research to perfect its accuracy and computational efficiency for application in engineering [149, 150]. It has found popular use in biology and palaeontology, as a method of assessing the strength of load bearing biological structures like bones [151–153]. There are many different types of FEA, which can be distinguished by the type of element a shape is broken down into. The most common is the simplex (a triangle in 2D or a tetrahedron in 3D), but square elements can also be used [150, 154, 155]. Also, FEA in biological literature is often associated purely with stress analysis, but there are many other physical processes that it can model, including the dynamics of heat transfer and fluid modelling [150]. Here, I will utilise a custom, low computational cost 2D constant strain triangular FEA in order to assess the structural strength and rotational efficiency of a large array of 2D theoretical morphologies.

Each performance metric can be measured on each theoretical morphology within a theoretical morphospace, to create a set of performance landscapes. Performance landscapes are similar to adaptive landscapes, in that they measure the functional ability of different regions of morphospace, but they do not represent the combined adaptive value of a structure. In a hypothetical case where a structure only has to perform a singular function, the functional performance landscape can be considered an adaptive landscape. However, I do not know of any such cases identified in the literature, and I do not think it is controversial to assume that no such structure exists in nature. Instead, the adaptive performance of biological structures is usually balanced by trade-offs [156].

1.3.4 Adaptivity and optimality

Raw functional performance is therefore not a measure of fitness or adaptive value. As most mechanical functional performances are dependent on some aspect of shape, they are likely to be correlated, as shape acts as a moderator variable between their relationship. This means that, in many cases, increasing the performance of one function may lead to decreasing performance in another, and thus the structure lies in balance, not able to maximise the performance in either function. Thus, in building the adaptive landscape, this trade-off must be measured. Also, as a structure's biomechanical performance does not necessarily denote its total performance, it is important to note that when biomechanical performance surfaces are combined into a single biomechanical optimality metric, this does not equate to true fitness either. In cases where a structure performs a heavily mechanical role, it can at most be considered a close approximation of fitness.

Measuring optimality or approximating fitness within a trade-off is the final stage in the process of building an adaptive landscape. This task is deceptively complex and is loaded

with implicit assumptions. One method might be to sum the total performance from all the metrics used in the analysis. However, it is unlikely that all performances are tested in the same units, so first they must be normalized by their variance, and then converted into a measure of their contributive value to fitness [157–159]. This is achieved by weighting each functional metric with its relative contribution to fitness, allowing a sum to generate a total fitness value [85]. Weights can be generated for each individual empirical morphology, using maximum likelihood to minimise its distance to an optimal point (or highest peak) in the adaptive landscape. This results in the generation of a unique fitness landscape for each empirical morphology or set of empirical morphologies, while providing some information about the relative importance of each functional performance metric in that organism's life. For example, in turtles, it has been used to show the relative importance of shell strength, hydrodynamics and self-righting ability (ability to get back on all fours after falling) in aquatic and terrestrial turtles [120]. The drawbacks to this method are that many taxa cannot be compared on a single adaptive landscape, and evolutionary trajectories through that landscape cannot be observed, as the landscape is constantly changing. Finally, these is an assumption that empirical shapes lie as close to their weighted optima as possible. Therefore, this method has some limitations when testing whether function has a strong control over form.

Alternatively, rather than assuming individual taxa are optimised, we can make assumptions about the adaptivity of functional performance metrics in order to test whether individual taxa are optimised. In the case of the weighted fitness formula, this would mean assigning prior arbitrary weights to each functional performance metric. Alternatively, we can consider all possible weight combinations together, by assessing the Pareto front [85, 121]. When assessing a set of solutions to a problem, that each have a set of measured performances, there exists a subset of solutions that cannot be improved in any performance without decreasing the performance of another metric. This subset is the Pareto Optimal Subset (POS), and together makes the Pareto front.

In the case of theoretical morphology and function, the solutions represent each individual theoretical morphology. The Pareto optimal morphologies can be considered optimal across the breadth of possible performance weights, provided that they have consistent optimality 'directions'. That is, that increasing one performance metric while maintaining all other performance metrics either increases or decreases optimality in the sample and cannot be reversed in different cases. This may seem like a large assumption, but the key point is that all other metrics are equal. A jaw with high strength and low rotational efficiency is still optimal when compared with a jaw with low strength and high efficiency. A jaw with lower strength and efficiency than both of those structures is suboptimal. If a new jaw enters the subset with higher strength AND efficiency than the others is considered optimal, and the previously optimal structures can no longer be considered optimal. This concept can be taken further by ranking each solution [160]. In chapter 2 of this thesis, I will develop a Pareto optimal metric for developing Pareto optimality landscapes.

1.4 Empirical occupation of the adaptive landscape

Finally, once a landscape has been constructed, the occupation of such a landscape by empirical morphologies can be observed. In a perfectly adaptive scenario, empirical taxa will be constrained to the peaks of the adaptive landscape. Otherwise, there are multiple possible reasons why empirical points may not lie on the adaptive peaks. Firstly, when assessing the spread of empirical morphospace, there must be careful consideration of the underlying morphospace structure. Euclidean morphometric methods should maintain consistent shape change with changing distance in morphospace but are often high dimensional. If a landscape is constructed in 2D by using a theoretical grid, a large proportion of shape variation may be lost to higher PC axes, and empirical data points will be projected into different regions of morphospace than their actual position. Additionally, the alternative morphodynamic biases should be considered where possible. These biases can explain why empirical shapes cannot reach the optima, as they are restricted in their construction. I will briefly discuss some methodologies for assessing these morphological biases.

1.4.1 Lost morphological variation

I have already discussed the problems associated with building high dimensional theoretical morphospaces. One issue I have highlighted is that many of the decisions made in building theoretical morphospace are arbitrary, with no assessment of validity available. In chapter 2 of this thesis, I will attempt to do so by comparing the Euclidean distance of each empirical morphology to the PC1-PC2 plane with its optimality value. Studies have used some landscape similarity metrics to assess the required number of theoretical shapes [97], but very little has been achieved in assessing the accuracy or precision of an adaptive landscape. Even the terms 'accuracy' and 'precision' here are ill defined. I will define the accuracy of a landscape as the amount of error in interpolation of performance or optimality at each point in morphospace. The precision of a landscape is how closely the troughs and peaks of a constructed landscape align to the troughs and peaks of the 'true' landscape (figure 1.6). Note, by this definition, a precise landscape does not need to be accurate, as it can have high error in its absolute value while still maintaining a precise landscape shape. However, an accurate landscape must also be precise. If the precision and accuracy of a theoretical morphospace can be measured compared to a 'true' landscape in higher dimensional empirical morphospace, we can understand the limitations of the analysis on a case-by-case basis.

In chapter 4 of this thesis, I will attempt to test the accuracy and precision of the constructed performance landscapes. This will be achieved by testing the function of theoretical morphospace and empirical morphospace. Thus, the reconstructive ability of theoretical morphospace can be compared to the actual functional results of the empirical morphospace. By plotting functional results of the empirical morphologies against their reconstructed function in theoretical morphospace against one another, they should have a directly proportional relationship, unless the landscape has very poor precision. We can then measure the precision of the landscape with a linear regression and quote the R^2 and significance values to determine its validity. The accuracy can be measured by assessing the

goodness of fit of this data to the $y = x$ line (figure 1.6). As empirical morphospace lies in all dimensions of morphospace, this can be a measure of the effect that lost morphological variation has on the landscape output.

1.4.2 Phylogenetic bias in morphospace

Assessing the bias of phylogeny on morphology is difficult, but it has been well researched due to the value of morphological phylogenetics in understanding the tree of life [161]. Some studies have suggested the use of random walks in morphospace, which can be Brownian or informed by the adaptive landscape, to statistically test the occupation of morphospace in a phylogenetically informed manner [162]. One way to visualise the effect of evolutionary history on morphospace exploration is the phylomorphospace [163]. This structure is achieved by computing an Ancestral State Reconstruction (ASR) using the raw morphometric dataset and a phylogenetic tree with branch lengths, then projecting the nodes of the tree back into morphospace and connecting them with lines. Like the random walks, ASR can be neutral (Brownian motion model) or informed by the adaptive landscape (Ornstein-Uhlenbeck) [164–167]. The neutral Brownian motion model assumes no functional impact, and so provides a good null model of morphospace dynamics. The phylomorphospace alone is not necessarily an analytical tool; it provides a good visualization of how morphospace has been explored over macroevolutionary time. If the lines diverge and spread, we can easily see an evolutionary story of radiation and exploration of new morphologies. If the lines cross over and over, this shows that evolution has repeatedly converged on similar morphologies.

The phylomorphospace (figure 1.3) can provide interesting extra utility to the adaptive landscape. Note that, under the definition within this thesis, ancestral states can be considered theoretical morphologies. This allows us to reconstruct their function or even optimality, either by directly testing the shapes, or interpolating from their position in theoretical morphospace. This allows us to visualise how function and optimality have changed throughout the phylogenetic tree, which may provide insight into how optimality evolves over time, or how evolutionary transitions at certain nodes in the tree alter the evolution of optimality. This in turn allows the researcher to investigate questions about the strength of functional bias through time and within separate clades. Thus, the phylomorphospace is a powerful interrogative tool, and I will utilise it within this thesis. It is worth noting, however, that it provides little statistical assessment of phylogenetic bias on morphology.

Fortunately, many phylogeneticists have developed statistical methodology for untangling the phylogenetic signal within biological shape data [103, 168–170]. In this thesis, I will utilise these concepts to understand the strength of phylogenetic signals within my datasets. Put simply, if closely related taxa are more likely to share morphological features than more distantly related taxa, there is a strong phylogenetic signal in the dataset. Statistically, a number is put to this signal by comparing the pairwise morphological distance matrix with the phylogenetic distance matrices. There is a hidden tautological trap within this. If the tree is built using the same morphological data as the morphological analysis, then the result will be biased towards higher phylogenetic signal ("these two

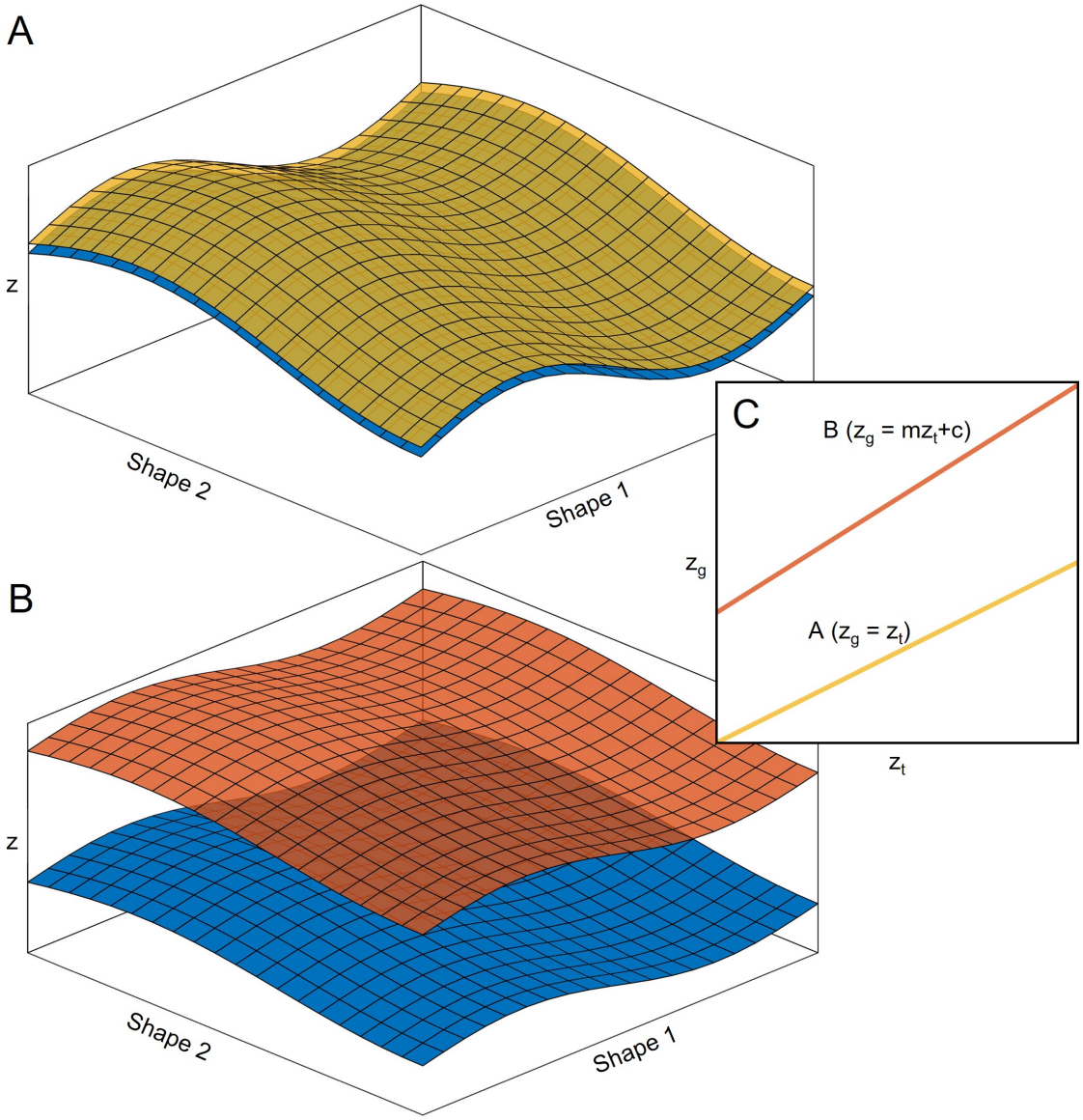

Figure 1.6: Testing the accuracy and precision of landscapes. (A) An accurate generated landscape (yellow) matches the true landscape (blue) well, where the value at each point on the generated landscape is equal to the equivalent point on the generated landscape. **(B)** A precise generated landscape (orange) does not have the same exact value as the true landscape (blue), but it has the same shape and the contours of each landscape match in morphospace. In the majority of studies interested in generating adaptive landscapes, accuracy is not necessary, but precision is. **(C)** The accuracy and precision of a generated landscape can be tested by plotting a sample from the true landscape (z_t) against its interpolated value on the generated landscape (z_g). An accurate landscape will fit tightly to the $y = x$ line, whereas a precise landscape will fit tightly to any monotonic function (here, it is tested against a linear function). z_g can be calculated empirically from emprical morphologies.

taxa share a recent common ancestor due to their similar jaw shape. Our tree shows that closely related taxa are more likely to share similar jaw shapes. Therefore, there is a high phylogenetic signal to jaw shape"). To minimise this bias, I will use trees published separately within the literature from my data, preferring molecular trees where possible.

1.4.3 Morphogenetic bias in morphospace

Morphogenetic bias is much more difficult to investigate. Usually, there is a requirement for morphological data throughout the development process. These can be plotted as a trajectory through morphospace. The distance in morphospace travelled through an organism's life history can then be measured, and compared with the adult morphological distances between taxa [171–174]. If this ontogenetic change is relatively large compared to the interspecific distance, we might expect morphogenetic bias to be a relatively weak control of form.

Ontogenetic data is not often present in the fossil record, however. An alternative route to understanding this bias in certain structures is to use developmentally informed morphometrics. Earlier, I wrote about the presence of logarithmic spirals in nature. By mapping the shapes of many 'pointed' biological structures (teeth, claws, horns and thorns, to name a few examples) to this developmentally informed formula, we can characterize shape in such a way in which morphometric distances can be considered morphogenetic distances [62, 64, 175–177]. These can be used to generate developmentally informed morphospaces, which can either be compared to developmentally naive morphospaces to measure morphogenetic bias or paired with phylogenetic and functional analyses to remove morphogenetic bias [178].

Finally, recent developments in the statistical analysis of developmental modules can provide further insight into morphogenetic bias. When measuring the morphology of a variety of morphological structures, the strength of covariance between these structures can be used to identify two things: 1) the number of modules within the dataset, and which morphological structures each module contains; 2) the strength of covariance within and between modules, which can in turn show which modules have stronger morphogenetic biases over one another [66, 67, 179–182]. Such analyses have shown generally high integration between the bones of many different vertebrates [74, 183–190].

1.5 Thesis overview

Investigating the functional controls of morphological macroevolution is critical in systematic biology, especially on large evolutionary scales. Identifying features of organisms that are functionally optimised may allow for more reliable ecological inference in palaeoecology, or provide more informed biomimetic practices [47, 85]. Further, it may inform researchers on whether to include or omit a morphological feature in morphological phylogenetics [161, 191]. Adaptivity, function and optimality have been assessed via the adaptive landscape within certain biological groups and structures in order to understand aspects of their ecomorphology. However, there is usually an implicit assumption that morphology is optimised, rather than an investigation of the optimality of morphology. Further, the performance surfaces used are often highly specific to certain morphologies that limit

comparison across broad macroevolutionary timescales. How does function limit and control the evolution of form in large taxonomic clades and long evolutionary timescales? How can we test this? Following this introduction, this thesis will consist of four separate analytical study chapters, and a final discussion chapter. Each will focus on a different case study in the evolution of form and apply the morphodynamical concepts I have discussed in this introduction. They will all be united in their attempts to assess the functional controls on form on large macroevolutionary timescales, while also providing new and alternative computational techniques in assessing the form function relationship.

1.5.1 Chapter 2:

Chapter 2 is an assessment of the shape and function of vertebrate jaws at their origin in the fossil record. The vertebrate jaw is a model study system for questions relating to form and function, as I have previously discussed. The origin of the jaw remains a mystery in terms of its functional evolution: when did vertebrate jaws develop a feeding function? This question has connections to deeper questions about the nature of functional evolution – can structures rapidly switch functions to explore new regions of morphospace, or do they experience a gradualistic change in functionality over time? In the case of the latter, how long does this take? Therefore, there are many interesting questions to ask of the earliest jaws in the fossil record, not least because jawed vertebrates make up the majority of vertebrates in evolutionary history, corroborating the view that the jaw is an extremely critical structure in the success of an organism.

This chapter introduces the custom code pipeline that I have spent much of my PhD developing. This MATLAB package, which I have called theofun (short for theoretical function), is built to facilitate optimality landscape generation for 2D morphometric data. It measures and generates a morphometric sample automatically from a sample of prepared image data. The package includes the methodology for creating and analysing large numbers of FEA models at relatively low computer effort. The chapter describes and utilises the Rotational Efficiency (RE) performance metric, defined as the speed of the tip of a jaw given one unit of rotational kinetic energy about its joint. Finally, the Pareto rank ratio metric is described, an algorithm developed from Goldberg Pareto ranking, to generate optimality values for a set of theoretical morphologies with multiple performance metrics.

1.5.2 Chapter 3:

In the third chapter of this thesis I will utilise the theofun package to assess the variety of jaw morphology during the terrestrialisation of tetrapods in the late Palaeozoic. While this period is defined by the extreme environmental change that these taxa underwent, and this change has marked effects on feeding function, very little change in jaw shape occurs until much later than the original colonisation of the land. This is surprising, but can be understood via optimality. This study measures the strength and rotational efficiency of theoretical morphospace, alongside the jaw height as a proxy for hydrodynamic performance. Together, these are combined into a single optimality metric, as Pareto optimality can combine any arbotrary number of functional performances. Although

the particular functional demands shift with changing ecology, the optimality within the trade-off between shape dependent functional performance remains the same.

1.5.3 Chapter 4:

The fourth chapter of this thesis builds on the methodology from the previous, utilising the theofun package once again. It will be applied to a much larger 2D jaw image dataset of extinct and extant mammals and closely related non-mammalian therapsids. The spread of taxa captures the transition from a lower jaw comprised of many different bones in extinct therapsids to the modern mammalian condition where the jaw is made up of just the dentary bone. There are also multiple key transitions in the dataset, from terrestrial to marine environments, and even the development of flight in bats, which may affect the selective pressures and thus the strength of functional bias on form in the dataset. A recent molecular phylogeny from the literature is employed to assess the evolution of jaw optimality through time.

I will also assess the complexity of shape in this study, as it is not known whether the reduction of complexity of parts in the mammal jaw also coincides with a reduction in shape complexity, and the link between complexity and optimality is not well understood. This may provide critical information in understanding how complexity evolves in natural systems. The complexity of theoretical morphs is assessed, allowing the generation of a complexity landscape as well as on adaptive landscape. Finally, the accuracy and precision of landscapes generated is measured via the relationship between measured and interpolated empirical function (figure 1.6) This is used to assess the power of two different theoretical morphospaces – a 2D grid theoretical morphospace, and a ND random point cloud morphospace.

1.5.4 Chapter 5:

The final analytical chapter will focus on 3D morphology and adapting EFA and theoretical morphospace construction to fit an entirely different vertebrate structure – the humeral bone shaft of modern birds. Limb bones are often input to morphometric analysis, as they can provide information about locomotor behaviour. However, assessing the shape of the bone usually involves landmarking the proximal and distal end morphologies, where it is easy to find Type I and II landmarks to place. This misses the variance in internal and external morphology in the shaft, which defines the resistance to bending and buckling of the structure. This in turn has important functional roles in supporting the mass of an organism, and in the case of birds, it is often critical to the performance of powered flight. The shapes of an empirical set of humeral shafts is measured, and a theoretical morphospace generated. This allows the measurement of the relationship between 3D morphology and locomotor ecology, as well as the creation of an adaptive landscape, to investigate whether the limb shaft morphology is related to ecology and whether this is due to functional constraint.

Most importantly, this chapter will provide the mathematical and algorithmic basis for systematically measuring 3D internal and external bone shaft morphology, in any bone. Due to the lack of homology, this is a difficult task. There is also an issue with the axis of

the bone, which is regularly twisted or bowed. I will describe an algorithm for measuring the bone axis, and automatically slicing 3D .stl and .ply objects such that a set of cross sections at regular intervals of a curved bone axis can be measured. Such structures will be entirely reconstructable from their position in morphospace, allowing the generation of theoretical morphospaces. In future, this algorithm will be adaptable to a variety of biological 'tubes', such as shells and teeth, both as a means of generating shape data and characterising morphology.

Chapter 2

Increasing morphological disparity and decreasing optimality for jaw speed and strength during the radiation of jawed vertebrates

Author's contribution This chapter has been published in its entirety [192]:

Deakin W.J., Anderson P.S.L., den Boer W., Smith T.J., Hill J.J., Rücklin M., Donoghue P.C.J., Rayfield E.J. "Increasing morphological disparity and decreasing optimality for jaw speed and strength during the radiation of jawed vertebrates". In: *Science Advances* 8.11 (2022).

W.J.D., P.C.J.D., and E.J.R. designed the study, interpreted the results, and drafted the manuscript, to which all authors contributed. **W.J.D.** and T.J.S. wrote the MATLAB code and performed analyses. **W.J.D.** and P.S.L.A. collected the image data.

Abstract

The Siluro-Devonian adaptive radiation of jawed vertebrates, which underpins almost all living vertebrate biodiversity, is characterized by the evolutionary innovation of the lower jaw. Multiple lines of evidence have suggested that the jaw evolved from a rostral gill arch, but when the jaw took on a feeding function remains unclear. We quantified the variety of form in the earliest jaws in the fossil record from which we generated a theoretical morphospace that we then tested for functional optimality. By drawing comparisons with the real jaw data and reconstructed jaw morphologies from phylogenetically inferred ancestors, our results show that the earliest jaw shapes were optimized for fast closure and stress resistance, inferring a predatory feeding function. Jaw shapes became less optimal for these functions during the later radiation of jawed vertebrates. Thus, the evolution of jaw morphology has continually explored previously unoccupied morphospace and accumulated disparity through time, laying the foundation for diverse feeding strategies and the success of jawed vertebrates.

2.1 Introduction

Almost all living vertebrates are jawed vertebrates [193]. The origin and early evolution of jaws is among the most formative of events in vertebrate evolutionary history, precipitating profound changes in predator-prey relationships and the foundations of extant vertebrate biodiversity [193, 194]. Many biomechanically novel feeding behaviors were established early in the evolution of jawed vertebrates, including complex linkage systems and high stress mitigation for durophagy and processing armored prey [195–197], all of which have contributed to the ecological success of vertebrates [193]. The tempo and mode of this evolutionary episode remains poorly characterized, but those few studies that have investigated jaw functional disparity have perceived stasis throughout much of the initial gnathostome radiation [198, 199], apparently contradicting the traditional view that gnathostome diversification was predicated on the innovation and broad ecological utility of the jaw. Here, we use an analytical approach to investigate this apparent limit on the evolution of the jaw via characterizing the range of theoretical forms accessible to early gnathostomes. We assess the functional capability of these theoretical gnathostome jaw shapes, testing which shapes are optimal for stress resistance, speed of closure, or a trade-off between these two traits. Following this, we document the temporal distribution of empirical jaw morphologies and those of inferred ancestors within theoretical morphospace to test whether gnathostome jaws were constrained by functional optimality during their early evolution. We evaluate the empirical record of jaw evolution in early jawed vertebrates within this functional context.

We characterized the mandibular morphology of 121 early gnathostomes (late Silurian to the end Devonian; 427 to 359 million years (Ma) through Elliptical Fourier Analysis (EFA) [112] of Two-Dimensional (2D) lateral images. We then generated a theoretical morphospace of mandible morphologies representing the tangent space of empirical shapes [87, 114, 125]. We used functional testing to establish how strength and Rotational Efficiency (RE) vary through theoretical shape space, as these metrics are critical to feeding function; speed of jaw closure has been implicated in capture of fast-moving prey, while jaw strength has been linked to bite ability and the procurement of harder foodstuffs [137, 200]. The two traits may trade-off due to the lever-like nature of the vertebrate jaw typically considered to generate fast versus forceful closure, although similar output metrics can be reached via different morphologies [e.g., [148]]. This allowed us to establish an adaptive landscape within the theoretical morphospace, as has been effective in previous studies constructing performance surfaces and adaptive landscapes [85, 119–121, 137, 201]. However, our adaptive landscape is constructed differently to those studies that fit models to performance data. Instead, we use a Pareto ranking approach (see Methods) that highlights optimal morphologies without using fitness functions weighted toward particular ecologies or groups [157, 159], providing a general picture of optimality among extinct taxa, where survival data [96] are unavailable and ecological data are incomplete (see figure 2.1 for an overview of methods). Pareto concepts have been used before in the interpretation of morphospace and adaptive landscapes; however, the construction of adaptive landscapes within a Pareto framework has not been previously used [85, 120, 121, 123, 201].

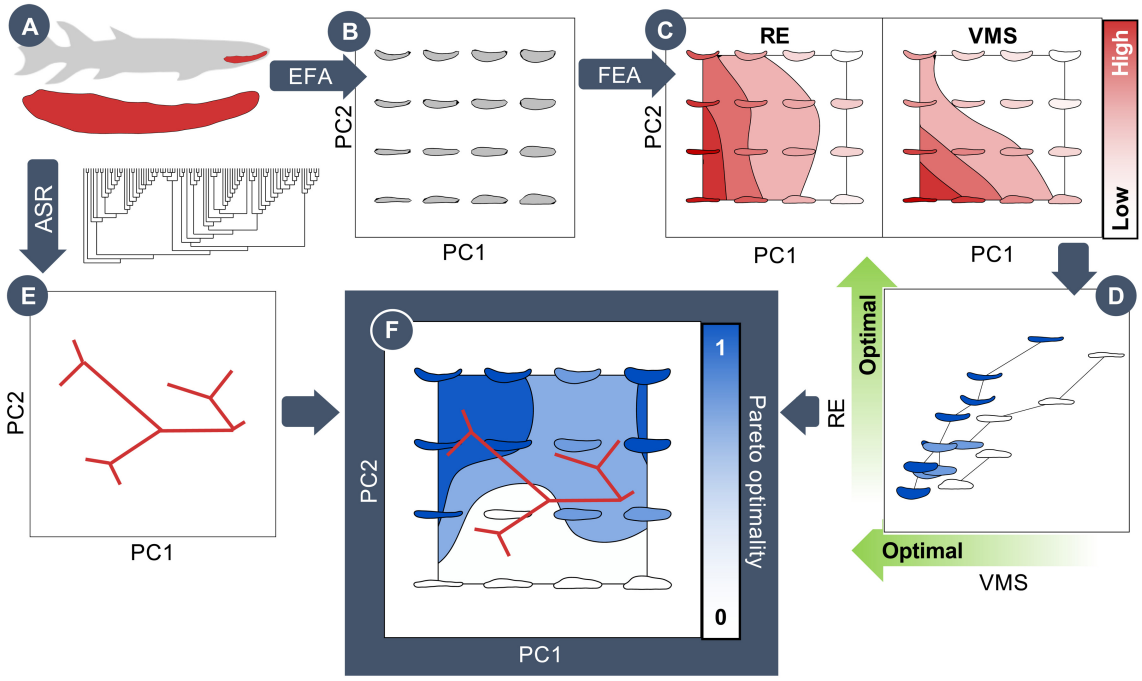

Figure 2.1: Example pipeline for adaptive landscape generation using Pareto methods. **(A)** Lateral images of 121 gnathostome jaws were collected and characterized via EFA. **(B)** EFA results were input to a PCA to build a theoretical morphospace of evenly spaced theoretical jaw shapes. **(C)** Each theoretical shape is tested 1000 times with random input constraints using finite element analysis (FEA) to assess their functional performance in RE and VMS. **(D)** Each shape was plotted in performance space with its individual performance metrics. These shapes are then ranked using a Pareto system, with the assumption that lower VMS (higher strength) is optimal and that higher RE (higher speed and efficiency) is optimal. **(E)** Ancestral state reconstruction (ASR) is used with EFA data and a timed phylogeny to construct a phylomorphospace. **(F)** The Pareto rank from the performance space is used to construct an adaptive landscape, and the evolution of taxa within this adaptive landscape is observed via the phylomorphospace.

Our metric of optimality refers to functional optimality, not true "fitness," which is much more complex. Using a phylomorphospace approach in which we model the mandibular shapes for the ancestors of the earliest known jawed vertebrates, we characterized the phylogenetic exploration of this adaptive landscape, demonstrating that the earliest mandibles exhibited morphologies that were optimal for strength and RE. Furthermore, far from plateauing, early jawed vertebrates explored an increasing range of jaw morphospace that tracked optimal adaptive regions early in their evolution. However, subsequent sarcopterygian evolution is characterized by a shift toward less optimal regions of morphospace, perhaps reflecting a shift away from the functional drivers that characterize the initial gnathostome radiation or that functional constraints weaken over time, becoming less restrictive in the evolution of jaw form.

2.2 Methods

2.2.1 Dataset

Our dataset consists of lower jaw shapes of 121 extinct gnathostome taxa ranging in age from the late Silurian to the end of the Devonian. Data were time binned, using age data sourced from the literature and the Paleobiology Database, to each of the Devonian stages, while Silurian taxa were grouped into one time bin representing the late Silurian due to the low data availability. Taxa that existed in more than one bin were ranged through and counted in all intermediate time bins. The dataset was also split into four clades: Sarcopterygii ($N = 57$), Placodermi ($N = 48$), Chondrichthyes (including acanthodians) ($N = 8$), and Actinopterygii ($N = 8$). Images of lower jaws were sourced from the literature using photographs of lateral shape, reconstructions, and, where available, computed tomography scans. The lateral 2D shape of the jaw was chosen because of its prevalence in the fossil record, in figures within journal articles and books, and its previous use in the literature as a model for functional processes [141, 197–199, 202] due to many jaw shapes approximating a 2D planar shape. However, it is noted that the jaw shape in these taxa does have some Three-Dimensional (3D) variation, and this will affect disparity and functional metrics [138].

Index	Genus	FAD	LAD	Clade	Image Type	Source
1	*Acanthostega*	Fras.	Fam.	Sarc.	Reconstruction	[203]
2	*Achoania*	Loch.	Loch.	Sarc.	Photograph	[204]
3	*Adololopas*	Fras.	Fras.	Sarc.	Photograph	[205]
4	*Angarichthys*	Eif.	Giv.	Plac.	Photograph	[206]
5	*Arquatichthys*	Prag.	Prag.	Sarc.	Drawing	[207]
6	*Atopacanthus*	Giv.	Giv.	Chon.	Photograph	[208]
7	*Barwickia*	Giv.	Fras.	Sarc.	Reconstruction	[209]
8	*Bothriolepis*	Fras.	Fam.	Plac.	μCT scan	[210]
9	*Brachydeirus*	Fras.	Fras.	Plac.	Photograph	NHM: 53180
10	*Brachyosteus*	Fras.	Fras.	Plac.	Reconstruction	[211]
11	*Brontichthys*	Fam.	Fam.	Plac.	Photograph	CMNH: 7575
12	*Bullerichthys*	Fras.	Fras.	Plac.	Photograph	WAM: 869703
13	*Bungartius*	Fam.	Fam.	Plac.	Drawing	[212]
14	*Camuropiscis*	Fras.	Fras.	Plac.	Photograph	[197]
15	*Cathlorhynchus*	Loch.	Eif.	Sarc.	Photograph	[213]
16	*Cavanosteus*	Ems.	Ems.	Plac.	Photograph	ANU: V77
17	*Cheiracanthus*	Eif.	Giv.	Chon.	Photograph	UCMZ: 1132
18	*Cheirolepis*	Ems.	Fras.	Acti.	Photograph	MNB: 5112
19	*Chirodipterus*	Fras.	Fras.	Sarc.	Photograph	MNB: 12875a
20	*Cladoselache*	Fam.	Fam.	Chon.	Drawing	[214]
21	*Coccosteus*	Eif.	Giv.	Plac.	Photograph	[215]
22	*Compagopiscis*	Fras.	Fras.	Plac.	μCT Scan	[210]
23	*Copanognathus*	Fras.	Fras.	Plac.	Drawing	[216]
24	*Denisonodus*	Fras.	Fras.	Plac.	Photograph	[217]
25	*Densignathus*	Fam.	Fam.	Sarc.	Reconstruction	[218]

26	*Diabolepis*	Loch.	Loch.	Sarc.	Photograph	[219]
27	*Diplocercides*	Giv.	Fras.	Sarc.	Reconstruction	[220]
28	*Diplognathus*	Fam.	Fam.	Plac.	Reconstruction	[211]
29	*Dipnorhynchus*	Ems.	Ems.	Sarc.	Photograph	NHM: 46773
30	*Dipterus*	Fam.	Fam.	Sarc.	Photograph	NHM: P34552
31	*Donnrosenia*	Giv.	Giv.	Acti.	Photograph	[221]
32	*Dunkleosteus*	Fam.	Fam.	Plac.	Photograph	[197]
33	*Eastmanosteus*	Giv.	Fam.	Plac.	Photograph	[197]
34	*Edenopteron*	Fam.	Fam.	Sarc.	Reconstruction	[222]
35	*Elginerpeton*	Fras.	Fras.	Sarc.	Reconstruction	[203]
36	*Enseosteus*	Fras.	Fras.	Plac.	Photograph	MNB: 18318
37	*Erromenosteus*	Fras.	Fras.	Plac.	Photograph	MNB: 139
38	*Eusthenopteron*	Giv.	Fam.	Sarc.	Reconstruction	[223]
39	*Fallacosteus*	Fras.	Fras.	Plac.	Photograph	[197]
40	*Gavinia*	Eif.	Giv.	Sarc.	Reconstruction	[224]
41	*Gogonasus*	Fras.	Fras.	Sarc.	Photograph	[225]
42	*Gogosardina*	Fras.	Fras.	Acti.	Photograph	[226]
43	*Gorgonichthys*	Fam.	Fam.	Plac.	Photograph	[197]
44	*Griphognathus*	Fras.	Fras.	Sarc.	Photograph	ANU: 21186
45	*Guiyu*	Sil.	Sil.	Sarc.	Photograph	[227]
46	*Gymnotrachelus*	Fam.	Fam.	Plac.	Photograph	CMNH: 8051
47	*Hadrosteus*	Fras.	Fras.	Plac.	Reconstruction	[211]
48	*Harrytoombsia*	Fras.	Fras.	Plac.	Photograph	WAM: 704254
49	*Heintzichthys*	Fras.	Fam.	Plac.	Photograph	[228]
50	*Holodipterus*	Fras.	Fras.	Sarc.	Reconstruction	[220]
51	*Holodus*	Fras.	Fras.	Sarc.	Drawing	[229]
52	*Holoptychius*	Giv.	Fam.	Sarc.	Photograph	[230]
53	*Homostius*	Ems.	Giv.	Plac.	Photograph	[231]
54	*Howidipterus*	Fras.	Fras.	Sarc.	Reconstruction	[209]
55	*Howittacanthus*	Giv.	Giv.	Chon.	Drawing	[232]
56	*Howqualepis*	Giv.	Giv.	Acti.	Drawing	[233]
57	*Hussakofia*	Fam.	Fam.	Plac.	Photograph	CMNH: 8082
58	*Hyneria*	Fam.	Fam.	Sarc.	Drawing	[234]
59	*Ichthyostega*	Fam.	Fam.	Sarc.	Reconstruction	[203]
60	*Incisoscutum*	Fras.	Fras.	Plac.	Photograph	[228]
61	*Ishnacanthus*	Sil.	Eif.	Chon.	Photograph	[235]
62	*Jarvikina*	Giv.	Fam.	Sarc.	Photograph	[236]
63	*Kendrichthys*	Fras.	Fras.	Plac.	Photograph	NHM: P51143
64	*Kenichthys*	Ems.	Ems.	Sarc.	Reconstruction	[204]
65	*Kimbryanodus*	Fras.	Fras.	Plac.	Photograph	[237]
66	*Laccognathus*	Giv.	Fras.	Sarc.	Photograph	[238]
67	*Lactocamurus*	Fras.	Fras.	Plac.	Photograph	[197]
68	*Latvius*	Giv.	Fras.	Sarc.	Reconstruction	MNB: f551
69	*Leptosteus*	Fras.	Fras.	Plac.	Photograph	MNB: 12709
70	*Malerosteus*	Fras.	Fras.	Plac.	Photograph	[239]
71	*Materpiscis*	Fras.	Fras.	Plac.	Drawing	[240]
72	*Meemannia*	Loch.	Loch.	Acti.	Drawing	[241]
73	*Megamastax*	Sil.	Sil.	Sarc.	Photograph	[242]

74	*Metaxygnathus*	Fam.	Fam.	Sarc.	Reconstruction	[203]
75	*Microsteus*	Fras.	Fras.	Plac.	Photograph	MNB: 18324
76	*Miguashaia*	Giv.	Fras.	Sarc.	Reconstruction	[243]
77	*Mimia*	Fras.	Fras.	Acti.	Reconstruction	[204]
78	*Moythomasia*	Giv.	Fam.	Acti.	Drawing	NHM: P53221
79	*Mylostoma*	Fam.	Fam.	Plac.	Photograph	CMNH: 7706
80	*Nesides*	Fras.	Fras.	Sarc.	Reconstruction	[224]
81	*Onychodus*	Ems.	Fam.	Sarc.	Reconstruction	[224]
82	*Orlovichthys*	Fam.	Fam.	Sarc.	Drawing	[244]
83	*Osteolepis*	Eif.	Giv.	Sarc.	Photograph	UCMZ: GN769
84	*Oxyosteus*	Fras.	Fras.	Plac.	Photograph	MNB: 296
85	*Pachyosteus*	Fras.	Fam.	Plac.	Photograph	MNB: 389
86	*Paledaphus*	Fras.	Fam.	Sarc.	Photograph	AMNH: 6560
87	*Panderichthys*	Giv.	Fras.	Sarc.	Drawing	[203]
88	*Pholidosteus*	Fras.	Fras.	Plac.	Photograph	MNB: 12797
89	*Pillararhynchus*	Fras.	Fras.	Sarc.	Photograph	[245]
90	*Platycephalichthys*	Fras.	Fras.	Sarc.	Reconstruction	[199]
91	*Plourdosteus*	Giv.	Fras.	Plac.	Photograph	[246]
92	*Porolepis*	Loch.	Prag.	Sarc.	Photograph	[247]
93	*Powichthys*	Loch.	Loch.	Sarc.	Reconstruction	[248]
94	*Promesacanthus*	Loch.	Loch.	Chon.	Drawing	[249]
95	*Protogonacanthus*	Fras.	Fam.	Chon.	Reconstruction	[250]
96	*Psarolepis*	Sil.	Loch.	Sarc.	Photograph	[204]
97	*Ptyctodus*	Eif.	Fam.	Plac.	Photograph	[216]
98	*Rhinodipterus*	Fras.	Fam.	Sarc.	Photograph	[245]
99	*Rhinosteus*	Fras.	Fras.	Plac.	Reconstruction	[211]
100	*Robinsondipterus*	Fras.	Fras.	Sarc.	Photograph	WAM: 011003
101	*Rolfosteus*	Fras.	Fras.	Plac.	Photograph	NHM: P50971
102	*Selenosteus*	Fras.	Fam.	Plac.	Photograph	CMNH: 8086
103	*Serenichthys*	Fam.	Fam.	Sarc.	Reconstruction	[251]
104	*Soederberghia*	Fras.	Fam.	Sarc.	Reconstruction	[220]
105	*Speonesydrion*	Prag.	Prag.	Sarc.	Photograph	ANU: 35647
106	*Spodichthys*	Fras.	Fras.	Sarc.	μCT Scan	[252]
107	*Stenognathus*	Fras.	Fras.	Plac.	Drawing	[216]
108	*Stenosteus*	Fras.	Fam.	Plac.	Photograph	CMNH: 8044
109	*Strunius*	Giv.	Fam.	Sarc.	Photograph	MNB: 161b
110	*Styloichthys*	Loch.	Loch.	Sarc.	Photograph	[204]
111	*Tegeolepis*	Fras.	Fam.	Acti.	Photograph	NHM: P45312
112	*Tiktaalik*	Fras.	Fras.	Sarc.	Photograph	[253]
113	*Titanichthys*	Fam.	Fam.	Plac.	Photograph	[254]
114	*Torosteus*	Fras.	Fras.	Plac.	Photograph	WAM: 8863
115	*Tungsenia*	Prag.	Prag.	Sarc.	Reconstruction	[255]
116	*Uranolophus*	Prag.	Eif.	Sarc.	Photograph	FMNH: PF3874
117	*Ventastega*	Fam.	Fam.	Sarc.	Drawing	[203]
118	*Watsonosteus*	Eif.	Giv.	Plac.	Drawing	[256]
119	*Xylacanthus*	Sil.	Prag.	Chon.	Photograph	[257]
120	*Ymeria*	Fras.	Fam.	Sarc.	Reconstruction	[258]
121	*Youngolepis*	Loch.	Prag.	Sarc.	Reconstruction	[204]

Table 2.1: Early gnathostome jaw image dataset. Abbreviations: First Appearance Date (FAD), Last Appearance Date (LAD), Silurian (Sil.), Lochkovian (Loch.), Pragian (Prag.), Emsian (Ems.), Eifelian (Eif.), Givetian (Giv.), Frasnian (Fras.), Famennian (Fam.), Sarcopterygii (Sarc.), Chondrichthyes and acanthodians (Chon.), Placodermi (Plac.), Actinopterygii (Acti.), Natural History Museum, London, UK (NHM), Museum für Naturkunde, Berlin, Germany (MNB), Cleveland Museum of Natural History, Cleveland, OH, USA (CMNH), Western Australian Museum, Perth, Australia (WAM), Australian National University, Canberra, Australia (ANU), University of Cambridge Museum of Zoology, Cambridge, UK (UCMZ), The Field Museum, Chicago, IL, USA (FMNH) and American Museum of Natural History, New York, NY, USA (AMNH).

2.2.2 Shape analysis

A further advantage to analyzing 2D jaw shape is that 2D filled polygons (such as the lateral jaw silhouette) can be characterized with zero converging error by curves with distinct functions, output from Fourier deconstructions [114, 259]. Specifically, EFA was the chosen method for morphometrics due to its shape characterization and reconstruction ability [112, 114, 260, 261]. Sensitivity tests of input outline data informed a decision to characterize the data with 600 outline landmarks, from which 12 EFA harmonics were generated. Six hundred were chosen, as it was the maximum number possible across all image files, and it was considerably beyond the point of convergence determined by a test of the EFA sensitivity to landmark number. Size and rotation variation of each curve was eliminated [112], with the goal of characterizing the jaw shape alone. This resulted in a dataset of 45 continuous characters ($4 \times 12 - 3$). From these data, a Principal Component Analysis (PCA) was used to build a morphospace of maximum variation [114] within empirical shape data (figure 2.2).

The empirical 2D shapes are generated via a mathematical formula that plots elliptic harmonics. Changing the input parameters of this formula generates a proportional change in 2D shape. We exploited this process to generate a grid of parameterized theoretical jaw shapes (figure 2.3). We produced a 23-by-21 grid of 483 of evenly spaced theoretical jaw shapes, which was plotted across the Principal Component (PC) 1-PC2 morphospace. These 483 jaws were designed to cover the space occupied by empirical data plus an extended border range of 20% to infer the patterns at the extremes of unoccupied morphospace. Of these 483 meshes, 53 self-intersecting loops were omitted from any functional analysis, leaving 430 testable meshes. Self-intersection is an ostensibly impossible feature of any 3D structure in 2D lateral view; thus, these regions were defined as a geometrically impossible space [118, 125].

2.2.3 Phylogeny

The phylogenetic tree used in all analyses was an informal supertree assembled from a multitude of literature sources (figure 2.4) [221, 227, 262–278]. The tree included 99 of the 121 taxa from the analysis that could be found in phylogenies from the literature and was dated using the "equal" method of the function bin_timePaleoPhy in the R package

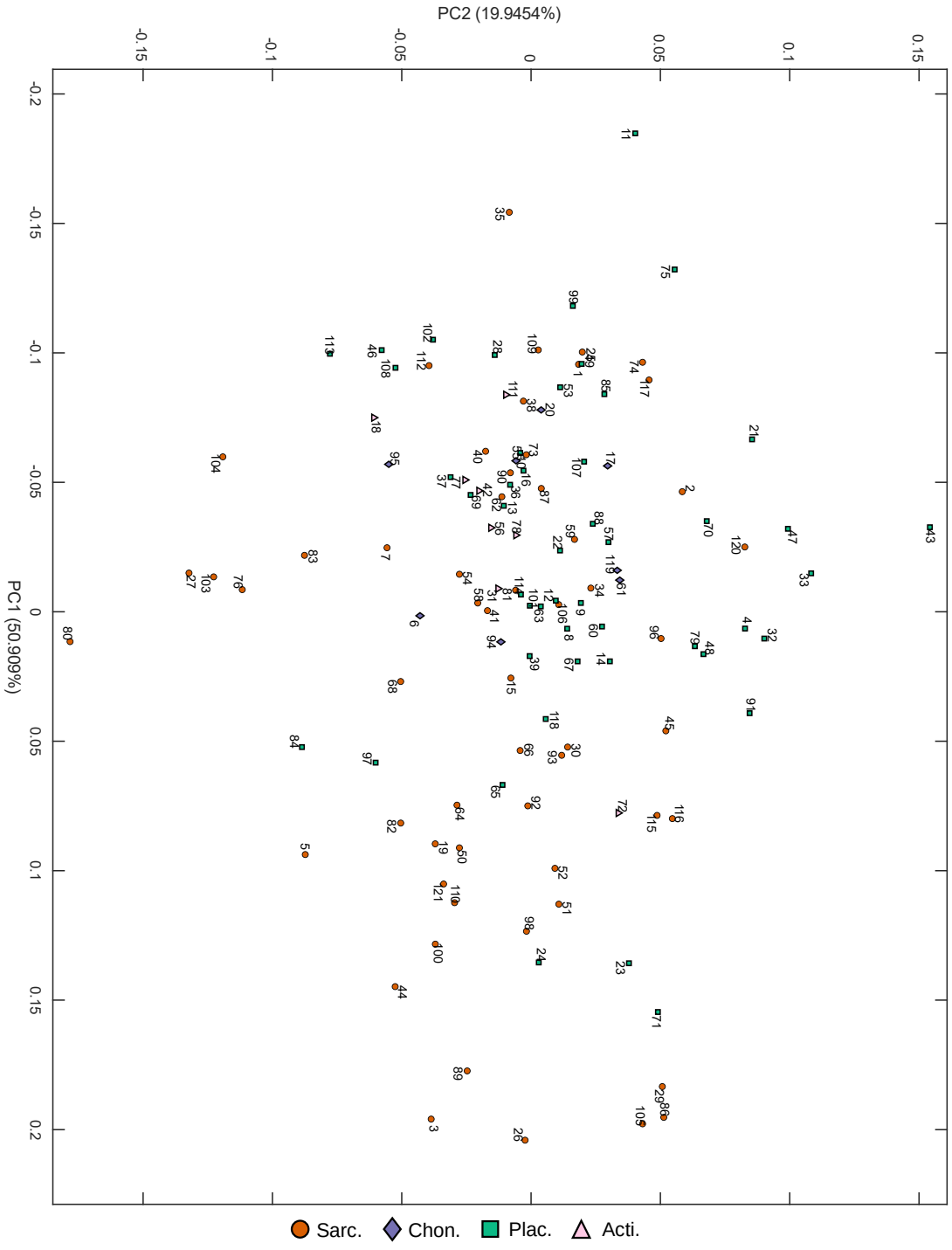

Figure 2.2: Empirical morphospace. Empirical morphospace is built from a Principal Component Analysis (PCA) of Elliptical Fourier Analysis (EFA) shape data. Coloured symbols represent individual taxa, with numbered labels referring to their index in table 2.1.

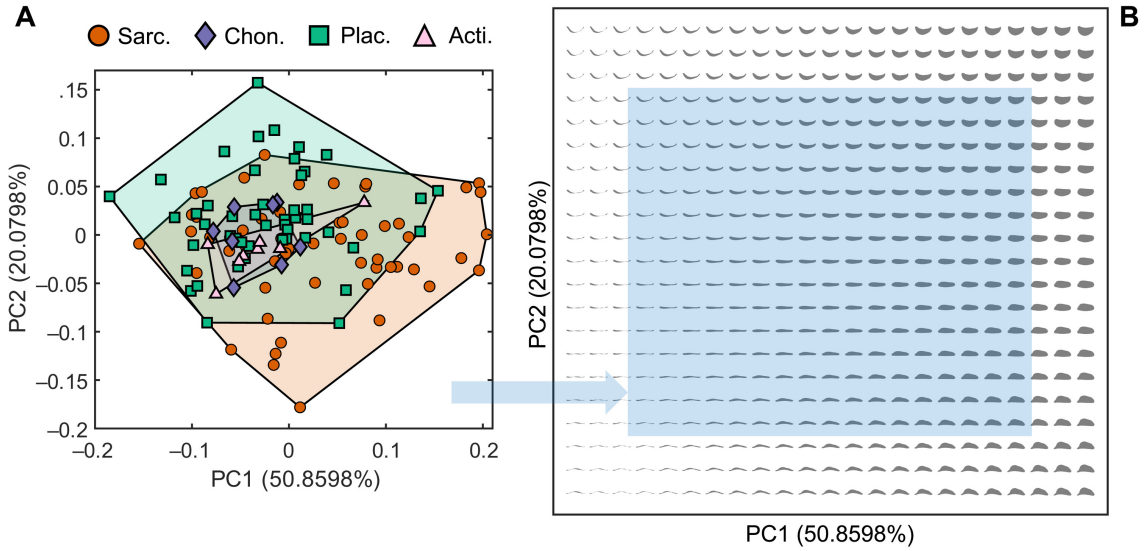

Figure 2.3: Empirical and theoretical morphospace. Theoretical morphospace **(B)** is built by extending the limits of empirical morphospace **(A)** and calculating the shape data at each point in a regular 23-by-21 grid. Legend shows symbols and colors for individual taxa from four clades: Sarcopterygii (Sarc.), Chondrichthyes and acanthodians (Chon.), Placodermi (Plac.), and Actinopterygii (Acti.). Blue area in theoretical morphospace represents the extent of empirical morphospace.

paleotree [279]. The R package geomorph was used to assess the phylogenetic signal of the data and perform maximum likelihood ancestral state reconstruction (functions physignal and gm.prcomp) [280]. These functions were used due to their applicability to coordinate data, matching the EFA output data. Each axis of each elliptical harmonic was considered as a single 2D coordinate. Ancestral states were not included in the EFA to build the morphospace; instead, they were transformed into the co-ordinate space using the PC coefficients. All R analyses were performed with R v.3.6.1.

2.2.4 Functional analysis

Each of the 483 theoretical jaws was converted into meshes of 2500 triangular elements. A sensitivity test performed on 10 meshes incremented by 500 elements showed that, at 1000 random replications, a mesh density of 2500 elements was adequate for convergence in both functional metrics. We calculated RE, defined as the velocity of the tip of the jaw when rotating about the jaw hinge given one unit of energy. RE can be considered a proxy for jaw closure speed. The RE was thus calculated for each theoretical shape as the velocity of the bite point (v) given a rotational energy of 1 Joule, where:

$$v = L\sqrt{\frac{2}{I}}$$

where L is the length of the distance between bite point and the rotational axis (jaw hinge) and I is the moment of inertia at the bite point, where I can be calculated with discrete finite elements using this formula [197]:

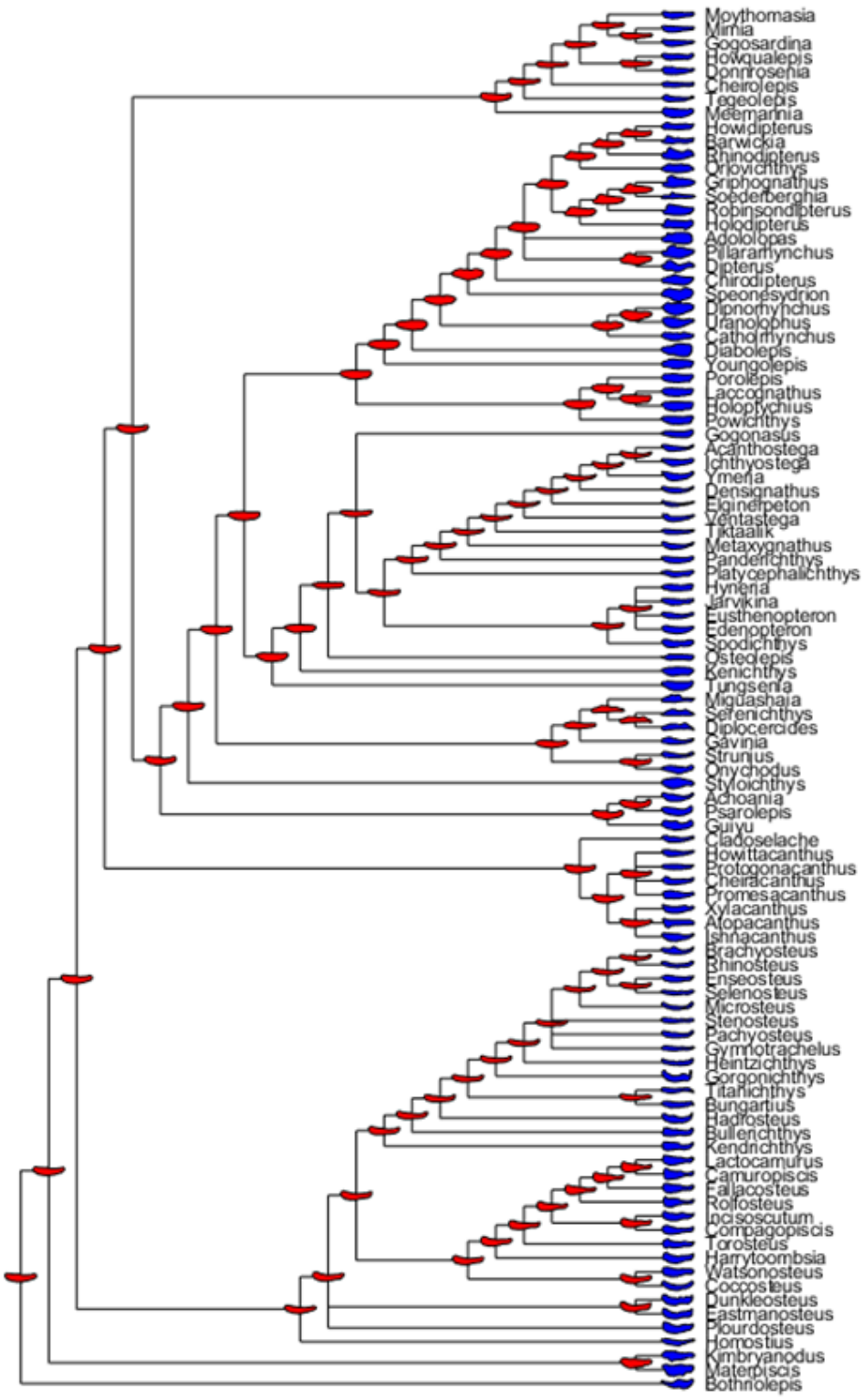

Figure 2.4: Morphological evolution of the jaw through the early gnathostome tree. Phylogeny with taxon jaw shapes and ancestral jaw shapes superimposed. Blue shapes are empirical jaw shapes of sample taxa, red shapes are reconstructed jaw shapes output from ancestral state reconstruction.

$$I \approx \sum_{i=1}^{N} m_i r_i^2$$

where m = element mass, r = distance from the element center of mass to rotational axis, and N = the number of elements. As each theoretical jaw shape is standardized by area, their lengths still vary. This calculation uses the length of the size-standardized jaws and thus is equivalent to the length divided by the square root of jaw area. RE was first calculated taking the posterior-most node of the jaw outline with a near vertical normal as the initial jaw joint and the anterior-most node of the jaw outline with a near vertical normal as the initial bite point. Jaw joint and bite point positions were then bootstrapped over 1000 randomizations that varied the joint and bite location along 5% of the total outline length on either side of the initial placement. Mean and 95% confidence intervals were then generated for each theoretical shape. The functional landscape of mean values is reported here (figure 2.5).

We calculated the Von Mises Stress (VMS) across each theoretical jaw shape mesh using a simple 2D constant strain triangle Finite Element Analysis (FEA) algorithm in MATLAB. Each jaw was modeled as a thin plate of uniform thickness with a Young's modulus of $2 \cdot 10^9$ Pa and Poisson's ratio of 0.3. VMS has been used a proxy for strength in recent functional adaptive landscape studies [121, 123, 281] and has been used for a number of years as a measure of skull strength, particularly in comparative studies. Our functional landscapes for mean, maximum, and media VMS showed little difference, so we use median VMS in this study, which is less susceptible to high stress outliers generated at constraints [85, 121, 137, 138, 141]. The same nodes were defined as bite and jaw joint positions as for the RE calculations. The location of muscle force is then interpolated along the perimeter of the jaw between these points, initially placed one-third of the length of the jaw from the jaw joint. Again, models were tested 1000 times with pseudo-randomized input conditions, shifting the force node position by 5% of the total outline length on either side of the initial node and orienting the force direction 45° either side of the force node normal. Constraints of the jaw joint and bite position were not randomized for stress calculation due to the exponential increase in computational time that this would require and their relatively small effect on overall strain energy [282].

To explore the effect of raw jaw length on shape, we plotted raw jaw length against PC1 and PC2 scores for the empirical dataset and assessed the significance with a Phylogenetic Generalized Least Squares (PGLS). We find a significant relationship between raw jaw size and PC1 ($p = 0.04129$, coefficient of determination (R^2)= 0.03485) and an insignificant relationship between size and PC2 ($p = 0.4846$, R^2= 0.0056). Both R^2 values were low; this appears to be due to the high shape variance in smaller jaws and the lower shape variance in larger jaws. This may suggest some developmental or functional restrictions on larger jaws. We also plotted each taxon data point as a function of jaw size on a PC1-PC2 plot. We find that some of the extremes of PC space are occupied by large jaws (e.g., the placoderms *Gorgonichthys*, *Titanichthys*, and *Dunkleosteus*); however, these taxa vary in shape from short deep jaws to longer thin jaws (figure 2.6).

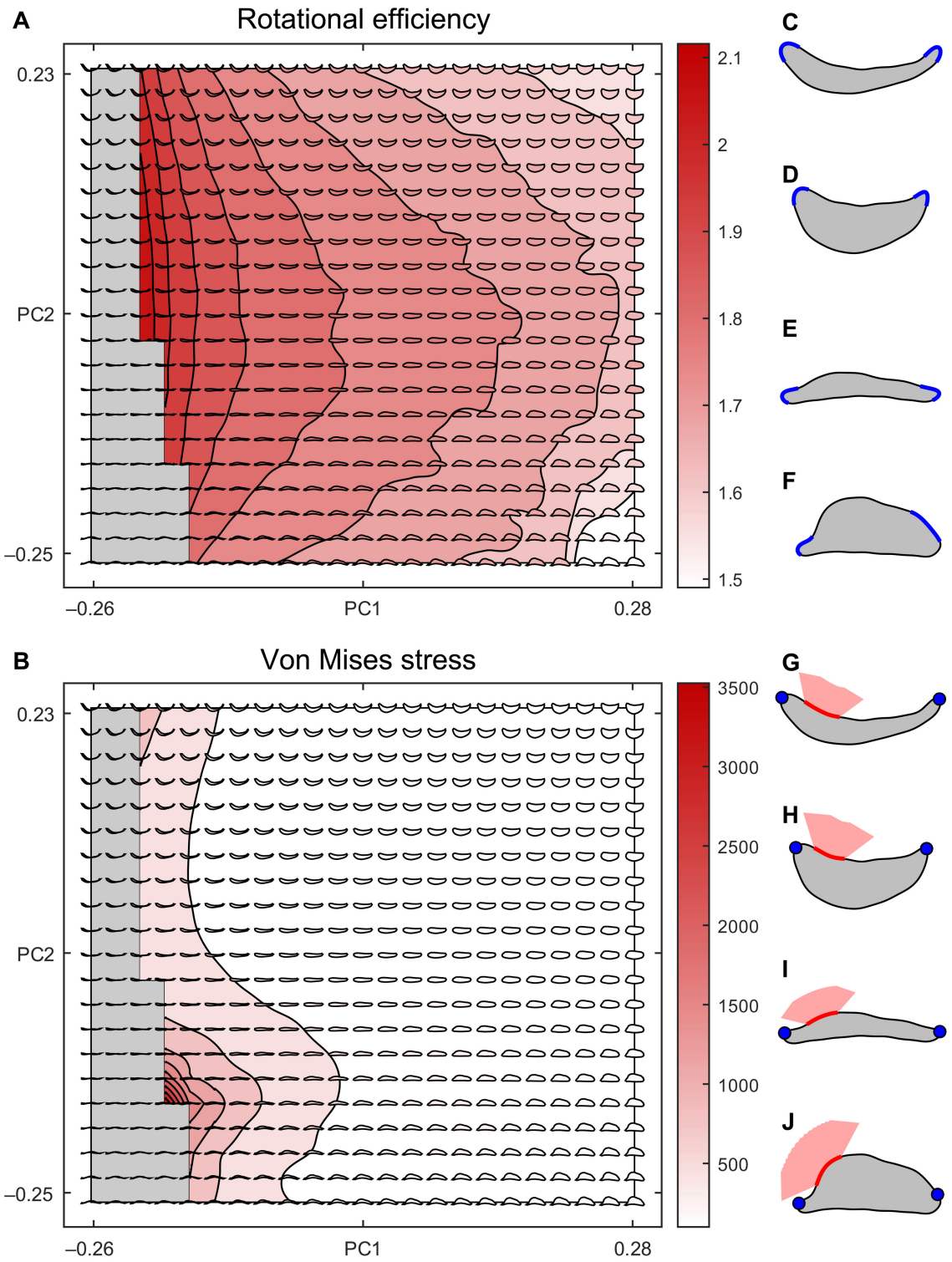

Figure 2.5: Performance surfaces generated from theoretical shapes. Rotational Efficiency (RE) **(A)** and median Von Mises Stress (VMS) **(B)** performance surfaces showing the mean value from 1000 random constraint inputs. Superimposed theoretical shapes are colored on the basis of their individual performance. Gray shapes and area represent geometrically impossible shapes and morphospace. **(C to J)** Random inputs shown on four theoretical shapes from different grid positions for RE **(C to F)** (blue lines represent the boundaries of random joint and tooth placement) and VMS **(G to J)** (blue dots represent constraint positions, red line represents boundaries of random force placement, and red area represents boundaries of random force direction).

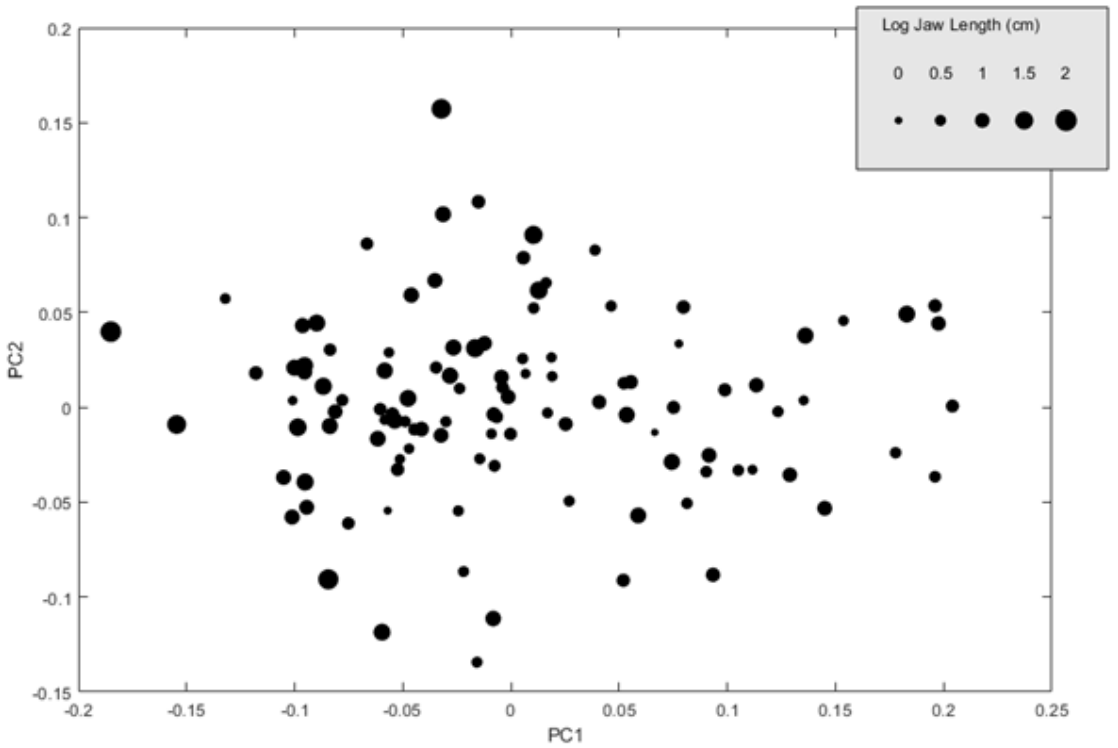

Figure 2.6: Relationship between log jaw length and shape. A Phylogenetic Generalized Least Squares (PGLS) shows a significant relationship between log jaw length and PC1 ($p = 0.00462$, $R^2 = 0.0627$), and no significant relationship between length and PC2 ($p = 0.3191$, $R^2 = 0.00954$)

The average median VMS value and 95% confidence intervals were then generated for each theoretical shape. As for RE, the functional landscape of mean values is reported (figure 2.5).

2.2.5 Pareto optimality

Building adaptive landscapes from functional metrics often uses least squares regressions or maximum likelihood to fit a first- or second-order polynomial relationship between morphology and performance and then performance and fitness [85, 121, 157, 159]. While this gives a good approximation of fitness under certain constraints and can highlight the relative importance of each functional trait measured, this approach cannot provide a single, universal fitness metric to disparate taxa with varying ecology. Instead, each group within the dataset (e.g., each ecology) has a unique adaptive landscape. Furthermore, in this study, the VMS surface is poorly characterized by the quadratic surface required for Arnold's fitness formulae [159]. Here, we develop a new rank-based method of combining functional metrics into a single fitness metric, adapted from Pareto ranking algorithms [47, 156]. Pareto optimality has been used as a method of morphospace optimality analysis elsewhere with very promising results, although these studies operate on large-scale assumptions about the relationship between morphospace and function [283, 284]. We use the foundational concepts of Pareto optimality to rank morphospace location based on its functional performance.

The optimality of each theoretical morphology was ranked using a modified Goldberg Pareto ranking system [285]. In many cases where the solutions to a problem (in this case, theoretical morphologies) experience a trade-off between N metrics of performance (in this case, there are two metrics: speed and strength), there exists a subset of those solutions that is Pareto optimal [Pareto Optimal Subset (POS)]. A solution is Pareto optimal if no other solution has better or equal performance in all metrics. We can take this concept further to generate a Pareto rank system, where the POS is assigned rank one and then removed from the sample of solutions. This allows a second POS to be found and assigned rank two. This POS is then removed from the second sample of solutions, and the process iterates until all solutions have been ranked. We develop this ranking for performance spaces with spatial occupation heterogeneity by ranking the dataset with Goldberg's ranking (optimal ranking, R_O) and then ranking it again with the optimality of each metric reversed (suboptimal ranking, R_S). The rank of the solution is then calculated via this equation

$$R_i = \frac{R_{Si} - 1}{R_{Oi} + R_{Si} - 2}$$

This results in a linear rank from 0 to 1, with 1 denoting Pareto optimal (not dominated by any solution) and 0 denoting Pareto suboptimal (not dominant over any solution). Other Pareto ranking systems have been shown to be more effective in evolutionary algorithms [286, 287]; however, these methods are biased by the relative scales of functional metrics and the density of occupation of performance space. We opt not to use these methods to eliminate the requirement for scaling functional metrics and the bias caused by heterogeneous occupation of performance space, as equidistant theoretical forms in morphospace converge and diverge in function (figure 2.7).

2.2.6 Disparity

Both disparity metrics were measured on EFA harmonic data and bootstrapped 10,000 times. The mean optimality of each time bin was calculated by bootstrapping taxon samples 10,000 times, extrapolating optimality from the surface at individual taxon PC scores, of which the mean was calculated. Trends in each signal were tested using a Spearman rank correlation test. The disparity (sum of variances and mean pairwise distance) against optimality relationships was tested with a standard Pearson's linear correlation test.

2.3 Results

2.3.1 Theoretical morphology

We used 12 size and rotation-corrected elliptical harmonics (45 metrics in total) output from EFA to characterize 121 gnathostome jaw shapes in 2D (figures 2.1 and 2.2). A PCA of the empirical shapes captures 88.6% of variation by the first five PC axes and 70.9% in the first two axes. By modifying the harmonic dataset, 483 theoretical shapes were generated in an evenly spaced 23-by-21 grid across the PC1-PC2 morphospace within an area that encompassed the range of realized jaw form plus a border of an extra 20% the range of PC1 (figure 2.3). This meets the expectations of a theoretical morphospace, since its

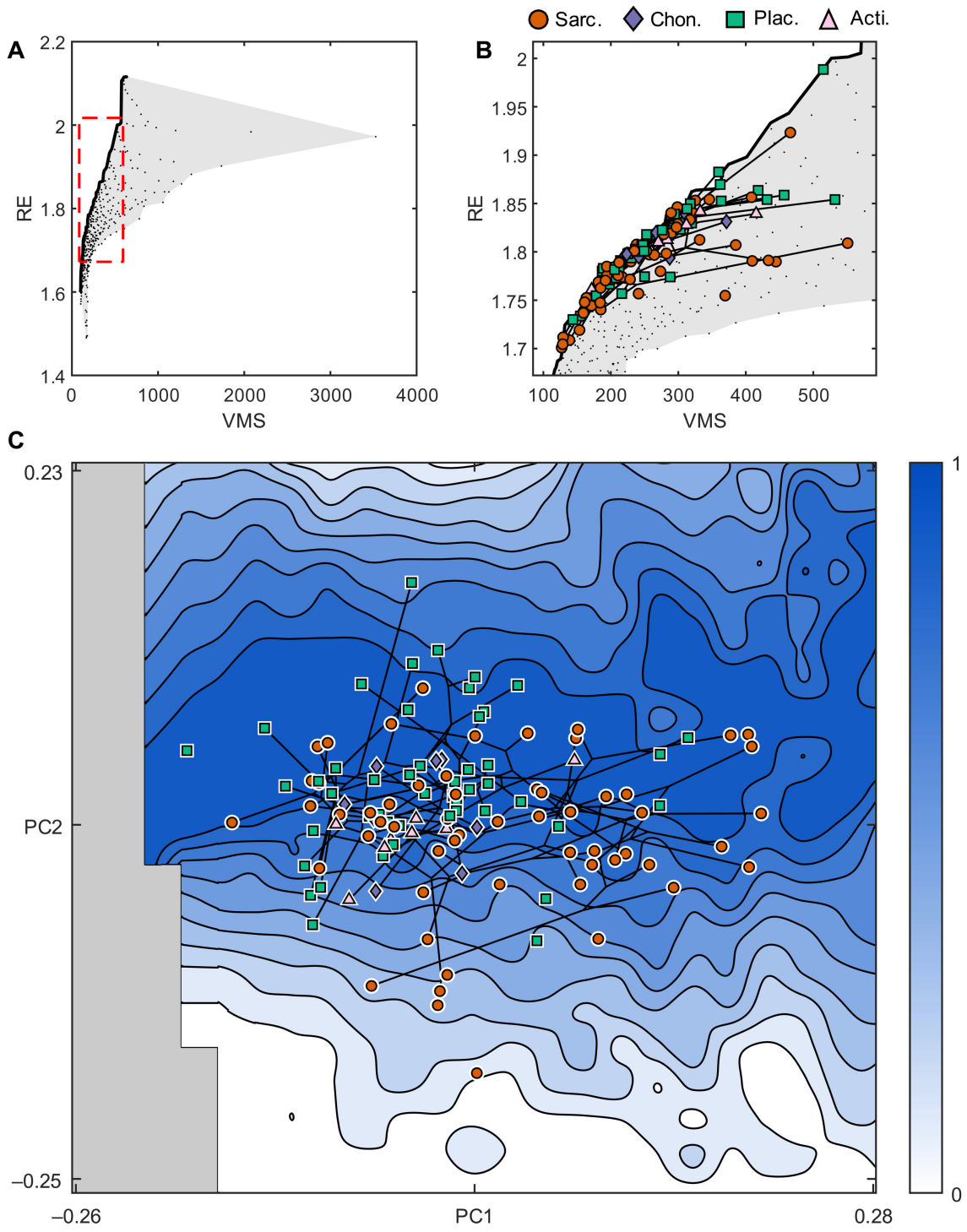

Figure 2.7: Pareto optimality and the adaptive landscape. (A) Performance space. Each theoretical shape is represented by a black dot, plotted by its individual VMS and RE performance. Note the heterogeneous occupation densities. Gray area represents the region of possible solutions. Solid black line represents the Pareto front. Red dashed area represents the area shown in **(B)**, a zoom of plot **(A)**, showing extrapolated taxon performances and their phylogenetic relationships. **(C)** The adaptive landscape, with phylomorphospace superimposed. Note that only 99 of the 121 taxa are included in the phylogeny; the remainder are plotted unconnected to the phylogeny. Pareto rank represents optimality, with 0 being least optimal and 1 representing optimal (on the Pareto front). Gray region represents geometrically impossible morphospace. Legend shows symbols and colors for individual taxa from four clades: Sarcopterygii (Sarc.), Chondrichthyes and acanthodians (Chon.), Placodermi (Plac.), and Actinopterygii (Acti.).

dimensions are geometric models of form and it encompasses morphological variation that extends beyond that observed in empirical data [87]. It is commonly argued that theoretical morphospaces are not constructed with reference to measurement data from existing form [87] as ours is. However, we reject this qualification, since, from their inception, theoretical morphospaces have been based on measurement data from existing form. For example, the seminal theoretical morphospace analyses by Raup [62, 288] were preceded and explicitly informed by his characterization of the coiling parameters of gastropods based on empirical measurement data [289]. Our approach allows for a much broader application of the theoretical morphospace approach, which has largely been limited to geometrically simple biological structures [e.g., [87]].

Within this article, we refer to jaw shapes by their position in theoretical morphospace, which spans from -0.26 to 0.28 in PC1 and -0.26 to 0.24 in PC2. In general, increasing PC1 represents increasing jaw depth and decreasing jaw length, while increasing PC2 represents the shift from a more convex to a more concave dorsal surface. Extended regions show geometrically viable jaw morphologies in high PC1 coordinates, but the lower PC1 borders show regions of self-intersecting geometry. Low PC1 regions are therefore geometrically impossible regions of morphospace [cf. [118, 125]]. Other extreme areas may be geometrically infeasible in nature due to poor articulation surfaces with the skull, but this is not testable with jaw morphology alone.

2.3.2 Functional performance of theoretical morphologies

We conducted functional analysis on the theoretical shapes. All taxa in the dataset are aquatic and encountered obstacles imposed by aquatic feeding, such as the bow wave produced by extending jaws [290]. Yet, they also benefit from feeding in a dense medium where suction feeding is feasible for prey capture [148, 291, 292]. The first functional metric that we analyzed therefore was the RE of the jaw as a proxy for speed of the jaw opening and closing due to its role in defining the time to peak gape and therefore suction feeding performance [197, 291, 293–295]. We defined RE as the speed of the jaw tip, given one unit of angular kinetic energy, which is dependent on the length and the moment of inertia of jaw shape [197]. Stress resistance was the second functional metric determined, as it is a common adaptive feature tested in feeding systems to gauge resistance to the forces generated during biting [119, 137]. For inferring stress resistance, we used the median VMS of a finite element model subject to jaw loading: Models were fixed at a jaw hinge and anterior bite point and loaded with muscle force. To account for uncertainty in boundary condition position and orientation for the theoretical jaw shapes, we varied the locations of the jaw hinge and bite position over 5% of the total length of the jaw for the calculation of RE (figure 2.5). Muscle force location was also varied over 5% total jaw length, and muscle force orientation was varied 45° in either direction. All theoretical shapes were analyzed with these constraints and randomized 1000 times, resulting in a total of 430,000 FEA models and 430,000 calculations of RE. To infer the performance of jaw shape only, we standardized all theoretical jaw morphologies to the same surface area. Performance surfaces were constructed from the mean performance values of each functional metric.

The RE performance surface (figure 2.5) shows a clear relationship between shape and speed. Geometrically viable regions at low PC1 show greater RE compared to high PC1 regions, and more intermediate PC2 values have greater RE than the extremes of PC2. The RE is well characterized by a second order polynomial surface [Sum of Squared Estimate of Errors (SSE) = 0.3619, Root Mean Square Error (RMSE) = 0.0293, $R^2 = 0.9280$, Degrees Of Freedom (DOF)–adjusted $R^2 = 0.9272$], specifically a hyperbolic paraboloid. The VMS performance surface (figure 2.5) shows a radically different shape. Regions of low PC1 and PC2 show extremely high VMS and by inference poor performance, and the variation in VMS across the majority of the theoretical morphospace is minimal in comparison to the magnitude of the low PC1-PC2 spike in stress. This surface is not well characterized by a quadratic surface (SSE = $1.2213 \cdot 10^7$, RMSE = 170.1191, $R^2 = 0.6669$, and DOF-adjusted $R^2 = 0.6630$). Given the assumption that, all else being equal, fitness increases with decreased VMS and increased RE, speed and strength are compromised within a trade-off, as longer structures with more mass distributed toward the pivot point (low PC1 values) rotate faster and experience larger stresses than shorter structures of more homogeneous thickness (high PC1 values).

2.3.3 Pareto optimality and the occupation of theoretical morphospace

Plotting the strength of each theoretical jaw morphology against its speed (figure 2.7) highlights the trade-off in our chosen performance metrics and reveals that many theoretical shapes have low stress scores and intermediate RE (many-to-one mapping of form to function) [148]. Within this "performance space," it is possible to establish the Pareto front of theoretical shapes, i.e., those theoretical shapes in which neither metric can be improved without deteriorating performance of the other [156].

To establish how early jaw evolution explored this performance space, we modeled the evolution of jaw shape on a time-scaled phylogeny of early jawed vertebrates, allowing us to reconstruct mandible morphology for the ancestors of the fossil jawed vertebrates sampled, including the ancestral jawed vertebrate (figure 2.4). These ancestral jaw shapes were projected into the performance landscape along with the sampled taxa (figure 2.7). On this basis, we find that most early gnathostomes occupy the Pareto front, corroborating our prior view of the adaptive value and trade-off of the functional metrics tested. However, some taxa plot further from the optimal boundary in regions of relatively high stress and intermediate RE. Many of the jaws occupying suboptimal regions of performance space independently migrated to this region from the Pareto front and did so by decreasing strength rather than decreasing RE (figure 2.7). This migration may be the result of another attractor in performance space caused by an additional functional metric not tested here or optimizing stress resistance becomes much less important to these taxa than optimizing RE or both.

We developed a Pareto rank algorithm that assigns each theoretical shape a value from 0 (suboptimal) to 1 (optimal) (see Methods). Plotting the Pareto rank of each theoretical shape on the z axis above the morphospace generates the adaptive landscape of theoretical shapes (figure 2.7, blue scale from 0 to 1). The optimality rank of empirical taxa was extrapolated from their location on this surface (figure 2.7, data points). The majority of

early jawed vertebrates occupy a Pareto optimal region of space, with some taxa showing extension into suboptimal space. One explanation for this phenomenon may be that "suboptimal" taxa in the PC1-PC2 plane lie in higher-dimensional space that is optimal. If this were the case, then we may expect taxa further away from the PC1-PC2 plane to lie in the less optimal regions on the PC1-PC2 plane. No significant correlation between the Euclidean distance from individual taxa to the plane of theoretical morphospace and their extrapolated optimality was found ($\rho = -0.0217$ and $p = 0.8127$). Therefore, taxon suboptimality is unlikely to be due to shape variation that is not captured by PC1 and PC2.

2.3.4 Disparity and optimality

Early jawed vertebrate taxa generally occupy only optimal regions of stress and speed function, with the exception of some sarcopterygian taxa that occupy suboptimal performance regions at lower PC2 values (figure 2.7). In particular, low optimality sarcopterygian taxa include *Nesides* (0.1239), *Soederberghia* (0.3389), *Diplocercides* (0.3462), *Serenichthys* (0.3781), and *Miguashaia* (0.4067). These are coelacanths and a lungfish, suggesting some phylogenetic correlation to suboptimality. The phylomorphospace (figure 2.7) shows that many taxa have independently evolved similar morphologies, evidencing a widespread convergence in jaw shape. A multivariate K statistic (K_{mult}) [170] showed a weak but significant phylogenetic signal in the shape data ($K_{mult} = 0.37425$, $p = 0.0001$). Focusing on the empirical data, we measure disparity in our dataset through two metrics (sum of variances and mean pairwise distance), which were chosen due to their robusticity to sample size [89]. Mean pairwise distance shows significant steady increase through evolutionary time, while the sum of variances shows a similar trend that is not significant (figure 2.8). However, measurements from consecutive time bins show large overlap in bootstrap confidence intervals in all metrics (figure 2.8). This shows the disconnection between patterns of morphological and functional disparity [198], which could be due to the "many forms, one function" nature of morphology, or the mechanical sensitivity of the system, which has been demonstrated to affect disparity measures [148, 296]. Mean taxon optimality for each time bin shows a steady decrease with time and has a significant negative relationship with mean pairwise distance (figure 2.8).

2.4 Discussion

We find that a large range of theoretical shapes exhibit optimal performance within a tradeoff for RE and jaw strength, particularly those with low curvature and a mass distribution that is weighted toward the jaw articulation (figure 2.7). This is because the jaws that harbor more mass close to their pivot have inherently lower rotational inertia and therefore higher RE while still maintaining large areas of mass for stress distribution. Pareto ranking characterizes the optimality of a set of solutions (in this case, theoretical morphologies) relative to one another when considering their individual performances (in this case, their strength and speed). This does not denote the adaptive value or fit of a jaw to a specific ecological role. We do not assess the relative importance of different functional metrics, as has been successful in studies of extant organisms where accurate ecological

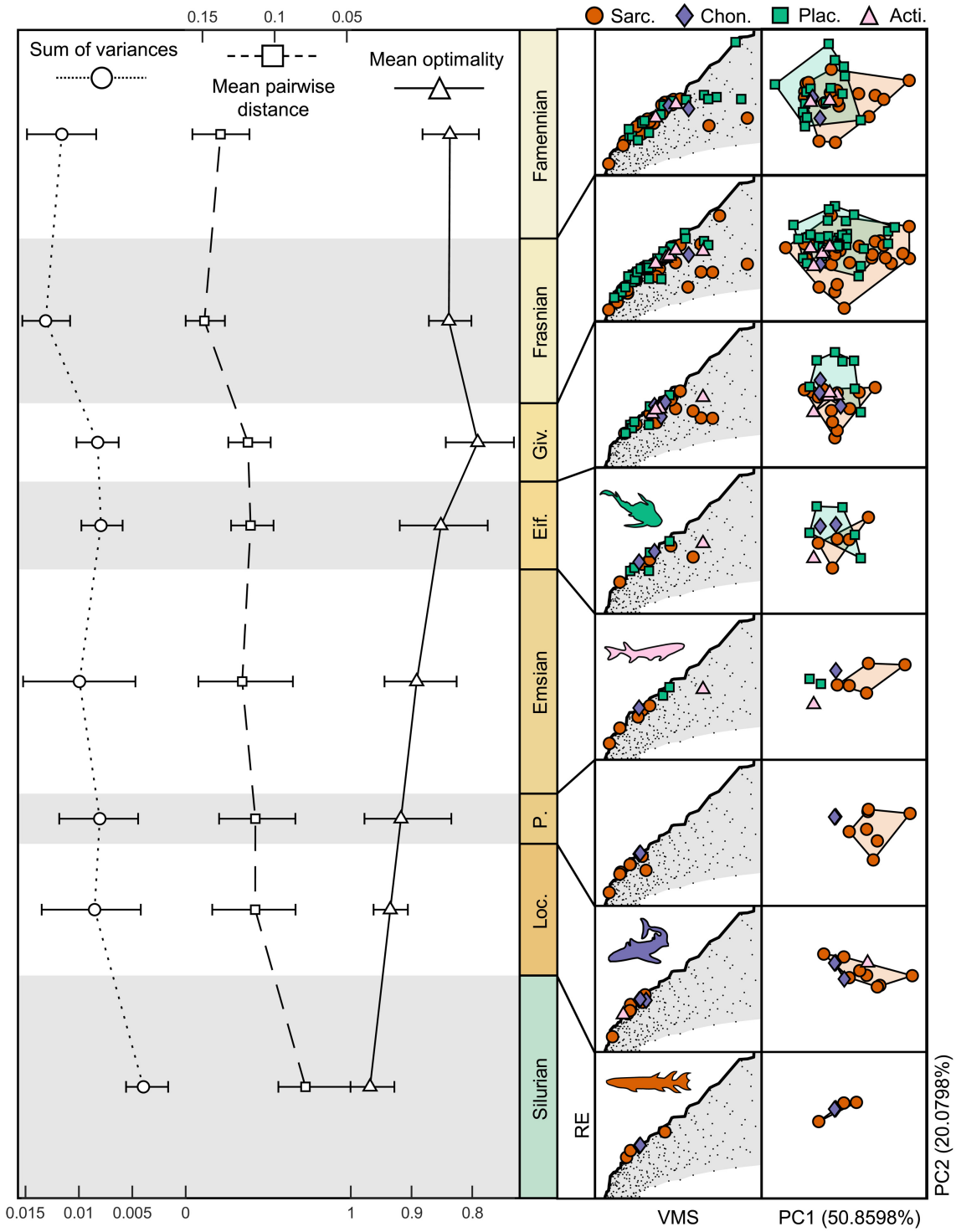

Figure 2.8: Disparity and optimality through time. Mean mechanical optimality decreases steadily through time, while the sum of variances and mean pairwise distance increase through the Devonian. White symbols and error bars represent mean and 95 confidence intervals of 10,000 bootstrap replicates. Columns on the right represent the occupation change in performance space (VMS versus RE) and morphospace (PC1 versus PC2) over time. Legend shows symbols and colors for individual taxa from four clades: Sarcopterygii (Sarc.), Chondrichthyes and acanthodians (Chon.), Placodermi (Plac.), and Actinopterygii (Acti.).

data are available [85, 120, 121, 137, 201]. Here, we interpret the optimality of each jaw as a 2D vector of weights, **w**, which determines the adaptive value of the two dimensions of performance (strength and speed, represented in a 2D performance space; figure 2.7). We do not need to know the precise magnitude or direction of **w**, as Pareto ranking allows us to identify the range of optimal morphologies given only the quadrant that **w** occupies. In practice, this is equivalent to our assumption that higher RE is adaptive and higher VMS is maladaptive. Despite many taxa exhibiting optimal ranking for the speed-strength trade-off, we also find that there are large areas of space unoccupied by empirical taxa that are ranked highly within our system. Taxa may not explore these areas, because they exhibit dichotomous performance—the morphologies in that space perform exceptionally in one metric but very poorly in the other.

We find that the earliest gnathostome jaws, and their inferred ancestral stages, have mandibles that are optimized for a tradeoff for speed and strength, therefore supporting a predatory function. The distribution of taxa within the boundaries of our theoretical jaw morphospace demonstrates that their jaws were optimized for this tradeoff (figures 2.7 and 2.9). Thus, optimality was achieved very early in jaw evolution, and our time-sliced performance space reveals that much of the subsequent exploration of shape space tracks the optimality front (figure 2.8). This pattern was maintained in each major clade or grade, with Placodermi, Chondrichthyes (here including acanthodians), Actinopterygii, and Sarcopterygii all exhibiting optimal jaw morphologies early in their evolution. Disparity increased as placoderms and sarcopterygians diversified into opposing regions of morphospace. Within the placoderms, many arthrodires occupy higher PC2 regions, representing a shift to stronger and less rotationally efficient morphologies. In the extreme case, *Gorgonichthys* represents a diversification into suboptimal shape space, reflecting a shift toward decreased strength while maintaining RE. Sarcopterygians diversified into shape space are also characterized by increased strength but lower speed efficiency (higher PC1 coordinates). Lungfish and actinistians independently evolved suboptimal morphologies that have characteristics comparable to *Gorgonichthys*: decreasing strength while maintaining RE. Lower strength in lungfish jaws is unexpected and perhaps inconsistent with the durophagous features of dipnoan jaws; we hypothesize that this is due to variation in the medial aspect not captured by our analysis or the loss of data to higher PC axes. Despite exploring different extremes of morphospace, Sarcopterygii and Placodermi exhibit functional convergence. Chondrichthyans and actinopterygians remained confined to their initial range of morphologies within Pareto optimal space.

Our results are compatible with the hypothesis that the mandibles of the earliest jawed vertebrates were optimized for prey acquisition and processing [297–299]. Rather than diversifying through shape space until an optimal morphology is achieved, the early evolution of jawed vertebrates is characterized by diffusion among equally optimal but morphologically disparate jaw morphologies. It is inevitable that the known fossil record misses an initial evolutionary episode of mandibular evolution, but our phylomorphospace approach, in which we infer morphologies ancestral to those sampled, diminishes the impact of this formal possibility. Deviation from morphologies optimized for prey acquisition

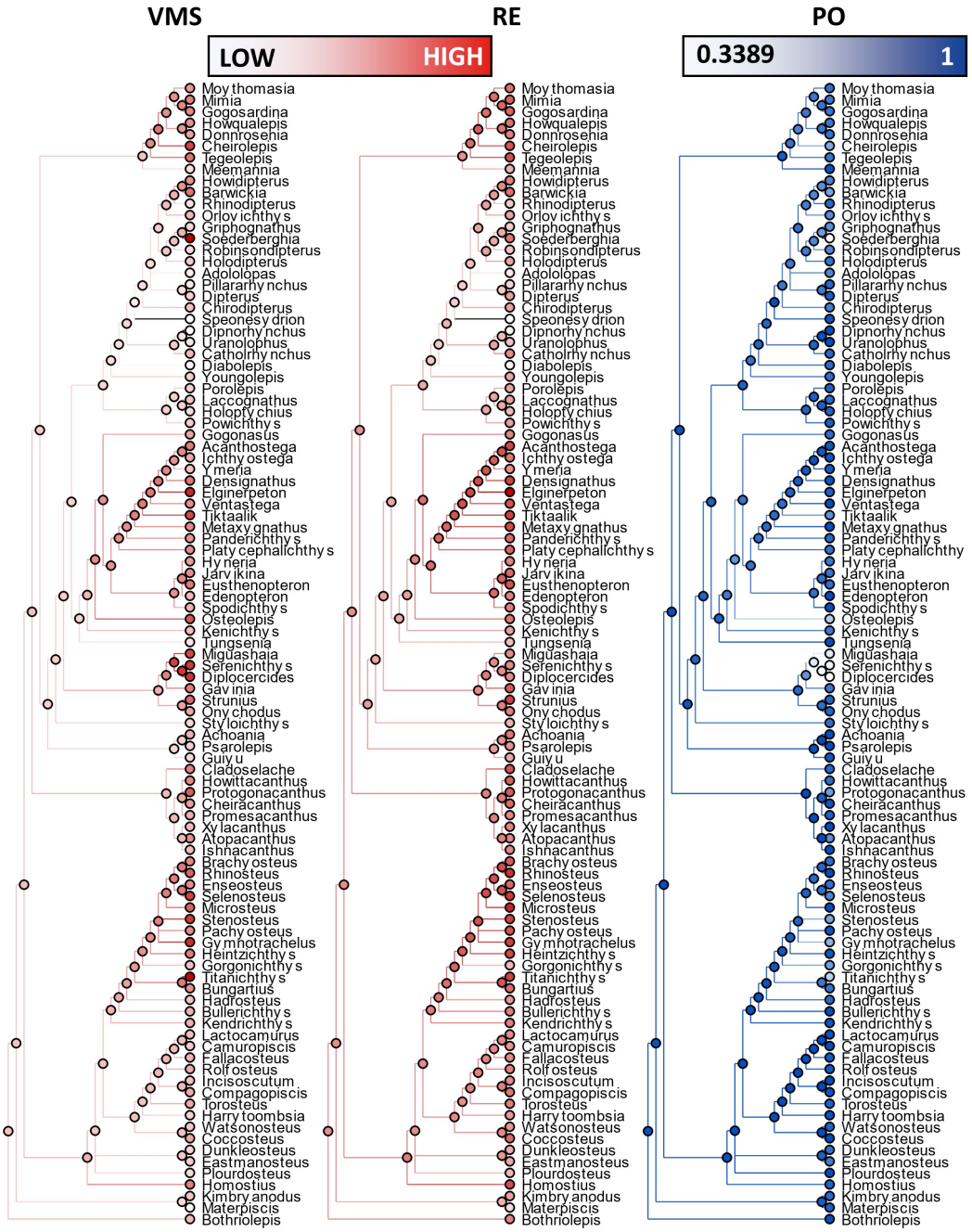

Figure 2.9: Functional optimality through the early gnathostome tree. Phylogeny with extrapolated performance values (shades of red) and optimality values (shades of blue) superimposed. Coloured circles represent values of individual nodes (both empirical taxa and inferred ancestral states)

and processing is a feature of later phylogenetic history. While the variety of mandibular functional morphology remains static [198], mandibular shape disparity increases through time (figure 2.8), made possible by the evolutionary discovery of morphologically divergent mandibles of the same optimality (figure 2.7). Despite the repeated evolution of Pareto optimal morphologies as taxa go extinct and new taxa originate, average jaw optimality decreases with increasing time and disparity.

Decreasing optimality is caused largely by the independent evolution of taxa with jaws that are weaker but otherwise maintain RE. The most optimal jaw shapes occupy a band of morphospace across PC1 coincident with largely straight jaws. Shifting into negative or positive PC2 space results in suboptimal jaws that are convex or concave, respectively. Thus, the shift from the Pareto front may be related to the repeated evolution of jaws that are concave or convex and therefore not optimized for a strength-speed trade-off. This may be due to the introduction of an ecological factor that may have changed the importance of the adaptive criterion of stress resistance or added new attractors in performance space. Examples of ecological change might be the emergence of ram feeding, lunge feeding, and other planktivorous strategies [300, 301] that are unlikely to require strong jaws but still rely on efficient jaw movement. Durophagy is another new feeding mode established within this evolutionary episode, but adaptation to hard food diets has often been associated with stronger jaw morphologies [119, 195, 302]. Decreasing optimality within our system is more likely driven by planktivorous feeding modes than durophagy, as the former is consistent with the pattern of decreasing strength and constant RE in suboptimal jaws. However, this pattern may be an artefact of our 2D approach, since, unlike the majority of jaws sampled for our study, durophagous jaws have a complex 3D morphology. Similarly, the perceived shift away from Pareto optimal morphologies may also reflect the evolution of new musculature systems that redefine the loading conditions of the biting mandible [202, 303, 304], resulting in contrasting stress patterns and magnitudes being subject to selection. Size may be another important factor, as larger (longer) jaws in our dataset occur at the limits of variation within the empirical data (figure 2.6). However, most of the size variation is evenly spread across morphospace. Alternatively, functional constraints on jaw morphology may have weakened through time or weakened with increasing disparity, as increasingly less of optimal morphospace remains to be discovered.

In any instance, our results reveal a pattern of increasing mandibular morphological disparity with clade diversification despite stasis in the evolution of jaw functional disparity [198]. This difference reflects the interrogative nature of our integrative theoretical morphology, functional optimality, and phylomorphospace approach to analyzing the evolution of form and function. It reveals that, although there may be a rapid rise to stasis in variance of phenotypic characters linked to function, this does not equate to stasis in phenotypic evolution, since our analyses demonstrate disparate morphologies that are equally Pareto optimal. The early evolution of jawed vertebrates is therefore characterized by the progressive exploration and convergence upon functionally equivalent phenotypes.

Following strong functional constraint early in gnathostome jaw evolution, increasing morphological disparity coupled with decreasing optimality suggests that the landscape of

optimality roughens with the emergence of new, functionally relevant anatomical innovations and that functional constraints (strength and speed) on morphospace occupation may have relaxed over time. This provides broader insight into questions surrounding the evolution of disparity through clade history, supporting a view that morphospace may not necessarily become saturated after an early burst in disparity [55, 56]. Rather, disparity can continue to increase, as patterns of functional optimality are rearranged and complexified within theoretical morphospace, reflecting the adaptation of taxa to different functions and trade-offs in response to their changing environment (exploitation of new prey or of old prey in a new way). Our results provide not only a further example of continuous disparity increase through clade history but also a causal mechanism for disparity accumulation: many divergent morphologies initially converging and then diverging from functional optima. Our approach to investigating disparity has allowed us to reach beyond traditional qualitative assessments of functional constraints on morphospace occupation by empirical datasets to quantitative testing of functional limits of theoretically plausible forms. By focusing functional analysis on theoretical morphospace, we can test adaptive hypotheses on the evolution of morphology and the accumulation of disparity while avoiding prior assumptions of fitness.

Chapter 3

Optimality landscapes reveal that functional constraint on tetrapod jaw morphology was released much later than their terrestrialisation

Author's contribution This chapter and all analyses within were completed by William J. Deakin.

Abstract

The origin of the tetrapod clade during the Devonian and Carboniferous was a period of major transition from aquatic to terretsrial environments. Tetrapod fossils from this region in time show great changes in their body plan, reflecting the changing functional demands between life in water and on life on land. However, the mandible exhibits morphological stasis during this transition, despite changes in diet and feeding mechanics. Here, I measure the variety of morphology in a dataset of late Palaeozoic tetrapod jaws that span this transition, and generate a theoretical morphospace of jaw shapes that could have evolved. Empirical morphologies show minimal change during terrestrialisation, until the evolution of herbivores and amniotes which expand the empirical occupation of morphospace. The overlapping regions of morphospace are optimised for a trade off between jaw strength, rotational efficiency and height, suggesting that functional constraints were defining the range of jaw morphologies during the terrestrialisation of tetrapods. While the functional demands of feeding in aquatic and terrestrial environments may change, the functional constraints acting on shape do not change, allowing aquatic jaw morphologies to perform adequately on land.

3.1 Introduction

The origin of tetrapods was a formative episode in vertebrate evolutionary history, the shift from aquatic to terrestrial ecology precipitating profound changes in anatomy, including feeding ecology [198, 199, 305, 306]. Terrestrialisation would have rendered suction feeding obsolete [306, 307], replaced by new mechanisms for food capture, transport and swallowing [306] and, in the Upper Carboniferous, the evolution of terrestrial herbivory [308]. These changes in feeding mode have been linked to morpho-functional changes in the skull. Specifically, skulls that are designed for aquatic suction feeding have greater flexibility and less consolidated skull elements compared to the more rigid skull sutures of biting taxa. During the tetrapod terrestrial transition, taxa appear to have variable, transitional skull forms: *Eusthenopteron* has a flexible, suction feeding skull with some adaptation to biting; *Acanthostega* has sutures and skull morphology associated with biting [309] and some suction ability [133, 310]. Recent studies have shown that the skull of *Tiktaalik* has a variable mix of traits that can be attributed to both aquatic and terrestrial feeding performance [311]. Combined with studies of extant fish that partake in some terrestrial feeding [306, 312–317], these studies of skull morphology have shown that the morpho-functional shift from suction to biting is not dichotomous. Morphological and functional studies have indicated similar shape and function in the jaws of sarcopterygian fish and early tetrapods, and a delayed onset of jaw morpho-functional evolution following terrestrialisation [198, 199, 318].

To achieve successful capture and processing of terrestrial prey, further cranial and postcranial modifications are required. In a terrestrial feeder, prey not only needs to be captured, but transported intraorally from the anterior to posterior jaws, and to the oesophagus for swallowing. Aquatic feeders and some aquatic taxa that feed on land utilise water pressure for transport and swallowing and some extant terrestrial feeders return to the water to swallow captured prey [306, 313, 315, 317, 319–321]. Separation of the head and shoulder girdle to create a mobile neck facilitates dorsoventral movement of the head independent to the body, aiding in prey capture[306]. Yet a neck first appears in the non-tetrapod elpistostegalid *Tiktaalik* [253]. A second feature crucial to terrestrial prey prehension and intraoral transport is a mobile tongue [306]. Stem tetrapods possessed a fish-like hyobranchial apparatus associated with the gills and an immobile tongue [258]. The 'terrestrial' tongue based hyobranchium evolved later [322]. It has been suggested that loss of gill-based respiration and remodelling of the hyobranchial system into lingual system bearing a tongue was the necessary step to achieve full terrestrial feeding [306].

A dichotomy therefore exists between the functional demands of shifting from aquatic suction and biting to terrestrial biting, but the shift in the functional morphology of transitional taxa is more gradual, before a terrestrial tongue system can evolve. How can a dramatic shift in environmental functional demands lead to limited change in functional morphology? The shift in environment had dramatic effects on many components of the appendicular skeleton [323–325], so why was the jaw so constrained? One explanation may be that the functional demands of biting and suction feeding on jaw morphology may be similar, and jaw morphologies of these taxa are constrained to similar optimal regions

of morphospace. To address this question, we investigate functional constraints acting on the morphological evolution of the jaw of sarcopterygian fishes and tetrapods during the terrestrialisation and subsequent radiation of tetrapods. Using an adaptive landscape approach, we use proxies to determine the strength, speed and hydrodynamic efficiency of the jaw across the terrestrialisation event, and the trade-off in these functional traits. We hypothesise that aquatic, semi-aquatic and terrestrial jaws are constrained within similar regions of morphospace that are optimised within a trade-off of their strength and rotational efficiency. We also hypothesise that aquatic taxa will be constrained to minimise jaw height, to reduce their hydrodynamic profile.

We test this using empirical and theoretical jaw morphospace, from which performance and optimality landscapes were generated. To do this we characterised the mandibular morphology of 137 species of stem- and early crown-tetrapods (including outgroup non-tetrapod sarcopterygians, ranging in age from Devonian to the end Permian), using Elliptical Fourier Analysis (EFA) of lateral images. From this sample we constructed a two dimensional theoretical morphospace of mandible morphologies that extended 20% beyond the range of variation observed within the sample data. Theoretical morphologies were sampled evenly across morphospace and subjected to functional analyses including Von Mises Stress (VMS), Rotational Efficiency (RE) and Jaw Height (JH), our proxies for jaw strength, speed and hydrodynamic efficiency, respectively. This allowed us to determine how these functional traits varied through theoretical shape space, which we present as performance surfaces. Additionally, we used a Pareto ranking approach [192] to identify the theoretical morphologies that manifest the optimal trade off between pairs of functional traits, as well as all traits combined. Considering functional performance and how it varies within theoretical shape space allows us to escape the limiting assumption that empirical samples are optimised by adaptation for their specific function [21]. This allows us to test such hypotheses based on the location of taxa or lineages relative to the performance surfaces within theoretical shape space. We achieved this by modelling the evolution of mandibular morphology within tetrapod phylogeny and projecting the position of our empirical samples and their inferred ancestors as a phylomorphospace.

Consistent with previous studies of functional morphology at the transition between aquatic and terrestrial feeding, we find that there is a wide overlap in mandibular morphology between each group of aquatic, semi-aquatic and terrestrial taxa. This overlap represents morphologies that are Pareto optimal for the trade off between our proxies for strength, speed and hydrodynamic efficiency, suggesting that the jaws of aquatic and terrestrial tetrapods can perform similar functional roles. However, we also see broader morphospace exploration in younger terrestrial taxa manifest as dispersion away from this trade off. This provides an explanation for the lack of a transition in jaw morphology during terrestrialisation, as aquatic jaw morphologies are functionally constrained to optimal shapes that can also perform adequately on land. This was followed by a combination of new functional feeding modes and a release of developmental constraint that may have allowed terrestrial amniotes to innovate jaw morphology.

3.2 Methods

3.2.1 Morphology

Jaw morphology was measured using 600 coordinates sampled from an outline traversal algorithm of 137 lateral images of tetrapod jaws. These were then input into an elliptical Fourier analysis. A total of 12 harmonics were used, which captured over 99% of shape in over 99% of taxa. A standard principal component analysis was used to find the 2 axes of maximum variation for the construction of theoretical morphospace. Theoretical morphospace was built from a 27-by-19 grid of evenly spaced points in this morphospace, extending through the range of real morphologies in morphospace plus a 20% border at each end of each axis (figure 3.1, 3.2).

Index	Genus	Clade	Ecology	Image Type	Source
1	*Acanthostega*	Stem.	SA	Reconstruction	Ahlberg and Clack (1998)
2	*Acanthostomatops*	Temn.	T	Reconstruction	Boy (1989)
3	*Adelogyrinus*	Stem.	A	Reconstruction	Carroll et al. (1998)
4	*Adelospondylus*	Stem.	A	Drawing	Smithson (1980)
5	*Aerosaurus*	Eupe.	T	Reconstruction	Spindler et al. (2018)
6	*Aletrimyti*	Micr.	T	μCT Scan	Szostakiwskyj et al. (2015)
7	*Anteosaurus*	Eupe.	T	Reconstruction	Barghusen (1975)
8	*Anthracosaurus*	Embo.	SA	Reconstruction	Panchen (1981)
9	*Araeoscelis*	Eure.	T	Reconstruction	Reisz et al. (1984)
10	*Archaeovenator*	Eupe.	T	Reconstruction	Spindler et al. (2018)
11	*Archegosaurus*	Temn.	A	Reconstruction	Romer (1947)
12	*Archeria*	Embo.	A	Drawing	Holmes (1989)
13	*Arctognathus*	Eupe.	T	Reconstruction	Sidor (2003)
14	*Ariekanerpeton*	Seym.	SA	Reconstruction	Klembara and Ruta (2005)
15	*Ascendonanus*	Eupe.	T	Reconstruction	Spindler et al. (2018)
16	*Balanerpeton*	Temn.	SA	Reconstruction	Ahlberg and Clack (1998)
17	*Banksiops*	Temn.	SA	Reconstruction	Cosgriff (1969)
18	*Batrachiderpeton*	Nect.	A	Drawing	Hancock and Atthey (1913)
19	*Belebey*	Para.	T	Reconstruction	Reisz et al. (2007)
20	*Biarmosuchus*	Eupe.	T	Reconstruction	Sidor (2003)
21	*Brachydectes*	Micr.	SA	μCT Scan	Pardo and Anderson (2016)
22	*Caerorhachis*	Stem.	T	Reconstruction	Holmes and Carroll (1977)
23	*Captorhinus*	Eure.	T	Reconstruction	Ahlberg and Clack (1998)
24	*Cardiocephalus*	Micr.	SA	Reconstruction	Carroll and Gaskill (1978)
25	*Carrolla*	Micr.	SA	Reconstruction	Maddin et al. (2011)
26	*Casea*	Case.	T	Reconstruction	Williston (1913)
27	*Cheliderpeton*	Temn.	SA	Reconstruction	Schoch and Milner (2000)
28	*Chomatobatrachus*	Temn.	SA	Reconstruction	Schoch and Milner (2000)
29	*Cochleosaurus*	Temn.	SA	Drawing	Sequiera (2003)
30	*Colobomycter*	Para.	T	Reconstruction	MacDougall et al. (2017)
31	*Coloraderpeton*	Aist.	SA	μCT Scan	Pardo et al. (2017)
32	*Cotylorhynchus*	Case.	T	Reconstruction	Reisz (2006)
33	*Crassigyrinus*	Stem.	A	Drawing	Ahlberg and Clack (1998)

34	*Ctenospondylus*	Eupe.	T	Reconstruction	Brink and Reisz (2014)
35	*Delorhynchus*	Para.	T	Photograph	Haridy et al. (2017)
36	*Deltasaurus*	Temn.	SA	Reconstruction	Cosgriff (1965)
37	*Deltavjatia*	Para.	T	Photograph	Tsuji (2013)
38	*Dendrerpeton*	Temn.	SA	Reconstruction	Godfrey et al. (1986)
39	*Densignathus*	Stem.	SA	Reconstruction	Daeschler (2000)
40	*Desmatodon*	Diad.	T	Reconstruction	Kissel (2010)
41	*Diadectes*	Diad.	T	Reconstruction	Welles (1941)
42	*Diictodon*	Eupe.	T	Reconstruction	Sidor (2003)
43	*Dimetrodon*	Eupe.	T	Reconstruction	Fröbisch et al. (2011)
44	*Diploceraspis*	Nect.	A	Reconstruction	Beerbower (1963)
45	*Doragnathus*	Stem.	A	Reconstruction	Anderson et al. (2013)
46	*Dvellacanus*	Micr.	SA	μCT Scan	Szostakiwskyj et al. (2015)
47	*Dvinosaurus*	Temn.	SA	Reconstruction	Romer (1947)
48	*Edaphosaurus*	Eupe.	T	Reconstruction	Reisz (2006)
49	*Elginerpeton*	Stem.	A	Reconstruction	Ahlberg and Clack (1998)
50	*Ennatosaurus*	Case.	T	Reconstruction	Maddin et al. (2008)
51	*Eodicynodon*	Eupe.	T	Reconstruction	Kemp (2005)
52	*Eoherpeton*	Embo.	T	Reconstruction	Smithson (1980)
53	*Eothyris*	Case.	T	Reconstruction	Reisz et al. (2009)
54	*Eryops*	Temn.	T	Reconstruction	Schoch and Milner (2014)
55	*Euryodus*	Micr.	SA	Reconstruction	Carroll and Gaskill (1978)
56	*Eusthenopteron*	Stem.	A	Reconstruction	Clack (2012)
57	*Greererpeton*	Stem.	A	Reconstruction	Bolt and Lombard (2001)
58	*Hapsidopareion*	Micr.	SA	Reconstruction	Carroll et al. (1998)
59	*Haptodus*	Eupe.	T	Reconstruction	Kemp (2005)
60	*Hylerpeton*	Micr.	SA	Reconstruction	Carroll et al. (1998)
61	*Ichthyostega*	Stem.	SA	Reconstruction	Ahlberg and Clack (1998)
62	*Ictidosuchoides*	Eupe.	T	Reconstruction	Sidor (2003)
63	*Intasuchus*	Temn.	SA	Reconstruction	Schoch and Milner (2000)
64	*Jarilinus*	Ungr.	T	Reconstruction	Carroll et al. (1972)
65	*Kotlassia*	Seym.	T	Reconstruction	Romer (1947)
66	*Labidosaurikos*	Eure.	T	Reconstruction	Reisz (2006)
67	*Labidosaurus*	Eure.	T	Reconstruction	Modesto et al. (2007)
68	*Leiocephalikon*	Micr.	SA	Reconstruction	Carroll et al. (1998)
69	*Leontosaurus*	Eupe.	T	Photograph	Kammerer (2016)
70	*Lethiscus*	Aist.	SA	Reconstruction	Pardo et al. (2017)
71	*Limnoscelis*	Diad.	T	Reconstruction	Kissel (2010)
72	*Lydekkerina*	Temn.	T	Reconstruction	Schoch and Milner (2000)
73	*Lystrosaurus*	Eupe.	T	Reconstruction	Kemp (2005)
74	*Megalocephalus*	Stem.	A	Reconstruction	Romer (1947)
75	*Megamolgophis*	Micr.	SA	Reconstruction	Lucas (2013)
76	*Melosaurus*	Temn.	SA	Reconstruction	Riabinin (1916)
77	*Mesenosaurus*	Eupe.	T	Reconstruction	Spindler et al. (2018)
78	*Mesosaurus*	Ungr.	A	Reconstruction	Modesto (2006)
79	*Metaxygnathus*	Stem.	A	Reconstruction	Ahlberg and Clack (1998)
80	*Micraroter*	Micr.	SA	Reconstruction	Carroll et al. (1998)
81	*Microbrachis*	Micr.	SA	Drawing	Carroll et al. (1998)

82	*Microvaranops*	Eupe.	T	Reconstruction	Spindler et al. (2018)
83	*Moradisaurus*	Eure.	T	Photograph	Modesto et al. (2019)
84	*Moschops*	Eupe.	T	Reconstruction	Boos et al. (2015)
85	*Neldasaurus*	Temn.	SA	Drawing	Chase (1965)
86	*Oedaleops*	Case.	T	Reconstruction	Langston (1965)
87	*Oestocephalus*	Aist.	SA	Reconstruction	Carroll et al. (1998)
88	*Onchiodon*	Temn.	SA	Reconstruction	Boy (1990)
89	*Ophiacodon*	Eupe.	T	Reconstruction	Sidor (2003)
90	*Orovenator*	Eure.	T	Reconstruction	Reisz et al. (2011)
91	*Palaeohatteria*	Eupe.	T	Reconstruction	Spindler (2016)
92	*Paleothyris*	Eure.	T	Reconstruction	Carroll (1969)
93	*Panderichthys*	Stem.	A	Drawing	Ahlberg and Clack (1998)
94	*Pantelosaurus*	Eupe.	T	Reconstruction	Spindler (2016)
95	*Pantylus*	Micr.	SA	Reconstruction	Carroll et al. (1998)
96	*Pareiasaurus*	Para.	T	Drawing	Olson and Broom (1937)
97	*Petrolacosaurus*	Eure.	T	Reconstruction	Reisz (1981)
98	*Phlegethontia*	Aist.	SA	Reconstruction	Carroll et al. (1998)
99	*Pholiderpeton*	Embo.	SA	Reconstruction	Clack (1987)
100	*Pholidogaster*	Embo.	SA	Reconstruction	Romer (1964)
101	*Platycephalichthys*	Stem.	A	Reconstruction	Anderson et al. (2013)
102	*Platyoposaurus*	Temn.	SA	Reconstruction	Schoch and Milner (2000)
103	*Protocaptorhinus*	Eure.	T	Reconstruction	Olson (1984)
104	*Protorothyris*	Eure.	T	Reconstruction	Kemp (2005)
105	*Pteroplax*	Embo.	SA	Reconstruction	Romer (1947)
106	*Ptyonius*	Nect.	SA	Reconstruction	Carroll et al. (1998)
107	*Reiszorhinus*	Eure.	T	Drawing	Sumida et al. (2010)
108	*Rhineceps*	Temn.	SA	Reconstruction	Schoch and Milner (2000)
109	*Rhizodus*	Stem.	A	Drawing	Jeffery (2003)
110	*Rhynchonkos*	Micr.	SA	μCT Scan	Szostakiwskyj et al. (2015)
111	*Sauropleura*	Nect.	SA	Reconstruction	Carroll et al. (1998)
112	*Schoenfelderpeton*	Temn.	SA	Drawing	Boy (1986)
113	*Sclerocephalus*	Temn.	SA	Reconstruction	Schoch and Milner (2000)
114	*Secodontosaurus*	Eupe.	T	Reconstruction	Reisz et al. (1992)
115	*Seymouria*	Seym.	T	Reconstruction	Romer (1947)
116	*Silvanerpeton*	Ungr.	T	Reconstruction	Ruta and Clack (2006)
117	*Solenodonsaurus*	Ungr.	T	Reconstruction	Carroll et al. (1972)
118	*Sphenacodon*	Eupe.	T	Reconstruction	Fröbisch et al. (2011)
119	*Suminia*	Eupe.	T	Reconstruction	Reisz (2006)
120	*Syodon*	Eupe.	T	Photograph	Kammerer (2011)
121	*Tetraceratops*	Eupe.	T	Reconstruction	Kemp (2005)
122	*Tiktaalik*	Stem.	A	Photograph	Daeschler et al. (2006)
123	*Titanophoneus*	Eupe.	T	Reconstruction	Barghusen (1975)
124	*Trimerorhachis*	Temn.	A	Reconstruction	Schoch and Milner (2014)
125	*Tryphosuchus*	Temn.	SA	Reconstruction	Schoch and Milner (2000)
126	*Tseajaia*	Diad.	T	Reconstruction	Kissel (2010)
127	*Ulemosaurus*	Eupe.	T	Reconstruction	Sidor (2003)
128	*Urocordylus*	Nect.	A	Reconstruction	Carroll et al. (1998)
129	*Utegenia*	Seym.	SA	Reconstruction	Klembara and Ruta (2004)

130	*Varanodon*	Eupe.	T	Reconstruction	Spindler et al. (2018)
131	*Varanops*	Eupe.	T	Reconstruction	Spindler et al. (2018)
132	*Varanosaurus*	Eupe.	T	Reconstruction	Reisz (2006)
133	*Ventastega*	Stem.	A	Drawing	Ahlberg and Clack (1998)
134	*Weigeltisaurus*	Eure.	T	Reconstruction	Bulanov and Sennikov (2015)
135	*Whatcheeria*	Stem.	SA	Drawing	Lombard and Bolt (2006)
136	*Ymeria*	Stem.	SA	Reconstruction	Clack et al. (2012)
137	*Zatrachys*	Temn.	T	Reconstruction	Langston (1953)

Table 3.1: Early tetrapod jaw image dataset. Abbreviations: Stem Tetrapoda (Stem.), Temnospondyli (Temn.), Microsauria (Micr.), Nectridea (Nect.), Aistopoda (Aist.), Embolomeri (Embo.), Seymouriamorpha (Seym.), Diadectomorpha (Diad.), Parareptilia (Para.), Eureptilia (Eure.), Caseasauria (Case.), Eupelycosauria (Eupe.), Aquatic (A), Semi-Aquatic (SA), Terrestrial (T).

3.2.2 Function

VMS was calculated using a simple constant strain triangle FEA, with input forces and constraints defined algorithmically as in chapter 2. The jaw joint was defined as the lowest x value node from the set of perimeter nodes with positive y values (i.e. the upper surface of the 2D jaw outline). The jaw tip was defined as the maximum x value node within the same set. The nodal force position was defined as the closest node within the upper surface node set to the point one quarter of the length along the vector from the jaw joint to the jaw tip (joint position + 0.25(tip position – joint position)). The force node was randomised within a set of nodes within a range of ±5% of the jaw outline from the calculated node. Force direction was randomised within a range of ±45° from the normal vector at the original force node position. RE was calculated using the rotational inertia of the theoretical mesh about the jaw joint, which was then used to find the speed of the jaw tip given one unit of rotational kinetic energy about the jaw joint. The jaw joint and tip were calculated the same way as the VMS algorithm, and were randomised within a range of ±5% of the jaw outline from the calculated node. Jaw height was taken as the range of a theoretical outline in its y axis, and a random range was placed on this value by randomly rotating the jaw outline by ±45°, to represent the range of flow angles the jaw might experience. Separate performance surfaces were combined into a single performance metric using a modified Goldberg ranking system [192].

3.2.3 Phylogeny

We constructed an informal supertree containing 99 out of 137 taxa based on published trees in the literature [264, 326, 327] (figure 3.3). This was timescaled using the function bin_timePaleoPhy in the R package paleotree [279], which allowed for ancestral state reconstruction for the generation of a phylomorphospace (figure 3.2) and allowed us to test for a phylogenetic signal in the morphological data using the package geomorph [280].

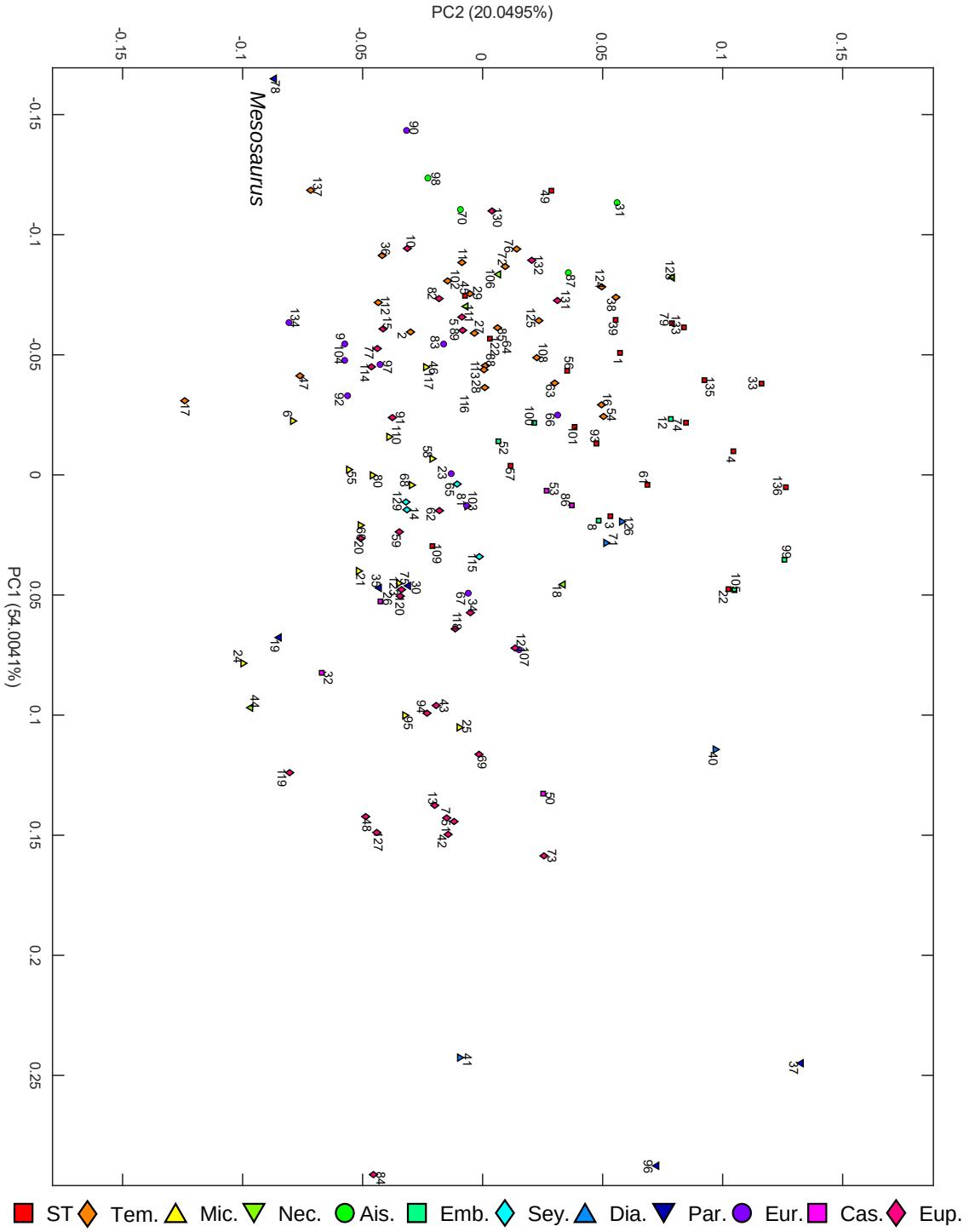

Figure 3.1: Empirical morphospace of early tetrapod jaws. PCA morphospace of an EFA dataset of 137 early tetrapod jaws, ranging from the mid Devonian to the end Permian. Coloured symbols represent the positions of empirical morphologies split into 12 clades: Stem Tetrapods (ST); Temnospondyli (Tem.); Microsauria (Mic.); Nectridea (Nec.); Aistopoda (Ais.); Embolomeri (Emb.); Seymouriamorpha (Sey.); Diadectomorpha (Dia.); Parareptilia (Par.); Eureptilia (Eur.); Caseasauria (Cas.) and Eupelycosauria (Eup.). Numbers represent taxon index (see table 3.1)

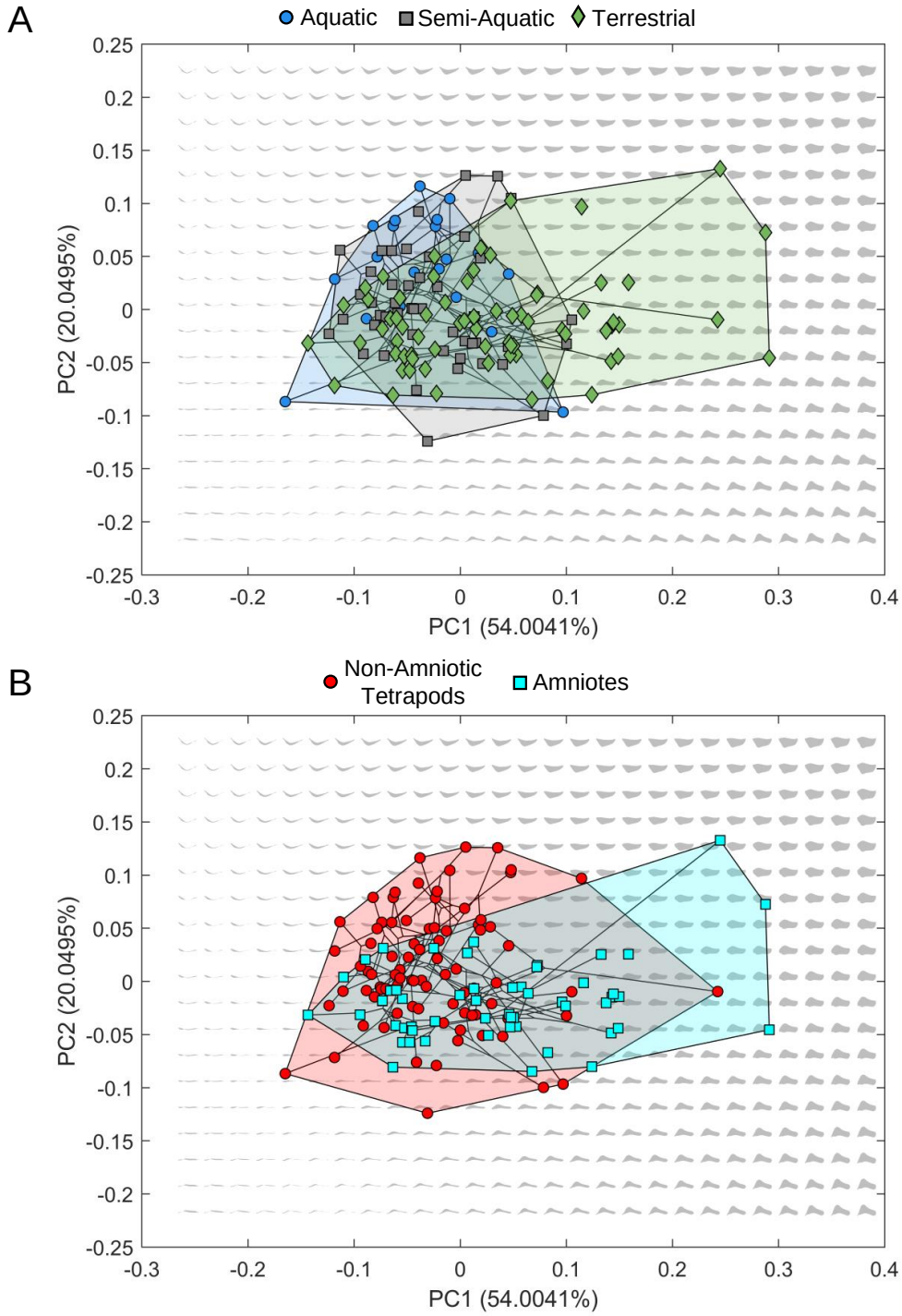

Figure 3.2: Empirical and theoretical morphospace of early tetrapod jaws. **(A)** Theoretical morphospace (grey shapes) with overlain empirical phylomorphospace grouped by ecology (coloured symbols and convex hulls). **(B)** Theoretical morphospace (grey shapes) with overlain empirical morphospace grouped by clade (coloured symbols and convex hulls).

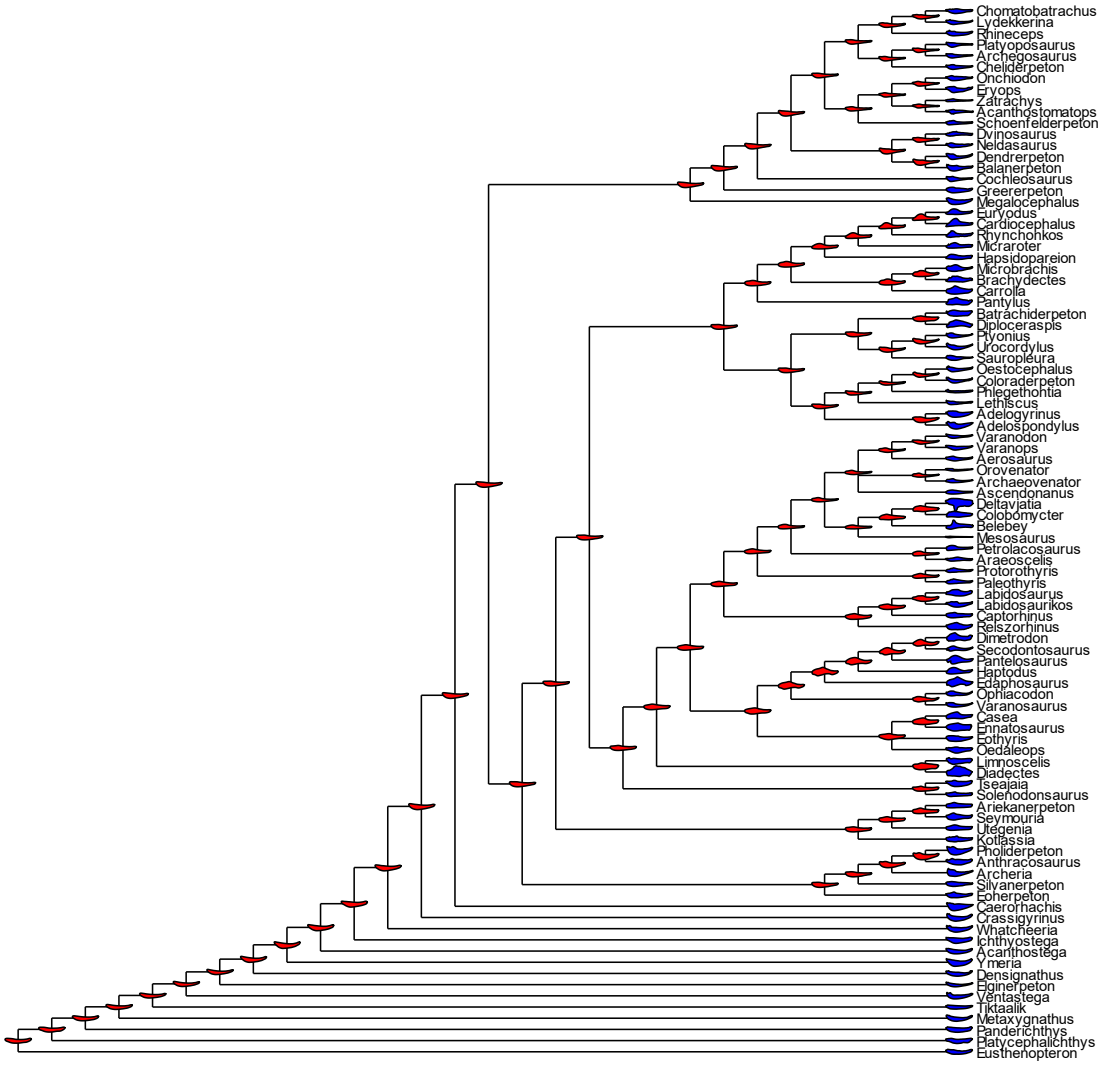

Figure 3.3: Phylogeny and Ancestral State Reconstruction (ASR) of early tetrapod jaw shape. Informal supertree used for phylogenetic analysis in this study. Blue shapes represent empirical morphologies, red shapes represent reconstructed ancestors.

3.2.4 Ecology

In order to assign ecological groups to all taxa, ecologies were defined broadly (aquatic, semi-aquatic and terrestrial) and were assigned based on fossil facies or appendicular skeletal morphology. These were assigned generally in accordamce with ecological interpretations in the literature, except in cases where those interpretations were dependent on jaw morphology. A list of the ecological assignment for each taxon is in table 3.1.

3.3 Results

3.3.1 Theoretical morphology

We used 12 elliptical harmonics from the EFA to capture over 99% of variation in the 2D shape data in over 99% of the 137 taxa. We used Principal Component Analysis (PCA) to construct a morphospace from the EFA shape data. Following the methods in chapter 2, we used Principal Component (PC) 1 and 2, which summarised 74.1% of the variation (PC1

= 54.0041%, PC2 = 20.0495%), to generate a theoretical morphospace of 513 theoretical jaw shapes in an evenly spaced, 27-by-19 grid of evenly spaced points, extending through the range of empirical morphologies plus a 20% border at each end of each axis.(figure 3.2). Theoretical shapes show an increase in jaw depth with increased PC1, and a change from convex to concave jaw curvature with increasing PC2. Of these 513 theoretical shapes, 78 were reconstructed as self-intersecting loops, representing impossible morphologies at low PC1 co-ordinates [87, 118, 125].

3.3.2 Performance landscapes

Omitting the 78 impossible morphologies from the theoretical morphology sample left jaw 435 meshes to be tested for functional performance. These were tested for strength through the metric of median VMS under loading, RE, JH, which we interpret as a proxy for hydrodynamic drag reduction (larger jaw height corresponding to increased hydrodynamic drag) (figure 3.4). These metrics are chosen for their relevance to biting and suction feeding performance (VMS should be important to biting jaws that experience large bite forces as high operational stress limits larger bite forces, RE should be important for suction feeding and kinetic inertial feeding modes, and JH here is a proxy for the hydrodynamic drag of the jaw) [119, 137, 328]. We find that the thinner jaws at low PC1 have increased RE, but also increased VMS, suggesting a tradeoff in strength and rotational efficiency. Jaw height shows a single minimum at low PC1 and mid PC2, marking these morphologies as hydrodynamically efficient ones. All three performance surfaces were tested for a fit to a second order polynomial surface, and all three could not adequately be described. Empirical jaw morphologies occur in the minimum trough of jaw height, while being spread across large differences in RE and VMS (figure 3.4). This suggests that jaws are either constrained to thinner shapes, or a trade-off between these functional performances.

3.3.3 Pareto optimality

To assess the different trade-offs these functional metrics impose on shape, we generated four Pareto optimal surfaces based on different combinations of the three functional metrics (figure 3.5). These can be further categorised by the three pair combinations (figure 3.5 A-C) and a separate triplet combination (figure 3.5 D). We see that each different pairing results in a vastly different optimality landscape: the trade-off between RE and JH favouring the thinner jaws at low PC1; JH and VMS favouring a large range of theoretical jaw shapes that spread out to largely unoccupied space at high PC1 and PC2; and RE and VMS generating separate islands of optimality, with a chasm of suboptimality flowing along the PC2 axis at intermediate PC1 values. When we incorporate all three performance metrics in our optimality ranking, much larger ranges of morphospace are optimal, and the gradient between optimal and suboptimal forms becomes very sharp.

3.3.4 Ecological signal

The most striking difference in morphospace occupation between the three major environmental ecologies (aquatic, semi-aquatic and terrestrial) is that terrestrial taxa occupy a significantly larger space (figure 3.2). This area of terrestrial occupation overlaps with aquatic and semi-terrestrial taxa but extends to higher PC1 than the other groups, an

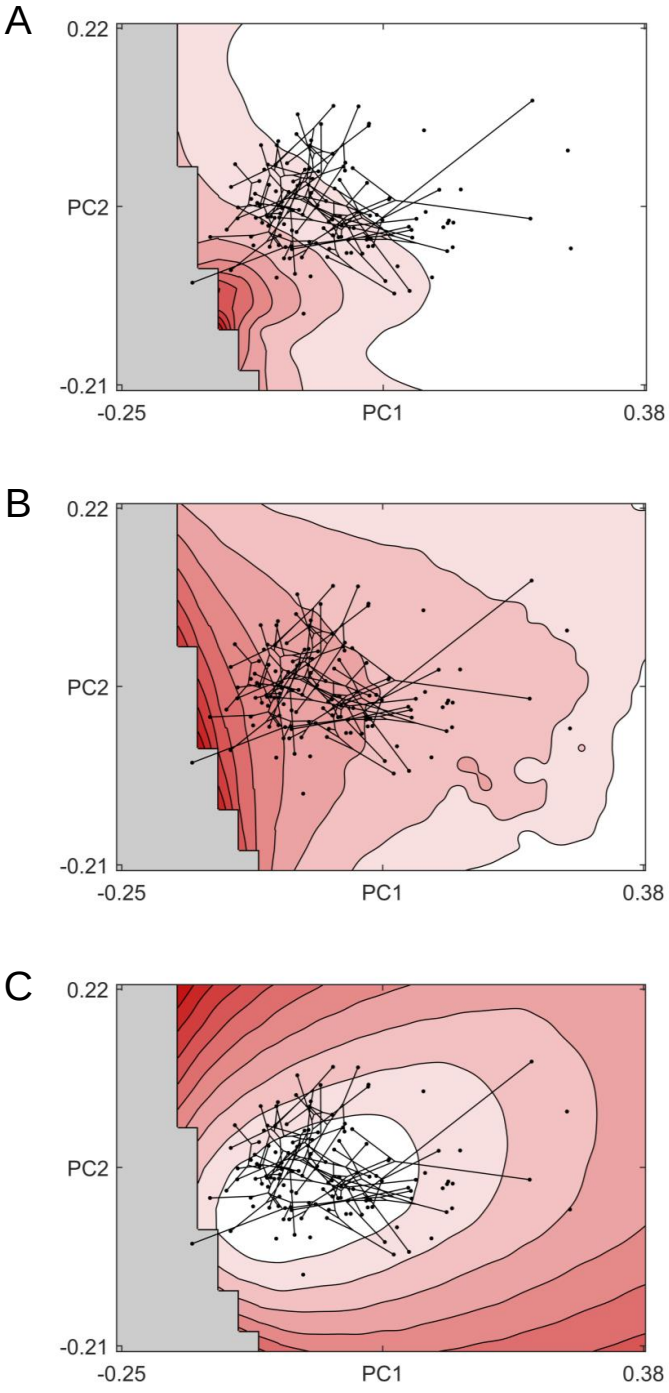

Figure 3.4: Functional performance landscapes of early tetrapod jaw shape. **(A)** Von Mises Stress (VMS), **(B)** Rotational Efficiency (RE) and **(C)** Jaw Height (JH). Darker colours represent higher functional metrics. Circles and black lines represent phylomorphospace.

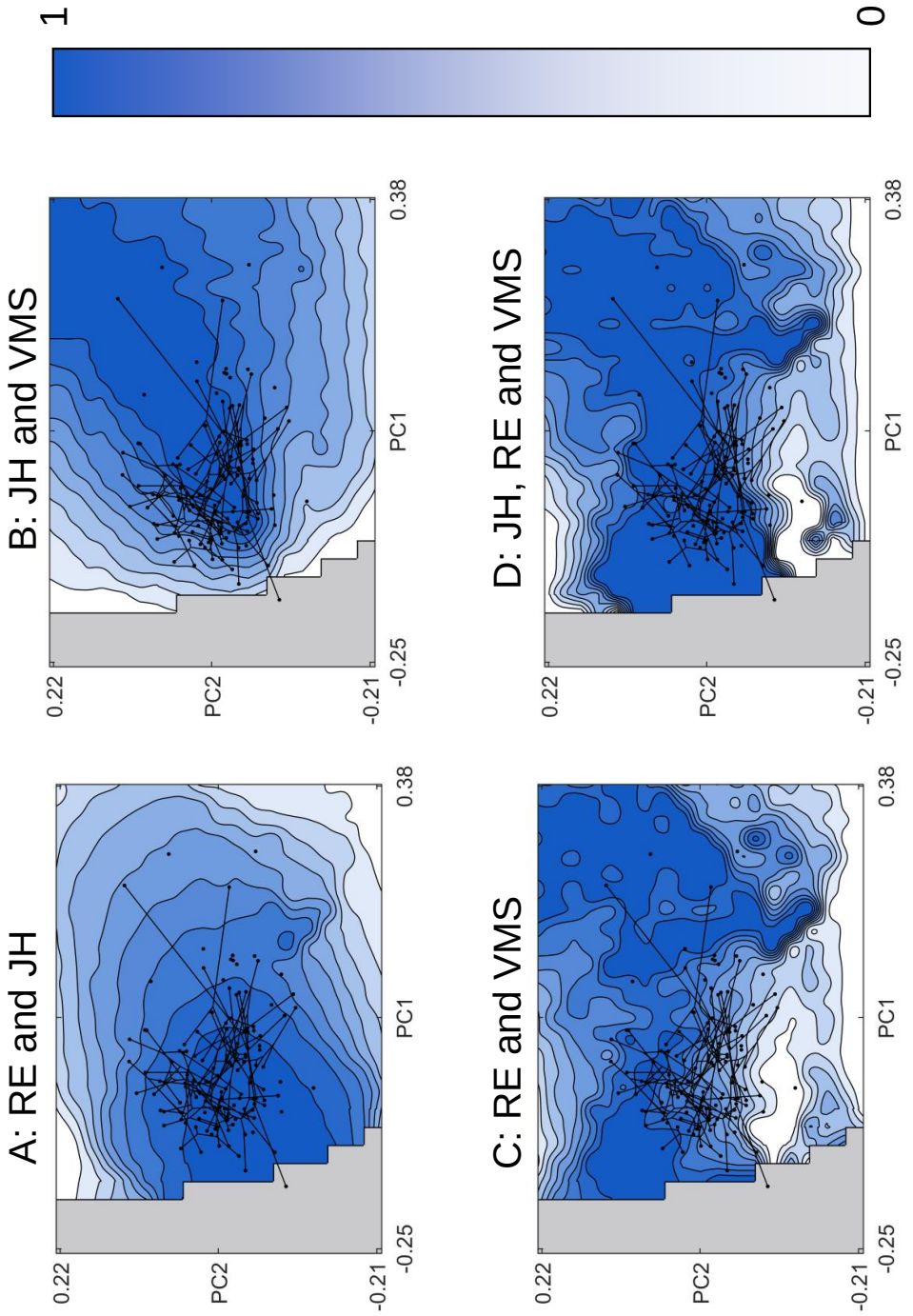

Figure 3.5: Pareto optimality landscapes of early tetrapod jaw shape. (A) Optimality in the tradeoff for Von Mises Stress (VMS) and Rotational Efficiency (RE). **(B)** Optimality in the tradeoff for Von Mises Stress (VMS) and Jaw Height (JH). **(C)** Optimality in the tradeoff for Rotational Efficiency (RE) and Jaw Height (JH). **(D)** Optimality in the tradeoff for Von Mises Stress (VMS),Rotational Efficiency (RE) and Jaw Height (JH). Circles and black lines represent phylomorphospace.

area that corresponds with deeper jaw shapes which are stronger but less rotationally efficient. However, the overlap is significant and results in similar functional qualities between all groups (figure 3.6). This shows that some aquatic jaw morphologies could function adequately on land. Our results show that terrestriality does not force a migration in jaw morpho-functional space, but allows new space to be explored.

We tested the optimality of aquatic, semi-aquatic and terrestrial taxa within each of the three performance and four Pareto surfaces. Firstly, we find that the range of performances occupied by each group does not vary significantly, with the exception that aquatic taxa occupy a much wider range of higher jaw heights compared to semi-aquatic and terrestrial taxa (figure 3.6). This is contrary to our hypothesis that aquatic taxa would be biased towards thinner jaws to minimise the hydrodynamic profile. When considering the Pareto surfaces, we expected that the surface that results in the highest mean optimality of real taxa with the fewest performance components would represent the functional trade-off acting on the jaw. We find that aquatic and semi-aquatic taxa are heavily optimised within the three-way trade-off between jaw strength, rotational efficiency and height (figure 3.6). However, terrestrial jaws are not constrained by this trade-off, or any other combination.

3.3.5 Phylogenetic signal

Using a multivariate K statistic [170] we find a significant, yet weak phylogenetic signal in the morphological data ($K_{mult} = 0.2502, p = 0.043$) suggesting that phylogenetic constraint on the evolution of early tetrapod mandibular morphology was weak. The phylomorphospace shows high convergence amongst jaw forms within the dataset, as the branches cross repeatedly (figure 3.2). Despite the weak phylogenetic signal, the amniote clade explores wider regions of morphospace, and their common ancestor is reconstructed outside the regions of non-amniotic tetrapod morphospace.

3.4 Discussion

Our results show that aquatic and semi-aquatic tetrapod jaws have tighter functional constraints than their terrestrial descendants. Terrestrialisation did not force a change in jaw morphology and function, but allowed some taxa greater freedom to explore broader jaw morphospace. Phylogenetic signal in jaw morphology is weak, with many lineages crossing one another in the phylomorphospace, however the radiation into new morphospace is limited to amniotic taxa (figure 3.2). Our optimality landscapes show that the trade-off between strength, speed and hydrodynamics plays a noteworthy role in constraining almost all aquatic jaw morphologies, however it is less important to terrestrial taxa. Terrestriality must bring with it some change in functional demands beyond these metrics, possibly due to the evolution of static pressure feeding systems and herbivory. Specifically, these feeding modes require large jaw musculature, giving selective advantage to jaws with greater area for muscle attachment [308]. The obsoletion of suction feeding during terrestrialisation does not appear to apply constraint on morphospace occupation. Specifically, the similarity in performance occupation between terrestrial and aquatic taxa suggests that additional functional metrics became important to terrestrial taxa, or a replacement of functional criteria. Ultimately, this may suggest that imposing new selective pressures on an evolving

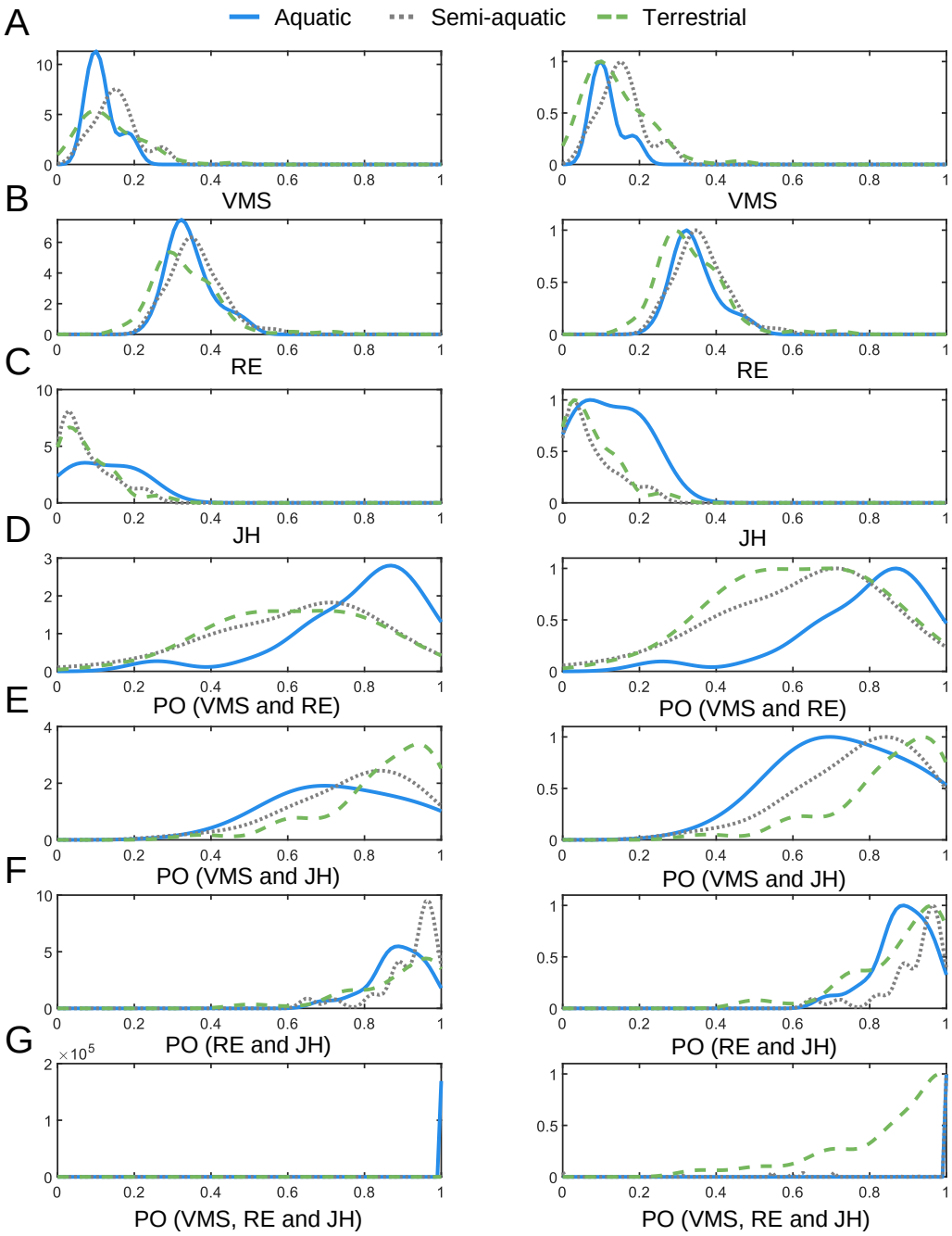

Figure 3.6: Distributions of functional performance and optimality in aquatic, semi-aquatic and terrestrial tetrapods. Kernel density probability distributions of performances and optimalities within each major ecological group. Kernel density is scaled to the maximum across all groups in the left column and to the maximum within each group in the right column. **(A-C)**, x axis represents individual trait measures, normalised to the range of theoretical performance. **(D-G)**, x axis represents Pareto optimality ranking, where 1 = most optimal jaw shapes for the combination of performance variables. Performance metrics are generally similar between groups, except in aquatic taxa where jaw height is more variable. The trade-off between VMS, RE and JH constrains aquatic and semi-aquatic taxa to optimal areas, but not terrestrial taxa.

system may allow more evolutionary freedom, rather than constraint. This hypothesis can be further tested by assessing the optimality during the many transitions from land to water in descendent tetrapod lineages, where the hypothesis expects aquatic taxa to be more constrained than their terrestrial ancestors.

While aquatic taxa (including semi-aquatic taxa) are constrained by optimality, they do not explore all Pareto optimal regions of morphospace. Therefore, there must exist some further constraint on their morphology not captured by our functional model. This could be a phylogenetic or morphogenetic constraint. While the phylogenetic signal in these morphological data is weak, wider areas of morphospace are occupied by amniotes and some diadectomorphs (figure 3.1, 3.2). However, amniotes in this dataset are almost entirely terrestrial, so untangling the phylogenetic and functional biases on jaw form is difficult. The aquatic amniote *Mesosaurus* lies beyond the range of non-amniotic aquatic taxa, suggesting that the constraint on aquatic taxa may be partially phylogenetic (figure 3.1). However, *Mesosaurus* also does not lie in the extended region of terrestrial morphospace. Still, areas of Pareto optimal morphospace remain unoccupied by all taxa within this dataset. This could be due to thresholds acting on the individual performance metrics - for example, there may be a minimum strength the jaw must exceed in order to perform. Theoretical morphologies below this threshold can still be considered optimal if they have high rotational efficiency or a low jaw height.

Morphogenetic constraints may also play a role in the constraint of non-amniotic tetrapod jaws. Metamorphosis has been characterised in non-amniotic tetrapod fossils from this period, with the majority of taxa exhibiting aquatic larval forms [329]. Aquatic larval stages can act to constrain and promote diversification in adults [174]. However, studies on salamander morphology have shown that metamorphosis has promoted morphological diversification in bones associated with feeding [330]. Instead, the limitation may arise from complex life cycle shifts during metamorphosis, between aquatic and terrestrial environments [331]. Furthermore, the need to return to water for reproduction may strongly enforce these constraints, which provides an explanation for the similar constraint acting on both aquatic and semi-aquatic jaws. The evolution of the amniotic egg would thus relieve this constraint, by allowing fully terrestrial juvenile forms, providing an explanation as to why some amniotes cross this morphospace boundary and explore greater PC1 regions.

Alternatively, this constraint may be lifted by the evolution of a fully terrestrial feeding system, with a mobile neck and the remodelling of the ancestral hyobranchial system [322] Some aquatic taxa can feed on terrestrial food sources by either carrying them back to the water, or pumping water through the mouth to aid in intraoral transport of food [306, 313, 315, 317, 319–321]. With the evolution of mobile necks and a prehensile tongue, the jaw may be alleviated from the evolutionary pressure to pump water efficiently. Future studies linking the morphology of the hyobranchial apparatus with jaw optimality can text this hypothesis.

Together, these results show that functional constraint is strong in defining aquatic jaw forms. Terrestriality does not represent a shift away from these functionally optimal morphologies, but a dispersion into new morphospace. Whether this release of constraint

is due to environmental change, the evolution of herbivory and amniotes, or modifications to the hyobranchial system is uncertain. Previous studies have shown a temporal delay in tetrapod jaw functional transition following terrestrialisation [198, 199], suggesting that the constraint is released by the evolution of herbivory and amniotes. While tetrapods were undertaking a radical transition in many aspects of their phenotype during the colonisation of terrestrial environments, their jaws were still constrained to ancestral aquatic morphologies and functions, which had already reached a peak in functional optimality. The evolution of amniotes and terrestrial herbivory relaxed constraint on jaw morphology, by shifting the functional demands on the jaw system and releasing morphogenetic constraint.

Chapter 4

The relationship between functional optimality and topological complexity in mammalian jaws

Author's contribution This chapter and all analyses within were completed by William J. Deakin. A large proportion of the dataset not collected by William J. Deakin was collected by (in alphabetical order): Josh Anderson, Sidney Davies, George Duffin, Soph Fasey, Jack Lovegrove, Spencer Pevsner, Iain Ratter, Andrew Shepherd, Philip Vixseboxse, Oliver Weeks, Winston Wilson and Alistaire Wu.

Abstract

The reduction in the number of mandible bones to a singular dentary bone is a characteristic feature of mammals. This change in jaw structure has interesting implications for the evolution of jaw function and complexity. The Zero Force Evolutionary Law (ZFEL) suggests that, in the absence of other evolutionary forces, the complexity of evolving structures should increase over time. The mammalian jaw therefore represents a counter example to this law, or a case in which evolutionary forces are selecting for jaws with lower complexity. To test the latter hypothesis, I measured the morphology of a large dataset of mammal jaws to generate a theoretical morphospace of jaw shape. The functional optimality in the trade-off between jaw strength and rotational efficiency was compared with the topological complexity of theoretical jaw shapes, and the evolution of mammalian jaw shape was observed within the resulting optimality and complexity landscapes. I find that mechanical optimality and complexity are inversely correlated, and that the majority of mammal jaws are constrained to morphospace regions of high optimality and low complexity. Complex jaw shapes are less functionally optimal, and are thus selected against on macroevolutionary timescales, providing an evolutionary force that overcomes the trend of the ZFEL.

4.1 Introduction

Mammals are a very successful and ecologically diverse group of vertebrates, with other 6,000 extant species [332–334]. Having developed from small nocturnal taxa in the Mesozoic to the wide variety of terrestrial and aquatic niches exhibited today, including the evolution of powered flight, mammals represent an evolutionary success story of radiation following the end Cretaceous extinction and the subsequent Cenozoic era [335–338]. Mammals share various autapomorphic traits that may help explain this success, including fur, the production of milk, and the evolution of the bones of the middle ear [339, 340]. The middle ear bones evolved from the posterior bones of the lower mandible, which has resulted in another unique adaptation of mammals – the reduction of the mandible to one bone, the dentary [339, 341, 342]. How did this transition effect the morphological evolution of the jaw? Here, I aim to test how this transition and the subsequent radiation of mammals impacted two aspects of the morphological evolution of their jaw: its functional optimality and complexity.

Functional constraint acts on morphological evolution in tandem with phylogenetic and morphogenetic constraint [22]. However, the interaction of functional and morphogenetic constraints on the mammalian jaw is not clear. In the case of mammals, the consolidation of the jaw may provide some functional advantage by allowing finer control at the jaw joint and increasing its total strength [332]. We may expect this to relax the functional constraint on jaw shape, as the total strength of all shapes is increased, allowing some freedom to explore weaker shapes. On the other hand, we may expect that the reduction in morphogenetic integration of the jaw structure allows functional constraint and integration to dominate, as has been demonstrated in other structures and clades [68, 343–347]. However, these changes in modularity can also have little effect on morphological constraint, or even promote diversification [346, 348]. It is worth noting that this reduction in jaw bones may not represent a total reduction in their modularity and integration, as the middle ear bones still develop together with the dentary during development, and the single dentary bone is comprised of a number of developmental modules [349, 350].

How does this reduction in bones relate to the evolution of complexity? The tempo and mode of the evolution of biological complexity is an unresolved problem in evolutionary science. At the largest scales, it is generally agreed that complexity has increased [351–353]. For example, it is intuitive that the diversity of multicellular eukaryotic organisms and structures hold more complex information in their structure than single celled prokaryotes. Yet, whether this increase represents an active trend towards complexity, or a passive trend with a hard minimum, is not well understood [352, 354, 355]. Williston's law postulates that the number of parts within a biological system tends to decrease over time, while the differentiation between those parts increases, and this has been ascribed to vertebrate skull morphology [343, 344, 356]. In the case of the mammalian jaw, the number of parts is reduced to one, so comparison between parts is impossible. However, we can measure the complexity of jaw shape to determine whether it has become more or less topologically complex following this transition.

At the heart of this question are the drivers of complexity. Are there evolutionary benefits to simpler or more complex systems? Many investigations into biological complexity and its evolution have drawn parallels with engineering, and the increasing complexity and optimality of modern technologies. A system with higher complexity between parts, where many different sub-systems cooperate to perform a vast array of different functions, does seem to be favoured in both biology and engineering [353]. In biological systems, this can in part be explained by the Zero Force Evolutionary Law (ZFEL), which is the tendency for complexity to increase in evolving systems [354]. However, many engineers will assure you that, often, the simplest solution is the best. How does the functional optimality of a jaw relate to its topological complexity? Finally, in the case of mammals, how do the two interact in the evolutionary time between their origin and their present diversity?

The distribution of optimality and complexity amongst evolved forms is not enough to answer these questions. To discern whether the evolving system has a bias towards either, the variety of evolved forms must be compared with a control group of non-evolved theoretical shapes. Theoretical morphology, therefore, has the potential to be a powerful tool for evolutionary biologists [87]. By allowing empirical assessment of not just evolved, but non-evolved shapes, theoretical morphology can help answer many questions about the biases and forces that shape morphological evolution. Before we implement this tool, however, we must have a good understanding of how to use it. One basic question to ask is how do we build those theoretical morphologies? There is an infinite spread of possible shapes that could be assessed, so how do we choose which ones to test? The common solution is to take the mean shape of an empirical dataset and extrapolate along each axis of morphological variation, as has been utilised on hypercarnivore skulls [119], turtle shells [85, 120], and on jaw shapes within this thesis [192]. Assuming that the metric being tested, z, is continuously associated with each morphological axis, z can be interpolated between empirically tested points.

This has been successful for morphospaces with low numbers of dimensions, as these can be densely populated with a grid, or a dense point cloud, which allows for high resolution surfaces [62, 284]. However, the ability to sample with an adequate resolution diminishes exponentially with increasing dimensionality. In cases where the morphospace has a high number of dimensions, it is common practice to perform a PCA and reduce the morphospace down to 2 or 3 main axes of variation [85]. This can then be gridded to assess the theoretical range of 'general' morphologies, representing average shapes in less important axes of morphology. When these PC component morphospaces represent a lower proportion of shape variation within a dataset, it is possible that the unassessed axes of morphological variation provide important informative value that is missed [78].

Here, I investigate the optimality of 1,735 2D lateral total-group mammal jaw morphologies, sampling across the transition to a single dentary jaw, and then interrogating the subsequent modern morphological diversity. As the functional biases acting on jaw shapes remain similar, while the morphogenetic processes defining the jaw change across this transition, I hypothesise that mammal jaws are optimised within a trade-off for strength and rotational efficiency, and that there is a difference in optimality between the ancestral

non-mammalian therapsid multi-bone jaw and the mammalian dentary. I hypothesise that this transition also leads to a change in topological complexity, and that complexity and functional optimality are correlated. I use a theoretical morphology, function and Pareto optimality approach to generate an optimality landscape of jaw strength and speed [192]. Following this, I assess the variation in shape complexity across theoretical morphospace, to visualise whether the reduction in jaw complexity by parts represents a concurrent change in topological complexity. This is then compared with the optimality landscape, to assess the relationship between optimality and complexity. This pipeline will be applied to two separate theoretical morphospaces, constructed through different algorithms. These theoretical morphospaces will be tested for their interpolative accuracy and precision compared to functional analysis of empirical morphologies. This will be combined with a phylomorphospace, to assess how the phylogenetic, morphogenetic and functional biases interact in the evolution of mammalian jaw morphology.

I find that all mammals exhibit remarkably conserved jaw morphologies, with a weak phylogenetic signal in the dataset. Early therapsid jaw forms lie in a subset of this mammalian dataset, suggesting that the reduction of lower jaw bones released some constraint on jaw form. Ancestral therapsid multi-bone jaws were significantly less optimised and complex than the dentary bones of their mammalian descendants. Following this transition, optimality remains consistently high and complexity relatively low in the majority of mammalian lineages, with the exception of the ungulates. Ungulate jaws show a marked decrease in optimality and an increase in topological complexity. Finally, the 2D grid theoretical morphologies, topological complexity is inversely correlated with optimality. These relationships break down when utilising an N-Dimensional (ND) point cloud theoretical morphospace, however this structure fails to sample large regions of unexplored morphospace. Thus, I conclude that the 2D grid is the preferable methodology for assessing trends in macroevolutionary data. Mammalian jaw morphology was released of some constraint following the evolution of the middle ear. This allowed further exploration of more functionally optimal morphospace, allowing functional constraint to become dominant over the majority of mammal clades, which further limited the evolution of their shape complexity.

4.2 Methods

4.2.1 Empirical and theoretical morphology

I used EFA [112] to characterise the 2D lateral outline shape of 1,735 extant and extinct therapsid taxa. 200 landmarks were automatically placed around the outline, which were then input to the EFA pipeline. 12 size and rotation corrected elliptical harmonics characterised $> 99\%$ of shape in $> 99\%$ of the jaw shape dataset, resulting in a morphospace with 45 (12×4–3) dimensions. A PCA of this dataset revealed that 58.9% of shape variation could be captured in the first two principal component axes, and 99% of shape is captured by the first 24 axes (figure 4.1). These data were then used to construct two distinct theoretical morphospaces.

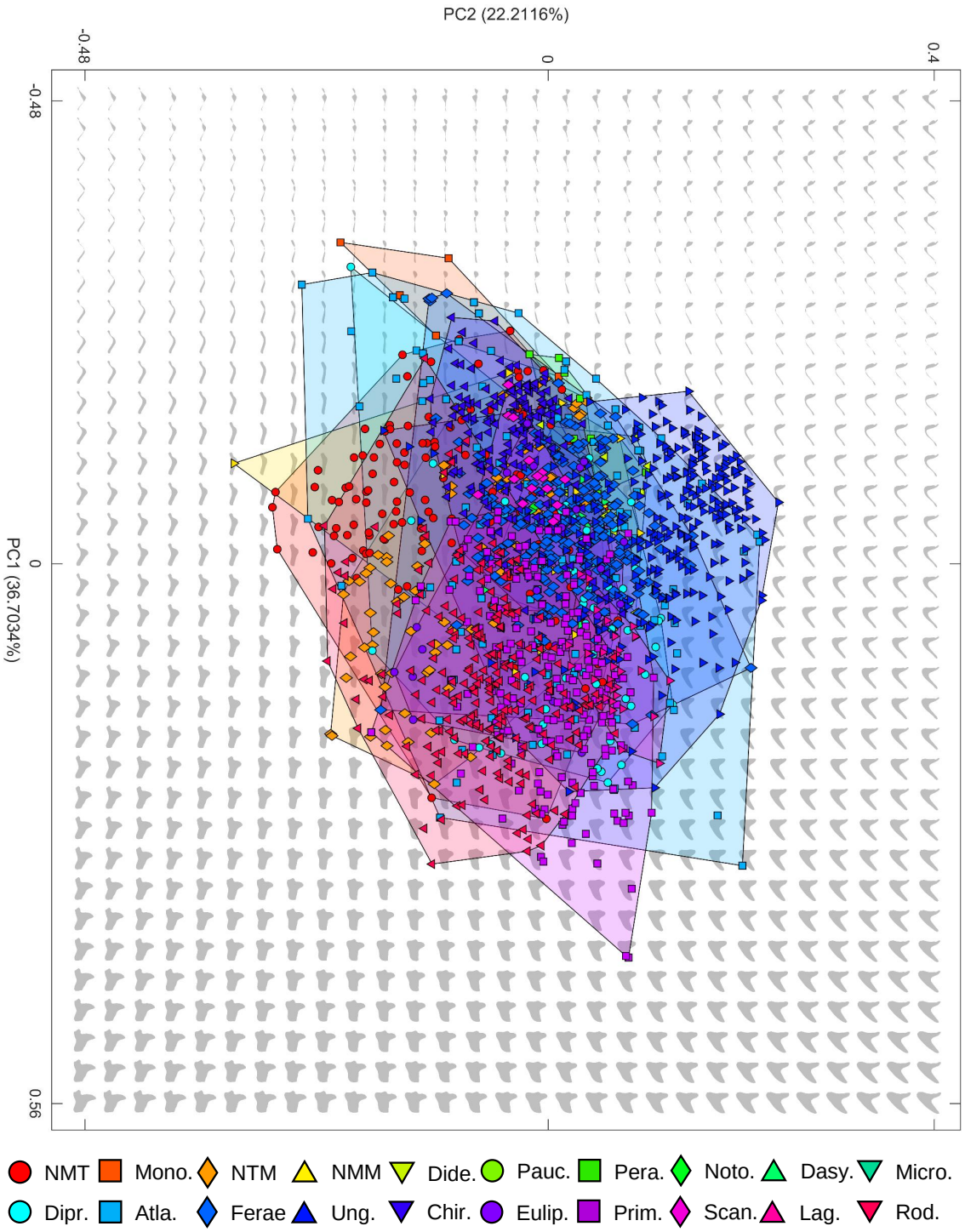

Figure 4.1: Empirical and theoretical morphospace of therapsid jaws. PCA morphospace of an EFA dataset of 1,735 therapsid jaws, ranging from Permian therapsids to the variety of extant mammals. Grey shapes represent the 2D grid theoretical morphospace, coloured symbols represent the empirical morphospace, split into 20 clades: Non-Mammalian Therapsids (NMT); Monotremata (Mono.); Non-Therian Mammals (NTM); Non-Marsupial Metatherians (NMM); Didelphimorpha (Dide.); Paucituberculata (Pauc.); Peramelemorphia (Pera.); Notoryctemorphia (Noto.); Dasyuromorphia (Dasy.); Microbiotheria (Micro.); Diprotodontia (Dipr.); Atlantogenata (Atla.); Ferae; Euungulata (Ung.); Chiroptera (Chir.); Eulipotyphla (Eulip.); Primates (Prim.); Scandentia (Scan.); Lagomorpha (Lag.) and Rodentia (Rod.).

The first theoretical morphospace sample was constructed using a 2D grid, similar to the majority of adaptive landscape studies (figure 4.1) [85, 120–123, 201]. The theoretical grid has advantages in its visual clarity, which helps interpretation of adaptive landscapes. It also allows spatially consistent sampling across morphospace. However, when incorporating higher dimensions of morphometry, the number of theoretical shapes generated increases exponentially, thus many of these studies have limited their scope to 1,2 or maybe 3 axes of variation. Finally, the limits of the theoretical grid are often arbitrarily set or confined to the bounding box of empirical data. This often obscures the nature of theoretical morphospace around extreme empirical morphologies. 986 theoretical jaw shapes were generated in a 34-by-29 grid across PC1 and PC2. 216 shapes were constructed as self-intersecting loops; therefore, they were identified as geometrically impossible structures and were omitted from the dataset.

The second theoretical morphospace was constructed via a random normally distributed sample of points with variation in all 45 axes of morphospace. The standard deviation of the random sample was matched to the variation in each PC axis. This results in a sample of theoretical morphologies that capture all axes of shape variation and fill the region of morphospace bounded by the empirical data. 1,000 random shapes were generated. Impossible structures were omitted, and another random shape generated to take their place. Similar approaches have been applied for understanding the limits of theoretical morphospace in discrete character data, given measured character contingency [124].

4.2.2 Functional performance and optimality

All functional analyses performed on theoretical jaw shape were following methodology described in chapter 2, with each analysis performed 1,000 times with pseudorandom input constraints. Each theoretical shape was converted to a mesh with approximately 2,500 elements. Thus, jaw optimality is here measured within the trade-off between rotational efficiency and strength. The algorithmic constraints, randomisation and functional analysis was also performed on the theoretical point cloud in the same manner. Finally, functional analysis was also performed on all 1,735 empirical jaw shapes, for comparison between the two theoretical morphospaces. This resulted in a total of 3,505,000 FEMs. Optimality within this trade-off is measured using the Pareto rank ratio.

After testing the function of the empirical shapes directly, I could assess how accurate and precise each performance surface was when interpolating function. There are four performance surfaces total: 1) The VMS surface generated from the 2D theoretical grid; 2) The RE surface generated from the 2D theoretical grid; 3) The VMS hypersurface generated from the N-Dimensional theoretical point cloud; 4) The RE hypersurface generated from the ND theoretical point cloud. Function was interpolated on each surface at the PC scores of empirical taxa. For the 2D grid surfaces, a cubic grid interpolation was used to infer empirical function. For the ND point cloud hypersurfaces, a linear extrapolation along the Delaunay triangulation of the point cloud was used. However, the computational processing time of the high dimensional interpolation grows exponentially with increased dimensionality, so no more than 7 PC axes could feasibly be used in this interpolation.

Furthermore, as more axes are added to the ND interpolation, more empirical taxa lie outside the bounds of the point cloud and thus could not be interpolated.

To assess the accuracy and precision of the surfaces, a linear regression was performed on the direct empirical function against the extrapolated empirical function. Here, I define the accuracy of a surface as its ability to interpolate the absolute value of the empirical data. I define the precision of the surface as its ability to interpolate the relative values of the empirical data with respect to one another. An accurate surface matches the 'real' surface perfectly, whereas a precise surface matches the shape and contours of the 'real' surface, though its absolute values are scaled and shifted. Thus, a linear regression between empirical and interpolated function should yield a relationship close to $y = x$ on an accurate surface, and the R^2 of this regression denotes the precision of the surface.

4.2.3 Topological complexity

I measured topological complexity via three separate metrics: Fractal Dimension (FD); Dirichlet Normal Energy (DNE); and Alpha Shape (AS) [357–359]. Each of these metrics is dependent on arbitrary input parameters, which were varied in order to observe their impact on both the scale of the output surface (the variation in magnitude of results) and the shape of the output surface (the location and shape of the surface contours).

FD was calculated by reconstructing each theoretical shape from its harmonic data at different resolutions and calculating the perimeter of the shape at each resolution. The fractal dimension is defined as the slope of the line formed by plotting the log of the size of each measurement and the log of the total perimeter measured. Therefore, it is somewhat dependent on the arbitrarily defined sample of measurements. As an example, you may get different results for FD if you measured 10 different perimeters varying from a ruler size of 10 units to 100 units, than if you measured 100 different perimeters varying form a ruler size of 50 units to 150 units. Therefore, I opted to calculate 3 FD surfaces with a variety of sampling: a sample of 10 perimeter calculations where the ruler varies from 1% of the shape outline to 0.5% of the shape outline; a sample of 40 perimeter calculations where the ruler varies from 1% of the shape outline to 0.2% of the shape outline; and a sample of 90 perimeter calculations where the ruler varies from 1% of the shape outline to 0.1% of the shape outline.

DNE was calculated following a modififcation of the ariaDNE protocol outlined in [358] to fit 2D data. The Dirichlet energy of a mathematical function is a measure of how much that function varies with changing input. In the case of DNE, the function being measured is the curvature of a surface in 2 or 3 dimensions. ariaDNE uses PCA of vertices within a 'bandwidth' around each point on the surface to approximate curvature and sum it across the entire shape. This has often been used on the 3D topology of teeth as a proxy for dietary ecology [360–363]. This metric is heavily dependent on the input bandwidth, so I calculated DNE surfaces using 4 different bandwidths: 0.02, 0.04, 0.08 and 0.16.

Finally, the AS metric is derived from a tool from computational geometry that fits a tight boundary around a point cloud, called an alpha shape. The alpha shape function takes in an input parameter called the alpha radius (α). As the α increases from zero to infinity, the resultant alpha shape becomes a 'looser' boundary around the point cloud

until it becomes the convex hull at $\alpha = \infty$. Here, the alpha shape function is utilised to try and reconstruct the original shape from a random point cloud. Firstly, a random point cloud is generated within the bounds of the original shape. Then, this point cloud is input into the alpha shape function, and the ratio between the area of the alpha shape and the original shape is recorded. This process is iterated with increasing alpha radius until this ratio between areas reaches its closest value to one. That is, the alpha shape that most closely resembles the original shape. This critical value of the alpha radius is recorded as the AS metric and used as a proxy for complexity. It is worth noting that this metric is inversely proportional with complexity. As complexity increases, AS decreases. This metric is dependent on the number of points in the initial point cloud generated [359]. Therefore, surfaces were generated at 3 different point cloud sizes: 100 points, 1,000 points, and 10,000 points.

Taxon complexity was extrapolated from each surface, along with their optimality, to observe the distribution of complexity and optimality across the transition from a multi-bone jaw to a single dentary jaw. These distributions were then compared against one another for each complexity metric and the Pareto rank ratio metric using a Wilcoxon rank sum test (figure 4.6).

4.2.4 Phylogenetic analysis

A consensus tree with branch lengths was generated from a downloaded sample of 1,000 trees from [364], which included 1,031 taxa from the sample of 1,735 taxa (figure 4.2). I achieved this using the consensus.edges function in the R package phytools [365], using the default settings (majority rule consensus with mean edge branch lengths). The R package geomorph was then used to assess the phylogenetic signal (K_{mult}) of the data and perform maximum likelihood ancestral state reconstruction (functions physignal and gm.prcomp) [280], as in chapter 2 and chapter 3. Ancestral state morphologies were then used to interpolate functional metrics from the performance surfaces, to visualise the evolution of function throughout the mammalian tree. Ancestral state interpolation was performed on both the 2D and ND hypersurfaces for VMS, RE and optimality. All R analyses were performed with R v.3.6.1.

4.3 Results

4.3.1 Morphology

The first two PC axes of shape variation represent a variety of jaw shapes that vary in their depth and curvature, similar to the range in chapter 2 and 3 (figure 4.1). However, the theoretical shapes generated differ from the previous chapter as they possess a distinct coronoid process. There is a considerable proportion of shape variation not captured by these axes as only 58.9% of shape variation is present in PC1 and PC2. There is also a considerable region of geometrically impossible space limited to the lower PC1 values on the left of the morphospace plot. Some slim mammalian jaws occupy impossible space.

Despite a broad variety in jaw shape within this morphological dataset, the majority of mammalian and non-mammalian therapsid groups overlap in the first two axes of jaw morphospace (figure 4.1). This is corroborated by a significant but weak phylogenetic

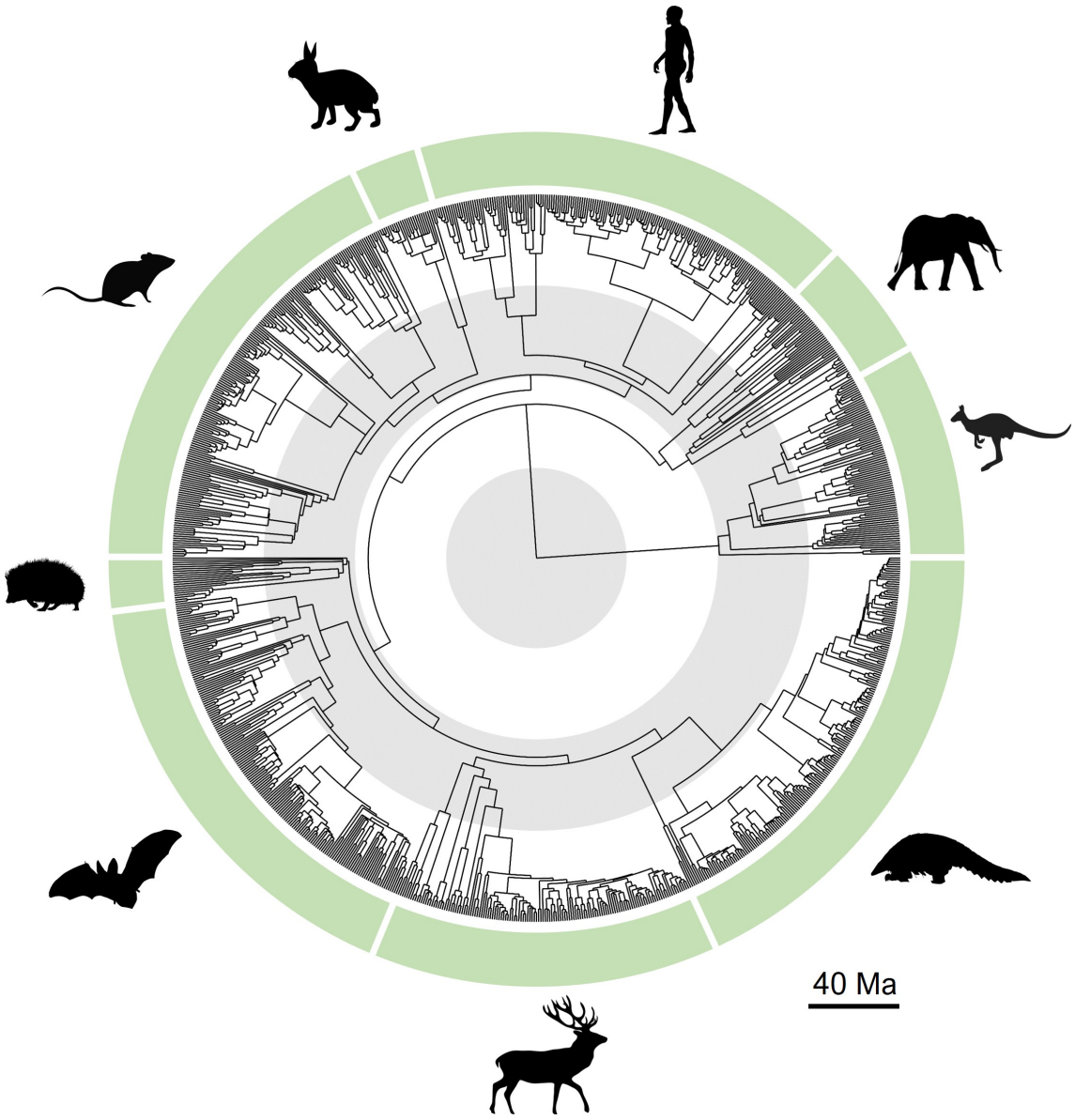

Figure 4.2: Phylogenetic relationships of study taxa. Dated phylogenetic tree used for all phylogenetic analyses in this study. This includes 1,031 taxa from the sample of 1,735 jaws. Grey and white bands represent 40 million years. Pruned from [364].

signal in the EFA data ($K_{mult} = 0.1997, p = 0.001$). Furthermore, the phylomorphospace is a complex web of intersecting branches. Together, these results indicate a high level of convergent evolution, as many similar shapes re-evolve in separate lineages. This in turn suggests that the phylogenetic control on mandibular form is weak when compared to other controls on form such as function and development.

4.3.2 Function

Within the 2D grid theoretical morphospace, there is a clear trade-off between jaw speed and strength (figure 4.3). The major axes of shape variation represent a trade-off between strong, deep jaws that are relatively short and rotationally inefficient, and long, thin jaws that are very energy efficient but also very weak. When testing the ND point cloud morphospace, this trade-off is still exhibited (figure 4.3) but a considerable variation in function dilutes the strength of the trade-off.

The accuracy and precision of each surface when interpolating empirical data was generally very low (figure 4.4). Even including 7 shape axes in the ND point cloud interpolation, which cumulatively represent approximately 87% of shape variation, the R^2 values of the linear regression are 0.5122 and 0.4246 for log VMS and RE respectively, indicating mediocre precision. The log VMS line has a slope of 0.5846 and an intercept of 2.2282, and the RE line has a slope of 0.5035 and an intercept of 0.9138. In both cases, an accurate surface would produce a line with a slope of 1 and an intercept of 0. The 2D theoretical grid morphospace performed worse, with an R^2 for log VMS and RE of 0.3346 and 0.1066 respectively; slopes of 0.4116 and 0.1979 respectively; and intercepts of 2.9443 and 1.4457 respectively. Overall, the VMS could be interpolated at higher precision and accuracy than the RE.

When interpolating the functional results on the mammalian tree, the results change dramatically depending on the surface used (figure 4.5). When using the 2D grids, there are consistent patterns within groups, with major changes focused along certain branches in the tree. Most notably, there is an increase in both VMS and RE within ungulates, conserved across the ruminant clade. However, when using the high dimensional interpolation, the evolution of both functional traits is more chaotic, with no clear conservation in the evolution of function within groups. Note, while the ND point cloud produces more accurate hypersurfaces, it is notably weaker in interpolating the function of more extreme shapes. This can be seen by the greater proportion of black branches in the ND point cloud interpolated trait phylogenies (figure 4.5), which represent shapes that could not be interpolated by the surface. There is also some phylogenetic bias to this phenomenon, most likely due to phylogenetic bias in shape. Lineages with extreme morphologies are less likely to be interpolated by the hypersurface.

4.3.3 Optimality

The differences in function between the different theoretical morphospaces propagate through to their optimality. When interpolating from a 2D grid, we see a pattern of extremely conserved, high optimality in almost all mammal jaws, except for ungulates and some primates. Even so, these relatively suboptimal taxa can still be considered optimal,

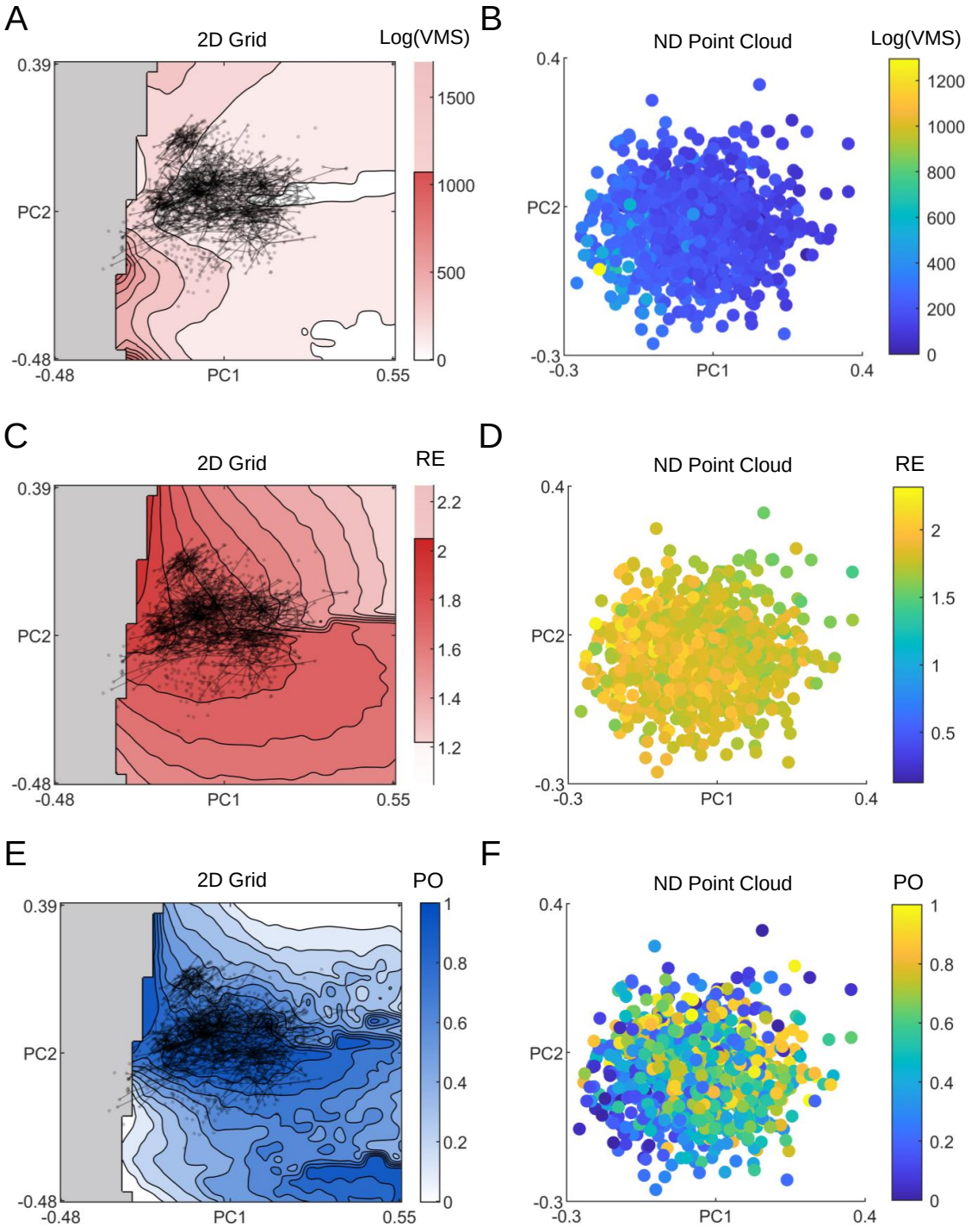

Figure 4.3: Functional performance and optimality surfaces. Two performance surfaces, Von Mises Stress (VMS) **(A,B)** and Rotational Efficiency (RE) **(C,D)**, were generated on each theoretical morphospace. Pareto Optimality surfaces **(E,F)** are then generated from these performance surfaces. Black lines overlain on the 2D grid landscapes represent the phylomorphospace. Point cloud positions represent the positions of ND point cloud theoretical morphospace projected into the PC1-PC2 plane.

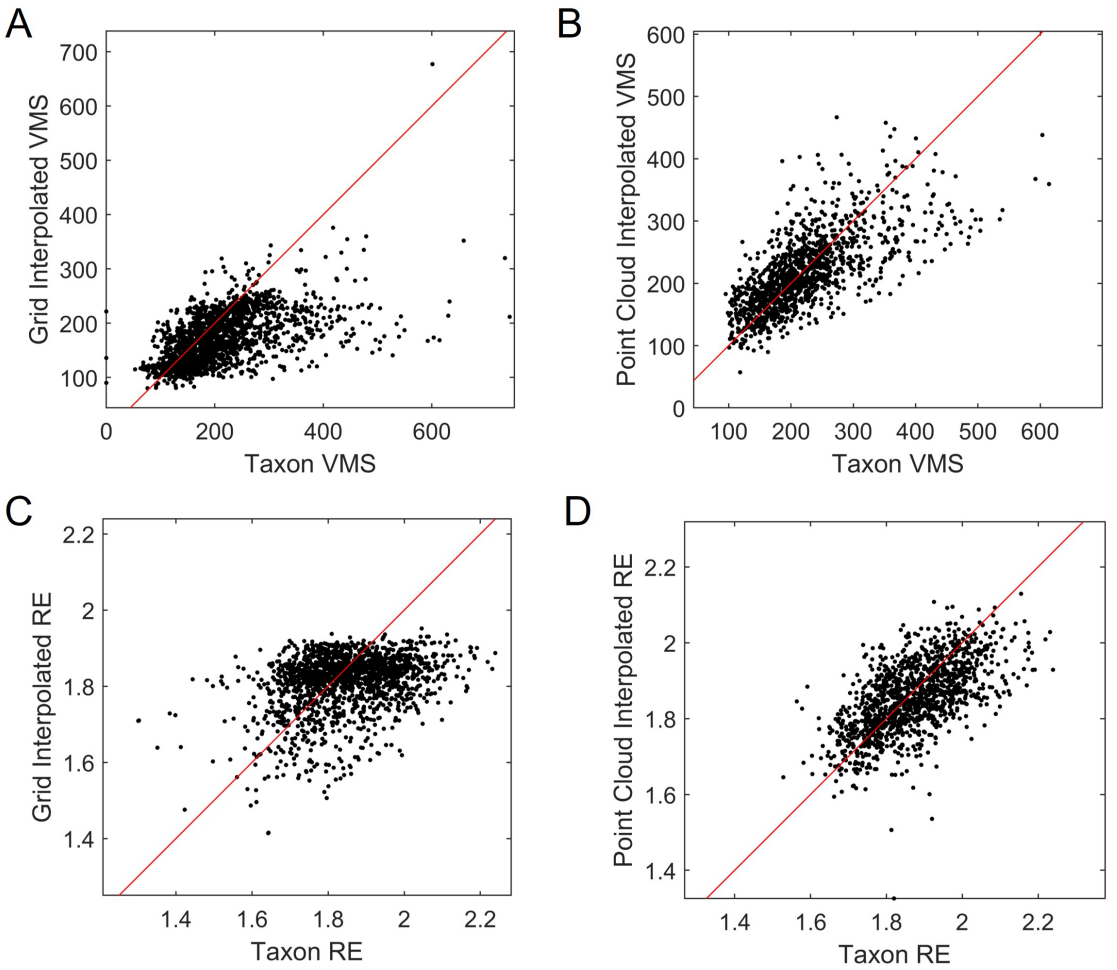

Figure 4.4: Accuracy and precision of theoretical morphospaces. (A) Empirical versus 2D grid interpolated VMS of study taxa. **(B)** Empirical versus ND point cloud interpolated VMS of study taxa. **(C)** Empirical versus 2D grid interpolated RE of study taxa. **(D)** Empirical versus ND point cloud interpolated RE of study taxa. A precise landscape will result in a tight correlation between measured and interpolated function, and an accurate landscape will generate a relationship close to $y = x$.

with Pareto rank ratio values above 0.5. This can be seen on the optimality landscape, as the phylomorphospace shows a convergent pattern of intersecting branches within optimal morphospace (figure 4.3). The optimality also seems to be conserved in time, with many deep nodes in the mammalian phylogeny remaining high on the optimality scale. This signal of high optimality throughout the mammalian tree is lost when interpolating from a hypersurface, however (figure 4.5). Single bone non-mammalian therapsid jaws showed a significantly lower distribution of optimality than the dentaries of their mammalian descendants ($p = 3.0276 \cdot 10^{-9}$) (figure 4.6).

4.3.4 Complexity

All three complexity metrics show consistent results across morphospace in all cases. Considering that the alpha shape metric is reversed (higher alpha shape radius = lower complexity), all three landscapes show the empirical taxa sitting within a trough of lower complexity compared to the theoretical range (figure 4.7). However, the ND point cloud

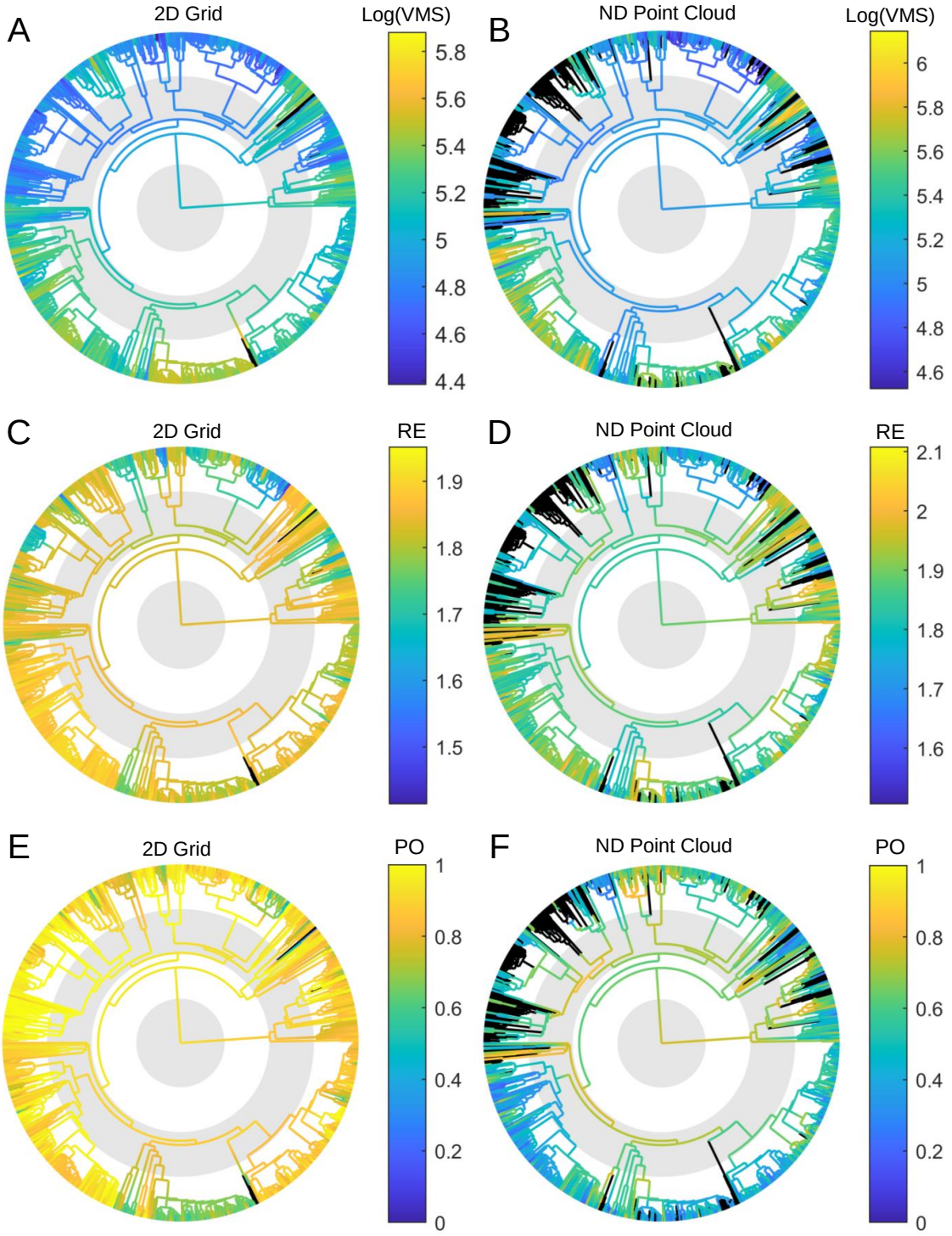

Figure 4.5: Functional results interpolated across the mammalian tree. The phylomorphospace was used to interpolate the function of each node in the phylogenetic tree according to each surface: **(A)** 2D grid log(VMS) surface; **(B)** ND point cloud log(VMS) hypersurface; **(C)** 2D grid RE surface; **(D)** ND point cloud RE hypersurface; **(E)** 2D grid Pareto optimality surface; **(F)** ND point cloud Pareto optimality hypersurface. Line colours represent trait values, black lines represent data that could not be interpolated by the surface.

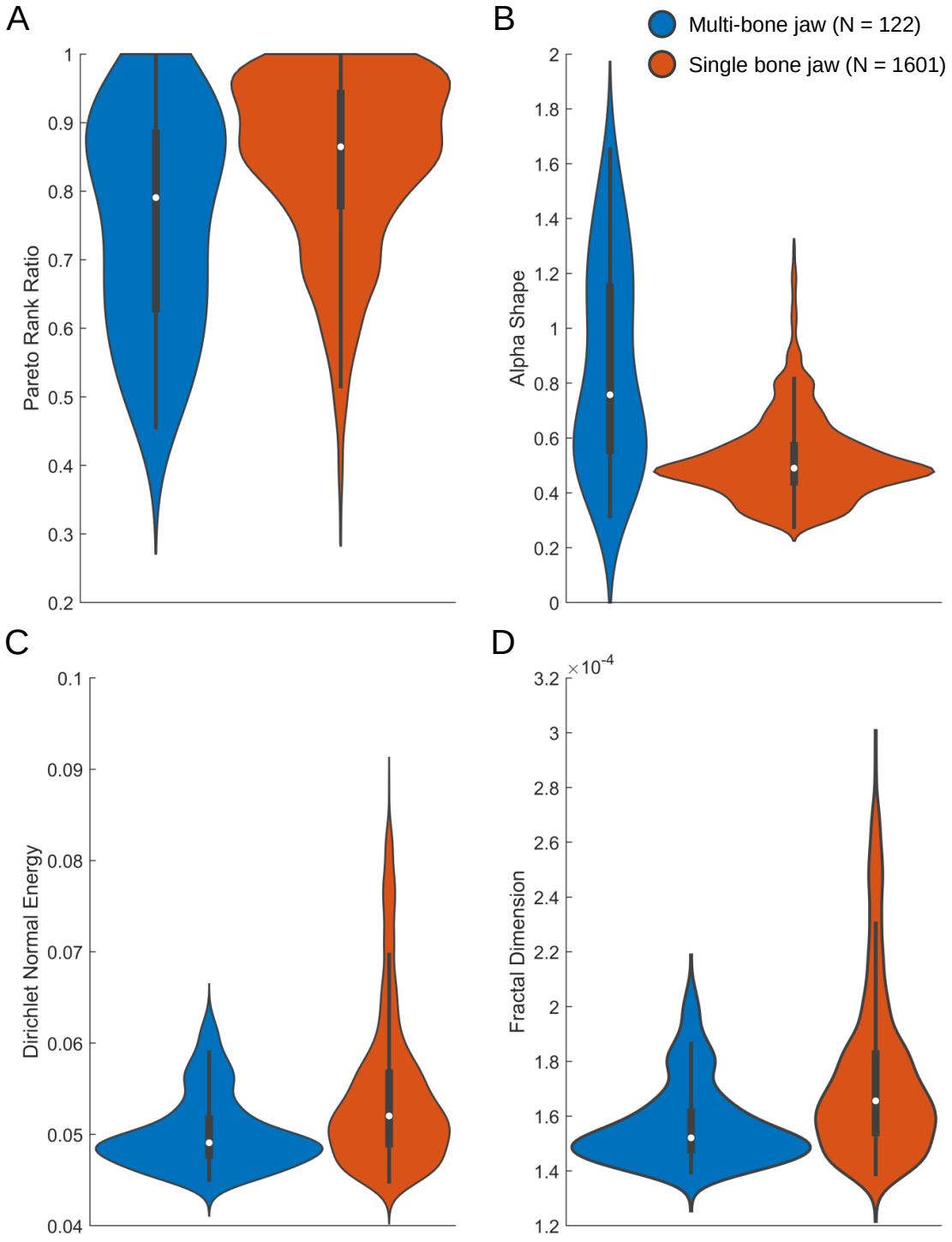

Figure 4.6: Optimality and complexity in single and multiple bone therapsid jaws. (A) Distribution of interpolated optimality values between different therapsid jaw constructions. **(B-D)** Distributions of interpolated complexity values between different therapsid jaw constructions. White dot represents median, thick black line represents interquartile range, thin black line represents data minimum and maximum, shaded region represents kernel density estimation of data.

shows that the higher PC axes of morphospace add considerable random variance to the landscape, suggesting that the complexity hypersurface is rough in higher dimensions. Similar to the functional metrics, the type of theoretical morphospace used has a dramatic effect on interpolated taxon values.

Across the mammalian tree, when interpolating from a 2D grid, there appears to be high conservation of low complexity (figure 4.8). There is an exception within the ungulates, consistent with the phylogenetic interpolation in function. When interpolating from the point cloud, the results still seem to show a conservation of relatively low complexity, with high complexity again evolving in ungulates. The ND hypersurfaces has less ability to interpolate the complexity of extreme morphologies, similar to the functional hypersurfaces, which results in some phylogenetic bias in interpolative ability.

The link between complexity and optimality is present when considering the 2D grid landscapes but is obscured in the ND point cloud hypersurfaces (figure 4.9, table 4.1). Within the 2D landscape, there is a consistent negative relationship between all three complexity metrics and optimality (the relationship between alpha shape radius and optimality is positive, due to the metric being reversed). This explains the link between complexity and optimality in ruminants; they are evolving more complex, less optimal shapes compared to the rest of the mammalian tree. However, this relationship is not statistically significant when interpolating from the point cloud hypersurfaces.

The difference between single and multiple bone jaw complexity distributions was significant in all three metrics ($p_{AS} = 7.9649 \cdot 10^{-25}$, $p_{DNE} = 4.8638 \cdot 10^{-9}$, $p_{FD} = 9.3957 \cdot 10^{-12}$), showing consistently higher complexity following the transition to a single bone jaw (figure 4.6).

		2D Grid		ND Point Cloud	
		Theoretical	**Taxon Interpolated**	**Theoretical**	**Taxon Interpolated**
AS	ρ	0.1846***	0.0555*	0.0531	-0.0074
	p	$2.48 \cdot 10^{-7}$	0.0217	0.0932	0.8148
DNE	ρ	-0.2668***	-0.1191***	-0.0062	0.0179
	p	$5.16 \cdot 10^{-14}$	$7.61 \cdot 10^{-7}$	0.8452	0.5719
FD	ρ	-0.0552	-0.1172***	-0.0623*	0.0443
	p	0.1256	$1.15 \cdot 10^{-6}$	0.0488	0.1622

Table 4.1: Statistical relationships between optimality and complexity. Correlation coefficients are measured for theoretical data and interpolated taxon data. Asterisks represent level of significance: $* = p < 0.05$, $*** = p < 0.001$.

4.4 Discussion

4.4.1 Theoretical morphospace construction

I aimed to test the effects that theoretical morphospace construction can have on test metric results, using a large synapsid jaw dataset and both functional and non-functional

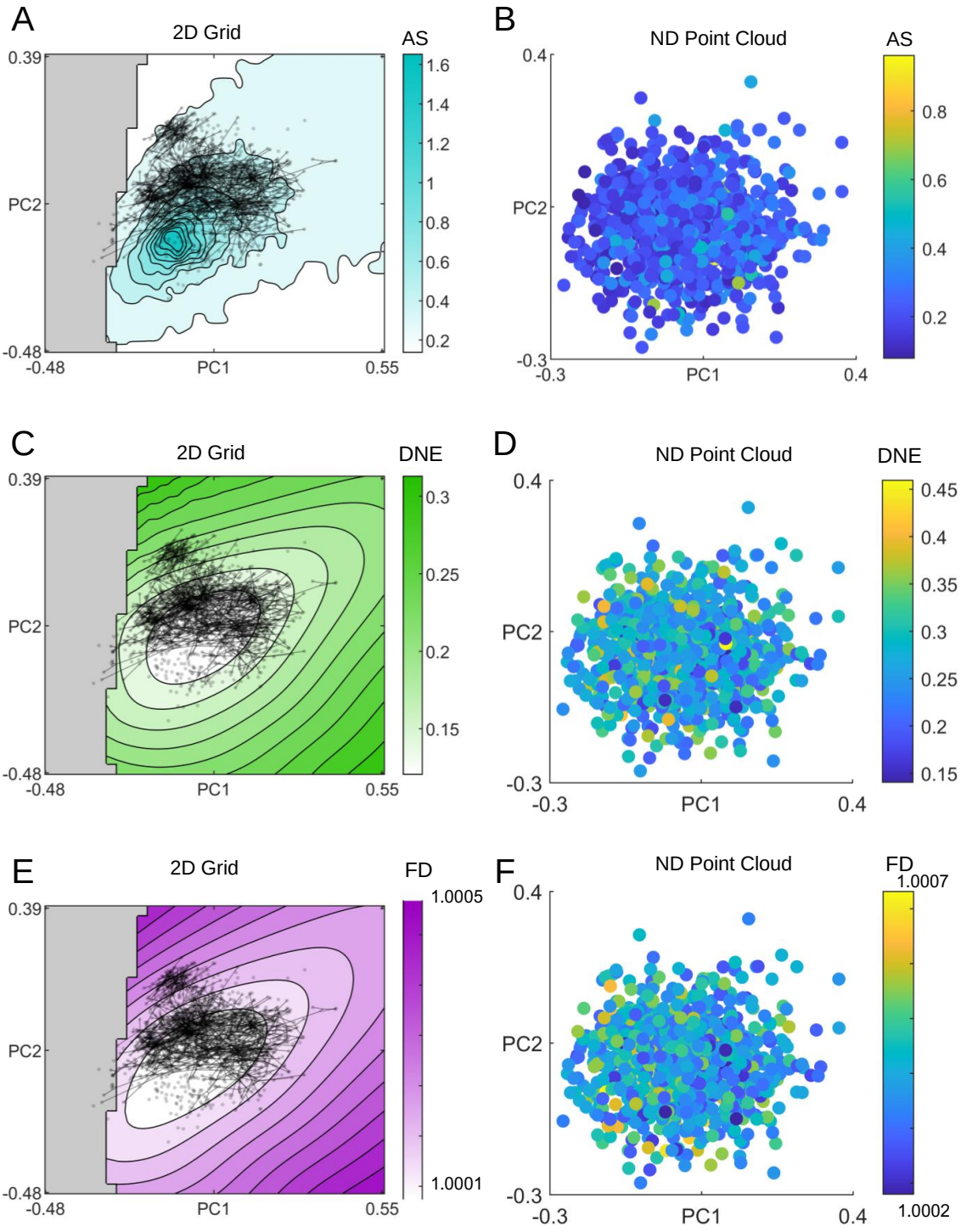

Figure 4.7: Topological complexity surfaces. Three complexity metrics were measured across both theoretical morphospaces: Alpha Shape (AS) **(A,B)**, Dirichlet Normal Energy (DNE) **(C,D)**, and Fractal Dimension (FD) **(E,F)**. Black lines overlain on the 2D grid landscapes represent the phylomorphospace. Point cloud positions represent the positions of ND point cloud theoretical morphospace projected into the PC1-PC2 plane.

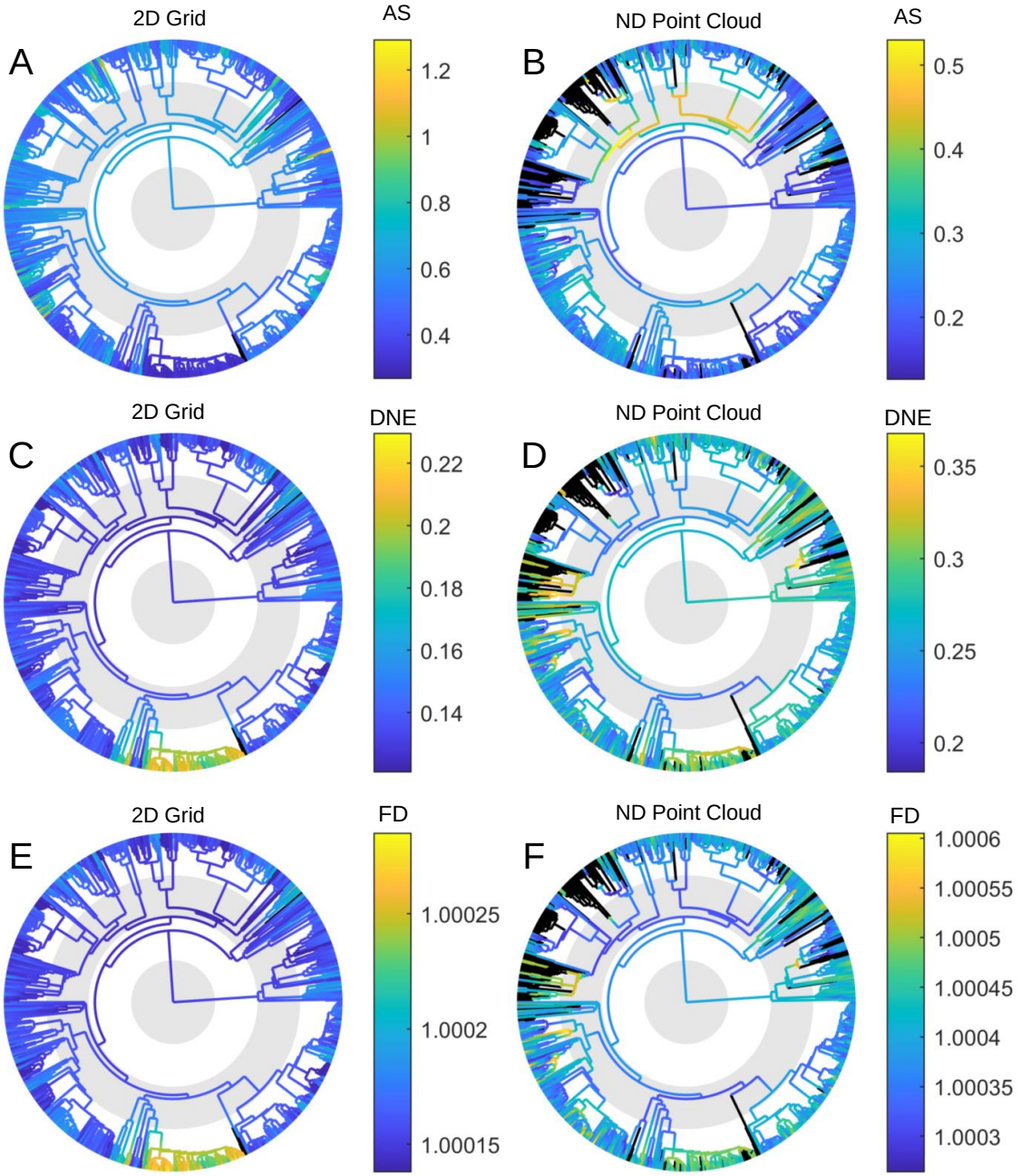

Figure 4.8: Topological complexity interpolated across the mammalian tree. The phylomorphospace was used to interpolate the complexity of each node in the phylogenetic tree according to each surface: **(A)** 2D grid AS surface; **(B)** ND point cloud AS hypersurface; **(C)** 2D grid DNE surface; **(D)** ND point cloud DNE hypersurface; **(E)** 2D grid FD surface; **(F)** ND point cloud FD hypersurface. Line colours represent complexity values, black lines represent data that could not be interpolated by the surface.

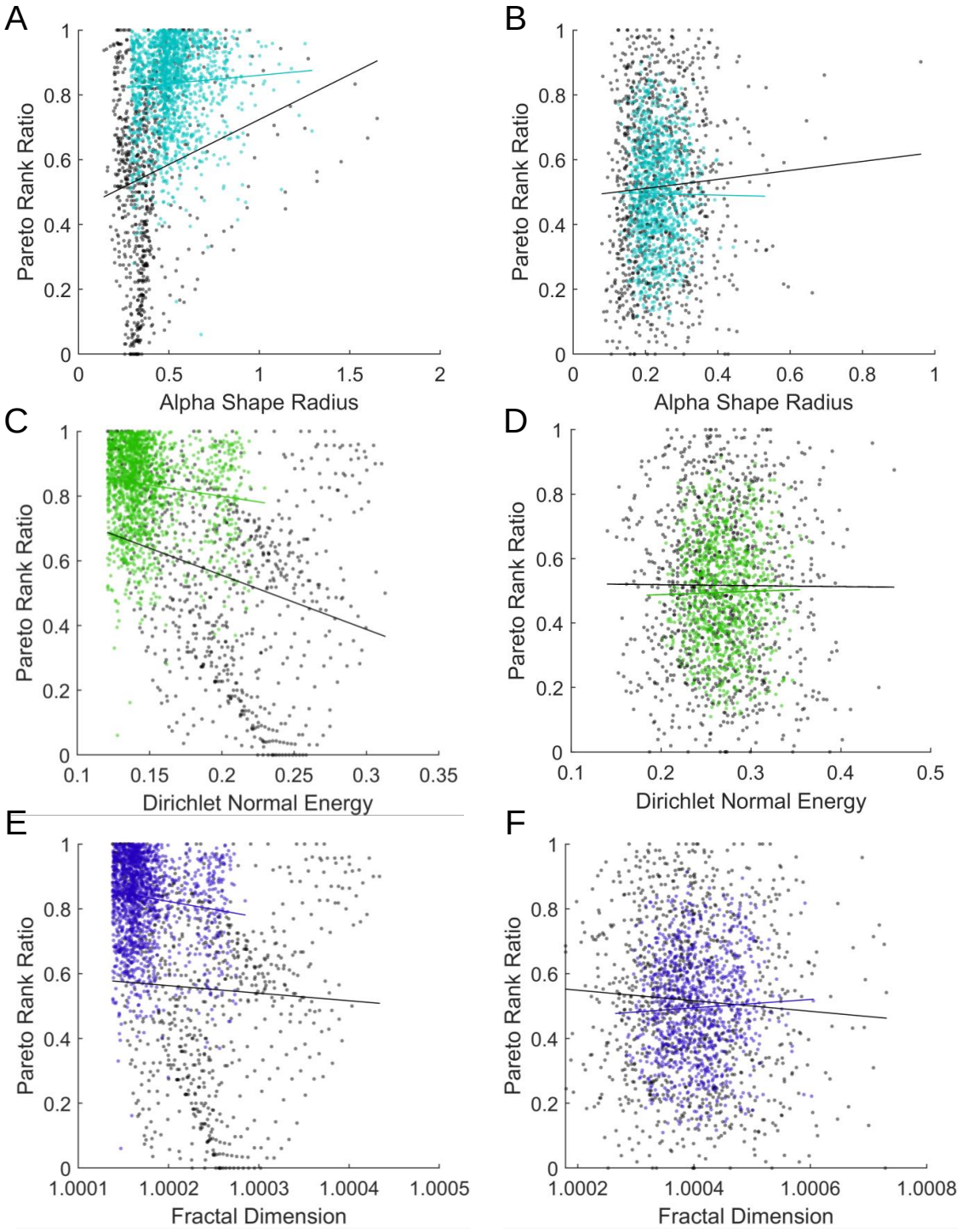

Figure 4.9: Relationship between topological complexity and functional optimality. (A,C,E) Relationship between optimality and complexity in a 2D grid theoretical morphospace. **(B,D,F)** Relationship between optimality and complexity in a ND point cloud theoretical morphospace. Optimality was compared with complexity in all theoretical morphologies (grey dots) and the interpolated results for empirical taxa (coloured dots). Black lines represent trend in theoretical data, coloured lines represent trend in interpolated empirical data.

(complexity) test metrics. Approaches to sampling high dimensional theoretical morphologies can be split in to two groups: dense samples in a subsample of morphological axes (here, a dense grid of theoretical shapes in the first 2 PC axes); and sparse samples in all morphological axes (here a random point cloud across all morphospace axes). I show that the latter generates more precise and accurate hypersurfaces, allowing for higher interpolative value. However, the computational cost of interpolation becomes infeasibly high as it increases exponentially with axis number. For example, sampling a maximum, minimum and mean shape for each axis would require 3^N shapes, where N is the number of axes. The morphospace in this study has 45 axes, so would require $3^{43} \approx 3 \cdot 10^{21}$ shapes to test. Testing each of these shapes with the computational time of analyses performed here would take longer than 1,000 times the age of the universe. Furthermore, the 2D gird is more visually intuitive, allowing for more accessible results that are less likely to be misinterpreted. The 2D grid also filters out morphological noise, by statistically assessing the axes of major variation with a PCA, which is more powerful when assessing general macroevolutionary trends.

High dimensionality also brings problems of sampling unexplored morphospace. As unexplored morphospace gains axes, it grows astronomically large very quickly, which means that it cannot be sampled as evenly as in a 2D grid. This is the most limiting factor of high dimensional theoretical morphospaces – they may be able to reconstruct individual empirical taxon data well, but they cannot compare to lower, more evenly sampled dimensions when sampling non-existent morphospace regions. This is shown in this dataset by the high percentage of empirical taxa that could not have their function interpolated (figure 4.5, black lines represent missing interpolated values). There is some phylogenetic bias to this interpolative ability, as clades with more extreme morphologies are less likely to be interpolated. This could cause unseen phylogenetic bias in results obtained this way. Further, the lack of ability to assess unexplored areas of morphospace reduces the overall optimality of the interpolated dataset, as function is more likely to be compared between empirical-like theoretical shapes, rather than theoretical shapes morphologically further form the empirical sample. In short, the 2D grid gives a less accurate comparisons between empirical and theoretical shapes, whereas the ND point cloud gives more accurate comparisons between the morphologically average shapes in the empirical sample.

Ideally, the best theoretical morphospace is one that captures as much morphological variation as possible. This includes assessing high resolution 3D morphological data and investigating as many morphologically important axes as possible. Perhaps there is a 'statistically significant' value of morphological variation that must be captured for interpreting results. This is common practice for p-values, and could help standardise the field, but is essentially arbitrary and limiting. Also, the data availability may not permit a wide taxonomic analysis with 3D morphometric data. Similarly, when assessing phylomorphospaces and their evolutionary trajectories through morphospace, it is important to remember the large uncertainty in ancestral state reconstruction [366]; so high accuracy in interpolated results may not be warranted at ancestral nodes in the tree. Thus, I argue that in most cases the highest amount of variation possible should be

captured to produce accurate values, but in large datasets, even sampling of explored and unexplored morphospace should be preferred, and the morphological filtering of a PCA can provide valuable information about general trends in morphological macroevolution. Here I will consider the results of both theoretical morphospaces within this framework – that individuals in the phylogenetic tree should be assessed via their accurate interpolations on the ND point cloud, while the general trends of morphological evolution in mammalian jaws should be investigated through the 2D theoretical grid.

4.4.2 The evolution of mammal jaw morphology and function

The mammalian jaw shows heavy shape conservation throughout their evolutionary history. The phylomorphospace shows consistent overlapping in evolutionary trajectories, with all branches crossing one another within a constrained, finite region of morphospace (figure 4.3). This, combined with a significant but weak phylogenetic signal in the dataset, suggests high constraint amongst all mammalian groups in jaw form. Even in a dataset spanning approximately 300 million years, groups rarely expand into morphospace previously unoccupied. This is surprising, considering that there is perhaps some developmental freedom due to the unique nature of the mammal jaw – it is comprised of a single dentary bone. While this reduction in bones does reduce the number of morphogenetic modules, there are still multiple developmental modules in the dentary [349, 350]. The PC1-2 plane represents changing jaw shape and curvature, similar to the theoretical morphospace in chapter 2 and 3. However, one key difference is the presence of the coronoid process, which appears large and narrow in curved jaws and shallow and thick in straighter jaws. This may represent a trade-off in jaw joint height, which can impact the mechanical advantage of the jaw [367].

This is further corroborated by the general trend of functional optimality through mammalian jaw macroevolution (figure 4.5). Considering the 2D grid data results, there is almost ubiquitous conservation of high optimality throughout mammal jaw evolution. There is a trade-off between rotational efficiency and strength in jaw shape, and many mammal jaws are constrained to optimise function within this trade-off. Non mammalian therapsids lie in a tighter range of morphospace, which is less functionally optimal than their mammalian descendants, then the reduction of jaw bones allowed the further exploration of jaws by subsequent mammalian taxa to diffuse into further optimal areas of morphospace. Indeed, the majority of functionally optimal morphospace is explored by mammals. This is consistent with the hypothesis that therapsid jaws were limited by their morphological integration, and mammalian jaws were released by this constraint, allowing functional constraint to dominate. An alternative explanation is that the diversity of mammalian jaws is limited by function, but the radiation into a variety of ecological niches in the Cenozoic allowed jaw shape to diversify through a wider variety of functionally optimal morphospace [335–338].

This high conservation of functional optimality in the majority of mammalian lineages is consistent with the hypothesis that mammal jaws are optimised for jaw rotational efficiency and strength. However, not all lineages are optimised. Specifically, ungulates show high levels of suboptimality, shown in individual function by relatively high stress and intermediate rotational efficiency. Ungulate feeding mechanics is complex and has

been discussed widely in the literature, with large variation in musculature and stress dissipation capability found within the clade [368–372]. Generally, this relative reduction in optimality could be explained by the unique feeding biomechanics in which ungulates have evolved enhanced grinding capability in mastication [368], or that the evolution of ruminant digestion requires less mechanical processing of food material, reducing the selective pressure on jaw strength [371, 372]. It could also be explained by the bias of the evolution of hypsodonty within the ungulate clade, which has been shown to bias jaw form [373].

4.4.3 Complexity in the mammal jaw

Shape complexity is difficult to define and measure. Here, I chose to utilise three separate metrics from the literature [357–359], so that their results could be compared to reliably measure topological complexity. The results show very high consistency between all three metrics, suggesting that they are all capturing the same aspect of shape. While topological complexity can be defined in different ways, these separate metrics and definitions can still capture a matching signal. When comparing the differences between therapsid multi-bone jaws and mammalian dentaries, there is a significant increase in complexity between during this transition (figure 4.6). This is consistent with the predictions of Williston's law.

The results show a story of highly conserved minimal complexity across many mammalian orders (figure 4.8). In the theoretical morphospace, taxa lie constrained in a region of minimum complexity, suggesting that complexity is being minimized on a macroevolutionary scale (figure 4.7). This is interesting considering that complexity is expected to increase over macroevolutionary timescales according to the Zero Force Evolutionary Law (ZFEL) [354, 355]. However, ungulates are an exception to this pattern. They extend into a region of complex morphospace, which coincides with their decreased functional optimality. Combined with the relationship between functional optimality and complexity (figure 4.9 Table X), this suggests that topological complexity is limited by high functional constraint in mammalian jaws, which is then released in ungulates, allowing optimality to decrease and complexity to increase. This provides an explanation for this limited complexity that is consistent with the predictions of the ZFEL: a consistent external 'force' (optimality) is limiting the evolution of complexity [354, 355].

4.4.4 Concluding remarks

These results show that mammalian jaw evolution is a story of repeated convergence for functional optimality, further corroborating the view that the mandible is a structure heavily controlled by its function. However, not all clades have optimal jaws within this dataset. The unique case of ungulate biology and how it defines their jaw evolution is marked in this dataset. The morphodynamic biases on morphology can vary significantly through the branches of a phylogenetic tree.

This study also highlights the benefits and limitations of different constructions of theoretical morphospace. The interpolative ability of including higher dimensions of morphological variation is significant, at the cost of higher computational times and limited characterisation of unexplored morphospace. The power of the grid theoretical

morphospace in sampling all regions of morphospace, while capturing the major aspects of morphological variation within an empirical dataset, allows for a better general picture of macroevolutionary trends. Going forward, significant work is required to unite these approaches into a dense sampling of all dimensions of morphospace.

Ascribing nomothetic laws to macroevolutionary processes is an ambitious and important goal of systematic biology. These laws have the potential to not only describe but explain organismal variety and its dynamics through time, which can give more informed views of current biodiversity. It is crucial to note, however, that nuances in evolution can cloud these patterns. This does not mean that they are not true, just that they can be obscured in specific cases. This is evident in two aspects of this investigation: first, that the bias of functional optimality on form can vary within lineages and clades, as in the ungulates; and second, that the neutral accumulation of complexity over time can be limited by the morphogenetic constraints on form.

Chapter 5

Assessing the optimality of bird limb shafts using theoretical 3D morphology and function

Author's contribution This chapter and all analyses within were completed by William J. Deakin. CT scan data was provided by Roger Benson.

Abstract

Birds exhibit extremely high diversity in locomotor ecology in comparison with other vertebrates. The evolution of the wing has facilitated the evolution of flight, both in air and in water. Some terrestrial birds have lost the ability to fly altogether. It is well known that these different types of locomotion have effects on the morphology of the wing. The wing spar must adapt to withstand the different functional loads of motion within different mediums, whilst remaining lightweight in aerial taxa. Here, I develop new methods for measuring the morphology of the limb shaft in the humerus, that incorporate the curvature of the bone to measure cross sectional geometry perpendicular to this curvature. The resulting morphometrics are used to generate a theoretical morphospace of bird limb shaft morphology which is tested for functional optimality, and the distribution of different groups of birds separated by their locomotor ecology is observed within the resulting functional landscapes.

5.1 Introduction

The analytical pipeline for measuring morphodynamic biases on biological form has been well refined in the literature and in this thesis. Phylogenetic bias can be measured in any morphological dataset [161], and there are mature mathematical models for assessing a wide range of biomechanical performance indices. Combined with the contemporary drive in comparative anatomy to scan the 3D morphology of many biological structures, while making them freely accessible via online repositories such as Morphosource [15], these studies are more accessible and feasible than ever. However, issues remain with the construction of theoretical morphospace, especially with generating detailed 3D theoretical shapes. In order to generate optimality landscapes for wide ranges of morphological structures within and between taxa, more theoretical morphological models are required, and a greater understanding of the geometric structure of their resultant morphospaces [78].

While 2D data can still be informative, 3D morphological and functional data is required to accurately model biomechanical systems [138, 374]. This is the main avenue through which theoretical morphology can improve – by developing models of 3D morphology. There already exist some ways to achieve this. A study on the skull shape of bone-cracking hypercarnivores, and how that relates to function, characterised shape variation via the aspect ratio of the skull, and generated theoretical morphologies by warping a detailed 3D model of an existing hyena skull [119]. This methodology is efficient, and facilitates the testing of extremely detailed theoretical morphologies. However, the detail in these warped theoretical shape models is constrained to the single deformed skull. Any variance in these details within the dataset is lost. The more popular approach has been to use 3D geometric morphometrics, and vary the position of landmarks to generate 3D theoretical morphologies, as has been performed on turtle shell shapes [85, 201]. This is extremely powerful for the majority of biological structures, however the heavy reliance on secondary homology for the placement of landmarks makes it difficult to analyse large taxonomic groups, or structures with complex shapes that are not defined by homologous structures.

For example, the humerus is a functionally important structure in many tetrapods that can be arbitrarily split into three parts: the proximal portion, often called the head, that forms a joint with the shoulder; the distal portion that forms part of the elbow, and the shaft connecting the two. The proximal and distal ends can be characterised well by landmarks, as there are many identifiable homologous structures. However, the shape of the shaft is more difficult. It has very few (if any) identifiable structures between taxa, despite having large variation in shape between taxa. Sliding surface semi-landmarks could provide a description of the surface, but the curvature and twisting of the shaft, as well as portions of internal morphology would be lost.

Characterising the shape of the shaft in limb bones can be an important goal in theoretical morphology. Indeed, by definition, secondarily homologous structures are heavily biased by phylogeny. Therefore, measuring the morphodynamic constraints on only these structures is likely to induce some systemic bias in results. In the case of the humeral shaft, it is likely to play important functional roles in an organism, specifically as a load

bearing structure. Mass estimates of extinct tetrapods rely on the geometry of the shafts of humeri and femora [375], and the length of the humerus is related to locomotor ecology in many tetrapods [376]. In birds, the geometric properties of the cross section of the humerus shaft has been shown to be mechanically important [377] and extensively linked with locomotor ecology [378–380]. These changes have been attributed to the changing functional demands of flying in water and in air, as well as the many different types of locomotion in air and water [33].

In this chapter, I describe a prototype methodology for measuring the axis of bone curvature in the humeral limb shaft. The methodology is broadly adaptable, such that it could be applied to a variety of biological 'tubes', like bone shafts, teeth, shells and plant stems. I then utilise this methodology to slice regular cross sections in 3D bird humerus scans, and characterise the internal and external perimeters with Elliptical Fourier Analysis (EFA). Finally, the dataset is used to build a 3D theoretical morphospace, which is tested for functional performance and optimality, to compare with ecological data.

5.2 Methods

5.2.1 Data collection

3D surface data of micro-CT scans of 165 bird humeri were collected from the TEMPO birds project on morphosource [15]. These models contained surface triangulation data of both the outside and inside surface of the bone, allowing characterisation of external and internal limb shaft morphology. The taxa included were separated by primary lifestyle and diet using data from the AVONET database [381]. For primary ecology, the divisions in AVONET were used (aerial ($N = 10$), aquatic ($N = 12$), generalist ($N = 9$), insessorial ($N = 72$) and terrestrial ($N = 62$)). For dietary ecology, taxa were split into two categories: aquatic (aquatic predator or aquatic herbivore) and non-aquatic (everything else). Each bone was checked for whether it was a right or left humerus, and all left humeri were mirrored so that the dataset contained only right humerus morphology. Finally, two Type II landmarks were placed on each bone to define the extent of the limb shaft. They will be referred to as landmark A (the base of the deltapectoral crest) and landmark B (the proximal limit of the entepicondylar foramen) (figure 5.1). Landmark A and B were chosen as identifiable points between taxa that define the proximal and distal limit of the bone shaft respectively.

5.2.2 Bone slicing

The process of collecting bone slice data is automated, and designed to generate accurate slices along the bone shaft, oriented perpendicular to the bone axis at that point. This can be broken down into 5 steps, which I will describe in detail in this section: **1) General orientation:** a general proximodistal axis of the bone is calculated; **2) Local orientation:** the local orientation of the bone axis is calculated at many points along the bone shaft; **3) Local centroid calculation:** the bone is sliced at each local orientation sample, to find the geometric centroid of the cross section in the plane; **4) Bone axis fitting:** a function is fitted to the local orientation and centroid data to generate a bone axis line; **5) Bone**

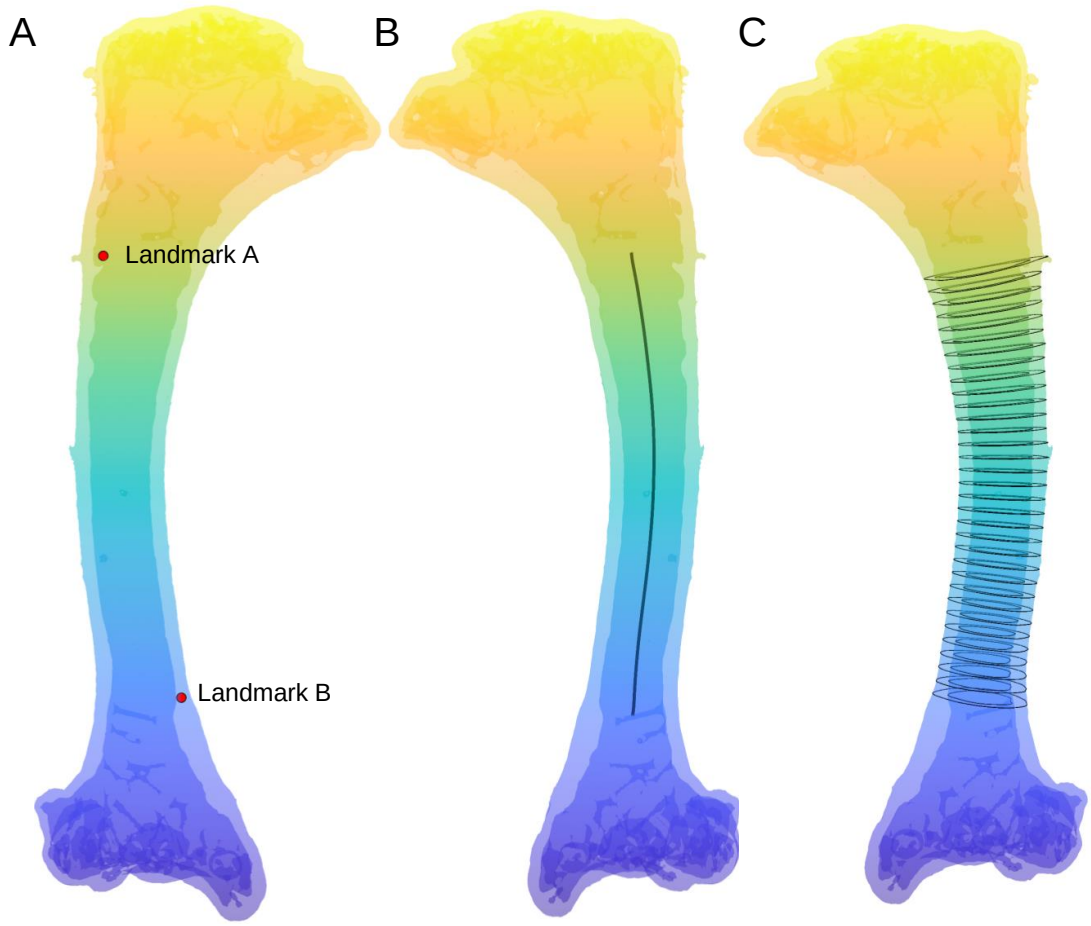

Figure 5.1: Bone slicing process. (A) Two landmarks are placed on the bone surface: landmark A at the base of the deltapectoral crest, and landmark B at the proximal limit of the entepicondylar foramen. **(B)** The bone axis (black curve) is fitted to the bone using the local centroid and local orientation at a set of query points along the bone. **(C)** Geometric data of cross sections at even points along the bone axis is collected. Colours represent the z coordinate at each point on the surface.

slicing: the bone is sliced perpendicular to the bone axis at evenly spaced intervals along the bone axis, and morphometric data is collected.

To aid in the generation of slices along the bone shaft, a general proximodistal orientation of the bone was found using an iterated Principal Component Analysis (PCA) of the vertex data of each bone. This process involved 4 steps: 1) indices of the vertices with z coordinates higher than the proximal end of the limb shaft (landmark A, figure 5.1) and lower than the distal end of the limb shaft (landmark B, figure 5.1) are recorded. 2) The major axis of variation (PC1) of the vertex data is found using a PCA (on the first iteration this is performed on the entire vertex set and on subsequent iterations the vertices indexed in the previous step are omitted). 3) The vertex and landmark data is rotated about the mean such that the z axis aligns with PC1. 4) The coefficients of PC1 are normalised and recorded. On all iterations excluding the first, the distance between the previous and current PC1 axis, d_g, is recorded and compared to an arbitrary threshold, D_g. If $d_g > D_g$, stages 1-4 are iterated again. If $d_g \leq D_g$, the iterative process is completed, and

the rotated vertex data is saved as the new aligned vertex data. This orientation process is shape specific, and can be considered an elimination of rotation, however it will not be the final rotation of the morphological data in this pipeline.

The general orientation of the bone shaft can then be used to sample slices along the shaft and calculate local orientations. At each point along the bone, the orientation of the local axis (local orientation) can be approximated using another iterative PCA. This process is similar to the previous step but on a smaller scale. To calculate the local orientation of the bone at a query point P_i, the process of iteration is as follows: 1) The z coordinate of P_i is subtracted from the vertex z data. 2) A weighted PCA is performed on the transformed vertex data. Vertices are weighted by a function, f_w, such that the weights decrease monotonically with an increase in the magnitude of their z coordinate. 3) The local orientation can be approximated by any of the three PC axes depending on the size of the cross section and the specific function used for f_w. To account for this, the coefficient closest to an expected local orientation (N_{ei}) is set to the new axis. 4) Points are rotated about their mean to align with the new axis. 5) If the difference between the new axis and the previous axis is greater than a threshold value, the query point P_i is also rotated to this new axis and steps 1-5 are repeated. If not, the local orientation, N_i, is set to the axis calculated in step 3.

While many functions could be used for f_w to calculate the vertex weights in each PCA iteration, after testing and analysing accuracy and computational time, I opted for the function:

$$f_w(z) = \frac{1}{z^2 + 1}$$

As it decreases exponentially with z distance to the query point, and reaches a maximum value of 1 at the same z coordinate as the query point. The process can also be put through a filter, such that values below a threshold are set to a negligible weight of 0.0001, which causes the iteration to converge quicker and saves computational time.

Here, I chose to characterise each slice of the bone as an annulus, described by two perimeters, the external surface and an internal surface. To find these, first the set of points where individual faces of the original bone intercept the slice plane are calculated. This is done by downsampling the faces of the original triangulation to those with points that lie a threshold distance h away from the slice plane. This threshold distance should be as small as possible, to save computational processing time, while also being large enough to capture all faces that intersect the slice plane. In the case of many .stl surface files generated from micro CT data, all triangles in the object will be congruent right angled triangles, and thus the farthest distance that any point in a triangle that intersects the slice plane will always be less than the hypotenuse (figure 5.2). Thus, in some cases, h can be calculated as the hypotenuse of any face in the triangulation object. However, .ply objects output from some segmenting software will use a marching squares algorithm to join the centre point of 3D pixels, rather than their faces. Also, in some CT scans, the scale of a particular axis may be different from the other two, depending on the settings of the original scan. A more general solution for h in all cases is to measure the maximum side

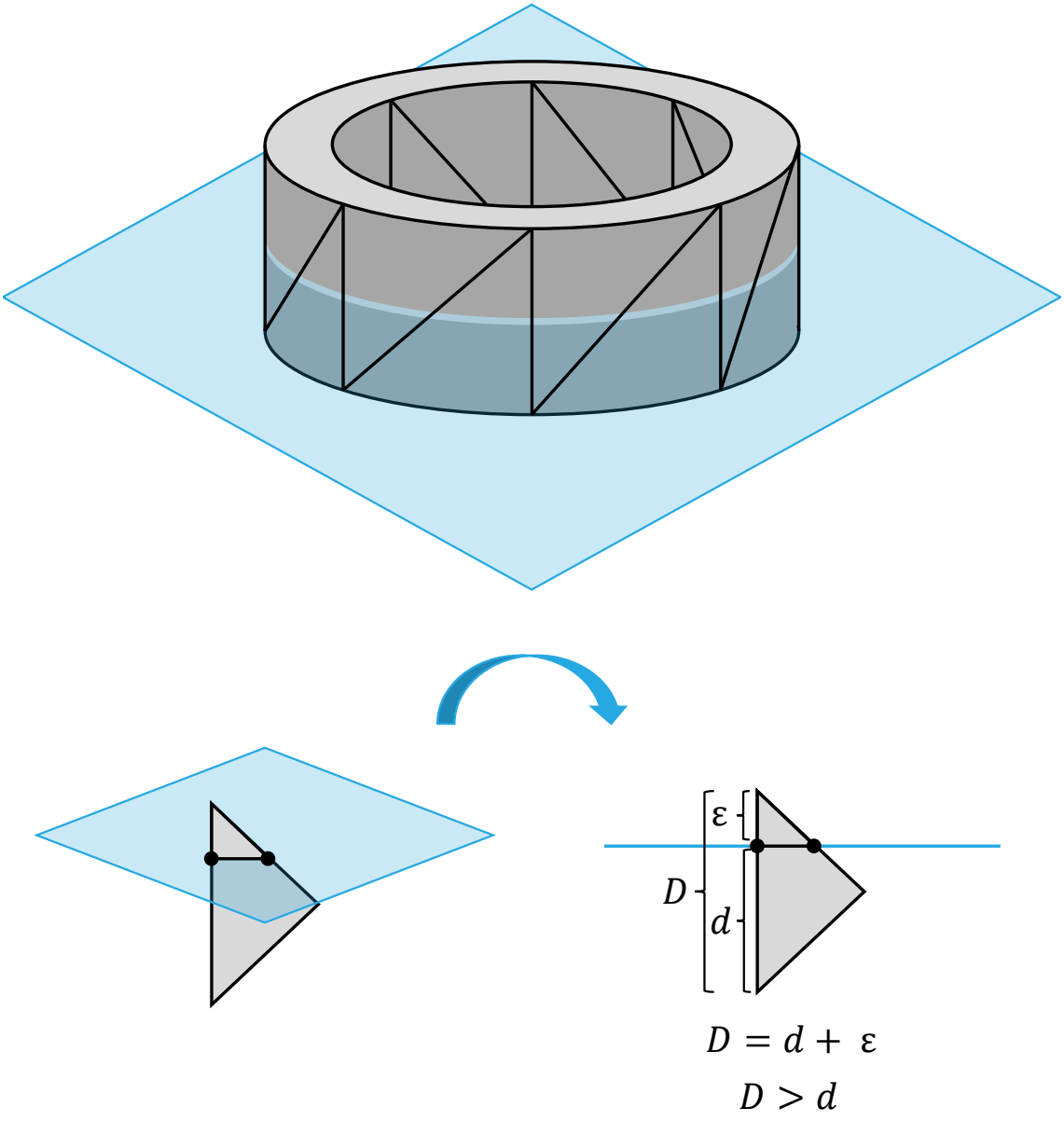

Figure 5.2: Downsampling the bone about a slice plane. Downsampling of faces is required to build efficient bone slicing algorithms. The maximum length of any triangle in the dataset, D, is measured. The maximum distance from the plane to any point in a triangle that intersects that plane, d, is always less than D. All points a distance greater than D from the plane, and their connected triangles, can be ommitted from the calculation.

length of all triangles in the triangulation. This will guarantee that all triangles intersecting a slice plane will be sampled, but may also sample extra triangles and find no intersections. Ultimately, this does not affect the results, but slows the computational time depending on the variation in aspect ratio amongst the faces of the triangulation.

Once the triangulation is downsampled, faces can be characterised by their connection to one another. In most cases, the outer surface will be separated from the inner surface, and thus the slice plane intersections of the two disconnected sets ('islands') of faces can be considered separately to generate an outer and inner perimeter (figure 5.3). However, in the case of many bird humeri, the internal bone structure has varying levels of pneumaticity between taxa and between points along the shaft. The surfaces cutting between sides of the bone complicate the internal structure, leading to many different islands in the cross section (figure 5.3). To account for this, the ordered set of perimeter points from the sampled intersections is chosen by finding the alpha radius of an alpha shape with zero holes of the set of points that minimises the perimeter of the shape. The outer surface is then set to the island with the largest bounding box in 3D space, and the inner surface is chosen from all points not in the outer surface island. Finally, in some cases, bones have holes in the shaft. In the case of this dataset, these are usually pathologies or holes drilled by scientists and museum curators. These will lead to the outer and inner islands being connected, and thus inseparable. In this case, the outer surface is calculated with the minimum perimeter alpha shape algorithm on the total set of slice plane intersection points, and the inner surface is calculated by transforming the points such that their distance from the center of the sample is inverted, and thus the inner surface lies on the outside of the outer surface. The minimum perimeter alpha shape algorithm performed on the transformed points can then define the inner surface.

To find the variation in local orientation along the bone shaft, a set of query points must be generated and sampled. Here, I chose to sample the end points of the limb shafts first, defined by the landmarks A and B. The midpoint between these two samples is sampled from the bone. The expected local orientation, N_{ei}, is set to the z axis in each of these three samples. The following samples are then generated by setting the query point: $P_{i+1} = \Delta t N_i + M_i$. Where Δt can be reduced to include more cross section samples along the bone. M_i is calculated by slicing the bone at each local orientation and calculating the cross section centroid. This essentially takes the middle slice of the bone shaft and moves up along the bone by a factor of Δt to the proximal limit defined by landmark A. Then, it returns to the middle sample, and moves down the bone shaft to the distal limit defined by landmark B. The expected orientation at each sample is set to the orientation of the previous sample, so that the normal vector varies continuously along the bone shaft.

Note that this process of sampling approximates equal sampling along the bone shaft, but does not account for the variation in curvature between successive samples. To get a true equal sampling, a formula for the local centroid must be generated with input parameter t, such that t is equal to the arc length of the formula between successive local centroid samples. Finally, the tangent at any point t between these samples should represent the local orientation at arc length t between these samples (figue 5.4).

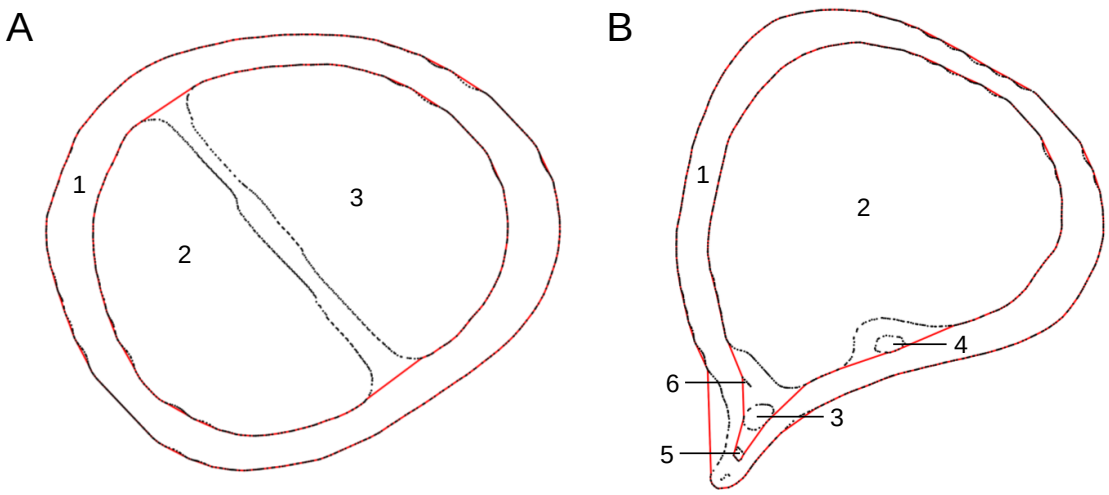

Figure 5.3: Imperfections in cross sections. The majority of bone cross sections can be split into two 'islands' (disconnected sets of points). Some imperfections, such as bone pneumaticity and holes in the bone surface, can disrupt this. **(A)** A single connection between edges of the bone splits the inner perimeter in two. **(B)** High pneumaticity can complicate the cross section dramatically. Here, the algorithm orders islands by their bounding box size (numbers in each island), then outlines the largest island and the union of all other islands. Black dots represent sampled triangle-plane intersections, red lines represent inner and outer perimeters. Note that the outline algorithm can fail to capture all of shape variation in complex shapes, as in **(B)**.

Let $\mu_i(t)$ denote the local centroid in cartesian coordinates at an arc length t from M_i to M_{i+1}. The local orientation in cartesian coordinates at t is therefore $\mu_i'(t)$ between M_i and M_{i+1}. The arc length of $\mu_i(t)$ is defined by:

$$\int |\mu_i'(t)|\, dt$$

Setting the arc length of the function equal to t:

$$t = \int |\mu_i'(t)|\, dt$$
$$1 = |\mu_i'(t)|$$

Therefore, by defining a function for $\mu_i'(t)$ such that the magnitude of $\mu_i'(t)$ is always equal to 1, we can ensure that $\mu_i(t)$ denotes the change in centroid along the arc such that the arc length is always equal to t, and can thus be sampled evenly. To ensure that $\mu_i'(t)$ always has a magnitude of 1, we can define it in polar coordinates, $\langle r, \theta, \phi \rangle$, and set $r = 1$. Thus, $\mu_i'(t)$ is a function of its rotation in the x-y plane ($\phi_i(t)$) and its angle from the z axis ($\theta_i(t)$). $\mu_i'(t)$ is thus defined as:

$$\mu_i'(t) = \langle x_i'(t), y_i'(t), z_i'(t) \rangle$$

Where:

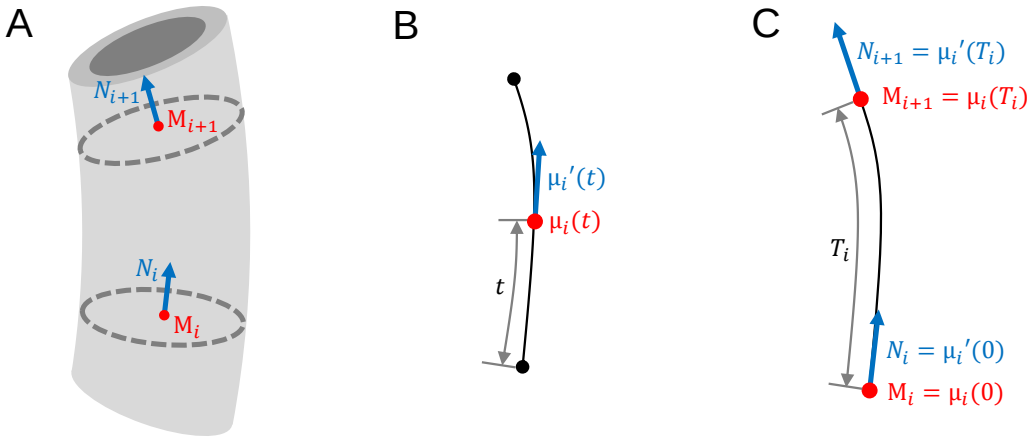

Figure 5.4: Interpolation between successive local centroids and local orientations. Even sampling along the bone axis is achieved by fitting a curve, $\mu_i(t)$, to the local centroid data such that the tangent at each point in the curve, $\mu_i'(t)$ is equal to the local orientation with a magnitude of 1. This ensures that the arc length from 0 to t of $\mu_i(t) = t$.

$$x_i'(t) = \sin(\theta_i(t))\cos(\phi_i(t))$$

$$y_i'(t) = \sin(\theta_i(t))\sin(\phi_i(t))$$

$$z_i'(t) = \cos(\theta_i(t))$$

And $\mu_i(t)$ is defined as:

$$\mu_i(t) = \langle x_i(t), y_i(t), z_i(t) \rangle$$

Where:

$$x_i(t) = \int \sin(\theta_i(t))\cos(\phi_i(t))\, dt$$

$$y_i(t) = \int \sin(\theta_i(t))\sin(\phi_i(t))\, dt$$

$$z_i(t) = \int \cos(\theta_i(t))\, dt$$

In order to generate a closed function for $\mu_i(t)$, we can assume that θ and ϕ vary linearly between each successive local sample. At a small number of samples, this assumption does not adequately define $\theta_i(t)$ and $\phi_i(t)$, but the error reduces to a limit of 0 as the distance between each sample is reduced. Let $N_i = \langle 1, \Theta_i, \Phi_i \rangle$ in normalised polar coordinates, and let T_i = the arc length from M_i to M_{i+1}. We define $\theta_i(t)$ as:

$$\theta_i(t) = a_i t + \Theta_i$$

Where:

$$a_i = \frac{\Theta_{i+1} - \Theta_i}{T_i}$$

And we define $\phi_i(t)$ as:

$$\phi_i(t) = b_i t + \Phi_i$$

Where:

$$b_i = \frac{\Phi_{i+1} - \Phi_i}{T_i}$$

This ensures that $\theta_i(0) = \Theta_i$ and $\phi_i(0) = \Phi_i$, and $\theta_i(T_i) = \Theta_{i+1}$ and $\phi_i(T_i) = \Phi_{i+1}$. We can now generate closed form functions for $\mu_i(t)$ and $\mu_i'(t)$:

$$x_i'(t) = \sin(a_i t + \Theta_i)\cos(b_i t + \Phi_i)$$

$$y_i'(t) = \sin(a_i t + \Theta_i)\sin(b_i t + \Phi_i)$$

$$z_i'(t) = \cos(a_i t + \Theta_i)$$

$$x_i(t) = \int \sin(a_i t + \Theta_i)\cos(b_i t + \Phi_i)\, dt$$

$$x_i(t) = \int \frac{\sin((a_i t + b_i t)t + \Theta_i + \Phi_i) + \sin((a_i t - b_i t)t + \Theta_i - \Phi_i)}{2}\, dt$$

$$x_i(t) = C_{xi} - \frac{\cos((a_i + b_i)t + \Theta_i + \Phi_i)}{2(a_i + b_i)} - \frac{\cos((a_i - b_i)t + \Theta_i - \Phi_i)}{2(a_i - b_i)}$$

$$y_i(t) = \int \sin(a_i t + \Theta_i)\sin(b_i t + \Phi_i)\, dt$$

$$y_i(t) = \int \frac{\cos((a_i t - b_i t)t + \Theta_i - \Phi_i) - \cos((a_i t + b_i t)t + \Theta_i + \Phi_i)}{2}\, dt$$

$$y_i(t) = C_{yi} - \frac{\sin((a_i + b_i)t + \Theta_i + \Phi_i)}{2(a_i + b_i)} + \frac{\sin((a_i - b_i)t + \Theta_i - \Phi_i)}{2(a_i - b_i)}$$

$$z_i(t) = \int \cos(a_i t + \Theta_i)\, dt$$

$$z_i(t) = C_{zi} + \frac{\sin(a_i t + \Theta_i)}{a_i}$$

Let $M_i = \langle X_i, Y_i, Z_i \rangle$ in cartesian coordinates. Setting $t = 0$:

$$\langle x_i(0), y_i(0), z_i(0) \rangle = M_i$$

$$\langle x_i(0), y_i(0), z_i(0) \rangle = \langle X_i, Y_i, Z_i \rangle$$

$$x_i(0) = C_{xi} - \frac{\cos(\Theta_i + \Phi_i)}{2(a_i + b_i)} - \frac{\cos(\Theta_i - \Phi_i)}{2(a_i - b_i)}$$

$$C_{xi} = X_i + \frac{\cos(\Theta_i + \Phi_i)}{2(a_i + b_i)} + \frac{\cos(\Theta_i - \Phi_i)}{2(a_i - b_i)}$$

$$y_i(0) = C_{yi} - \frac{\sin(\Theta_i + \Phi_i)}{2(a_i + b_i)} + \frac{\sin(\Theta_i - \Phi_i)}{2(a_i - b_i)}$$

$$C_{yi} = Y_i + \frac{\sin(\Theta_i + \Phi_i)}{2(a_i + b_i)} - \frac{\sin(\Theta_i - \Phi_i)}{2(a_i - b_i)}$$

$$z_i(0) = C_{zi} + \frac{\sin(\Theta_i)}{a_i}$$

$$C_{zi} = Z_i - \frac{\sin(\Theta_i)}{a_i}$$

We can now calculate T_i:

$$z_i(T_i) = Z_{i+1}$$

$$Z_{i+1} = Z_i + \frac{\sin(a_i T_i + \Theta_i)}{a_i} - \frac{\sin(\Theta_i)}{a_i}$$

$$Z_{i+1} - Z_i = \frac{\sin(\Theta_{i+1}) - \sin(\Theta_i)}{a_i}$$

$$Z_{i+1} - Z_i = \frac{T_i(\sin(\Theta_{i+1}) - \sin(\Theta_i))}{\Theta_{i+1} - \Theta_i}$$

$$T_i = \frac{(Z_{i+1} - Z_i)(\Theta_{i+1} - \Theta_i)}{\sin(\Theta_{i+1}) - \sin(\Theta_i)}$$

Using T_i, a_i and b_i can be calculated using these formulae:

$$a_i = \frac{\Theta_{i+1} - \Theta_i}{T_i}$$

$$b_i = \frac{\Phi_{i+1} - \Phi_i}{T_i}$$

Once the parameters are fit to the bone axis formula, a set of N_s slices can be calculated evenly spaced along the axis. Here, I chose to set $N_s = 33$, because it is $2^5 + 1$, allowing multiple downsamples that preserve the positions of the end slices and preserve equal spacing between slices. The bone is sliced in the same set of algorithms described previously, and then an unscaled EFA is performed on the points of each perimeter, generating two samples of elliptical harmonic data. The EFA data is stored along with the position of its centroid in 3D space and the normal vector of the slice plane. These can then be scaled down by the bone axis length, such that all shapes have a bone length of 1. Finally, a PCA is used to generate am empirical morphospace (figure 5.5) and a theoretical grid of humerus shaft shape (figure 5.6).

5.2.3 Theoretical morphology and performance

From the PCA morphospace, a 20-by-20 theoretical grid of limb shaft bones was generated at evenly spaced PC1 and PC2 coordinates spanning the range of morphological variation in the dataset plus a border of 10% (figure 5.6). These were then tested for five characteristics

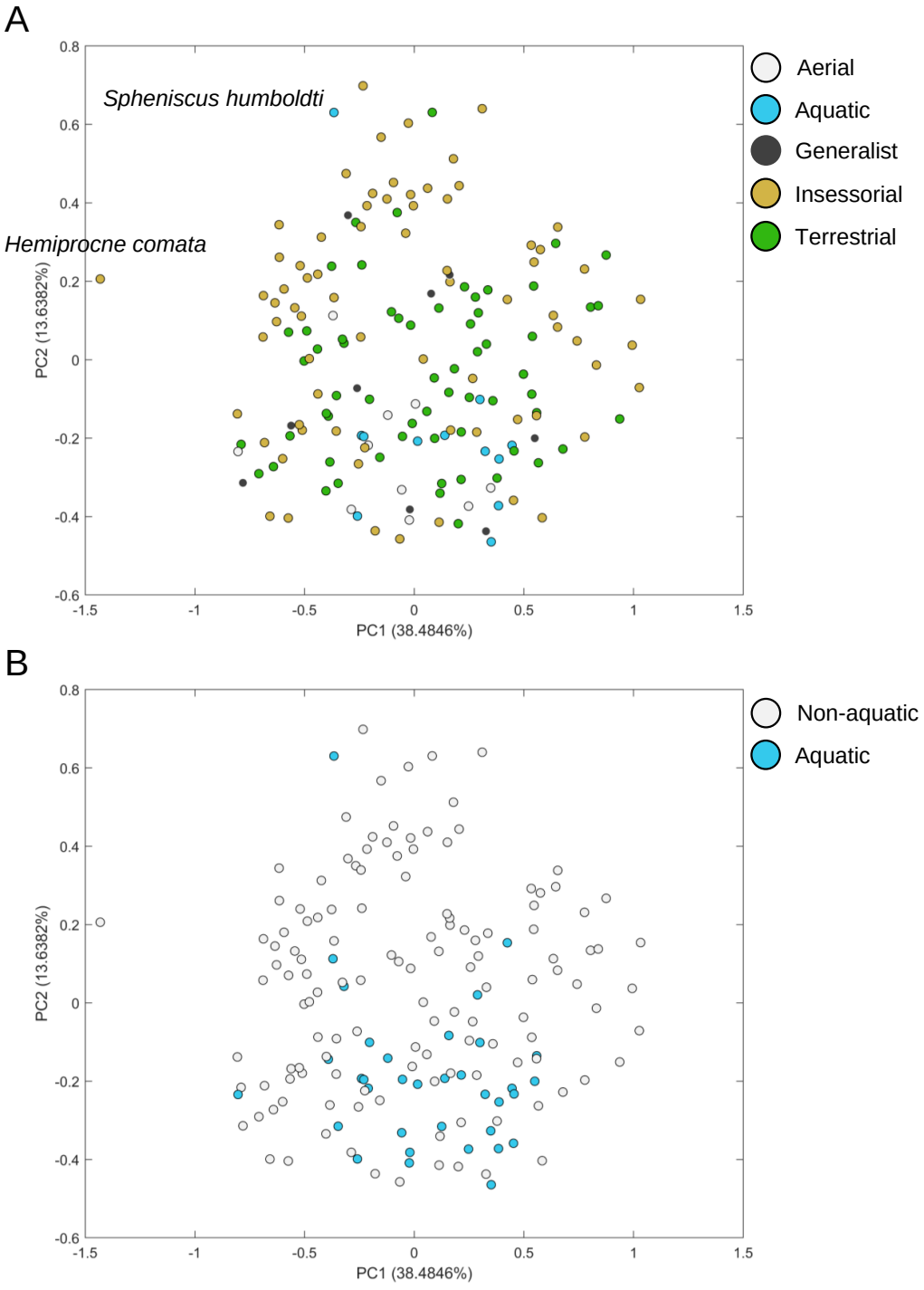

Figure 5.5: Bird humeral limb shaft empirical morphospace. Morphospace is built from a PCA of axis parameter and cross sectional EFA data. **(A)** Taxa grouped by primary ecology: aerial (white dots); aquatic (blue dots); generalist (black dots); insessorial (brown dots); terrestrial (green dots). **(B)** Taxa grouped by dietary ecology, split into aquatic diets (blue dots) and non-aquatic diets (white dots).

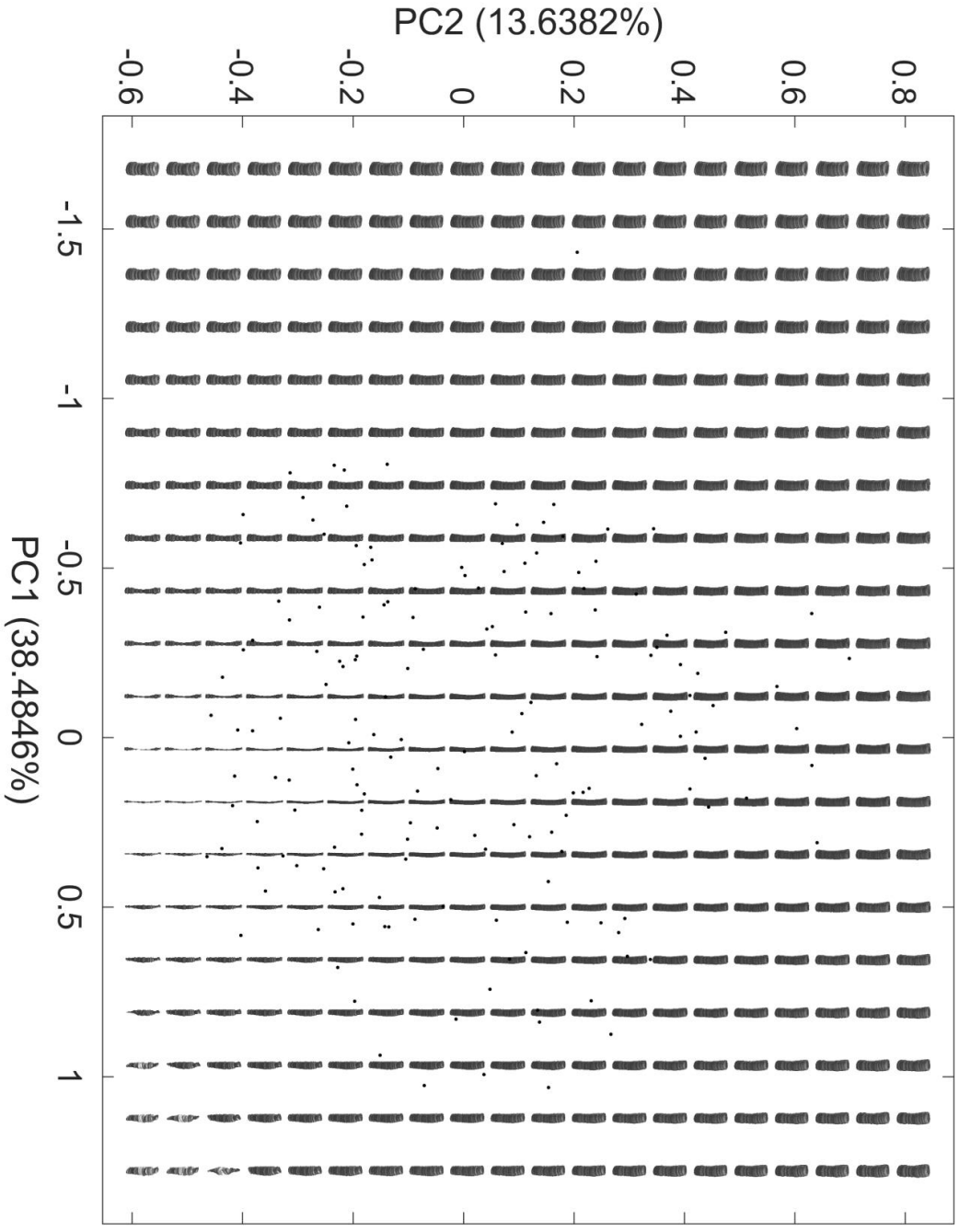

Figure 5.6: Bird humeral limb shaft theoretical morphospace. Grey shapes represent 20-by-20 grid of 3D theoretical limb shaft morphologies, spanning the range of empirical morphospace plus an extra 10% border. Black dots represent empirical data.

of their shape: volume, rotational efficiency in the mediolateral direction, rotational efficiency in the anteroposterior orientation, resistance to bending in the mediolateral direction and resistance to bending in the anteroposterior direction.

The rotational efficiency metrics are calculated using a finite element model of each bone shape to approximate the rotational inertia of the shape when rotated about the mediolateral axis and the anteroposterior axis. These were then used to calculate the speed of the distal centroid of the limb shaft, given one unit of rotational kinetic energy about each axis at the proximal end of the limb shaft. The resistance to bending in each direction was approximated by the sum of the second moment of areas of each cross section slice, in the mediolateral and anteroposterior axes. These were then combined using the Pareto rank ratio into a single optimality surface [192].

5.3 Results

5.3.1 Empirical and Theoretical Morphospace

The PC1-PC2 morphospace of limb shaft variation captures a total of $\sim 52\%$ of shape variation (PC1 = 38.5%, PC2 = 13.6%) (figure 5.5). Due to the inclusion of rotational information in this shape characterization, changes in shape in this space occur radially about a point in the mid PC1 and low PC2 coordinates. This point represents an infinitely thin and long bone, with bones getting thicker and more curved along radial vectors from this point in morphospace. Extreme theoretical morphologies tend to have ridges along the bone shaft, as the differences in variation between slices is magnified at extreme morphospace positions.

The occupation of empirical taxa within this morphospace is evenly spread about the mean, with the exception of one outlier taxon: the whiskered treeswift (*Hemiprocne comata*). These organisms are known for high flight manoeuvrability, with very long primary wing feathers and short wing spars, which may explain this bias in humeral limb shaft shape. Taxa which specialise in aquatic and aerial lifestyles (figure 5.5 A, blue and white dots respectively) occupy limited regions of morphospace compared to the ranges of other groups, which overlap significantly across the breadth of empirical morphospace. The exception is the Humboldt penguin (*Spheniscus humboldti*), an organism with modified wings for underwater flying. Similarly, when splitting the empirical morphospace by aquatic and non-aquatic diet, those birds that feed in aquatic environments lie in similarly limited regions of morphospace compared to the total occupation of morphospace.

5.3.2 Functional landscapes

All theoretical morphologies are corrected for bone shaft length before being subject to functional analysis. This means that the volume of theoretical shapes varies across morphospace. The pattern of volume change across morphospace is not smooth: it tends to increase from the mid PC1, low PC2 point, but with a periodic banding pattern at regular intervals along PC1.

The rotational efficiency of limb shaft shape is controlled by the mass distribution of bone in the shaft, with a preference for long, thin bones with mass concentrated at the center. For this reason, the resulting rotational efficiency landscapes are biased by

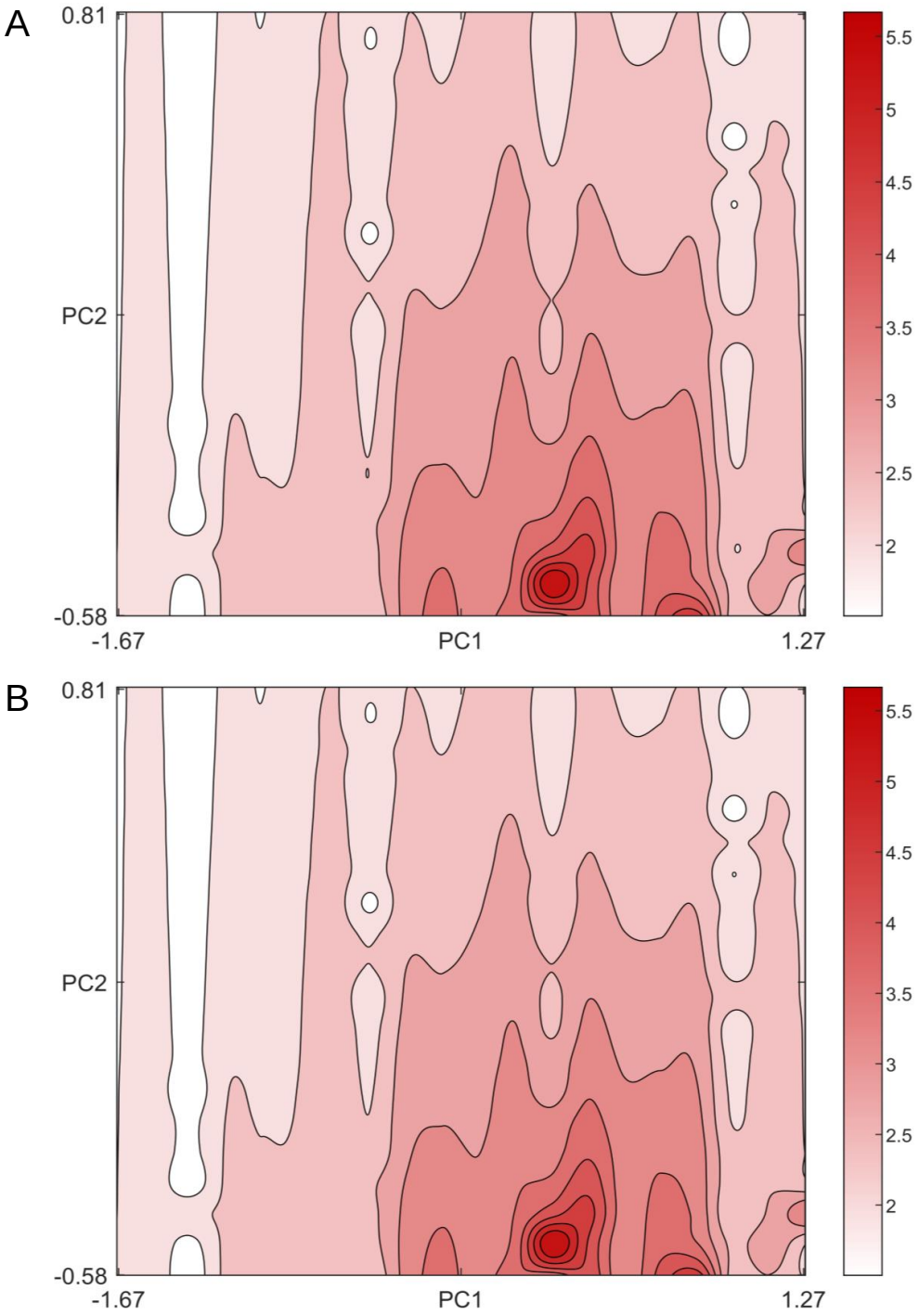

Figure 5.7: Rotational efficiency landscapes. **(A)** Performance landscape of rotational efficicency of theoretical morphospace in the mediolateral direction. **(B)** Performance landscape of rotational efficicency of theoretical morphospace in the dorsoventral direction. Darker bands represent higher rotational efficiency. 'Banding' patterns appear due to the cyclical variation in theoretical bone volume.

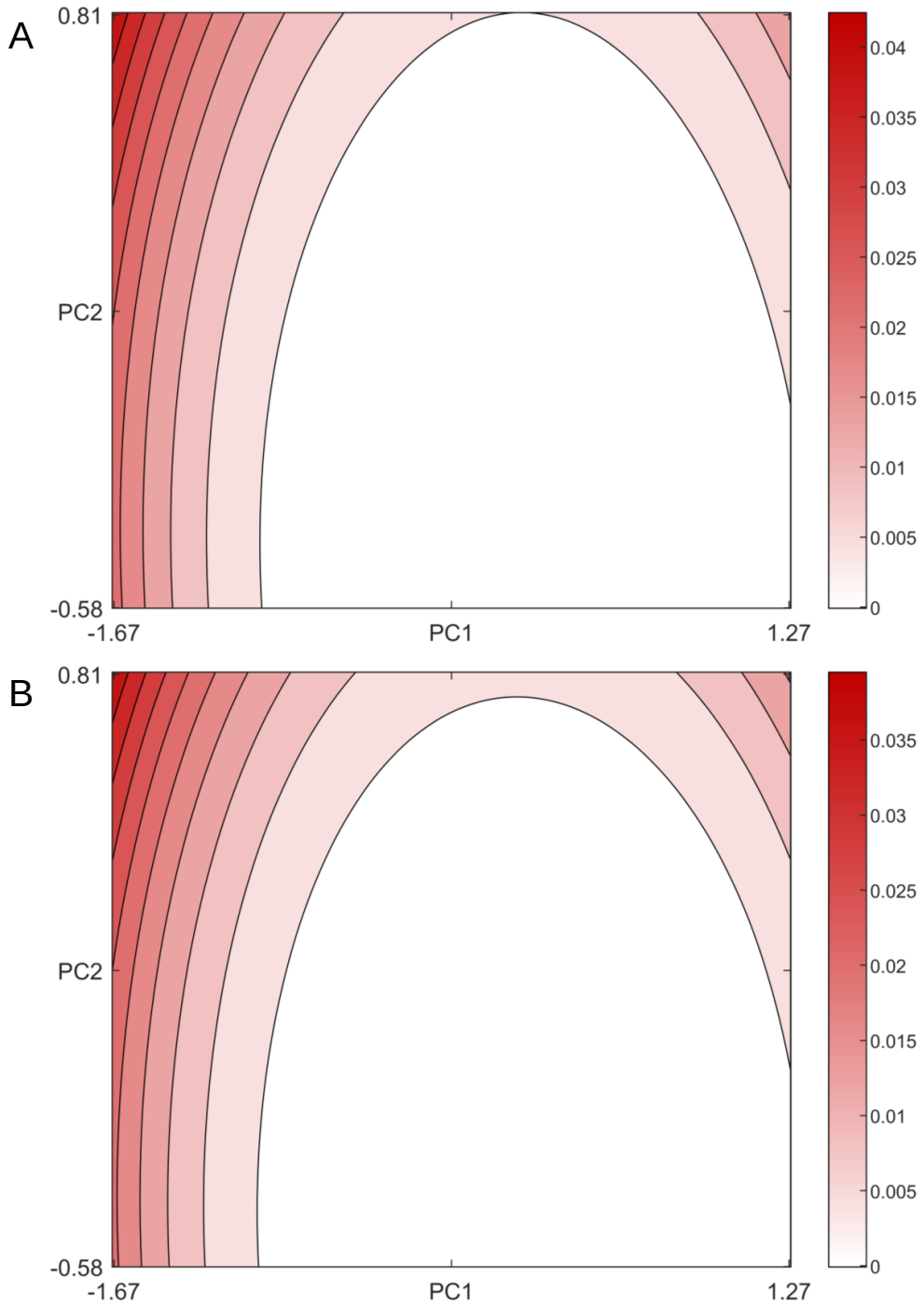

Figure 5.8: Resistance to bending landscapes. (A) Performance landscape of resistance to bending (sum of second moment of area of cross sectional geometries) of theoretical morphospace in the mediolateral direction. **(B)** Performance landscape of resistance to bending (sum of second moment of area of cross sectional geometries) of theoretical morphospace in the dorsoventral direction. Darker bands represent higher resistance to bending.

the arbitrarily thin bones in mid PC1 and low PC2 regions (figure 5.6, 5.7). I correct for this by plotting the log scaled rotational efficiency landscape, which preserves the rank order of functional performance between theoretical morphologies, and thus does not affect Pareto optimality calculations, despite modifying the ratios of performance between theoretical morphologies. The banding from the volume surface persists through this surface at regular PC1 intervals, as the rotational inertia, and thus the rotational efficiency, is largely dependent on the total bone volume. The total second moment of area varies more smoothly across morphospace, with bending resistance increasing as you move further from the center of morphospace (figure 5.8).

The difference in morphospace occupation by different ecological groups results in different distributions in function between the ecological groups (figure 5.9). In terms of primary ecology, aquatic and aerial taxa are biased towards morphologies with higher rotational efficiency, lower bone volume and lower resistance to bending. Similarly, taxa that have predominantly aquatic diets are also biased towards morphologies with higher rotational efficiency, lower bone volume and lower resistance to bending.

5.3.3 Optimality

When considering the Pareto optimality within the trade-off for the rotational efficiency, resistance to bending and bone volume of limb shafts, the periodic bands in the surface at regular intervals along PC1 become more apparent (figure 5.10). The bands in the performance surfaces bias the optimality surface, as the peaks tend to represent much more optimal performance than their neighbouring troughs, therefore spreading high optimality along PC1.

5.4 Discussion

5.4.1 Ecology and limb shaft morphology

These results show that the morphology of the humeral shaft is linked to the primary ecology in this dataset. Most notably, aquatic and aerial birds exhibit a limited range of humeral shaft morphologies compare to the range of all other birds, characterised by long, thin shapes with high rotational efficiency. This is unsurprising, as similar results have been found when characterising patterns of cross sectional geometry in bird limb bones [378, 379], and forelimb musculature [382], but this study has shown that the link holds to the total shape of the shaft, including cross sectional geometry, curvature and length. The differences in morphology reflect a preference for lightweight and rotationally efficient bones in aerial and aquatic birds. Many aquatic birds rely on flight to travel between aquatic habitats, which may require long distance flight, and oceanic birds tend to soar long distances with a requirement for wing shape with high aspect ratio [33]. Organisms that fly for long distances would then prefer longer and more efficient humeral shafts, at the cost of proportional strength.

5.4.2 Morphometrics

The pipeline here is designed to assess the structure of the limb shaft of bones within tetrapods. Taking regular slices along a bone is a common practice in comparative studies,

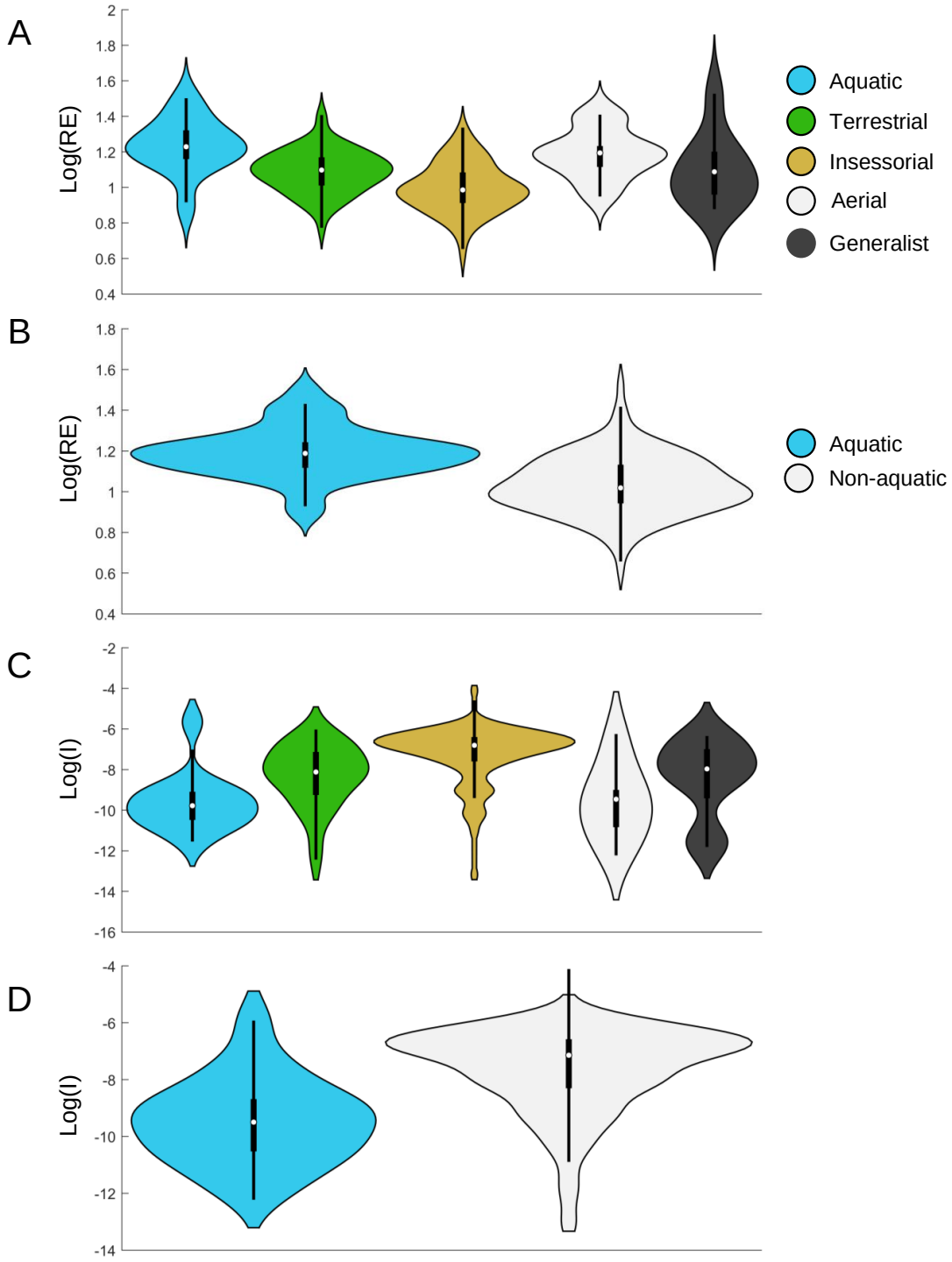

Figure 5.9: Distribution of performances between ecological groups. Violin plots of the distribution of empirical interpolated performance, split by ecology: **(A)** Log scaled rotational efficiency of each primary ecology; **(B)** Log scaled rotational efficiency of each dietary ecology; **(C)** Log scaled resistance to bending of each primary ecology; **(D)** Log scaled resistance to bending each dietary ecology. All performance metrics are taken from the mediolateral axis, due to similarity in results between different axes.

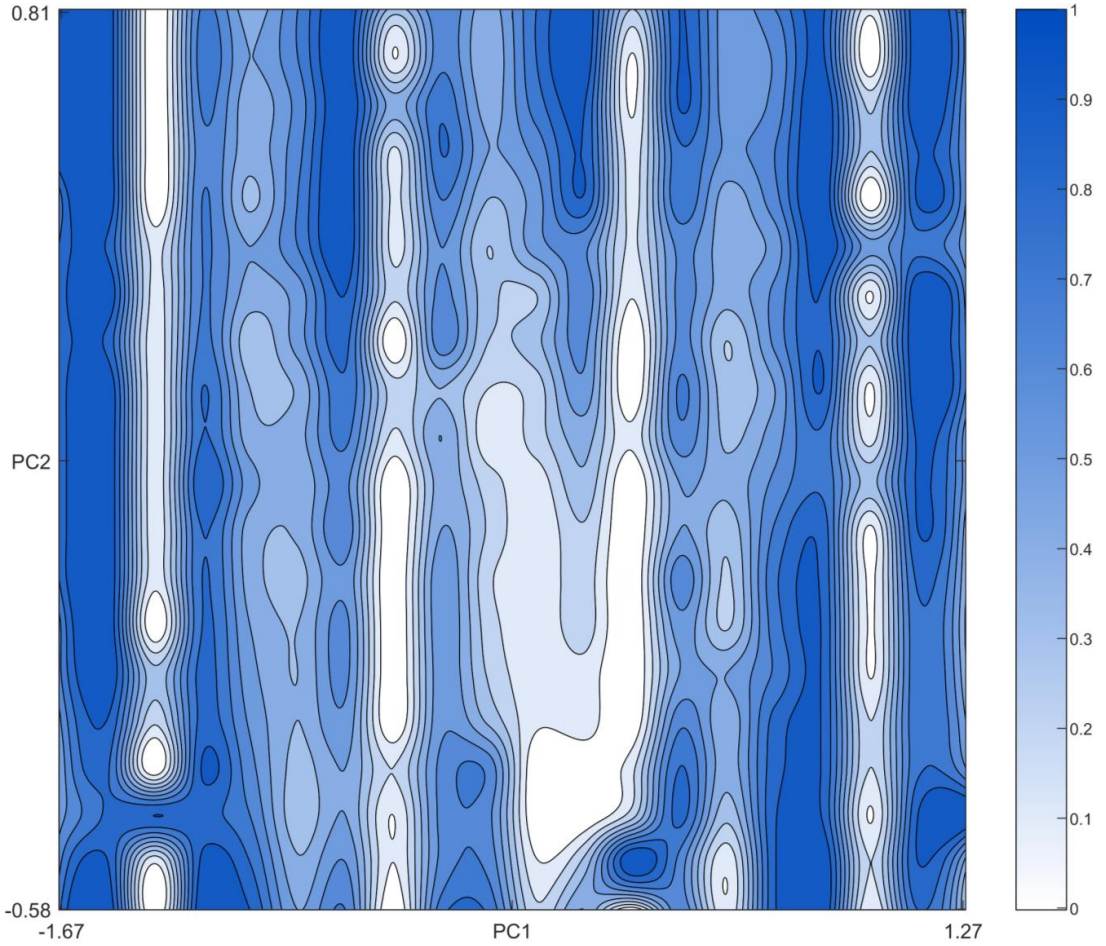

Figure 5.10: Pareto optimality landscape. Pareto optimality is calculated via the Pareto rank ratio of all four performance metrics. The 'banding' pattern arises from cyclical variation in theoretical bone volume, which in turn affects the pattern of the rotational efficiency landscape.

and has been combined with morphometric analysis and beam theory extensively within mammal humeri [383–386] and the humeri of birds [377, 379]. It has also found uses in the teeth and skulls of dinosaurs and crocodiles [387, 388] and the teeth of conodonts [389]. Finally, cross sectional morphology has been used to generate and validate models of morphological growth in a wide range of pointed biological structures [64]. While cross sections are measured differently between these studies, the position and plane in which to slice the geometry is defined manually. That is, human input is used to estimate the position and orientation of a cross section at a point along the structure; or a landmark is used to define the initial position of the cross section and the orientation is arbitrarily defined; or, as is often the case where multiple cross sections along the bone are used, the positions and orientations are defined by a biological axis. The ability to algorithmically define a curved axis for a shaft may help future studies to slice geometry in such a way that is conscious of axis curvature, while requiring minimal human input and error.

Within this study, the comparison of shape along the shaft necessitates a conservation of rotation along the shaft – that is, all EFA contours must not be aligned to remove rotation, and should be aligned to a common axis between taxa. Similarly, the separate contours used for the inner and outer perimeter of each cross section must be aligned to preserve cross-sectional geometry. This results in some issues with orientation when extrapolating theoretical morphospace, as shapes are not aligned, so all orientations of a single shape are considered different morphologies. This can be seen in the resulting radial pattern of theoretical morphospace, where rotation about the mid PC1, low PC2 point results in change in shape rotation but not necessarily the geometry. More work on this pipeline is needed to remedy this issue (figure 5.6).

Another issue with reconstructed morphologies within this pipeline is the banded ridges that appear in the extremes of theoretical morphospace (figure 5.6). This is a result of the different magnitudes of variance between bands, which cause variation along a PC axis to vary between cross sections. A potential solution is to factor in the covariance between successive morphologies along the shaft. As the distance between successive cross sections decreases to a limit of zero, the morphological distance must also decrease to a limit of zero. Thus, the function mapping the length along the bone axis of a cross section to its location in cross sectional morphospace is continuous, and can be modelled via an infinite polynomial. The parameters of the best fit polynomial could then be used as the axes of morphospace, allowing reconstruction of theoretical morphospace at arbitrary slice densities. Issues with this method may arise with the nature of the resulting morphospace, which would be a non-Euclidean affine space [78].

In order to generate a theoretical morphospace, the data from each bone must be vectorised in a way that allows reconstruction of the original data from the vector. In most cases this is simple, as the algorithm used to generate the vector from morphological data can be reversed. However, issues arise with the normalisation of data. When normalising these morphometric data for size, how should the normal vector of each slice be scaled? In the morphometric process, we defined that the normal vector of each slice has a magnitude of one. However, scaling the rest of the data while leaving the normal vector will artificially inflate its variance and thus its impact on the resulting PC coordinates. Further, a 3D vector of length one can be characterised by a 2D vector, as its third dimension is dependent on the other two dimensions. Thus, if the normal vectors are scaled such that their length does not equal one, they must be described in 3D space, resulting in the morphospace increasing by $N_s = 33$ dimensions.

The 'banding' nature of the bone volume and rotational efficiency landscapes can be attributed to the construction of morphospace. While the pipeline for generating curved axes for slicing the bone is robust and widely applicable, the use of an unscaled EFA and the lack of consideration of the correlation between successive slice morphologies results in chaotic and unpredictable theoretical morphologies. The distance within morphospace is still Euclidean, and thus empirical morphospace can be interpreted, but the theoretical morphospace is ill defined and requires further development.

Chapter 6

Conclusion

Author's contribution This chapter was written by William J. Deakin.

Functional constraint in the evolution of biological shape is important to our understanding of the diversity of morphology in nature. There is no doubt that morphology is at least in part adapted, such that it is fit for purpose, but the precise role that functional adaptation plays in defining shape is still not clear. Throughout evolutionary biology's 150 year history, perspectives have shifted on how we should interpret shape in terms of function. Today, it is uncontroversial to use morphological and biomechanical proxies to elucidate behaviours in life history. This is particularly true of palaeontology, where in the absence of extremely rare direct fossilised evidence of ecosystem interactions, the majority of our understanding of palaeoecology is from morphological inference. This often has a solid empirical basis, where observational evidence from extant taxa shows a statistical link between shape, function and ecology. This breaks down in cases where the links between form, function and ecology are not so clear. The extrapolation to extinct taxa relies on an adaptationist assumption that both the extinct morphologies being measured and the control group of extant morphologies are functionally optimized by evolution.

In this thesis I have aimed to explore this problem from a different perspective, by attempting to test the optimality of morphologies for particular functions, and observing this change in evolutionary history. I aimed to develop a 'post-spandrels' framework for removing adaptationist bias in further biomechanical and morphological studies. This framework is built from a combination of previous concepts such as morphodynamics, theoretical morphology, biomechanics and Pareto optimality. This is not novel work; many studies in the last few decades have asked similar questions in similar ways, utilizing theoretical morphospaces to build performance and adaptive landscapes [85, 120, 121, 123, 201, 282, 319]. These have generally found high conformity of their samples to their generated landscapes, but this may be expected as the methodology makes prior assumptions of functional optimisation. The difference in this work comes from the Pareto optimality metric, along with the broadening of methods for defining theoretical morphologies.

I have utilized these concepts to analyse 2D jaw shape throughout the evolutionary history of gnathostomes. This has yielded interesting and insightful results in itself, not just about the role of functional optimality in the evolution of morphology as a whole, but in each particular study group it has revealed information about their evolution. It has also prompted further questions about the jaw structure, that I will discuss in the next

part of this conclusion. That being said, I do not think this framework is complete. The jaw has been a useful case study through which to apply these methodologies, but it is not the only structure in biological systems. I spent time developing chapter 5 of this thesis in order to show that the methodology is more broadly applicable, and expandable to 3D morphology, but more work is needed to refine these processes for building theoretical morphospaces. In part two of this conclusion, I will discuss the potential of theoretical morphology, and its future requirements. I will finish this thesis with a brief discussion of future projects and methodologies that could be explored to further develop and utilise the analytical pipeline for measuring functional constraint.

6.1 Functional constraint in vertebrate jaw morphology

Hopefully this thesis has provided a convincing case that the variety in jaw morphology of many gnathostomes is largely controlled by two inversely correlated functional properties of form: its strength in resistance to loading, and the energy required to open and close it at high speeds. There is large variety in preference for these two performance metrics, which may be related with diet, but many jaws are optimized within this trade-off. This has been shown in three major transitions in the history of gnathostome jaw evolution: the origin of jaws, the terrestrialisation of vertebrates, and the transition to the mammalian single dentary mandible structure.

At the origin of jaws, we see that functional optimality is reached very quickly in geological time scales [192]. In its current condition, the jaw fossil record shows that the earliest jaws were optimised for jaw function, suggesting that the developmental and functional transition from agnathan gill arches to gnathostome mandibles was very quick. In the terrestrialisation of vertebrates, results in this thesis and the literature suggest a temporal delay between the transition from water to land and jaw functional morphology [198]. Despite very different environmental constraints imposed by water and land, the functional demands of jaw shape remain the same. Finally, the reduction of mandibular bones in mammals allows more optimal forms to evolve, while simultaneously reducing the shape complexity. This highlights the links between functional optimality and complexity in the jaw, providing an explanation for the reduction in jaw complexity throughout tetrapod evolution that is consistent with the Zero Force Evolutionary Law (ZFEL).

Overall, the shape of the jaw in gnathostomes appears to be heavily controlled by functional demands. Most jaws in vertebrate evolutionary history can be explained as balancing the demands of efficiency and strength. However, there are exceptions to this rule, found in herbivorous Palaeozoic amniotes and in the ungulates within mammals. This prompts further questions about the mechanical demands of different feeding mechanisms – why are the functional constraints on jaw morphology in some herbivorous animals different from all other feeding styles? Herbivory tends to require high bite forces to process tough plant material, which may shift the demand away from rotational efficiency and towards mechanical advantage. In herbivorous lizards, higher mechanical advantage is convergently evolved in the lower jaw multiple times [390]. Further, within this pattern there may also be some explanations for previously unexplained macroevolutionary phenomena. Many large marine macropredatory lineages have evolved filter feeding lifestyles, including marine

reptiles, mammals, actinopterygians and sharks. The similarity in functional demands on the jaw may help explain this phenomenon, as jaws adapted for both dietary ecologies are optimised within the trade-off for rotational efficiency and strength.

Overall, this may seem like a support of adaptationist logic. The morphology of jaws can be understood as an optimisation of functional performances, thus it is perfectly adapted. However, as previously noted, not all jaws are optimised within this trade-off. Furthermore, herein lies the new approach for dealing with topics such as assumed adaptivity. The solution to the issue is not to assume all structures are optimised, nor is it to assume that no structure is optimised. The solution is to investigate optimality within structures and lineages, and test whether optimality is reached. In this thesis, I believe I have laid convincing evidence that the jaw morphology of many vertebrates, particularly aquatic animals and terrestrial predators, is heavily optimised.

6.2 Broader applications of theoretical morphology

Much more work is needed to develop and formalise the methodology when asking questions of optimality. Many components of the pipeline are already mature fields of evolutionary science: we already have reliable metrics for measuring phylogenetic bias on morphology, and the classical mechanics used to infer functional performance are commonplace in contemporary biomechanics. Further, the Pareto rank ratio metric provides a means to combine any number of functional performances into a single optimality metric. In order to improve this workflow, and definitively test the roles of morphodynamic constraints on form, there needs to be more sophisticated and informed models of theoretical morphology.

Theoretical morphology has great potential to investigate evolutionary constraints. By definition, the question requires the analysis of unevolved shapes as a control group in an investigation. Developing these models is difficult, but some biological structures can be modelled with precise, developmentally informed formulae [64]. Further work must also be done to standardise the construction of theoretical morphospace. In chapter 4 of this thesis, I intended to test the random point cloud theoretical morphospace as an alternative to the grid that is commonplace in the literature. While the results were unpredictable, and the sampling of unexplored morphospace was insufficient to provide meaningful inference at large macroevolutionary scales, with fine tuning and more computationally efficient algorithms there is a future where all dimensions of shape can be characterised.

Finally, models of 3D morphology should be developed and optimised such that all aspects of shape can be investigated. While 2D morphology is still informative, and large datasets can be built with 2D data, some information is still lost from the full Three-Dimensional (3D) shape, including morphological variation and some properties of functional performance [138, 374]. For these reasons, I spent time in my PhD attempting to develop models of 3D shape in the limb shaft of birds. This morphology has been hard to measure with traditional landmark methods, and no algorithms for the description and reconstruction of theoretical morphologies exist in this structure. The methodology described is applicable to a wide variety of bone shafts, as well as many biological ‘tubes’, such as plant stems and blood vessels. Of particular importance is the methodology for describing the bone axis, which may help future investigations of cross-sectional geometry,

as well as further investigating trajectories in morphospace which I will discuss briefly in the next part of this conclusion.

6.3 Future directions

In the future, I hope to continue the investigation of jaw shape and functional optimality. Gnathostomes make up the majority of taxa in vertebrate evolutionary history, and the fossil record of the jaw is extensive, allowing complete description of optimality within certain trade-offs throughout macroevolutionary time. Particularly, investigations of more environmental transitions could provide interesting insight into how optimality changes with varying functional demands. Further, I hope to incorporate more functional performance metrics in order to elucidate the different functional constraints acting on terrestrial herbivorous gnathostomes. More informed models of theoretical morphology that include data about jaw joint structure may help this, and allow the construction of mechanical advantage performance landscapes. I would like to test the many transitions from marine macropredators to giant filter feeders, as this is a consistently repeating pattern in vertebrate evolutionary history, suggesting that functional convergence and constraint may provide insight.

I would also like to spend more time developing theoretical models of morphology, particularly to capture 3D skeletal morphology. There are many possible methodologies available, such as spherical harmonic analyses (SPHARM) [391]. Issues also arise in theoretical morphology due to topological non homeomorphism between shapes, which cannot be mapped easily to one another mathematically. In general, structures with the same number of holes can be mapped within the same morphospace, like a torus can be continuously deformed into a coffee mug. However, biological structures often evolve new holes, or close old ones, and these can have impacts on functional morphology [392]. If these problems can be solved and topologically distinct structures can be compared, and new standardised algorithms for the construction of high dimensional theoretical morphospaces formulated, there is a possibility to investigate all of theoretical morphospace.

Finally, empirical data can perhaps inform of the structure of underlying morphospace. Any parameterisation of shape space can be understood as a high dimensional manifold, the curvature of which representing the 'evolvability' of shape over morphospace. This can be measured through a vector field derived from the phylomorphospace, as a function of the average vector of morphological change at each point in morphospace. In a 'flat' morphospace, the average direction of evolution at any point is the adaptive landscape. More likely, however, is that phylogenetic bias and morphogenetic bias distort the morphospace manifold. Differences between optimality landscapes and the curvature of the phylomorphospace may provide further insight into the strength of functional controls in comparison with phylogenetic controls on form. Furthermore, this can be applied to any trajectory in morphospace – for example, the developmental trajectories of structures through ontogeny.

6.4 The role of mechanical function in the evolution of skeletal morphology

The evolution of morphology is dependent on many factors. Understanding these factors, and how they contribute together in creating biological form, is an imperative goal of contemporary systematic biology. Outside of biological science, the public perception of nature is largely visual, and thus we connect with nature through its form. Engineers model trains with the shape of a kingfisher beak and artists design alien creatures with the visual inspiration of our own animals. Our connection with nature relies on our understanding of it, and during a period of ecosystem collapse and anthropogenic climate change this connection is more important than ever. Despite current biological science firmly agreeing that biological shape is contingent on many factors, the widespread view of evolution is that it is determined by function. The engineers building the bullet train assumed that the kingfisher beak was functionally optimised. The creature artists working on James Cameron's *Avatar 2: The Way of Water* assumed that the structures found in our spread of modern marine taxa would convergently evolve elsewhere. These may be true assumptions, but deep in their logical pathways lie problematic views of evolution: that it is an almost perfect optimiser, akin to an intelligent designer. In the past and still today, these views promote dangerous beliefs about human culture, our relation to one another, and our superiority over nature.

The rationale and methodological basis for understanding the limits of evolution's optimising power have been outlined here in this thesis. By using morphometrics, biomechanics, theoretical morphology and optimality theory, we can assess how true these assumptions are. We can understand how shape evolves, how the nuances of evolutionary history push and pull evolution in all directions, sometimes in direct opposition to the nearest optimal front. Within a morphodynamic framework, we can understand these contingencies as phylogenetic and morphogenetic, which can be measured. Put together, there is a future in science where comprehensive adaptive landscapes can be built, allowing for more informed morphological phylogenetics, biologically inspired engineering, and maybe even inspiring a deeper understanding of our own connection to natural systems. I don't claim to solve the original questions posed at the beginning of this thesis, though I believe that one day evolutionary biologists will. These are extremely difficult problems to solve analytically, and we may not yet have the tools to do so. But I believe that with patience exploration and testing of new methodology, we can get closer to answering the question: *How much of form is controlled by function?*

References

[1] C. Darwin. *On the origin of species*. 1859.

[2] P. R. Grant and B. R. Grant. "The breeding and feeding characteristics of Darwin's finches on Isla Genovesa, Galapagos". In: *Ecological Monographs* 50.3 (1980), pp. 381–410.

[3] M. Foote. "The evolution of morphological diversity". In: *Annual Review of Ecology and Systematics* 28.1 (1997), pp. 129–152.

[4] J. G. Kingsolver and R. B. Huey. "Introduction: the evolution of morphology, performance, and fitness". In: *Integrative and Comparative Biology* 43.3 (2003), pp. 361–366.

[5] J. Hausser. "Genetic drift and selection: their respective weights in the morphological and genetic differentiation of four species of shrews in southern Europe (Insectivora, Soricidae)". In: *Journal of Zoological Systematics and Evolutionary Research* 22.4 (1984), pp. 302–320.

[6] S. M. Clegg et al. "Microevolution in island forms: the roles of drift and directional selection in morphological divergence of a passerine bird". In: *Evolution* 56.10 (2002), pp. 2090–2099.

[7] R. R. Ackermann and J. M. Cheverud. "Detecting genetic drift versus selection in human evolution". In: *Proceedings of the National Academy of Sciences* 101.52 (2004), pp. 17946–17951.

[8] R. Araya-Donoso et al. "Integrating genetics, physiology and morphology to study desert adaptation in a lizard species". In: *Journal of Animal Ecology* 91.6 (2022), pp. 1148–1162.

[9] P. C. J. Donoghue and M. J. Benton. "Rocks and clocks: calibrating the Tree of Life using fossils and molecules". In: *Trends in ecology & evolution* 22.8 (2007), pp. 424–431.

[10] F. Ronquist et al. "A total-evidence approach to dating with fossils, applied to the early radiation of the Hymenoptera". In: *Systematic biology* 61.6 (2012), pp. 973–999.

[11] L. Pozzi and A. Penna. "Rocks and clocks revised: new promises and challenges in dating the primate tree of life". In: *Evolutionary Anthropology: Issues, News, and Reviews* 31.3 (2022), pp. 138–153.

[12] G. G. Simpson. *Tempo and mode in evolution*. 15. Columbia University Press, 1944.

[13] M. Tamborini. "A plea for a new synthesis: from twentieth-century paleobiology to twenty-first-century paleontology and back again". In: *Biology* 11.8 (2022), p. 1120.

[14] J. A. Cunningham et al. "A virtual world of paleontology". In: *Trends in ecology & evolution* 29.6 (2014), pp. 347–357.

[15] D. M. Boyer et al. "Morphosource: archiving and sharing 3-D digital specimen data". In: *The Paleontological Society Papers* 22 (2016), pp. 157–181.

[16] L. E. Copes et al. "A collection of non-human primate computed tomography scans housed in MorphoSource, a repository for 3D data". In: *Scientific data* 3.1 (2016), pp. 1–8.

[17] G. Taylor and A. Thomas. *Evolutionary biomechanics: selection, phylogeny, and constraint*. OUP Oxford, 2014.

[18] S. Broyde et al. "Evolutionary biomechanics: hard tissues and soft evidence?" In: *Proceedings of the Royal Society B* 288.1945 (2021), p. 20202809.

[19] J. Wiemann et al. "Fossil biomolecules reveal an avian metabolism in the ancestral dinosaur". In: *Nature* 606.7914 (2022), pp. 522–526.

[20] A. K. Behrensmeyer, S. M. Kidwell, and R. A. Gastaldo. "Taphonomy and paleobiology". In: *Paleobiology* 26.S4 (2000), pp. 103–147.

[21] S. J. Gould and R. C. Lewontin. "The Spandrels of San Marco and the Panglossian Paradigm: A Critique of the Adaptationist Programme". In: *Proceedings of the Royal Society of London. Series B, Biological Sciences* (1979), pp. 581–598.

[22] A. Seilacher. "Arbeitskonzept zur konstruktions-morphologie". In: *Lethaia* 3.4 (1970), pp. 393–396.

[23] A. Seilacher and A. D. Gishlick. *Morphodynamics*. Taylor & Francis Oxfordshire, UK, 2015.

[24] D. E. G. Briggs. "Seilacher, konstruktions-morphologie, morphodynamics, and the evolution of form". In: *Journal of Experimental Zoology Part B: Molecular and Developmental Evolution* 328.3 (2017), pp. 197–206.

[25] A. Herrel et al. "Bite performance and morphology in a population of Darwin's finches: implications for the evolution of beak shape". In: *Functional Ecology* 19.1 (2005), pp. 43–48.

[26] J. Soons et al. "Mechanical stress, fracture risk and beak evolution in Darwin's ground finches (Geospiza)". In: *Philosophical Transactions of the Royal Society B: Biological Sciences* 365.1543 (2010), pp. 1093–1098.

[27] J. Soons et al. "Is beak morphology in Darwin's finches tuned to loading demands?" In: *PLoS One* 10.6 (2015), e0129479.

[28] L. P. Lawson and K. Petren. "The adaptive genomic landscape of beak morphology in Darwin's finches". In: *Molecular ecology* 26.19 (2017), pp. 4978–4989.

[29] S. Al-Mosleh et al. "Geometry and dynamics link form, function, and evolution of finch beaks". In: *Proceedings of the National Academy of Sciences* 118.46 (2021), e2105957118.

[30] M. E. Alfaro, D. I. Bolnick, and P. C. Wainwright. "Evolutionary consequences of many-to-one mapping of jaw morphology to mechanics in labrid fishes". In: *The American Naturalist* 165.6 (2005), E140–E154.

[31] P. G. Cox et al. "Functional evolution of the feeding system in rodents". In: *PLoS One* 7.4 (2012), e36299.

[32] A. L. Pigot et al. "Macroevolutionary convergence connects morphological form to ecological function in birds". In: *Nature Ecology & Evolution* 4.2 (2020), pp. 230–239.

[33] S. L. Baumgart, P. C. Sereno, and M. W. Westneat. "Wing shape in waterbirds: morphometric patterns associated with behavior, habitat, migration, and phylogenetic convergence". In: *Integrative Organismal Biology* 3.1 (2021), obab011.

[34] D. B. Booher et al. "Functional innovation promotes diversification of form in the evolution of an ultrafast trap-jaw mechanism in ants". In: *PLoS biology* 19.3 (2021), e3001031.

[35] S. Gutarra and I. A. Rahman. "The locomotion of extinct secondarily aquatic tetrapods". In: *Biological Reviews* 97.1 (2022), pp. 67–98.

[36] B. Chong et al. “Coordinating tiny limbs and long bodies: Geometric mechanics of lizard terrestrial swimming”. In: *Proceedings of the National Academy of Sciences* 119.27 (2022), e2118456119.

[37] I. Menéndez et al. “Diet versatility and functional trade-offs shape tooth morphology in squirrels”. In: *Evolution* 77.1 (2023), pp. 83–96.

[38] F. E. Fish. “Influence of hydrodynamic-design and propulsive mode on mammalian swimming energetics”. In: *Australian Journal of Zoology* 42.1 (1994), pp. 79–101.

[39] F. E. Fish. “Biomechanics and energetics in aquatic and semiaquatic mammals: platypus to whale”. In: *Physiological and Biochemical Zoology* 73.6 (2000), pp. 683–698.

[40] S. Gutarra et al. “Effects of body plan evolution on the hydrodynamic drag and energy requirements of swimming in ichthyosaurs”. In: *Proceedings of the Royal Society B* 286.1898 (2019), p. 20182786.

[41] T. Fletcher et al. “Hydrodynamics of fossil fishes”. In: *Proceedings of the Royal Society B: Biological Sciences* 281.1788 (2014), p. 20140703.

[42] M. Rincon-Sandoval et al. “Evolutionary determinism and convergence associated with water-column transitions in marine fishes”. In: *Proceedings of the National Academy of Sciences* 117.52 (2020), pp. 33396–33403.

[43] H. G. Ferrón et al. “Functional assessment of morphological homoplasy in stem-gnathostomes”. In: *Proceedings of the Royal Society B* 288.1943 (2021), p. 20202719.

[44] F. E. Fish. “The myth and reality of Gray’s paradox: implication of dolphin drag reduction for technology”. In: *Bioinspiration & biomimetics* 1.2 (2006), R17.

[45] T. McKeag. “How one engineer’s birdwatching made Japan’s bullet train better”. In: *The Biomimicry Column* (2012).

[46] F. Mathews. “Towards a deeper philosophy of biomimicry”. In: *Organization & Environment* 24.4 (2011), pp. 364–387.

[47] D. Adriaens. “Evomimetics: the biomimetic design thinking 2.0”. In: *Bioinspiration, Biomimetics, and Bioreplication IX*. Vol. 10965. SPIE. 2019, pp. 41–53.

[48] G. Sansalone et al. “Trapped in the morphospace: The relationship between morphological integration and functional performance”. In: *Evolution* 76.9 (2022), pp. 2020–2031.

[49] M. Hawkins and M. Hawkins. *Social Darwinism in European and American thought, 1860-1945: Nature as model and nature as threat*. Cambridge university press, 1997.

[50] Mariette Manktelow. “History of taxonomy”. In: *Lecture from Dept. of Systematic Biology, Uppsala University* 29 (2010).

[51] C. Linnaeus. *Systema naturae*. Vol. 1. Stockholm Laurentii Salvii, 1758.

[52] Mario CC De Pinna. “Concepts and tests of homology in the cladistic paradigm”. In: *Cladistics* 7.4 (1991), pp. 367–394.

[53] S. J. Gould and N. Eldredge. “Punctuated equilibria: an alternative to phyletic gradualism”. In: *Models in paleobiology* 1972 (1972), pp. 82–115.

[54] L. R. Heasley, N. M. V. Sampaio, and J. L. Argueso. “Systemic and rapid restructuring of the genome: a new perspective on punctuated equilibrium”. In: *Current genetics* 67 (2021), pp. 57–63.

[55] L. J. Harmon et al. “Early bursts of body size and shape evolution are rare in comparative data”. In: *Evolution* 64.8 (2010), pp. 2385–2396.

[56] M. Hughes, S. Gerber, and M. A. Wills. “Clades reach highest morphological disparity early in their evolution”. In: *Proceedings of the National Academy of Sciences* 110.34 (2013), pp. 13875–13879.

[57] K. L. Baab, K. P. McNulty, and K. Harvati. “Homo floresiensis contextualized: a geometric morphometric comparative analysis of fossil and pathological human samples”. In: *PLoS One* 8.7 (2013), e69119.

[58] M. D. Dumbravă et al. “A dinosaurian facial deformity and the first occurrence of ameloblastoma in the fossil record”. In: *Scientific reports* 6.1 (2016), p. 29271.

[59] J. M. Fahlke and O. Hampe. “Cranial symmetry in baleen whales (Cetacea, Mysticeti) and the occurrence of cranial asymmetry throughout cetacean evolution”. In: *The Science of Nature* 102 (2015), pp. 1–16.

[60] E. J. Coombs et al. “Wonky whales: the evolution of cranial asymmetry in cetaceans”. In: *BMC biology* 18.1 (2020), pp. 1–24.

[61] A. Lanzetti et al. “The ontogeny of asymmetry in echolocating whales”. In: *Proceedings. Biological sciences* 289.1980 (2022), p. 20221090.

[62] D. M. Raup and A. Michelson. “Theoretical morphology of the coiled shell”. In: *Science* 147.3663 (1965), pp. 1294–1295.

[63] H. Vogel. “A better way to construct the sunflower head”. In: *Mathematical biosciences* 44.3-4 (1979), pp. 179–189.

[64] A. R. Evans et al. “A universal power law for modelling the growth and form of teeth, claws, horns, thorns, beaks, and shells”. In: *BMC biology* 19.1 (2021), pp. 1–14.

[65] D. R. Diedrichs. “Archimedean, Logarithmic and Euler spirals- intriguing and ubiquitous patterns in nature”. In: *The Mathematical Gazette* 103.556 (2019), pp. 52–64.

[66] C. P. Klingenberg. “Morphological integration and developmental modularity”. In: *Annual review of ecology, evolution, and systematics* 39 (2008), pp. 115–132.

[67] A. Goswami and P. D. Polly. “Methods for studying morphological integration and modularity”. In: *The Paleontological Society Papers* 16 (2010), pp. 213–243.

[68] C. P. Klingenberg. “Studying morphological integration and modularity at multiple levels: concepts and analysis”. In: *Philosophical Transactions of the Royal Society B: Biological Sciences* 369.1649 (2014), p. 20130249.

[69] M. W. J. Ferguson and T. Joanen. “Temperature of egg incubation determines sex in Alligator mississippiensis”. In: *Nature* 296.5860 (1982), pp. 850–853.

[70] S. Renaud et al. “Morphological evolution, ecological diversification and climate change in rodents”. In: *Proceedings of the Royal Society B: Biological Sciences* 272.1563 (2005), pp. 609–617.

[71] J. Babin-Fenske, M. Anand, and Y. Alarie. “Rapid morphological change in stream beetle museum specimens correlates with climate change”. In: *Ecological Entomology* 33.5 (2008), pp. 646–651.

[72] A. Mikis et al. “Temporal variability in foraminiferal morphology and geochemistry at the West Antarctic Peninsula: a sediment trap study”. In: *Biogeosciences* 16.16 (2019), pp. 3267–3282.

[73] R. D. McCulloch, P. Mathiasen, and A. C. Premoli. “Palaeoecological evidence of pollen morphological changes: A climate change adaptation strategy?” In: *Palaeogeography, Palaeoclimatology, Palaeoecology* 601 (2022), p. 111157.

[74] A. Goswami. "Morphological integration in the carnivoran skull". In: *Evolution* 60.1 (2006), pp. 169–183.

[75] C. M. Martinez and J. S. Sparks. "Malagasy cichlids differentially limit impacts of body shape evolution on oral jaw functional morphology". In: *Evolution* 71.9 (2017), pp. 2219–2229.

[76] K. L. Foster et al. "Skink ecomorphology: forelimb and hind limb lengths, but not static stability, correlate with habitat use and demonstrate multiple solutions". In: *Biological Journal of the Linnean Society* 125.4 (2018), pp. 673–692.

[77] A. J. Conith et al. "Ecomorphological divergence and habitat lability in the context of robust patterns of modularity in the cichlid feeding apparatus". In: *BMC Evolutionary Biology* 20 (2020), pp. 1–20.

[78] P. Mitteroecker and S. M. Huttegger. "The concept of morphospaces in evolutionary and developmental biology: mathematics and metaphors". In: *Biological Theory* 4 (2009), pp. 54–67.

[79] S. Wright. "The roles of mutation, inbreeding, crossbreeding, and selection in evolution". In: *Proceedings of the Sixth International Congress on Genetics* 1.8 (1932), pp. 355–366.

[80] E. Svensson and R. Calsbeek. *The adaptive landscape in evolutionary biology*. OUP Oxford, 2012.

[81] J. N. Pitt and A. R. Ferré-D'Amaré. "Rapid construction of empirical RNA fitness landscapes". In: *Science* 330.6002 (2010), pp. 376–379.

[82] T. Hinkley et al. "A systems analysis of mutational effects in HIV-1 protease and reverse transcriptase". In: *Nature genetics* 43.5 (2011), pp. 487–489.

[83] R. D. Kouyos et al. "Exploring the complexity of the HIV-1 fitness landscape". In: *PLoS genetics* 8.3 (2012), e1002551.

[84] J. Otwinowski and I. Nemenman. "Genotype to phenotype mapping and the fitness landscape of the E. coli lac promoter". In: *PloS one* 8.5 (2013), e61570.

[85] P. D. Polly et al. "Combining geometric morphometrics and finite element analysis with evolutionary modeling: towards a synthesis". In: *Journal of Vertebrate Paleontology* 36.4 (2016), e1111225.

[86] G. R. McGhee. "Theoretical morphology: the concept and its applications". In: *Short courses in paleontology* 4 (1991), pp. 87–102.

[87] G. R. McGhee. *The geometry of evolution: adaptive landscapes and theoretical morphospaces*. Cambridge University Press, 2006.

[88] J. M. C. Hutchinson. "But which morphospace to choose?: Theoretical Morphology by GR McGhee, Jr". In: *Trends in Ecology & Evolution* 14.10 (1999), p. 414.

[89] C. N. Ciampaglio, M. Kemp, and D. W. McShea. "Detecting changes in morphospace occupation patterns in the fossil record: characterization and analysis of measures of disparity". In: *Paleobiology* 27.4 (2001), pp. 695–715.

[90] P. C. Wainwright et al. "A functional morphospace for the skull of labrid fishes: patterns of diversity in a complex biomechanical system". In: *Biological Journal of the Linnean Society* 82.1 (2004), pp. 1–25.

[91] B. Shen et al. "The Avalon explosion: evolution of Ediacara morphospace". In: *Science* 319.5859 (2008), pp. 81–84.

[92] K. C. Prentice, M. Ruta, and M. J. Benton. "Evolution of morphological disparity in pterosaurs". In: *Journal of Systematic Palaeontology* 9.3 (2011), pp. 337–353.

[93] S. A. Price et al. “Building a body shape morphospace of teleostean fishes”. In: *Integrative and Comparative Biology* 59.3 (2019), pp. 716–730.

[94] C. M. Lowery and A. J. Fraass. “Morphospace expansion paces taxonomic diversification after end Cretaceous mass extinction”. In: *Nature Ecology & Evolution* 3.6 (2019), pp. 900–904.

[95] P. E. Jardine et al. “Why does pollen morphology vary? Evolutionary dynamics and morphospace occupation in the largest angiosperm order (Asterales)”. In: *New Phytologist* 234.3 (2022), pp. 1075–1087.

[96] C. H. Martin and P. C. Wainwright. “Multiple fitness peaks on the adaptive landscape drive adaptive radiation in the wild”. In: *Science* 339.6116 (2013), pp. 208–211.

[97] S. M. Smith, C. T. Stayton, and K. D. Angielczyk. “How many trees to see the forest? Assessing the effects of morphospace coverage and sample size in performance surface analysis”. In: *Methods in Ecology and Evolution* 12.8 (2021), pp. 1411–1424.

[98] G. R. McGhee. “Limits in the evolution of biological form: a theoretical morphologic perspective”. In: *Interface focus* 5.6 (2015), p. 20150034.

[99] C. Bardua et al. “A practical guide to sliding and surface semilandmarks in morphometric analyses”. In: *Integrative Organismal Biology* 1.1 (2019), obz016.

[100] M. L. Zelditch, D. L. Swiderski, and H. D. Sheets. *Geometric morphometrics for biologists: a primer*. academic press, 2012.

[101] A. Palci and M. S. Y. Lee. “Geometric morphometrics, homology and cladistics: review and recommendations”. In: *Cladistics* 35.2 (2019), pp. 230–242.

[102] M. L. Zelditch, W. L. Fink, and D. L. Swiderski. “Morphometrics, homology, and phylogenetics: quantified characters as synapomorphies”. In: *Systematic Biology* 44.2 (1995), pp. 179–189.

[103] N. MacLeod. “Phylogenetic signals in morphometric data”. In: *SYSTEMATICS ASSOCIATION SPECIAL VOLUME* 64 (2002), pp. 100–138.

[104] F. J. Rohlf and D. Slice. “Extensions of the Procrustes method for the optimal superimposition of landmarks”. In: *Systematic biology* 39.1 (1990), pp. 40–59.

[105] P. O’Higgins. “The study of morphological variation in the hominid fossil record: biology, landmarks and geometry”. In: *The Journal of Anatomy* 197.1 (2000), pp. 103–120.

[106] S. B. Cooke and C. E. Terhune. “Form, function, and geometric morphometrics”. In: *The Anatomical Record* 298.1 (2015), pp. 5–28.

[107] A. M. Lawing and P. D. Polly. “Geometric morphometrics: recent applications to the study of evolution and development”. In: *Journal of Zoology* 280.1 (2010), pp. 1–7.

[108] D. D. Kassam et al. “Morphometric analysis on ecomorphologically equivalent cichlid species from Lakes Malawi and Tanganyika”. In: *Journal of Zoology* 260.2 (2003), pp. 153–157.

[109] C. Meloro and D. Tamagnini. “Macroevolutionary ecomorphology of the Carnivora skull: adaptations and constraints in the extant species”. In: *Zoological Journal of the Linnean Society* 196.3 (2022), pp. 1054–1068.

[110] G. P. Lohmann. “Eigenshape analysis of microfossils: a general morphometric procedure for describing changes in shape”. In: *Journal of the International Association for Mathematical Geology* 15 (1983), pp. 659–672.

[111] N. MacLeod. “Generalizing and extending the eigenshape method of shape space visualization and analysis”. In: *Paleobiology* 25.1 (1999), pp. 107–138.

[112] F. P. Kuhl and C.R. Giardina. “Elliptic Fourier features of a closed contour”. In: *Computer graphics and image processing* 18.3 (1982), pp. 236–258.

[113] J. Caple, J. Byrd, and C. N. Stephan. “Elliptical Fourier analysis: fundamentals, applications, and value for forensic anthropology”. In: *International Journal of Legal Medicine* 131.6 (2017), pp. 1675–1690.

[114] J. J. Hill et al. “Evolution of jaw disparity in fishes”. In: *Palaeontology* 61.6 (2018), pp. 847–854.

[115] K. Roy and M. Foote. “Morphological approaches to measuring biodiversity”. In: *Trends in Ecology & Evolution* 12.7 (1997), pp. 277–281.

[116] D. H. Erwin. “Disparity: morphological pattern and developmental context”. In: *Palaeontology* 50.1 (2007), pp. 57–73.

[117] D. M. Raup. “Geometric analysis of shell coiling: general problems”. In: *Journal of paleontology* (1966), pp. 1178–1190.

[118] D. M. Raup. “Geometric analysis of shell coiling: coiling in ammonoids”. In: *Journal of Paleontology* (1967), pp. 43–65.

[119] Z. J. Tseng. “Testing adaptive hypotheses of convergence with functional landscapes: a case study of bone-cracking hypercarnivores”. In: *PLOS one* 8.5 (2013), e65305.

[120] C. T. Stayton. “Performance in three shell functions predicts the phenotypic distribution of hard-shelled turtles”. In: *Evolution* 73.4 (2019), pp. 720–734.

[121] B. V. Dickson and S. E. Pierce. “Functional performance of turtle humerus shape across an ecological adaptive landscape”. In: *Evolution* 73.6 (2019), pp. 1265–1277.

[122] K. E. Jones et al. “Adaptive landscapes challenge the “lateral-to-sagittal” paradigm for mammalian vertebral evolution”. In: *Current Biology* 31.9 (2021), pp. 1883–1892.

[123] B. V. Dickson et al. “Functional adaptive landscapes predict terrestrial capacity at the origin of limbs”. In: *Nature* 589.7841 (2021), pp. 242–245.

[124] B. Deline et al. “Evolution and development at the origin of a phylum”. In: *Current Biology* 30.9 (2020), pp. 1672–1679.

[125] G. R. McGhee. “Shell form in the biconvex articulate Brachiopoda: a geometric analysis”. In: *Paleobiology* 6.1 (1980), pp. 57–76.

[126] W. G. Eberhard et al. “Sexual selection and static allometry: the importance of function”. In: *The Quarterly Review of Biology* 93.3 (2018), pp. 207–250.

[127] A. J. Klinkhamer et al. “Head to head: the case for fighting behaviour in *Megaloceros giganteus* using finite-element analysis”. In: *Proceedings of the Royal Society B* 286.1912 (2019), p. 20191873.

[128] Philip Jay Motta. “Mechanics and functions of jaw protrusion in teleost fishes: a review”. In: *Copeia* (1984), pp. 1–18.

[129] P. S. L. Anderson and M. W. Westneat. “Feeding mechanics and bite force modelling of the skull of *Dunkleosteus terrelli*, an ancient apex predator”. In: *Biology Letters* 3.1 (2007), pp. 77–80.

[130] R. S. Mehta. “Ecomorphology of the moray bite: relationship between dietary extremes and morphological diversity”. In: *Physiological and Biochemical Zoology* 82.1 (2009), pp. 90–103.

[131] P. S. L. Anderson, S. Renaud, and E. J. Rayfield. “Adaptive plasticity in the mouse mandible”. In: *BMC Evolutionary Biology* 14.1 (2014), pp. 1–9.

[132] F. J. Larabee and A. V. Suarez. “The evolution and functional morphology of trap-jaw ants (Hymenoptera: Formicidae)”. In: *Myrmecological News* 20 (2014), pp. 25–36.

[133] J. M. Neenan et al. “Feeding biomechanics in Acanthostega and across the fish–tetrapod transition”. In: *Proceedings of the Royal Society B: Biological Sciences* 281.1781 (2014), p. 20132689.

[134] S. Serrano-Fochs et al. “Finite element analysis of the Cingulata jaw: an ecomorphological approach to armadillo’s diets”. In: *PLoS One* 10.4 (2015), e0120653.

[135] M. L. Zelditch et al. “Rare ecomorphological convergence on a complex adaptive landscape: body size and diet mediate evolution of jaw shape in squirrels (Sciuridae)”. In: *Evolution* 71.3 (2017), pp. 633–649.

[136] F. J. Larabee, A. A. Smith, and A. V. Suarez. “Snap-jaw morphology is specialized for high-speed power amplification in the Dracula ant, Mystrium camillae”. In: *Royal Society open science* 5.12 (2018), p. 181447.

[137] M. N. Simon et al. “Bite performance surfaces of three ecologically divergent Iguanidae lizards: relationships with lower jaw bones”. In: *Biological Journal of the Linnean Society* 127.4 (2019), pp. 810–825.

[138] N. M. Morales-Garcıa et al. “The use of extruded finite-element models as a novel alternative to tomography-based models: a case study using early mammal jaws”. In: *Journal of the Royal Society Interface* 16.161 (2019), p. 20190674.

[139] K. F. Liem and S. L. Sanderson. “The pharyngeal jaw apparatus of labrid fishes: a functional morphological perspective”. In: *Journal of Morphology* 187.2 (1986), pp. 143–158.

[140] S. Ginot et al. “Morphometric models for estimating bite force in Mus and Rattus: mandible shape and size perform better than lever-arm ratios”. In: *Journal of Experimental Biology* 222.12 (2019), jeb204867.

[141] J. Marcé-Nogué et al. “Broad-scale morpho-functional traits of the mandible suggest no hard food adaptation in the hominin lineage”. In: *Scientific Reports* 10.1 (2020), p. 6793.

[142] K. Kotrschal. “Trophic ecomorphology in eastern Pacific blennioid fishes: character transformation of oral jaws and associated change of their biological roles”. In: *Environmental Biology of Fishes* 24 (1989), pp. 199–218.

[143] M. W. Westneat. “Feeding mechanics of teleost fishes (Labridae; Perciformes): A test of four-bar linkage models”. In: *Journal of morphology* 205.3 (1990), pp. 269–295.

[144] P. C. Wainwright. “Ecomorphology: experimental functional anatomy for ecological problems”. In: *American Zoologist* 31.4 (1991), pp. 680–693.

[145] L. M. Witmer and K. D. Rose. “Biomechanics of the jaw apparatus of the gigantic Eocene bird Diatryma: implications for diet and mode of life”. In: *Paleobiology* 17.2 (1991), pp. 95–120.

[146] T. B. Waltzek and P. C. Wainwright. “Functional morphology of extreme jaw protrusion in Neotropical cichlids”. In: *Journal of Morphology* 257.1 (2003), pp. 96–106.

[147] M. E. Alfaro, D. I. Bolnick, and P. C. Wainwright. “Evolutionary dynamics of complex biomechanical systems: an example using the four-bar mechanism”. In: *Evolution* 58.3 (2004), pp. 495–503.

[148] P. C. Wainwright. “Functional morphology of the pharyngeal jaw apparatus”. In: *Fish physiology* 23 (2005), pp. 77–101.

[149] E. Stein, M. Rüter, and S. Ohnimus. "Adaptive finite element analysis and modelling of solids and structures. Findings, problems and trends". In: *International Journal for Numerical Methods in Engineering* 60.1 (2004), pp. 103–138.

[150] J. N. Reddy. *An Introduction to Nonlinear Finite Element Analysis Second Edition: with applications to heat transfer, fluid mechanics, and solid mechanics*. OUP Oxford, 2014.

[151] Callum F Ross. "Finite element analysis in vertebrate biomechanics". In: *The Anatomical Record Part A: Discoveries in Molecular, Cellular, and Evolutionary Biology: An Official Publication of the American Association of Anatomists* 283.2 (2005), pp. 253–258.

[152] E. J. Rayfield. "Finite element analysis and understanding the biomechanics and evolution of living and fossil organisms". In: *Annu. Rev. Earth Planet. Sci.* 35 (2007), pp. 541–576.

[153] O. Panagiotopoulou. "Finite element analysis (FEA): applying an engineering method to functional morphology in anthropology and human biology". In: *Annals of human biology* 36.5 (2009), pp. 609–623.

[154] J. Donea, S. Giuliani, and J. P. Halleux. "An arbitrary Lagrangian-Eulerian finite element method for transient dynamic fluid-structure interactions". In: *Computer methods in applied mechanics and engineering* 33.1-3 (1982), pp. 689–723.

[155] R. W. Lewis et al. *The finite element method in heat transfer analysis*. John Wiley & Sons, 1996.

[156] J. F. V. Vincent. "The trade-off: a central concept for biomimetics". In: *Bioinspired, Biomimetic and Nanobiomaterials* 6.2 (2016), pp. 67–76.

[157] S. J. Arnold. "Morphology, performance and fitness". In: *American Zoologist* 23.2 (1983), pp. 347–361.

[158] S. J Arnold, M. E. Pfrender, and A. G. Jones. "The adaptive landscape as a conceptual bridge between micro-and macroevolution". In: *Microevolution rate, pattern, process* (2001), pp. 9–32.

[159] S. J. Arnold. "Performance surfaces and adaptive landscapes". In: *Integrative and comparative biology* 43.3 (2003), pp. 367–375.

[160] J. Horn, N. Nafpliotis, and D. E. Goldberg. "A niched Pareto genetic algorithm for multiobjective optimization". In: *Proceedings of the first IEEE conference on evolutionary computation. IEEE world congress on computational intelligence*. Ieee. 1994, pp. 82–87.

[161] M. S. Y. Lee and A. Palci. "Morphological phylogenetics in the genomic age". In: *Current Biology* 25.19 (2015), R922–R929.

[162] M. R. Pie and J. S. Weitz. "A null model of morphospace occupation". In: *The American Naturalist* 166.1 (2005), E1–E13.

[163] B. Sidlauskas. "Continuous and arrested morphological diversification in sister clades of characiform fishes: a phylomorphospace approach". In: *Evolution* 62.12 (2008), pp. 3135–3156.

[164] W. P. Maddison. "Squared-change parsimony reconstructions of ancestral states for continuous-valued characters on a phylogenetic tree". In: *Systematic Biology* 40.3 (1991), pp. 304–314.

[165] M. Royer-Carenzi and G. Didier. "A comparison of ancestral state reconstruction methods for quantitative characters". In: *Journal of Theoretical Biology* 404 (2016), pp. 126–142.

[166] J. B. Smaers, C. S. Mongle, and A. Kandler. “A multiple variance Brownian motion framework for estimating variable rates and inferring ancestral states”. In: *Biological Journal of the Linnean Society* 118.1 (2016), pp. 78–94.

[167] E. W. Goolsby. “Rapid maximum likelihood ancestral state reconstruction of continuous characters: A rerooting-free algorithm”. In: *Ecology and Evolution* 7.8 (2017), pp. 2791–2797.

[168] C. P. Klingenberg and N. A. Gidaszewski. “Testing and quantifying phylogenetic signals and homoplasy in morphometric data”. In: *Systematic biology* 59.3 (2010), pp. 245–261.

[169] T. Münkemüller et al. “How to measure and test phylogenetic signal”. In: *Methods in Ecology and Evolution* 3.4 (2012), pp. 743–756.

[170] D. C. Adams. “A generalized K statistic for estimating phylogenetic signal from shape and other high-dimensional multivariate data”. In: *Systematic biology* 63.5 (2014), pp. 685–697.

[171] J. R. Stone. “Ontogenic tracks and evolutionary vestiges in morphospace”. In: *Biological Journal of the Linnean Society* 64.2 (1998), pp. 223–238.

[172] F. Witzmann, H. Scholz, and M. Ruta. “Morphospace occupation of temnospondyl growth series: a geometric morphometric approach”. In: *Alcheringa* 33.3 (2009), pp. 237–255.

[173] B. A. S. Bhullar et al. “Birds have paedomorphic dinosaur skulls”. In: *Nature* 487.7406 (2012), pp. 223–226.

[174] K. E. Powder et al. “Constraint and diversification of developmental trajectories in cichlid facial morphologies”. In: *EvoDevo* 6.1 (2015), pp. 1–14.

[175] O. Ellers. “A mechanical model of growth in regular sea urchins: predictions of shape and a developmental morphospace”. In: *Proceedings of the Royal Society of London. Series B: Biological Sciences* 254.1340 (1993), pp. 123–129.

[176] G. J. Eble. “Developmental and non-developmental morphospaces in evolutionary biology”. In: *Morphospace concepts and applications* (1999).

[177] J. Tyszka. “Morphospace of foraminiferal shells: results from the moving reference model”. In: *Lethaia* 39.1 (2006), pp. 1–12.

[178] S. Gerber. “Not all roads can be taken: development induces anisotropic accessibility in morphospace”. In: *Evolution & Development* 16.6 (2014), pp. 373–381.

[179] J. A. Bolker. “Modularity in development and why it matters to evo-devo”. In: *American Zoologist* 40.5 (2000), pp. 770–776.

[180] C. P. Klingenberg. *Integration, modules, and development*. Oxford University Press New York, 2004.

[181] M. Pigliucci and K. Preston. *Phenotypic integration: studying the ecology and evolution of complex phenotypes*. Oxford University Press, 2004.

[182] A. Goswami et al. “The fossil record of phenotypic integration and modularity: a deep-time perspective on developmental and evolutionary dynamics”. In: *Proceedings of the National Academy of Sciences* 112.16 (2015), pp. 4891–4896.

[183] B. Hallgrımsson, K. Willmore, and B. K. Hall. “Canalization, developmental stability, and morphological integration in primate limbs”. In: *American Journal of Physical Anthropology: The Official Publication of the American Association of Physical Anthropologists* 119.S35 (2002), pp. 131–158.

[184] M. Bastir and A. Rosas. “Hierarchical nature of morphological integration and modularity in the human posterior face”. In: *American Journal of Physical Anthropology* 128.1 (2005), pp. 26–34.

[185] A. G. Drake and C. P. Klingenberg. “Large-scale diversification of skull shape in domestic dogs: disparity and modularity”. In: *The American Naturalist* 175.3 (2010), pp. 289–301.

[186] M. Randau and A. Goswami. “Morphological modularity in the vertebral column of Felidae (Mammalia, Carnivora)”. In: *BMC evolutionary biology* 17 (2017), pp. 1–12.

[187] C. López-Aguirre et al. “Postcranial heterochrony, modularity, integration and disparity in the prenatal ossification in bats (Chiroptera)”. In: *BMC Evolutionary Biology* 19.1 (2019), pp. 1–17.

[188] M. Randau, D. Sanfelice, and A. G. “Shifts in cranial integration associated with ecological specialization in pinnipeds (Mammalia, Carnivora)”. In: *Royal Society Open Science* 6.3 (2019), p. 190201.

[189] A. Watanabe et al. “Ecomorphological diversification in squamates from conserved pattern of cranial integration”. In: *Proceedings of the National Academy of Sciences* 116.29 (2019), pp. 14688–14697.

[190] B. Figueirido, A. Pérez-Ramos, and A. Martın-Serra. “Intravertebral vs. intervertebral integration and modularity in the vertebral column of mammalian carnivorans”. In: *Journal of Anatomy* (2022).

[191] J. N. Keating et al. “Morphological phylogenetics evaluated using novel evolutionary simulations”. In: *Systematic Biology* 69.5 (2020), pp. 897–912.

[192] W. J. Deakin et al. “Increasing morphological disparity and decreasing optimality for jaw speed and strength during the radiation of jawed vertebrates”. In: *Science Advances* 8.11 (2022), eabl3644.

[193] P. C. J. Donoghue and J. N. Keating. “Early vertebrate evolution”. In: *Palaeontology* 57.5 (2014), pp. 879–893.

[194] R. H. Denison. “Feeding mechanisms of agnatha and early gnathostomes”. In: *Integrative and Comparative Biology* 1 (1961), pp. 177–181.

[195] K. Dennis and R. S. Miles. “New durophagous arthrodires from Gogo, Western Australia”. In: *Zoological Journal of the Linnean Society* 69.1 (1980), pp. 43–85.

[196] P. S. L. Anderson and M. W. Westneat. “Feeding mechanics and bite force modelling of the skull of *Dunkleosteus terrelli*, an ancient apex predator”. In: *Biology Letters* 3.1 (2006), pp. 77–80.

[197] E. Snively, P. S. L. Anderson, and M. J. Ryan. “Functional and ontogenetic implications of bite stress in arthrodire placoderms”. In: *Kirtlandia* 57 (2010), pp. 53–60.

[198] P. S. L. Anderson et al. “Initial radiation of jaws demonstrated stability despite faunal and environmental change”. In: *Nature* 476.7359 (2011), pp. 206–209.

[199] P. S. L. Anderson, M. Friedman, and M. Ruta. “Late to the Table: Diversification of tetrapod mandibular biomechanics lagged behind the evolution of terrestriality”. In: *Integrative and Comparative Biology* 53.2 (2013), pp. 197–208.

[200] B. Figueirido, Z. J. Tseng, and A. Martín-Serra. “Skull shape evolution in durophagous carnivorans”. In: *Evolution* 67.7 (2013), pp. 1975–1993.

[201] C. T. Stayton, L. F. O’Connor, and N. M. Nisivoccia. “The influence of multiple functional demands on morphological diversification: a test on turtle shells”. In: *Evolution* 72.9 (2018), pp. 1933–1949.

[202] P. S. L. Anderson. “Cranial muscle homology across modern gnathostomes”. In: *Biological Journal of the Linnean Society* 94.1 (2008), pp. 195–216.

[203] P. E. Ahlberg and J. A. Clack. “Lower jaws, lower tetrapods–a review based on the Devonian genus Acanthostega”. In: *Transactions of the Royal Society of Edinburgh: Earth Sciences* 89.1 (1998), pp. 11–46.

[204] M. Zhu and X. B. Yu. “Lower jaw character transitions among major sarcopterygian groups—a survey based on new materials from Yunnan, China”. In: *Recent advances in the origin and early radiation of vertebrates* (2004), pp. 271–286.

[205] K. S. W. Campbell and R. E. Barwick. “A new tooth-plated dipnoan from the Upper Devonian Gogo Formation and its relationships”. In: *Memoirs-Queensland Museum* 42 (1998), pp. 403–437.

[206] A. Heintz. “Fischreste aus dem Unterperm Norwegens”. In: *Norsk geologisk tidsskrift* 14.1-2 (1934), pp. 176–194.

[207] J. Lu and M. Zhu. “An Early Devonian (Pragian) sarcopterygian from Zhaotong, Yunnan, China”. In: *Vertebrata PalAsiatica* 46.3 (2008), p. 161.

[208] H. Jessen. “Weitere Fischreste aus dem Oberen Plattenkalk der Bergisch-Gladbach-Paffrather Mulde (Oberdevon, Rheinisches Schiefergebirge)”. In: *Palaeontographica Abteilung A* (1973), pp. 159–187.

[209] J. A. Long. “Cranial anatomy of two new late Devonian lungfishes (Pisces: Dipnoi) from Mount Howitt, Victoria”. In: *Records of the Australian Museum* 44.3 (1992), pp. 299–318.

[210] M. Rücklin et al. “Development of teeth and jaws in the earliest jawed vertebrates”. In: *Nature* 491.7426 (2012), pp. 748–751.

[211] R. K. Carr. “Placoderm diversity and evolution”. In: *Bulletin du Muséum national d’histoire naturelle: Sciences de la terre, paléontologie, géologie, minéralogie. Section C* 17 (1995), p. 85.

[212] D. H. Dunkle. “A new genus and species of arthrodiran fish from the Upper Devonian Cleveland Shale”. In: *Scientific Publications of the Cleveland Museum of Natural History* 8 (1947), pp. 103–117.

[213] K. S. W. Campbell, R. E. Barwick, and T. J. Senden. “Evolution of dipnoans (lungfish) in the Early Devonian of southeastern Australia”. In: *Alcheringa* 33.1 (2009), pp. 59–78.

[214] J. E. Harris. *The dorsal spine of* Cladoselache*: The neurocranium and jaws of* Cladselache. Vol. 8. 1. 1938.

[215] A. Heintz. “Revision of the structure of *Coccosteus decipiens* Ag.” In: *Norwegian Journal of Geology* 12 (1931), pp. 291–313.

[216] L. Hussakof and W. L. Bryant. “Catalog of the fossil fishes in the Museum of the Buffalo Society of Natural Sciences.—Buffalo, Soc”. In: *Nat. Sci., Bull* 12 (1918), pp. 1–346.

[217] H. G. Johnson and D. K. Elliott. “A new ptyctodont (Placodermi) from the Upper Devonian Martin Formation of northern Arizona, and an analysis of ptyctodont phylogeny”. In: *Journal of Paleontology* 70.6 (1996), pp. 994–1003.

[218] E. B. Daeschler. “Early tetrapod jaws from the Late Devonian of Pennsylvania, USA”. In: *Journal of Paleontology* 74.2 (2000), pp. 301–308.

[219] M. M. Smith and M. M. Chang. “The dentition of *Diabolepis speratus* Chang and Yu, with further consideration of its relationships and the primitive dipnoan dentition”. In: *Journal of Vertebrate Paleontology* 10.4 (1990), pp. 420–433.

[220] M. Friedman. "*Styloichthys* as the oldest coelacanth: implications for early osteichthyan interrelationships". In: *Journal of Systematic Palaeontology* 5.3 (2007), pp. 289–343.

[221] J. A. Long, B. Choo, and G. C. Young. "A new basal actinopterygian fish from the Middle Devonian Aztec Siltstone of Antarctica". In: *Antarctic Science* 20.4 (2008), pp. 393–412.

[222] B. Young et al. "A gigantic sarcopterygian (tetrapodomorph lobe-finned fish) from the Upper Devonian of Gondwana (Eden, New South Wales, Australia)". In: *PLOS ONE* 8 (2013), pp. 1–30.

[223] J. A. Clack. *Gaining ground: the origin and evolution of tetrapods*. Indiana University Press, 2012.

[224] J. A. Long. "A new genus of fossil coelacanth (Osteichthyes: Coelacanthiformes) from the Middle Devonian of southeastern Australia". In: *Records of the Western Australian Museum* 57 (1999), pp. 37–53.

[225] J. A. Long, R. E. Barwick, and K. S. W. Campbell. "Osteology and functional morphology of the osteolepiform fish *Gogonasus andrewsae* Long, 1985, from the Upper Devonian Gogo Formation, Western Australia". In: *Records of the Australian Museum* 53 (1997), pp. 1–89.

[226] B. Choo, J. A. Long, and K. Trinajstic. "A new genus and species of basal actinopterygian fish from the Upper Devonian Gogo Formation of Western Australia". In: *Acta Zoologica* 90.s1 (2009), pp. 194–210.

[227] M. Zhu et al. "The oldest articulated osteichthyan reveals mosaic gnathostome characters". In: *Nature* 458.7237 (2009), pp. 469–474.

[228] P. S. L. Anderson. "Shape variation between arthrodire morphotypes indicates possible feeding niches". In: *Journal of Vertebrate Paleontology* 28.4 (2008), pp. 961–969.

[229] Z. Gorizdro-Kulczycka. "Dwudyszne ryby dewońskie Gór Swietokrzyskich". In: *Acta Geologica Polonica* 1.2 (1950), pp. 53–105.

[230] J. P. Downs. "*Holoptychius bergmanni* sp. nov.(Sarcopterygii, Porolepiformes) from the Upper Devonian of Nunavut, Canada, and a review of *Holoptychius* taxonomy". In: *Proceedings of the Academy of Natural Sciences of Philadelphia* 162.1 (2013), pp. 47–59.

[231] E. Mark-Kurik. "The inferognathal in the Middle Devonian arthrodire Homostius". In: *Lethaia* 25.2 (1992), pp. 173–178.

[232] J. A. Long. "A new Late Devonian acanthodian fish from Mt. Howitt, Victoria, Australia, with remarks on acanthodian biogeography". In: *Proceedings of the Royal Society of Victoria* 98.1-2 (1986), pp. 1–17.

[233] J. A. Long. "New palaeoniscoid fishes from the Late Devonian and Early Carboniferous of Victoria". In: *Mem. Assoc. Australas. Palaeontol.* 7 (1988), pp. 1–64.

[234] E. B. Daeschler and J. P. Downs. "New description and diagnosis of *Hyneria lindae* (Sarcopterygii, Tristichopteridae) from the Upper Devonian Catskill Formation in Pennsylvania, USA". In: *Journal of Vertebrate Paleontology* 38.3 (2018), e1448834.

[235] E. I. White. "The Old Red Sandstone of Brown Clee Hill and the adjacent area II. Palaeontology". In: *Bulletin of the British Museum (Natural History), Geology* 5 (1961), pp. 243–310.

[236] E. I. Vorobyeva. “Morphology and nature of evolution of crossopterygian fish”. In: *Trudy Paleontologicheskogo Instituta* 163 (1977), pp. 1–239.

[237] K. Trinajstic and J. A. Long. “A new genus and species of Ptyctodont (Placodermi) from the Late Devonian Gneudna Formation, Western Australia, and an analysis of Ptyctodont phylogeny”. In: *Geological Magazine* 146.5 (2009), pp. 743–760.

[238] E. I. Vorobyeva. “A new species of *Laccognathus* (Porolepiform Crossopterygii) from the Devonian of Latvia”. In: *Paleontological Journal* 40.3 (2006), pp. 312–322.

[239] J. Kulczycki. “Upper Devonian fishes from the Holy Cross Mountains (Poland)”. In: *Acta Palaeontologica Polonica* 2.4 (1957).

[240] J. A. Long et al. “Live birth in the Devonian period”. In: *Nature* 453.7195 (2008), pp. 650–652.

[241] M. Zhu, W. Wang, and X. Yu. “*Meemannia eos*, a basal sarcopterygian fish from the Lower Devonian of China–expanded description and significance”. In: *Morphology, Phylogeny and palaeobiogeography of Fossil Fishes* (2010), pp. 199–214.

[242] B. Choo et al. “The largest Silurian vertebrate and its palaeoecological implications”. In: *Scientific Reports* 4.1 (2014), pp. 1–8.

[243] P. L. Forey et al. “A new coelacanth from the Middle Devonian of Latvia”. In: *Journal of Vertebrate Paleontology* 20.2 (2000), pp. 243–252.

[244] N. I. Krupina, R. R. Reisz, and D. Scott. “The skull and tooth system of *Orlovichthys limnatis*, a Late Devonian dipnoan from Russia”. In: *Canadian Journal of Earth Sciences* 38.9 (2001), pp. 1301–1311.

[245] A. M. Clement. “The anatomy, evolution and interrelationships of Devonian Dipnoans, with insights from the extant Australian lungfish, *Neoceratodus forsteri*”. PhD thesis. Australian National University., 2011.

[246] T. Ørvig. “Histologic studies of Ostracoderms, Placoderms and fossil Elasmobranchs: 3. Structure and growth of the gnathalia of certain arthrodires ‘”. In: *Zoologica Scripta* 9.1-4 (1980), pp. 141–159.

[247] E. Jarvik. “Middle and Upper Devonian Porolepiformes from East Greenland with special reference to *Glyptolepis groenlandica* n. sp. and a discussion on the structure of the head in the Porolepiformes”. In: *Medd. Grønland* 187 (1972), pp. 1–307.

[248] H. L. Jessen. “Lower Devonian Porolepiformes from the Canadian Arctic with special reference to *Powichthys thorsteinssoni* Jessen”. In: *Palaeontographica Abt. A* 167 (1980), pp. 180–214.

[249] G. F. Hanke. “*Promesacanthus eppleri* n. gen., n. sp., a mesacanthid (Acanthodii, Acanthodiformes) from the Lower Devonian of northern Canada”. In: *Geodiversitas* 30.2 (2008), pp. 287–302.

[250] R. S. Miles. “The acanthodian fishes of the Devonian Plattenkalk of the Paffrath Trough in the Rhineland, with an appendix containing a classification of the Acanthodii and a revision of the genus *Homalacanthus*”. In: *Arkiv Zool* 18 (1966), pp. 147–194.

[251] R. W. Gess and M. I. Coates. “Fossil juvenile coelacanths from the Devonian of South Africa shed light on the order of character acquisition in actinistians”. In: *Zool. J. Linnean Soc.* 175 (2015), pp. 360–383.

[252] D. Snitting. “A redescription of the anatomy of the Late Devonian *Spodichthys buetleri* Jarvik, 1985 (Sarcopterygii, Tetrapodomorpha) from East Greenland”. In: *Journal of Vertebrate Paleontology* 28.3 (2008), pp. 637–655.

[253] E. B. Daeschler, N. H. Shubin, and F. A. Jenkins. "A Devonian tetrapod-like fish and the evolution of the tetrapod body plan". In: *Nature* 440.7085 (2006), pp. 757–763.

[254] J. Boyle and M. J. Ryan. "New information on *Titanichthys* (Placodermi, Arthrodira) from the Cleveland Shale (Upper Devonian) of Ohio, USA". In: *Journal of Paleontology* 91.2 (2017), pp. 318–336.

[255] J. Lu et al. "The earliest known stem-tetrapod from the Lower Devonian of China". In: *Nature Communications* 3 (2012), p. 1160.

[256] R. S. Miles and T. S. Westoll. "IX.—Two new genera of coccosteid arthrodira from the Middle Old Red Sandstone of Scotland, and their Stratigraphical distribution". In: *Trans. R. Soc. Edinburgh* 65 (1962), pp. 179–210.

[257] T. Ørvig. "Some new acanthodian material from the Lower Devonian of Europe". In: *Zool. J. Linnean Soc.* 47 (1967), pp. 131–153.

[258] J. A. Clack et al. "A new genus of Devonian tetrapod from North-East Greenland, with new information on the lower jaw of *Ichthyostega*". In: *Palaeontology* 55.1 (2012), pp. 73–86.

[259] M. Ruta et al. "The evolution of the tetrapod humerus: Morphometrics, disparity, and evolutionary rates". In: *Earth and Environmental Science Transactions of the Royal Society of Edinburgh* 109.1-2 (2018), pp. 351–369.

[260] F. Márquez et al. "Use of different geometric morphometrics tools for the discrimination of phenotypic stocks of the striped clam *Ameghinomya antiqua* (Veneridae) in north Patagonia, Argentina". In: *Fisheries Research* 101.1-2 (2010), pp. 127–131.

[261] J. M. Carlo, M. S. Barbeitos, and H. R. Lasker. "Quantifying complex shapes: elliptical Fourier analysis of octocoral sclerites". In: *The Biological Bulletin* 220.3 (2011), pp. 224–237.

[262] A. Kemp, L. Cavin, and G. Guinot. "Evolutionary history of lungfishes with a new phylogeny of post-Devonian genera". In: *Palaeogeography, Palaeoclimatology, Palaeoecology* 471 (2017), pp. 209–219.

[263] B. King et al. "Bayesian morphological clock methods resurrect placoderm monophyly and reveal rapid early evolution in jawed vertebrates". In: *Systematic Biology* 66.4 (2017), pp. 499–516.

[264] J. D. Pardo et al. "Hidden morphological diversity among early tetrapods". In: *Nature* 546.7660 (2017), pp. 642–645.

[265] N. Takezaki and H. Nishihara. "Support for lungfish as the closest relative of tetrapods by using slowly evolving ray-finned fish as the outgroup". In: *Genome Biology and Evolution* 9.1 (2017), pp. 93–101.

[266] A. M. Clement et al. "Neurocranial anatomy of an enigmatic Early Devonian fish sheds light on early osteichthyan evolution". In: *Elife* 7 (2018), e34349.

[267] M. I. Coates et al. "An early chondrichthyan and the evolutionary assembly of a shark body plan". In: *Proceedings of the Royal Society B: Biological Sciences* 285.1870 (2018), p. 20172418.

[268] T. J. Challands et al. "A lungfish survivor of the end-Devonian extinction and an Early Carboniferous dipnoan radiation". In: *Journal of Systematic Palaeontology* 17.21 (2019), pp. 1825–1846.

[269] B. Choo et al. "A new actinopterygian from the Late Devonian Gogo Formation, Western Australia". In: *Papers in Palaeontology* 5.2 (2019), pp. 343–363.

[270] J. A. Clack et al. “Newly recognized Famennian lungfishes from East Greenland reveal tooth plate diversity and blur the Devonian–Carboniferous boundary”. In: *Papers in Palaeontology* 5.2 (2019), pp. 261–279.

[271] L. Frey et al. “The early elasmobranch *Phoebodus*: phylogenetic relationships, ecomorphology and a new time-scale for shark evolution”. In: *Proceedings of the Royal Society B* 286.1912 (2019), p. 20191336.

[272] M. D. Brazeau. “The braincase and jaws of a Devonian ‘acanthodian’ and modern gnathostome origins”. In: *Nature* 457.7227 (2009), pp. 305–308.

[273] K. Trinajstic and K. Dennis-Bryan. “Phenotypic plasticity, polymorphism and phylogeny within placoderms”. In: *Acta Zoologica* 90 (2009), pp. 83–102.

[274] B. Choo. “Revision of the actinopterygian genus *Mimipiscis* (= *Mimia*) from the Upper Devonian Gogo Formation of Western Australia and the interrelationships of the early Actinopterygii”. In: *Earth and Environmental Science Transactions of the Royal Society of Edinburgh* 102.2 (2012), pp. 77–104.

[275] V. Dupret et al. “A primitive placoderm sheds light on the origin of the jawed vertebrate face”. In: *Nature* 507.7493 (2014), pp. 500–503.

[276] M. D. Brazeau and M. Friedman. “The origin and early phylogenetic history of jawed vertebrates”. In: *Nature* 520.7548 (2015), pp. 490–497.

[277] S. Giles, M. Friedman, and M. D. Brazeau. “Osteichthyan-like cranial conditions in an Early Devonian stem gnathostome”. In: *Nature* 520.7545 (2015), pp. 82–85.

[278] M. Zhu et al. “A Silurian maxillate placoderm illuminates jaw evolution”. In: *Science* 354.6310 (2016), pp. 334–336.

[279] D. W. Bapst. “paleotree: an R package for paleontological and phylogenetic analyses of evolution”. In: *Methods in Ecology and Evolution* 3.5 (2012), pp. 803–807.

[280] D. C. Adams and E. Otárola-Castillo. “geomorph: an R package for the collection and analysis of geometric morphometric shape data”. In: *Methods in ecology and evolution* 4.4 (2013), pp. 393–399.

[281] P. D. Polly. “Functional tradeoffs carry phenotypes across the valley of the shadow of death”. In: *Integrative and Comparative Biology* 60.5 (2020), pp. 1268–1282.

[282] Z. J. Tseng et al. “Model sensitivity and use of the comparative finite element method in mammalian jaw mechanics: mandible performance in the gray wolf”. In: *PLOS ONE* 6.4 (2011), e19171.

[283] O. Shoval et al. “Evolutionary trade-offs, Pareto optimality, and the geometry of phenotype space”. In: *Science* 336.6085 (2012), pp. 1157–1160.

[284] A. Tendler, A. Mayo, and U. Alon. “Evolutionary tradeoffs, Pareto optimality and the morphology of ammonite shells”. In: *BMC systems biology* 9.1 (2015), pp. 1–12.

[285] D. E. Goldberg. *Genetic Algorithms in Search, Optimization and Machine Learning*. 1st. USA: Addison-Wesley Longman Publishing Co., Inc., 1989. ISBN: 0201157675.

[286] C. M. Fonseca and P. J. Fleming. “Multiobjective optimization and multiple constraint handling with evolutionary algorithms. I. A unified formulation”. In: *IEEE Transactions on Systems, Man, and Cybernetics-Part A: Systems and Humans* 28.1 (1998), pp. 26–37.

[287] I. Alberto et al. “Multiobjective evolutionary algorithms. Pareto rankings”. In: *Monografias del Seminario Matematico Garcia de Galdeano* 27 (2003), pp. 25–35.

[288] D. M. Raup. “Computer as aid in describing form in gastropod shells”. In: *Science* 138.3537 (1962), pp. 150–152.

[289] D. M. Raup. "The geometry of coiling in gastropods". In: *PNAS* 47.4 (1961), pp. 602–609.

[290] S. Van Wassenbergh et al. "Hydrodynamic constraints on prey-capture performance in forward-striking snakes". In: *Journal of the Royal Society Interface* 7.46 (2010), pp. 773–785.

[291] S. W. Day et al. "Spatial and temporal patterns of water flow generated by suction-feeding bluegill sunfish Lepomis macrochirus resolved by particle image velocimetry". In: *Journal of Experimental Biology* 208.14 (2005), pp. 2661–2671.

[292] P. C. Wainwright et al. "Origins, innovations, and diversification of suction feeding in vertebrates". In: *Integrative and Comparative Biology* 55.1 (2015), pp. 134–145.

[293] S. Van Wassenbergh et al. "A dynamic model of mouth closing movements in clariid catfishes: the role of enlarged jaw adductors". In: *Journal of Theoretical Biology* 234.1 (2005), pp. 49–65.

[294] C. P. Kenaley. "Exploring feeding behaviour in deep-sea dragonfishes (Teleostei: Stomiidae): jaw biomechanics and functional significance of a loosejaw". In: *Biological Journal of the Linnean Society* 106.1 (2012), pp. 224–240.

[295] S. Van Wassenbergh et al. "Suction power output and the inertial cost of rotating the neurocranium to generate suction in fish". In: *Journal of Theoretical Biology* 372 (2015), pp. 159–167.

[296] M. M. Muñoz et al. "Strong biomechanical relationships bias the tempo and mode of morphological evolution". In: *Elife* 7 (2018), e37621.

[297] C. Gans and R. G. Northcutt. "Neural Crest and the Origin of Vertebrates: A New Head". In: *Science* 220.4594 (1983), pp. 268–273.

[298] R. G. Northcutt. "Evolution of the optic tectum in ray-finned fishes". In: *Fish Neurobiology* 2 (1983), pp. 1–42.

[299] C. Gans. "Stages in the origin of vertebrates: analysis by means of scenarios". In: *Biological Reviews* 64.3 (1989), pp. 221–268.

[300] L. A. Ferry, E. M. Paig-Tran, and A. C. Gibb. "Suction, ram, and biting: deviations and limitations to the capture of aquatic prey". In: *Integrative and Comparative Biology* 55.1 (2015), pp. 97–109.

[301] S. J. Coatham et al. "Was the Devonian placoderm *Titanichthys* a suspension feeder?" In: *Royal Society Open Science* 7.5 (2020), p. 200272.

[302] A. M. Herbert and P. J. Motta. "Biomechanics of the jaw of the durophagous bonnethead shark". In: *Zoology* 129 (2018), pp. 54–58.

[303] J. Mallatt. "Ventilation and the origin of jawed vertebrates: a new mouth". In: *Zoological Journal of the Linnean Society* 117.4 (1996), pp. 329–404.

[304] T. Miyashita. "Fishing for jaws in early vertebrate evolution: a new hypothesis of mandibular confinement". In: *Biological Reviews* 91.3 (2016), pp. 611–657.

[305] J. Fortuny et al. "Temnospondyli bite club: ecomorphological patterns of the most diverse group of early tetrapods". In: *Journal of evolutionary biology* 24.9 (2011), pp. 2040–2054.

[306] E. Heiss, P. Aerts, and S. Van Wassenbergh. "Aquatic–terrestrial transitions of feeding systems in vertebrates: a mechanical perspective". In: *Journal of Experimental Biology* 221.8 (2018), jeb154427.

[307] S. Van Wassenbergh et al. "Hydrodynamic constraints on prey-capture performance in forward-striking snakes". In: *Journal of the Royal Society Interface* 7.46 (2010), pp. 773–785.

[308] H. D. Sues and R. R. Reisz. "Origins and early evolution of herbivory in tetrapods". In: *Trends in Ecology & Evolution* 13.4 (1998), pp. 141–145.

[309] M. J. Markey and C. R. Marshall. "Terrestrial-style feeding in a very early aquatic tetrapod is supported by evidence from experimental analysis of suture morphology". In: *Proceedings of the National Academy of Sciences* 104.17 (2007), pp. 7134–7138.

[310] Laura B Porro, Emily J Rayfield, and Jennifer A Clack. "Descriptive anatomy and three-dimensional reconstruction of the skull of the early tetrapod *Acanthostega gunnari* Jarvik, 1952". In: *PLoS One* 10.3 (2015), e0118882.

[311] J. B. Lemberg, E. B. Daeschler, and N. H. Shubin. "The feeding system of Tiktaalik roseae: an intermediate between suction feeding and biting". In: *Proceedings of the National Academy of Sciences* 118.7 (2021), e2016421118.

[312] S. Van Wassenbergh et al. "A catfish that can strike its prey on land". In: *Nature* 440.7086 (2006), pp. 881–881.

[313] S. Van Wassenbergh. "Kinematics of Terrestrial Capture of Prey by the Eel-Catfish *Channallabes apus*". In: *Integrative and Comparative Biology* 53.2 (2013), pp. 258–268.

[314] K. B. Michel et al. "Functional anatomy and kinematics of the oral jaw system during terrestrial feeding in *Periophthalmus barbarous*". In: *Journal of morphology* 275.10 (2014), pp. 1145–1160.

[315] K. B. Michel et al. "A fish that uses its hydrodynamic tongue to feed on land". In: *Proceedings of the Royal Society B: Biological Sciences* 282.1805 (2015), p. 20150057.

[316] K. B. Michel et al. "Functional morphology and kinematics of terrestrial feeding in the largescale foureyes (*Anableps anableps*)". In: *Journal of Experimental Biology* 218.18 (2015), pp. 2951–2960.

[317] S. Van Wassenbergh, C. Bonte, and K. B. Michel. "Terrestrial capture of prey by the reedfish, a model species for stem tetrapods". In: *Ecology and Evolution* 7.11 (2017), pp. 3856–3860.

[318] J. R. G. Rawson et al. "Early tetrapod cranial evolution is characterized by increased complexity, constraint, and an offset from fin-limb evolution". In: *Science Advances* 8.36 (2022), eadc8875.

[319] C. T. Stayton. "Terrestrial feeding in aquatic turtles: environment-dependent feeding behavior modulation and the evolution of terrestrial feeding in Emydidae". In: *Journal of Experimental Biology* 214.24 (2011), pp. 4083–4091.

[320] J. Cucherousset et al. ""Freshwater killer whales": beaching behavior of an alien fish to hunt land birds". In: *PloS one* 7.12 (2012), e50840.

[321] E. Heiss, P. Aerts, and S. Van Wassenbergh. "Masters of change: seasonal plasticity in the prey-capture behavior of the Alpine newt *Ichthyosaura alpestris* (Salamandridae)". In: *Journal of Experimental Biology* 216.23 (2013), pp. 4426–4434.

[322] F. Witzmann. "Phylogenetic patterns of character evolution in the hyobranchial apparatus of early tetrapods". In: *Earth and Environmental Science Transactions of the Royal Society of Edinburgh* 104.2 (2013), pp. 145–167.

[323] J. A. Long and M. S. Gordon. "The greatest step in vertebrate history: a paleobiological review of the fish-tetrapod transition". In: *Physiological and Biochemical Zoology* 77.5 (2004), pp. 700–719.

[324] P. E. Ahlberg, J. A. Clack, and H. Blom. "The axial skeleton of the Devonian tetrapod *Ichthyostega*". In: *Nature* 437.7055 (2005), pp. 137–140.

[325] V. Callier, J. A. Clack, and P. E. Ahlberg. "Contrasting developmental trajectories in the earliest known tetrapod forelimbs". In: *Science* 324.5925 (2009), pp. 364–367.

[326] M. Ruta, M. I. Coates, and D. L. J. Quicke. "Early tetrapod relationships revisited". In: *Biological Reviews* 78.2 (2003), pp. 251–345.

[327] M. Ruta, J. E. Jeffery, and M. I. Coates. "A supertree of early tetrapods". In: *Proceedings of the Royal Society of London. Series B: Biological Sciences* 270.1532 (2003), pp. 2507–2516.

[328] P. Wainwright et al. "Suction feeding mechanics, performance, and diversity in fishes". In: *Integrative and comparative biology* 47.1 (2007), pp. 96–106.

[329] R. R. Schoch. "Evolution of life cycles in early amphibians". In: *Annual Review of Earth and Planetary Sciences* 37 (2009), pp. 135–162.

[330] A. C. Fabre et al. "Metamorphosis shapes cranial diversity and rate of evolution in salamanders". In: *Nature ecology & evolution* 4.8 (2020), pp. 1129–1140.

[331] R. M. Bonett and A. L. Blair. "Evidence for complex life cycle constraints on salamander body form diversification". In: *Proceedings of the National Academy of Sciences* 114.37 (2017), pp. 9936–9941.

[332] T. S. Kemp. *The origin and evolution of mammals*. Oxford University Press on Demand, 2005.

[333] G. A. Feldhamer et al. *Mammalogy: adaptation, diversity, ecology*. JHU press, 2007.

[334] C. J. Burgin et al. "How many species of mammals are there?" In: *Journal of Mammalogy* 99.1 (2018), pp. 1–14.

[335] J. J. Saarinen et al. "Patterns of maximum body size evolution in Cenozoic land mammals: eco-evolutionary processes and abiotic forcing". In: *Proceedings of the Royal Society B: Biological Sciences* 281.1784 (2014), p. 20132049.

[336] R. Maor et al. "Temporal niche expansion in mammals from a nocturnal ancestor after dinosaur extinction". In: *Nature ecology & evolution* 1.12 (2017), pp. 1889–1895.

[337] G. L. Benevento, R. B. J. Benson, and M. Friedman. "Patterns of mammalian jaw ecomorphological disparity during the Mesozoic/Cenozoic transition". In: *Proceedings of the Royal Society B* 286.1902 (2019), p. 20190347.

[338] N. Brocklehurst et al. "Mammaliaform extinctions as a driver of the morphological radiation of Cenozoic mammals". In: *Current Biology* 31.13 (2021), pp. 2955–2963.

[339] N. Anthwal, L. Joshi, and A. S. Tucker. "Evolution of the mammalian middle ear and jaw: adaptations and novel structures". In: *Journal of anatomy* 222.1 (2013), pp. 147–160.

[340] G. Fleischer. *Evolutionary principles of the mammalian middle ear*. Vol. 55. Springer Science & Business Media, 2013.

[341] Z. X. Luo. "Transformation and diversification in early mammal evolution". In: *Nature* 450.7172 (2007), pp. 1011–1019.

[342] Z. X. Luo. "Developmental patterns in Mesozoic evolution of mammal ears". In: *Annual Review of Ecology, Evolution, and Systematics* 42 (2011), pp. 355–380.

[343] W. K. Gregory. "'Williston's law' relating to the evolution of skull bones in the vertebrates". In: *American Journal of Physical Anthropology* 20.2 (1935), pp. 123–152.

[344] Christian A Sidor. "Simplification as a trend in synapsid cranial evolution". In: *Evolution* 55.7 (2001), pp. 1419–1442.

[345] L. T. Shirai and G. Marroig. “Skull modularity in neotropical marsupials and monkeys: size variation and evolutionary constraint and flexibility”. In: *Journal of Experimental Zoology Part B: Molecular and Developmental Evolution* 314.8 (2010), pp. 663–683.

[346] K. J. Parsons, E. Márquez, and R. C. Albertson. “Constraint and opportunity: the genetic basis and evolution of modularity in the cichlid mandible”. In: *The American Naturalist* 179.1 (2012), pp. 64–78.

[347] M. Oudot et al. “Functional integration for enrolment constrains evolutionary variation of phacopid trilobites despite developmental modularity”. In: *Palaeontology* 62.5 (2019), pp. 805–821.

[348] T. J. Sanger et al. “Roles for modularity and constraint in the evolution of cranial diversity among Anolis lizards”. In: *Evolution* 66.5 (2012), pp. 1525–1542.

[349] W. R. Atchley and B. K. Hall. “A model for development and evolution of complex morphological structures”. In: *Biological Reviews* 66.2 (1991), pp. 101–157.

[350] W. R. Atchley. “Genetic and developmental aspects of variability in the mammalian mandible”. In: *The skull* 1 (1993), pp. 207–247.

[351] C. Adami, C. Ofria, and T. C. Collier. “Evolution of biological complexity”. In: *Proceedings of the National Academy of Sciences* 97.9 (2000), pp. 4463–4468.

[352] S. B. Carroll. “Chance and necessity: the evolution of morphological complexity and diversity”. In: *Nature* 409.6823 (2001), pp. 1102–1109.

[353] M. E. Csete and J. C. Doyle. “Reverse engineering of biological complexity”. In: *science* 295.5560 (2002), pp. 1664–1669.

[354] D. W. McShea and R. N. Brandon. *Biology’s first law: the tendency for diversity and complexity to increase in evolutionary systems*. University of Chicago Press, 2010.

[355] D. W. McShea. “Evolution of complexity”. In: *Evolutionary developmental biology: A reference guide* (2021), pp. 169–179.

[356] B. Esteve-Altava et al. “Structural constraints in the evolution of the tetrapod skull complexity: Williston’s law revisited using network models”. In: *Evolutionary Biology* 40 (2013), pp. 209–219.

[357] B. B. Mandelbrot. “How long is the coastline of Great Britian”. In: *Statistical selfsimilarity and fractional dimension Science* 155 (1967), pp. 636–638.

[358] S. Shan et al. “ariaDNE: A robustly implemented algorithm for Dirichlet energy of the normal”. In: *Methods in Ecology and Evolution* 10.4 (2019), pp. 541–552.

[359] J. D. Gardiner, J. Behnsen, and C. A. Brassey. “Alpha shapes: determining 3D shape complexity across morphologically diverse structures”. In: *BMC evolutionary biology* 18.1 (2018), pp. 1–16.

[360] J. M. Bunn et al. “Comparing Dirichlet normal surface energy of tooth crowns, a new technique of molar shape quantification for dietary inference, with previous methods in isolation and in combination”. In: *American journal of physical anthropology* 145.2 (2011), pp. 247–261.

[361] L. R. Godfrey et al. “Dental topography indicates ecological contraction of lemur communities”. In: *American Journal of Physical Anthropology* 148.2 (2012), pp. 215–227.

[362] K. A. Prufrock, D. M. Boyer, and M. T. Silcox. "The first major primate extinction: an evaluation of paleoecological dynamics of North American stem primates using a homology free measure of tooth shape". In: *American Journal of Physical Anthropology* 159.4 (2016), pp. 683–697.

[363] S. López-Torres et al. "Dental topographic analysis of paromomyid (Plesiadapiformes, Primates) cheek teeth: more than 15 million years of changing surfaces and shifting ecologies". In: *Historical Biology* 30.1-2 (2018), pp. 76–88.

[364] N. S. Upham, J. A. Esselstyn, and W. Jetz. "Inferring the mammal tree: species-level sets of phylogenies for questions in ecology, evolution, and conservation". In: *PLoS biology* 17.12 (2019), e3000494.

[365] L. J. Revell. "phytools: an R package for phylogenetic comparative biology (and other things)". In: *Methods in ecology and evolution* 2 (2012), pp. 217–223.

[366] J. B. Losos. *Uncertainty in the reconstruction of ancestral character states and limitations on the use of phylogenetic comparative methods*. 1999.

[367] N. M. Morales-Garcıa et al. "Jaw shape and mechanical advantage are indicative of diet in Mesozoic mammals". In: *Communications biology* 4.1 (2021), p. 242.

[368] L. Radinsky. "Patterns in the evolution of ungulate jaw shape". In: *American Zoologist* 25.2 (1985), pp. 303–314.

[369] F. J. Pérez-Barberıa and I. J. Gordon. "The functional relationship between feeding type and jaw and cranial morphology in ungulates". In: *Oecologia* 118 (1999), pp. 157–165.

[370] M. Mendoza, C. M. Janis, and P. Palmqvist. "Characterizing complex craniodental patterns related to feeding behaviour in ungulates: a multivariate approach". In: *Journal of Zoology* 258.2 (2002), pp. 223–246.

[371] T. M. Fletcher, C. M. Janis, and E. J. Rayfield. "Finite element analysis of ungulate jaws: can mode of digestive physiology be determined". In: *Palaeontologia Electronica* 13.3 (2010), pp. 1–15.

[372] Z. Zhou et al. "Why ruminating ungulates chew sloppily: biomechanics discern a phylogenetic pattern". In: *PLoS One* 14.4 (2019), e0214510.

[373] P. Raia et al. "The shape of contention: adaptation, history, and contingency in ungulate mandibles". In: *Evolution* 64.5 (2010), pp. 1489–1503.

[374] A. L. Smith et al. "Does the model reflect the system? When two-dimensional biomechanics is not 'good enough'". In: *Journal of the Royal Society Interface* 20.198 (2023), p. 20220536.

[375] N. E. Campione and D. C. Evans. "A universal scaling relationship between body mass and proximal limb bone dimensions in quadrupedal terrestrial tetrapods". In: *BMC biology* 10 (2012), pp. 1–22.

[376] A. E. Maher et al. "Body size, shape and ecology in tetrapods". In: *Nature Communications* 13.1 (2022), p. 4340.

[377] E. De Margerie et al. "Torsional resistance as a principal component of the structural design of long bones: comparative multivariate evidence in birds". In: *The Anatomical Record Part A: Discoveries in Molecular, Cellular, and Evolutionary Biology: An Official Publication of the American Association of Anatomists* 282.1 (2005), pp. 49–66.

[378] M. B. Habib and C. B. Ruff. "The effects of locomotion on the structural characteristics of avian limb bones". In: *Zoological Journal of the Linnean Society* 153.3 (2008), pp. 601–624.

[379] E. L. R. Simons, T. L. Hieronymus, and P. M. O'Connor. "Cross sectional geometry of the forelimb skeleton and flight mode in pelecaniform birds". In: *Journal of Morphology* 272.8 (2011), pp. 958–971.

[380] F. J. Serrano et al. "Morphological disparity of the humerus in modern birds". In: *Diversity* 12.5 (2020), p. 173.

[381] J. A. Tobias et al. "AVONET: morphological, ecological and geographical data for all birds". In: *Ecology Letters* 25.3 (2022), pp. 581–597.

[382] F. Bribiesca-Contreras, B. Parslew, and W. I. Sellers. "Functional morphology of the forelimb musculature reflects flight and foraging styles in aquatic birds". In: *Journal of Ornithology* 162 (2021), pp. 779–793.

[383] D. J. Wescott and D. L. Cunningham. "Temporal changes in Arikara humeral and femoral cross-sectional geometry associated with horticultural intensification". In: *Journal of Archaeological Science* 33.7 (2006), pp. 1022–1036.

[384] B. A. Patel et al. "Humeral cross-sectional shape in suspensory primates and sloths". In: *The Anatomical Record* 296.4 (2013), pp. 545–556.

[385] B. M. Kilbourne and J. R. Hutchinson. "Morphological diversification of biomechanical traits: mustelid locomotor specializations and the macroevolution of long bone cross-sectional morphology". In: *BMC evolutionary biology* 19.1 (2019), pp. 1–16.

[386] C. López-Aguirre et al. "Variation in cross-sectional shape and biomechanical properties of the bat humerus under Wolff's law". In: *The Anatomical Record* 304.9 (2021), pp. 1937–1952.

[387] E. Snively, D. M. Henderson, and D. S. Phillips. "Fused and vaulted nasals of tyrannosaurid dinosaurs: implications for cranial strength and feeding mechanics". In: *Acta Palaeontologica Polonica* 51.3 (2006).

[388] A. R. Cuff and E. J. Rayfield. "Feeding mechanics in spinosaurid theropods and extant crocodilians". In: *PLoS One* 8.5 (2013), e65295.

[389] D. J. E. Murdock, I. J. Sansom, and P. C. J. Donoghue. "Cutting the first 'teeth': a new approach to functional analysis of conodont elements". In: *Proceedings of the Royal Society B: Biological Sciences* 280.1768 (2013), p. 20131524.

[390] C. T. Stayton. "Testing hypotheses of convergence with multivariate data: morphological and functional convergence among herbivorous lizards". In: *Evolution* 60.4 (2006), pp. 824–841.

[391] L. Shen, H. Farid, and M. A. McPeek. "Modeling three-dimensional morphological structures using spherical harmonics". In: *Evolution* 63.4 (2009), pp. 1003–1016.

[392] E. J. Rayfield et al. "Functional morphology of spinosaur 'crocodile-mimic' dinosaurs". In: *Journal of Vertebrate Paleontology* 27.4 (2007), pp. 892–901.

Acronyms

R^2 coefficient of determination. 19, 37, 39, 43, 75, 78

2D Two-Dimensional. i, 7, 10–17, 19, 23, 24, 28, 30, 33, 35, 37, 40, 46, 48, 57, 60, 71–76, 78–81, 83–88, 92, 110, 111, 113

3D Three-Dimensional. i, 9, 10, 16, 17, 24, 25, 30, 33, 48, 92, 93, 95, 97, 101, 103, 110, 112–114

AS Alpha Shape. 75, 76, 83–85

ASR Ancestral State Reconstruction. v, 8, 20, 60

DNE Dirichlet Normal Energy. 75, 83–85

DOF Degrees Of Freedom. 43

EFA Elliptical Fourier Analysis. v, 12–14, 16, 24, 28, 33–35, 40, 53, 58, 60, 72, 73, 78, 93, 101, 102, 110

FAD First Appearance Date. 30, 33

FD Fractal Dimension. 75, 83–85

FEA Finite Element Analysis. 17, 23, 37, 42, 57

FEM Finite Element Model. 74

JH Jaw Height. 53, 61–63, 65

LAD Last Appearance Date. 30, 33

ND N-Dimensional. 7, 15, 24, 72, 74–76, 78–81, 83–86

PC Principal Component. 15, 19, 33, 35, 37, 40, 42–46, 48, 60, 61, 66, 71, 74, 76, 79, 83, 84, 87, 88, 94, 95, 101, 104, 107, 110

PCA Principal Component Analysis. 8, 12, 15, 16, 33, 34, 40, 58, 60, 71–73, 75, 87, 88, 94, 95, 101, 102

PGLS Phylogenetic Generalized Least Squares. 37, 39

POS Pareto Optimal Subset. 18, 40

RE Rotational Efficiency. 23, 28, 29, 35, 37–39, 41–46, 48, 53, 57, 61–63, 65, 74, 76, 78–81

RMSE Root Mean Square Error. 43

SSE Sum of Squared Estimate of Errors. 43

VMS Von Mises Stress. 37–39, 41–43, 45, 46, 53, 57, 61–63, 65, 74, 76, 78–81

ZFEL Zero Force Evolutionary Law. 69, 71, 112